NOTICE

AVIS

The quality of this microform is heavily dependent upon the quality of the original thesis submitted for microfilming. Every effort has been made to ensure the highest quality of reproduction possible.

If pages are missing, contact the university which granted the degree.

Some pages may have indistinct print especially if the original pages were typed with a poor typewriter ribbon or if the university sent us an inferior photocopy.

Reproduction in full or in part of this microform is governed by the Canadian Copyright Act, R.S.C. 1970, c. C-30, and subsequent amendments.

La qualité de cette microforme dépend grandement de la qualité de la thèse soumise au microfilmage Nous avons tout fait pour assurer une qualité supérieure de reproduction.

S'il manque des pages, veuillez communiquer avec l'université qui a conféré le grade

La qualité d'impression de certaines pages peut laisser a désirer, surtout si les pages originales ont été dactylogra phiées à l'aide d'un ruban usé ou si l'université nous a fait parvenir une photocopie de qualité inférieure

La reproduction, même partielle, de cette microforme est soumise à la Loi canadienne sur le droit d'auteur, SRC 1970, c. C-30, et ses amendements subséquents

**Optimization of Prestressed Concrete Bridge Ties
for Open Deck Railway Bridges**

Nigel William Peters

A Thesis

in

The Department

of

Civil Engineering

Presented in Partial Fulfilment of the Requirements
for the Degree of Master of Applied Science at
Concordia University
Montreal, Quebec, Canada

March 1992

National Library
of Canada

Bibliothèque nationale
du Canada

Canadian Theses Service   Service des thèses canadiennes

Ottawa, Canada
K1A 0N4

The author has granted an irrevocable non-exclusive licence allowing the National Library of Canada to reproduce, loan, distribute or sell copies of his/her thesis by any means and in any form or format, making this thesis available to interested persons.

The author retains ownership of the copyright in his/her thesis. Neither the thesis nor substantial extracts from it may be printed or otherwise reproduced without his/her permission.

L'auteur a accordé une licence irrévocable et non exclusive permettant à la Bibliothèque nationale du Canada de reproduire, prêter, distribuer ou vendre des copies de sa thèse de quelque manière et sous quelque forme que ce soit pour mettre des exemplaires de cette thèse à la disposition des personnes intéressées.

L'auteur conserve la propriété du droit d'auteur qui protège sa thèse. Ni la thèse ni des extraits substantiels de celle-ci ne doivent être imprimés ou autrement reproduits sans son autorisation.

ISBN   0-315-73613-5

Canada

ABSTRACT

**Optimization of Prestressed Concrete Bridge Ties
for Open Deck Railway Bridges**

Nigel W. Peters

This thesis presents a study in the optimization of
prestressed concrete bridge tie design. A historical review
of both the development of the bridge tie and the design of
the existing tie is presented. The problem of the existing
tie design cracking from rebound and the need for redesign is
also outlined.

The data obtained from field investigations of a short span
bridge was analyzed in order to determine the effect of
various types of rail-tie and tie-girder pads on attenuating
impacts from railway vehicles. Also, maximum bending strains
from these impacts were determined.

A mathematical model is presented which predicts both the
maximum static and dynamic strains experienced by the ties
under impact. This model was then compared to the field
results which led to the design of three types of prestressed
concrete bridge ties.

Eighteen full scale samples (six of each type) were fabricated

iii

for laboratory testing consisting of static load tests to destruction. Measurements of strains and deflections were obtained.

The purpose of the laboratory testing was to determine the effect of increasing prestress levels in the compressive zone of the tie on the cracking moment and ultimate moment capacity of the tie.

As this is a joint Concordia University - Canadian National Railway research undertaking, the conclusions and recommendations presented will be of great interest to the railway in assisting in the possible redesign of the existing C.N. Rail prestressed concrete bridge tie.

ACKNOWLEDGEMENTS

TABLE OF CONTENTS

TABLE OF CONTENTS

TABLE OF CONTENTS

TABLE OF CONTENTS

LIST OF FIGURES

LIST OF FIGURES

LIST OF FIGURES

LIST OF FIGURES

LIST OF FIGURES

LIST OF TABLES

LIST OF TABLES

LIST OF NOTATIONS

a   - depth of equivalent rectangular stress block

a   - shear span length

b   - overall bottom width of ties

b_1 - overall top width of tie

b   - shear span length

b   - axle to axle distance of railway vehicle bogie

d   - depth of tie

d   - length of skid flat on steel wheel

d_1 - distance from extreme compression fibre to first level of tension zone reinforcement

d_2 - distance from extreme compression fibre to second level of tension zone reinforcement

d_3 - distance from extreme compression fibre to third level of tension zone reinforcement

d_4 - distance from extreme compression fibre to fourth level of tension zone reinforcement

e   - eccentricity of design prestressing force parallel to the axis measured from the centroid of the tie

f_b - stress in the bottom fibre of the tie

f_c - compressive stress in concrete

f_c' - specified compressive strength of concrete

f_{ci} - compressive strength of concrete at the time of prestress transfer

f_{ct} - compressive strength of concrete under combined bi-directional compression and tension

f_{cts} - compressive strength of concrete under combined bi-directional compression and tension due to prestress

f_{pu} - ultimate tensile strength of tendon

f_r - modulus of rupture of concrete

LIST OF NOTATIONS

f_{sc} - effective prestress in steel after losses

f_t - stress in top fibre of tie

f_{tc} - tensile strength of concrete under bi-directional tension and compression

f_{tcs} - tensile strength of concrete under bi-directional tension and compression due to prestress

f_{to} - pure tensile strength of concrete

f_{tself} - stress in top fibre of the tie due to prestress and self weight

g - acceleration due to force of gravity

h - overall height of tie

n - modular ratio

n - tie number

r - radius of steel railway vehicle wheel

r_y - vertical displacement between axle and rail

$\dot{r}_y$ - velocity of rail with respect to the wheel

t - time

A - cross-sectional area of concrete tie

A_c - concrete cross-sectional area

A_i - initial cross-sectional area of the tie

A_n - mode coefficient of the tie

A_{ps}, A_s - area of prestressed reinforcement

A_{s1} - area of prestressed reinforcement at depth d_1

A_{s2} - area of prestressed reinforcement at depth d_2

A_{s3} - area of prestressed reinforcement at depth d_3

A_{s4} - area of prestressed reinforcement at depth d_4

A_T - transformed cross-sectional area of the tie

LIST OF NOTATIONS

C — compressive force due to stress block

C_1 — force due to prestressed reinforcement in the compressive zone

E_c — modulus of elasticity of concrete

E_s — modulus of elasticity of prestressed reinforcement

F — frictional force at the wheel rail interface

$\hat{F}$ — frictional force at the wheel rail interface due to impulse loading

I — impact factor

I — moment of inertia

I_0 — moment of inertia calculated on the apparent linear mass

I_T — transformed moment of inertia

K — spring constant

L — overall length of tie

L — sprung load of the railway vehicle over one wheel

$\hat{L}$ — sprung load, due to the impulse loading, of the railway vehicle, over one wheel

ℓ — length of tie between supports

M_{cr} — flexural cracking moment

M_D — moment due to dead load

M_f — fatigue moment

M_{L+I} — moment due to live loading and impact

M_{LL} — moment due to live loading

M_{SD} — moment due to super-imposed dead loading

M_{self} — moment due to self weight

M_T — mass of tie per unit length

LIST OF NOTATIONS

M_{tot} — moment due to all applied loads

M_R — mass of rail per unit length

M_u — ultimate moment capacity

M_w — mass of wheel

P — prestressing force

P_{cr} — applied load at moment of first cracking

P_{eff} — effective prestressing force after losses

P_f — applied load which causes fatigue

P_i — initial prestressing force applied to tendons

P_u — applied load at ultimate failure

R — reaction of rail beneath the wheel

$\hat{R}$ — reaction due to dynamic impulse loading of the rail beneath the wheel

S — prestressing force

S_b — section modulus - bottom of tie

S_t — section modulus - top of tie

T — tractive force on coupler

T — period (inverse of frequency)

$\hat{T}$ — tractive force on coupler due to impulse loading

T_1 — tensile force due to prestressed reinforcement at depth d_1

T_2 — tensile force due to prestressed reinforcement at depth d_2

T_3 — tensile force due to prestressed reinforcement at depth d_3

T_4 — tensile force due to prestressed reinforcement at depth d_4

U — stored energy

LIST OF NOTATIONS

U_D — energy stored in the tie due to the downward deflection

U_u — energy stored in the tie due to the upward deflection

V — velocity

V_{split} — shear force to cause splitting

W — wheel loading

X — depth of stress block

X — length along tie

X_{max} — maximum depth of stress block

Y — vertical displacement

Y_b — distance from the top fibre of the tie to the centroid

Y_{max} — maximum vertical displacement

Y_o — downward deflection of centre of the tie

$Y_{o'}$ — upward deflection of the centre of the tie

Y_R — displacement of the rail

Y_s — compression of the railway vehicle springs

Y_t — distance from the bottom fibre of the tie to the centroid

Y_T — displacement of the tie

Y_{TR} — displacement of the tie at the rail seat

Y_w — displacement of the wheel

$\dot{Y}_R$ — vertical velocity of the rail

$\dot{Y}_T$ — vertical velocity of the tie

$\dot{Y}_{TN}$ — vertical velocity of the nth tie

$\dot{Y}_{TR}$ — velocity of the tie at the rail seat

$\dot{Y}_w$ — vertical velocity of the wheel

Z — gap between rail and wheel at skid flat

LIST OF NOTATIONS

θ_0 — one half the angle of the skid flat as measured from the centre of the wheel

α — angular decleleration of the axle due to impact

ϵ_b — strain at bottom fibre of the tie

ϵ_{cu} — ultimate strain in concrete

ϵ_t — strain at top fibre of the tie

ϵ_{sc} — strain in prestressing steel after losses

ϵ_{su} — strain in prestressing steel when the tendon reaches its ultimate tensile strength

ϵ_1 — strain in prestressing steel at depth d_1

ϵ_2 — strain in prestressing steel at depth d_2

ϵ_3 — strain in prestressing steel at depth d_3

ϵ_4 — strain in prestressing steel at depth d_4

ϵ_{max} — maximum strain

ϵ_x — tensile strain

λ — length along rail of ties under consideration

μ — poissons ratio

ρ_c — mass density of concrete

σ — stress

σ_b — stress at bottom outer fibre of the tie

σ_t — stress at top outer fibre of the tie

ω — angular velocity

F — frequency

Σ — summation

ϕ — capacity reduction factor

xxiii

CHAPTER 1

BACKGROUND HISTORY

1.1 THE OPEN DECK BRIDGE

The floor systems of railway bridges are divided into two classes. These are open deck, where the floor consists of timber bridge ties, and solid or ballast decks comprised of steel or reinforced concrete decks supporting a ballasted track structure. In open deck bridges the bridge ties in a deck girder or beam bridge rest directly on the top flanges of the girders or beams. In through span bridges the ties are supported by longitudinal stringers. A comparison of an open deck and ballast deck bridge is shown in Figure 1.1.

Open deck structures were popular because they were less costly to construct and they induced less dead loading to the substructure. In addition because of their reduced depth they were practically suited to locations where overhead clearances were restricted, such as underpasses. A diagram of a short span open deck bridge is shown in Figure 1.2.

1.2 CONCRETE VERSUS TIMBER TIES

Up until the last twenty years or so timber remained the dominant material for both track and bridge ties in North America. This was because of the relative abundance of timber in North America and the generally satisfactory performance of both hardwood and softwood ties. In addition the state of
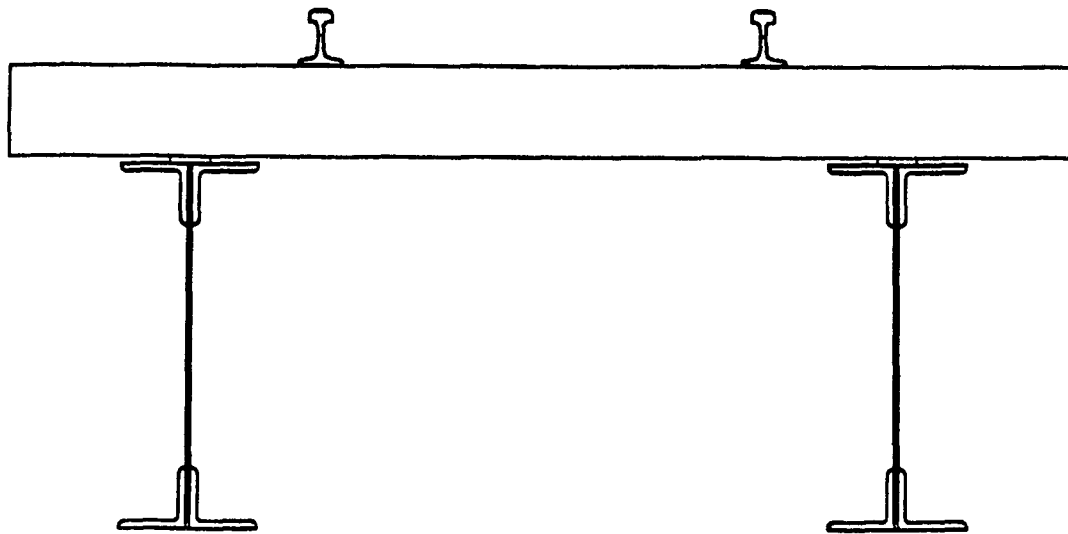
TYPICAL OPEN DECK RAILWAY BRIDGE
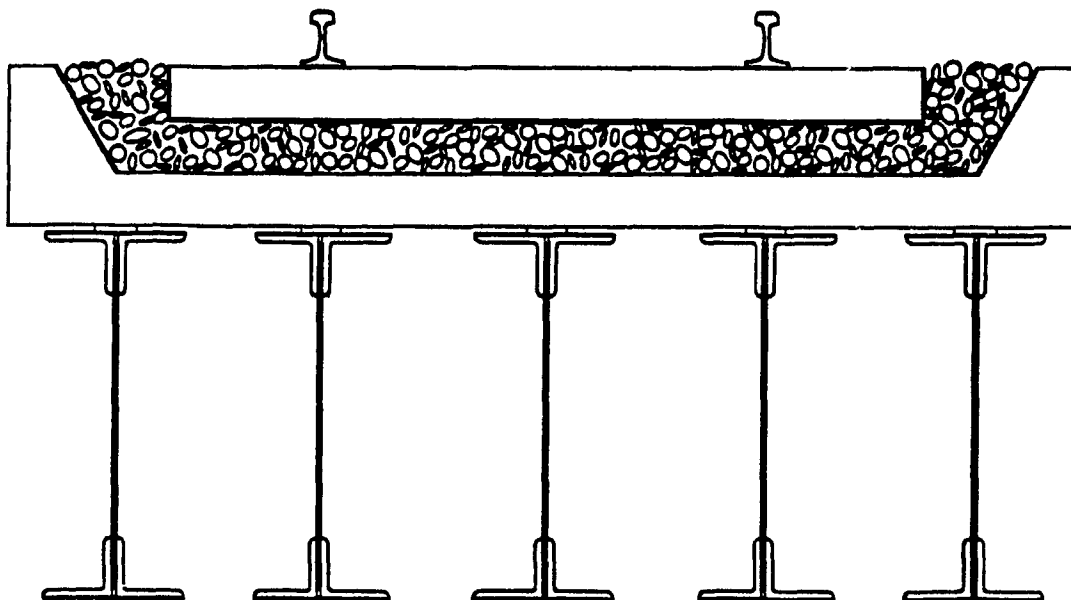
TYPICAL BALLAST DECK RAILWAY BRIDGE

Figure 1.1 Comparison of Open Deck and Ballast Deck Railway
Bridge

prestressed concrete technology in regards to the performance of the ties was not fully understood.

There is now a greater tendency in North America towards the acceptance and use of prestressed concrete ties as an acceptable alternative to the use of timber ties. This is primarily due to the fact that in the last twenty to thirty years rail traffic frequency, axle loadings, train lengths and speeds have all risen dramatically. Under these large increases the service life and performance of timber ties, both hardwood and softwood, has decreased especially on curves and open deck bridges.

The second reason is the growing scarcity of timber of the size required for railway ties, especially in the hardwood species. With the reduction in the availability of the so called old growth timber, new growth timber is being used. However, the performance of this new growth timber is not nearly as satisfactory as that of the old growth timber. For these reasons concrete ties are a viable alternative.

There are several disadvantages in using timber bridge ties on open deck bridges. The close spacing, usually 14" (356.0 mm), on centre of the ties on such decks and their exposure on all sides makes them vulnerable to fire. Such fires can spread rapidly over the length of a bridge causing considerable

3

damage to the deck and supporting structure, often in the millions of dollars. In addition these ties are susceptible to rot, checking, splitting, warping, crushing and mechanical abrasion.

Because of the above problems, the railways often found it difficult to maintain proper alignment, gauge or level across open deck bridges in heavy usage.

1.3 THE CONCRETE BRIDGE TIE

In the late 1970's the Canadian Prestressed Concrete Institute established a liaison committee to promote the use of prestressed concrete on Canadian railways. In consultation with Canada's two major railways it was concluded that, due to the problems associated with timber bridge ties, a prestressed concrete bridge tie for use on open deck bridges would be an ideal place to start.

The Engineering Departments of both major railways proceeded to prepare design drawings for prestressed bridge ties, while the liaison committee compiled the specifications for the rigorous laboratory testing.

The laboratory testing was subsequently conducted at Queen's (12) and McGill Universities (8, 9), who obtained grants from the National Sciences and Engineering Research Council (14).

4
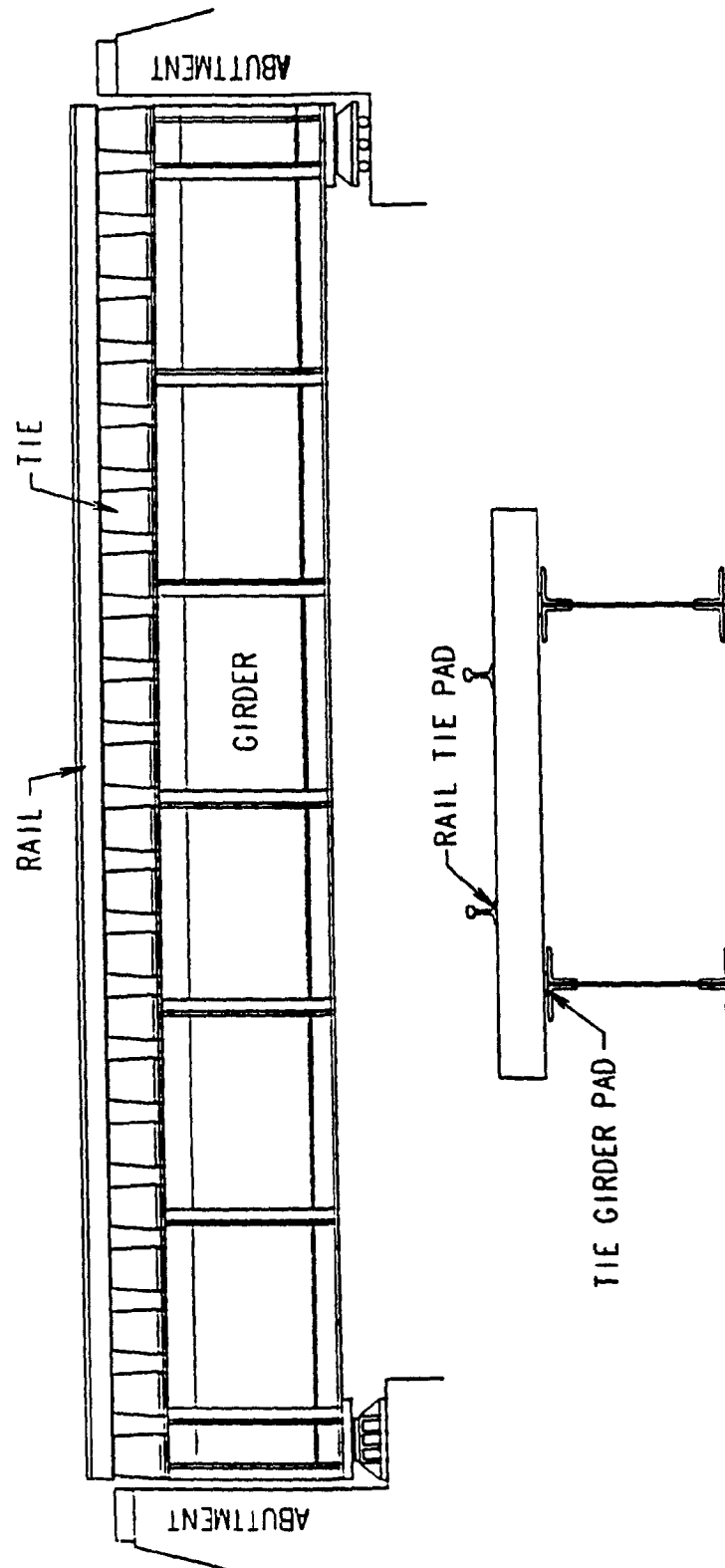
Figure 1.2   Diagram of Short Span Open Deck Railway Bridge

5

In addition the Transportation Development Centre of Transport Canada was retained to provide a technical review. Within a period of three years a great deal of research was conducted.

Based upon this research, C.N. Rail decided to design its' ties based on a 60 percent impact factor. In September of 1984, C.N. Rail installed 22 of these ties on a short span bridge located at mile 122.4 (km 198.3) of its Drummondville Subdivision, some 50 miles (80.5 km) from Montreal. These ties were installed on 16" (406 mm) centres and are shown in Figure 1.3.

The test ties are 12' (3.66 m) long, 12" (305 mm) deep, 10" (254 mm) wide at the top and 12" (305 mm) wide at the bottom. They are prestressed with 32 - 0.196" (5 mm) diameter indented steel wires which provided a static moment capacity of 640" kips (72.3 kN.m) in positive downward bending. The design is based on a steel bridge girder support spacing of 8'-0" (2.44 m) and Cooper's E-80 loading. In addition, each prestressed concrete tie is assumed to carry 1/3 of the static axle loading plus a 60 percent impact factor.

A total of 10 prestressed bridge ties had 44 strain gauge circuits connected to them. The circuits had previously been calibrated so as to establish the relationship between bending moment and strain. In 1984 and again in 1986 C.N. Rail
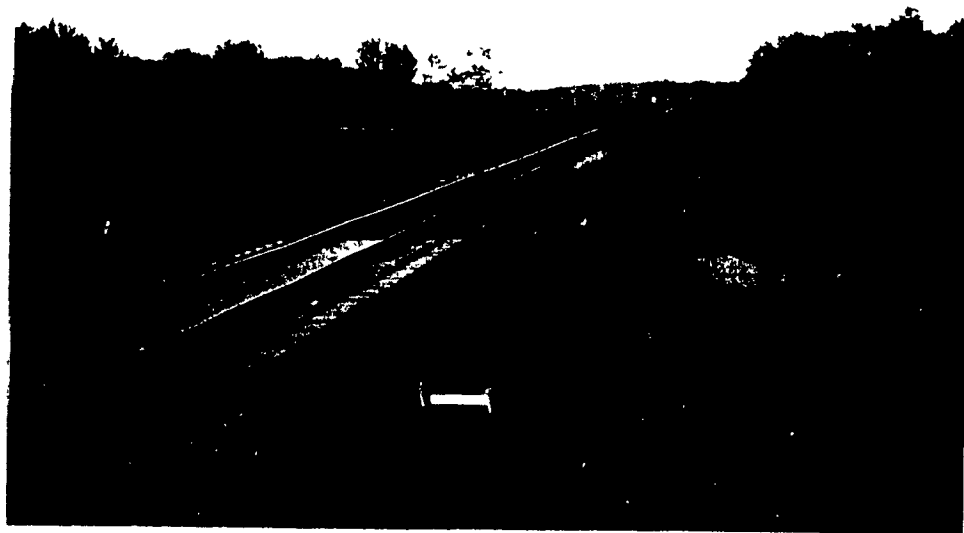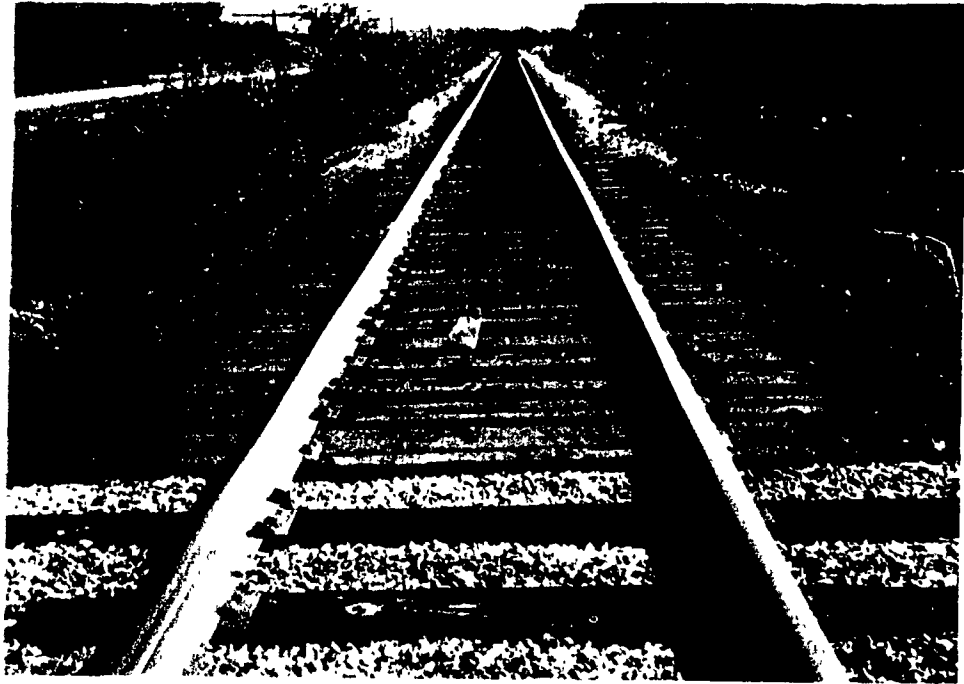
Figure 1.3   Test Bridge Before and After the Installation of
Prestressed Concrete Bridge Ties

recorded the strains caused by both passenger and freight train traffic over this bridge.

In 1988 during an inspection it was found that 17 of the 22 bridge ties had cracks in their centres. The cracks start at the top of the ties and progress towards the middle of the tie. It was obvious that the ties were cracking due to negative bending and must be subjected to rebound. There were no cracks from positive bending. In a follow up inspection conducted in May of 1990, it was determined that the number of cracked ties had increased to 18.

1.4 THE CURRENT PROBLEM

Although 18 of the 22 existing C.N. bridge ties have cracks at their top centres, tests performed (15, 16) indicate that these ties can carry axle loads for 20 million cycles. However, the problem is not one of impending structural failure, but one of durability and resistance to damaging freeze thaw cycles. This problem has previously been recognized (6, 11, 15, 16) and therefore the need to design ties which do not crack from rebound is a must.

CHAPTER 2

THE EXISTING C.N. BRIDGE TIE

2.1 GENERAL

The existing C.N. prestressed concrete bridge tie, designated as the Type A modified design, is trapezoidal in cross section. It has a top width of 10" (254 mm) and a bottom width of 11-23/32" (298 mm). It has an overall height of 12" (305 mm) and an overall length of 12'-0" (3,658 mm). It is prestressed by the use of 32 - 0.196" (5 mm) diameter indented steel wires. The existing C.N. design concrete bridge tie is illustrated in Figure 2.1.

2.2 DESIGN PARAMETERS

The Type A modified ties were designed assuming the following design parameters:

1)   track gauge = 4'-8-1/2" (1,435 mm)

2)   centre to centre of rails ≈ 5'-0" (1,524 mm)

3)   rail section is 132 lb. R.E.

4)   centre to centre of girder supports = 8'-0" (2.44 m)
      actual spacing of girders = 7'-10" (2.39 m)

5)   tie spacing to be 16" (406 mm) on centre

6)   design loading based on Cooper's E-80

7)   impact based on 60 percent

8)   static wheel load distribution = 33.33 percent

10"

4 WIRES

1.3/4"

SLOPE 14:1

TIE CENTERLINE

12"

4 WIRES

8 WIRES

8 WIRES

5.1/2"

8 WIRES

3"

4.1/4"

1.3/4"

1"

1"

2.1/4" 2.1/4"

3.1/2" 3.1/2"
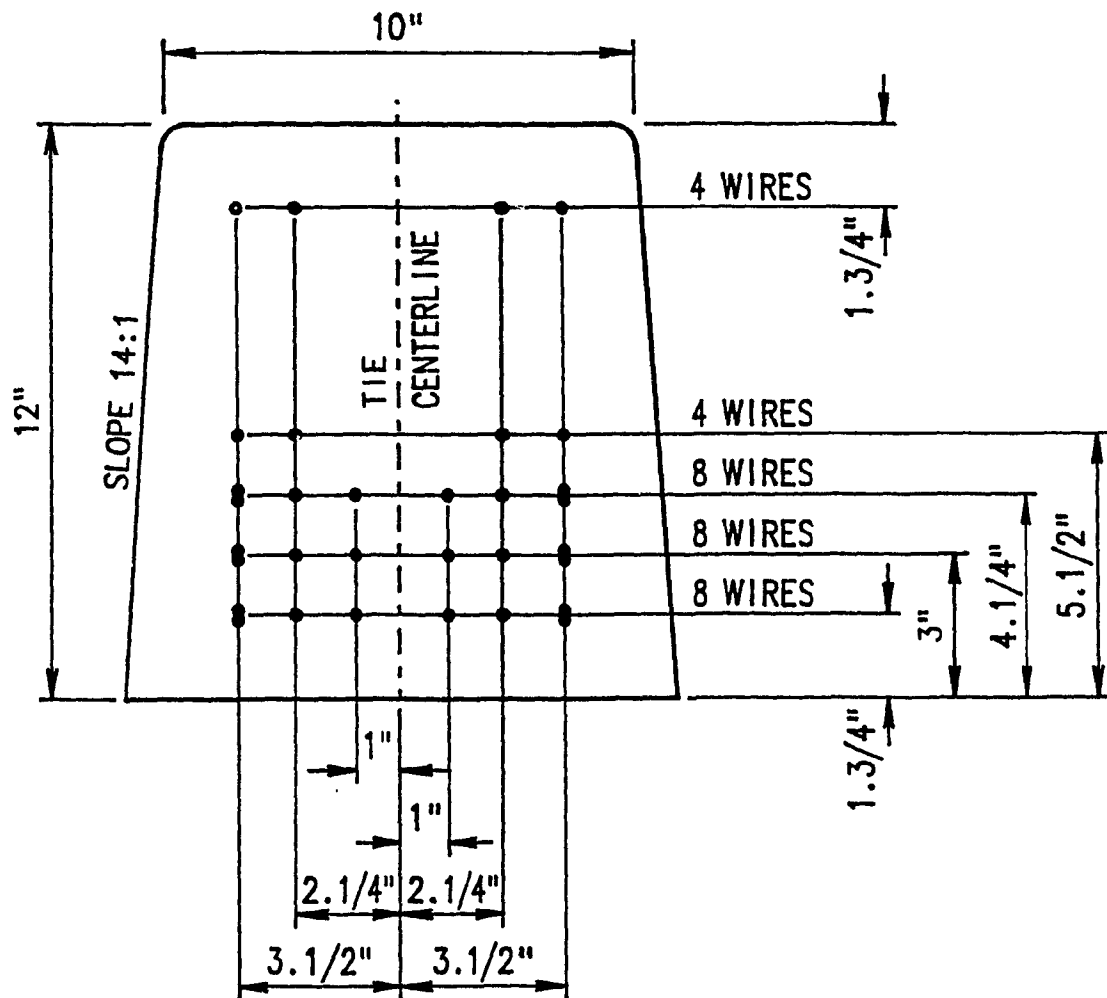
32 – 0.193" (5mm) DIAMETER INDENTED STEEL WIRES

Figure 2.1   Cross Section of C.N. Rail Prestressed Concrete
Bridge Tie

10

2.3 MATERIAL PROPERTIES

The type A modified ties were constructed from materials having the following minimum specified material properties:

a) Concrete:

Compressive strength at 28 days = 6,000 psi (41.4 MPa)

Compressive strength at transfer = 4,500 psi (31.0 MPa)

Flexural stresses after transfer:

Compression: $0.6f_{ci}' = 0.6 \times 4,500 = 2,700$ psi (18.6 Mpa)

Tension: $3(f_{ci}')^{1/2} = 3(4,500)^{1/2} = 201$ psi (1.4 MPa)

Flexural stresses at service loading after losses:

Compression: $0.4f_c' = 0.4 \times 6,000 = 2,400$ psi (16.5 MPa)

Tension: $3(6,000)^{1/2} = 232$ psi (1.6 MPa)

(although in actual design no tension was allowed)

b) Prestressing Steel:

0.193" (4.9 mm) diameter indented wire

Area of prestressing wire; $A_{ps} = 0.029$ in^2 (18.9 mm^2)

Minimum tensile strength; $f_{pu} = 237,000$ psi (1,634 MPa)

Jacking stress; $0.80f_{pu} = 189,600$ psi (1,307 MPa)

Stress at transfer; $0.7f_{pu} = 165,900$ psi (1,144 MPa)

Stress at service load; $0.6f_{pu} = 142,200$ psi (980 MPa)

Modulus of elasticity; $E_s = 29 \times 10^6$ psi (200 x 10^3 MPa)

2.4 GEOMETRIC PROPERTIES

The ties also possess the following geometric properties:

The area of the cross section is:

$A_c = d(b + b_1)/2 = 12(10 + 11.71)/2$

$A_c = 130.28$ in^2 $(84,064$ mm$^2)$

The moment of inertia of the tie is:

$I = d^3(b^2 + 4bb_1 + b_1^2)/36(b + b_1)$

$I = 12^3(11.71^2 + 4 \times 11.71 \times 10 + 10^2)/36(10 + 11.71)$

$I = 1,560.16$ in^4 $(649.4 \times 10^6$ mm$^4)$

The distance from the neutral axis to the top of concrete fibre is:

$Y_t = d(2b + b_1)/3(b + b_1)$

$Y_t = 12(2 \times 11.71 + 10)/3(10 + 11.71)$

$Y_t = 6.16$ in $(156.5$ mm$)$

The distance from the neutral axis to the bottom outer concrete fibre is:

$Y_b = d - Y_t = 12 - 6.26 = 5.84$" $(148.3$ mm$)$

The top and bottom section moduli are:

$S_t = I/Y_t = 1,560.16/6.16 = 253.27$ in^3 $(4,150 \times 10^3$ mm$^3)$

$S_b = I/Y_b = 1,560.16/5.84 = 267.15$ in^3 $(4,378 \times 10^3$ mm$^3)$

The distance from the centroid of the prestressing wire to the top of tie is:

$\Sigma n_i d_i/\Sigma n_i = 7.78$" $(198$ mm$)$

The distance from the centroid of the prestressing wire to the neutral axis (the eccentricity) is:

$e = 7.78 - 6.16 = 1.62$" $(41.1$ mm$)$

The static wheel load distribution factor = 33.33 percent

The prestressing loss = 27 percent

The initial prestressing force was:

$P_i = 32 \times 5,170 = 165,440$ lbs. $(735.9$ kN.$)$

The effective prestress force was:

$P_{eff} = P_i \times 0.73 = 165,440 \times 0.73 = 120,771$ lbs. (537.2 kN)

2.5 DESIGN LOADS

In determining the loads on the tie Cooper's E-80 loading, 60 percent impact factor and 33.33 percent static wheel load distribution were used.

The service live load moment is:

$M_{L+I} = 80 \times 1.60 \times 33.33 \times 18 \times 1/2 \times 1/100$

$M_{L+I} = 384$ in.kips (43.4 kN.m)

The moment due to self weight of the ties is:

$M_D = 6 \times 12 \times 138 \times 1/1,000 = 9.94$ in.k (1.12 kN.m)

The moment due to superimposed dead loads (rail & fasteners)

$M_{SD} = 4 \times 12 \times 62 \times 1/1,000 = 2.98$ in.k (0.34 kN.m)

The total moment $M_{tot} = M_D + M_{SD} + M_{L+I}$ is:

$M_{tot} = 9.94 + 2.98 + 384.0 = 396.9$ in.k (44.85 kN.m)

2.6 CONCRETE STRESSES

The top fibre stress with no service live load is:

$$f_t = \frac{P}{A} - \frac{P\,e\,Y_t}{I} + \frac{(M_D + M_{SD})\,Y_t}{I}$$

$$f_t = \frac{120.77}{130.28} - \frac{120.77 \times 1.62 \times 6.16}{1,560.16} + \frac{12.92 \times 6.16}{1,560.16}$$

$f_t = 0.21$ ksi (1.5 MPa) compression

The bottom fibre stress with no service live load is:

$$f_b = \frac{P}{A} + \frac{P\,e\,Y_b}{I} - \frac{(M_D + M_{SD})\,Y_b}{I}$$

13

$$f_b = \frac{120.77}{130.28} + \frac{120.77 \times 1.62 \times 5.84}{1,560.16} - \frac{12.92 \times 5.84}{1,560.16}$$

f_b = 1.61 ksi (11.1 MPa) compression

The top fibre stress with service live loading is:

$$f_t = \frac{P}{A} - \frac{P\, e\, Y_t}{I} + \frac{M_{tot}\, Y_t}{I}$$

$$f_t = \frac{120.77}{130.28} - \frac{120.77 \times 1.62 \times 6.16}{1,560.16} + \frac{396.9 \times 6.16}{1,560.16}$$

f_t = 1.72 ksi (11.9 MPa) compression

The bottom fibre stress with service live loading is:

$$f_b = \frac{P}{A} + \frac{P\, e\, Y_b}{I} - \frac{M_{tot}\, Y_b}{I}$$

$$f_b = \frac{120.77}{130.28} + \frac{120.77 \times 1.62 \times 5.84}{1,560.16} - \frac{396.9 \times 5.84}{1,560.16}$$

f_b = 0.21 ksi (1.5 MPa) compression

2.7 TIE CRACKING STRENGTH

The concrete bridge ties were manufactured in June of 1984 by Conforce Costain of Edmonton, Alberta. Although there were no 28 day cylinder tests performed specifically on these ties, there were 28 day cylinder tests done on all batches of concrete poured that month. The average 28 day cylinder tests for concrete poured during the month of June, 1984 at the Costain plant was 8,620 psi (59.4 MPa). This was well above the minimum specified 28 day compressive strength of 6,000 psi (41.4 MPa).

Concrete is assumed to crack when the tensile stress reaches the modulus of rupture, f_r or $0.1f_c'$.

The modulus of rupture is given by:

$$f_r = 7.5(f_c')^{1/2}$$

where $f_c' = 6,000$ psi (41.4 MPa)

$$f_r = 7.5(6,000)^{1/2} = 696 \text{ psi } (4.8 \text{ MPa})$$

Under positive bending the cracking moment M_{cr} is:

$$M_{cr} = \frac{(f_r + f_b) \ I}{Y_b}$$

$$M_{cr} = \frac{(0.58 + 1.66) \ x \ 1,560.16}{5.84} = 598.4 \ in.k \ (71.2 \ kN.m)$$

Under negative bending the cracking moment M_{cr} is:

$$M_{cr} = \frac{(f_r + f_t) \ I}{Y_t}$$

$$M_{cr} = \frac{(0.58 + 0.16) \ x \ 1,560.16}{6.16} = 187.4 \ in.k \ (21.2 \ kN.m)$$

$$P_{cr} = \frac{M_{cr}}{18} = \frac{187.4}{18} = 10.41 \ kips \ (46.3 \ kN)$$

2.8 ULTIMATE MOMENT CAPACITY

The ultimate moment capacity of the CN concrete bridge tie was calculated by the stress - strain compatability method outlined in Chapter 6.

The ultimate moment capacity of the tie in positive bending has been calculated to be:

M_u = 1,176.75 in.k (133.0 kN.m)

P_u = 65.38 k (290.8 kN)

The ultimate moment is therefore achieved by the application of two loads equal to 65.38 k (290.8 kN) on each rail, as outlined below.

P_u = 65.38 k P_u = 65.38 k

(290.8 kN)   (290.8 kN)

Figure 2.2   Diagram of Load Application

2.9   FATIGUE CRACKING MOMENT

The fatigue strength of concrete is very much dependent on; the range of loading, the rate of loading, prior loading history, material properties and environmental conditions. Of these, the most important influence is the range of loading which in turn dictates the stress range within the concrete. This stress range is the difference between the minimum and maximum stresses experienced by the concrete under repetitive loading.

In the calculation of the fatigue cracking moment of the concrete tie (method used by the CN Technical Research Centre), it has been assumed that concrete has zero tensile strength in fatigue. This is a valid assumption as it indicates that the fatigue bending capacity of the tie is directly related to the level of precompression within the tie.

The positive fatigue moment is given by:

$M_f = (f_b \times I)/Y_b$

$M_f = (1.66 \times 1,560.16)/5.84 = 443.5$ in.k (50.1 kN.m)

$P_f = \dfrac{M_f}{18} = \dfrac{443.5}{18} = 24.6$ *kips* (109.4 *kN*)

The negative fatigue moment is given by:

$M_f = (f_t \times I)/Y_t$

$M_f = (0.16 \times 1,560.16)/6.16 = 40.5$ in.k (4.6 kN.m)

$M_f = 40.5$ in.k (4.6 kN.m)

CHAPTER 3

THE C.N. FIELD TESTS

3.1 EVALUATION

In order to evaluate the design of the 22 prestressed ties testing was carried out in September of 1984 and again in April of 1986. For each test a different rail-tie and tie-girder pad configuration was used. In addition, the type of approach ties to the bridge were varied.

3.2 THE 1984 BRIDGE CONFIGURATION

The 22 prestressed concrete ties were installed at 16" (406 mm) centres on two girders, at 8'-0" (2.44 m) centres, spanning 29' (8.84 m). The ties were numbered consecutively from 1 to 22 starting at the east end of the bridge. The approach ties to the bridge consisted of 11 timber ties on 20" (508 mm) centres.

3.3 RAIL-TIE AND TIE-GIRDER PADS (1984)

Two types of tie-girder pads were used which determined two regions of influence. These were:

a)   the hard SA-47 tie-girder pads placed under ties numbered 1 to 11.

b)   the soft AASHTO, 60 durometer tie-girder pads placed under ties numbered 12 to 22.

Two types of rail-tie pads were used which were placed over each type of tie-girder pad. These were as follows:

a)   the hard EVA rail-tie pads placed on ties numbered 1 to

4 inclusive and ties numbered 12 to 18 inclusive.

b)   the soft SBR, 60 durometer rail-tie pads placed on ties

numbered 5 to 11 inclusive and ties numbered 19 to 22

inclusive.

Figure 3.1 indicates the areas of influence of the rail-tie

and the tie-girder pads.

3.4 STRAIN GAUGE CONFIGURATION (1984)

The following structural members were instrumented with strain

gauge rosettes:

i)   the concrete ties at top and bottom of their vertical

faces.

ii)   the girders at the top and bottom flanges on either

side of the web.

Due to the symmetry of the structure the instrumentation was

applied on one side of the structure only. A list of the

strain gauges monitored in 1984 is shown in Table 3.1.

The following abbreviations are used to designate the location

of the strain gauges on the structure:

3GT and 3GB   -   strain gauges located on the vertical

face of concrete tie number 3, over the

girder support. "T" indicates top of

vertical face, 2" (51 mm) from the top;

"B" indicates the bottom of the vertical

19
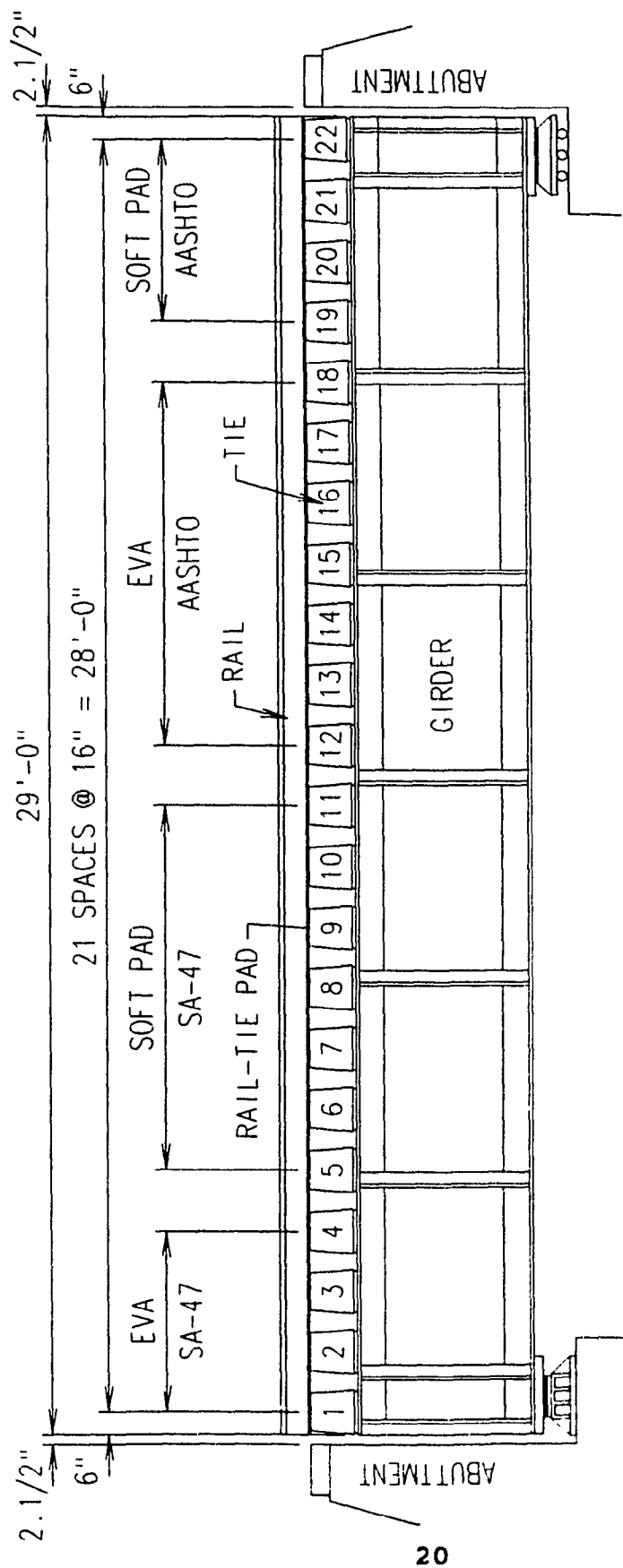
Figure 3.1 Regions of Influence for Rail-Tie and Tie-Girder Pads

TIE NO.	GIRDER TOP	GIRDER BOTTOM	RAIL SEAT TOP	RAIL SEAT BOTTOM	TIE TOP	CENTRE BOTTOM	WIRE/STEEL GIRDER
1	1GT	1GB	1RT	1RB	1CT	1CB	
3	3GT	3GB	3RT	3RB	3CT	3CB	
7					7CT	7CB	
8	8GT	8GB	8RT	8RB	8CT	8CB	W1 AND W2
9					9CT	9CB	
11							G1,G2,G3,G4
14					14CT	14CB	
15	15GT	15GB	15RT	15RB	15CT	15CB	W3 AND W4
16					16CT	16CB	
20	20GT	20GB	20RT	20RB	20CT	20CB	
22	22GT	22GB	22RT	22RB	22CT	22CB	

TABLE 3.1   Concrete Bridge Tie Strain Gauge Circuits for the 1984 Tests Location and Designation

face 1-1/2" (38 mm) from the bottom.

8RT and 8RB   -   strain gauges located on the vertical face of the concrete tie number 8 under the rail seat at the top and bottom of the vertical face as indicated above.

15CT and 15CB   -   strain gauges located on vertical face of concrete tie number 15 at the centre of the tie, at the top and bottom of the vertical face as indicated above.

W1 and W2   -   two strain gauges located on prestressing wires, 7" (177.8 mm) apart and 1-3/4" (44.5 mm) from the base of tie number 8.

W3 and W4   -   two strain gauges located on prestressing wires, 7" (177.8 mm) apart and 1-3/4" (44.5 mm) from the base of tie number 15.

G1, G2, G3, & G4   -   the four strain gauges located on the four flanges of one of the girders directly under tie number 4.

Figure 3.2 illustrates the locations of the strain gauges on the C.N. field test ties.

3.5 THE 1986 BRIDGE CONFIGURATION

Between 1984 and 1986 hairline positive bending cracks were detected in the two end ties of the bridge, namely ties 1 and 22. These cracks were initiated from the high impact loading associated with the transition from the timber approach ties

CONCRETE STRAIN GAUGE
TYPICAL

(267mm)

(51mm)

2 CONCRETE GAUGES

10.1/2"

2"

SECTION

CONCRETE TIES 7, 9, 14 & 16

PRESTRESS WIRES — ┌─STEEL STRAIN GAUGE

CONCRETE GAUGE ⌐

6 CONCRETE AND
2 STEEL GAUGES

SECTION

CONCRETE TIES 8 & 15

8'-0" (2.44m)

┌─RAIL TIE PAD

GIRDER PAD ⌐

6 CONCRETE GAUGES

SECTION

CONCRETE TIES 1, 3, 20 & 22
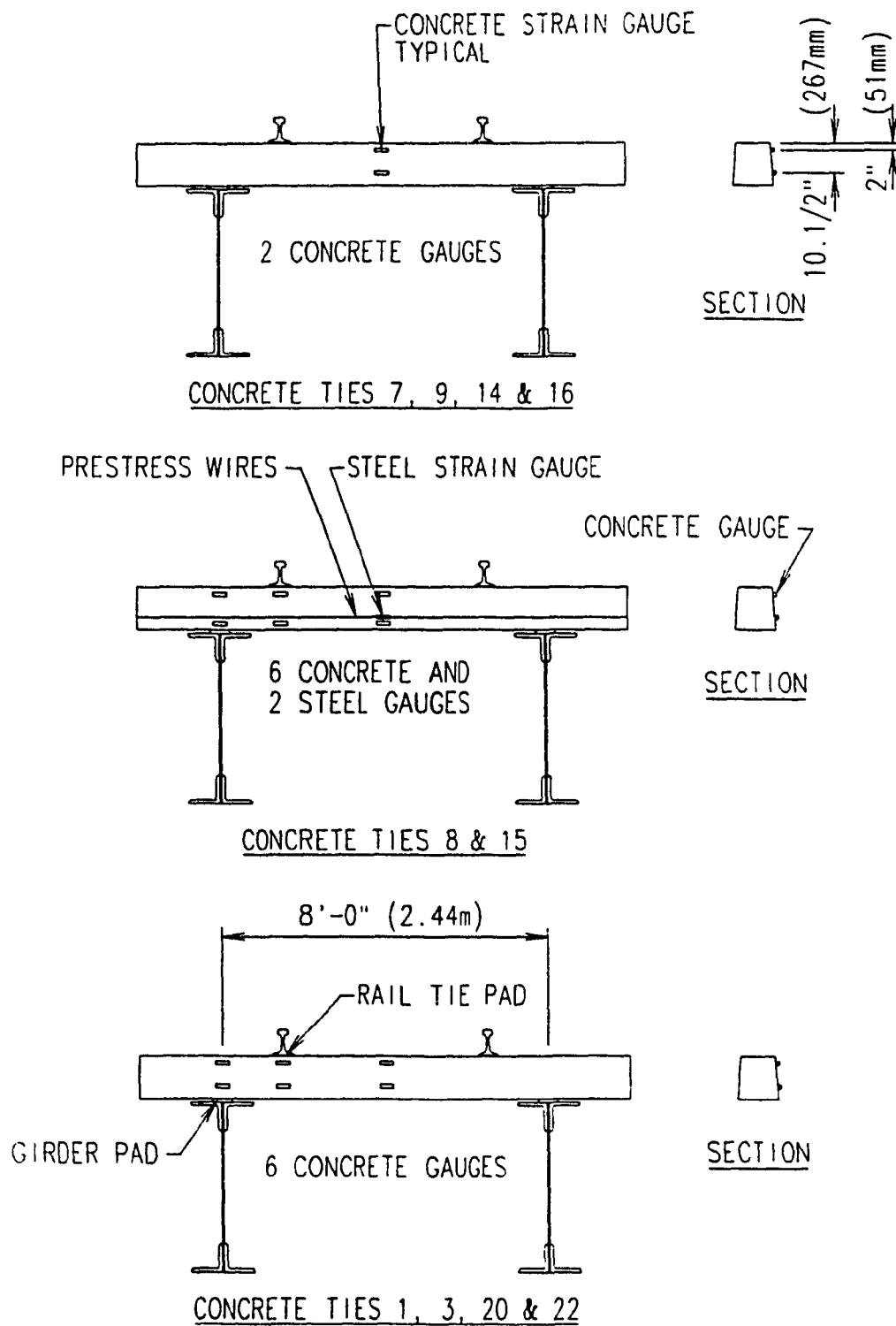
Figure 3.2   Location of Strain Gauges on Field Test Ties

23

on ballast to the concrete ties at the abutments of the bridge. This is commonly referred to as a variation in track modulus.

To reduce the impact at the abutments, the timber approach ties at each end of the bridge were replaced by 50 concrete track ties, spaced at 24" (610 mm) centre to centre. In addition the cracked bridge ties (numbers 1 and 22) at the abutments were replaced with spares.

3.6 RAIL AND TIE GIRDER PADS (1986)

The 1986 test configuration was identical to the 1984 configuration except that the 5 mm EVA rail-tie pads were removed and replaced by 6.5 mm Hytrel studded pads. The measurements and data analysis focused on the evaluation of the new Hytrel rail-tie pads, in order to determine if there was any improvement in the reduction of high strains. These strains would be reduced by the attenuation of impact by the pads and the smoother transition at the abutments provided by the 50 concrete track ties.

3.7 STRAIN GAUGE CONFIGURATION (1986)

From a preliminary analysis of the 1984 results, it was found that the maximum static strains occurred as expected between the rail seats at the bottom fibre of the tie. However, the maximum dynamic strains occurred at the rail seat bottom

locations. Therefore, the 1986 test concentrated primarily on the rail seat bottom (RB) locations as these were the locations of maximum strain. In the 1986 tests a total of 8 prestressed concrete bridge ties were instrumented with 10 strain gauge rosettes. The list of strain gauges monitored in the 1986 test is shown in Table 3.2.

3.8 CALIBRATION MEASUREMENTS

In the evaluation of the 1984 and 1986 data on concrete bridge ties two types of measurements were calibrated with respect to the applied moment, these were:

1) bending strain measurements of the concrete ties and

2) tensile strain measurements of the prestressing wire

3.9 BENDING STRAINS ON CONCRETE BRIDGE TIES

The result of the calibrations of the concrete ties is plotted in the graph shown in Figure 3.3. This curve was used for the calibration of the 1984 and 1986 measurements for all concrete bridge tie bending strain gauges.

It should be noted that the strain gauge rosette readings are expressed in terms of $\epsilon_x(1+\mu)$ where:

μ is Poisson's Ratio for concrete (determined to be $\mu = 0.18$) and ϵ_x is the bending strain.

TIE NO.	RAIL SEAT TOP	RAIL SEAT BOTTOM	TIE CENTRE BOTTOM
1		1RB	
3		3RB	
14		14RB	
15	15RT	15RB	15CB
16		16RB	
20		20RB	
22	22RT	22RB	

TABLE 3.2 Concrete Bridge Tie Strain Gauge Circuits for the 1986 Tests – Location and Designation
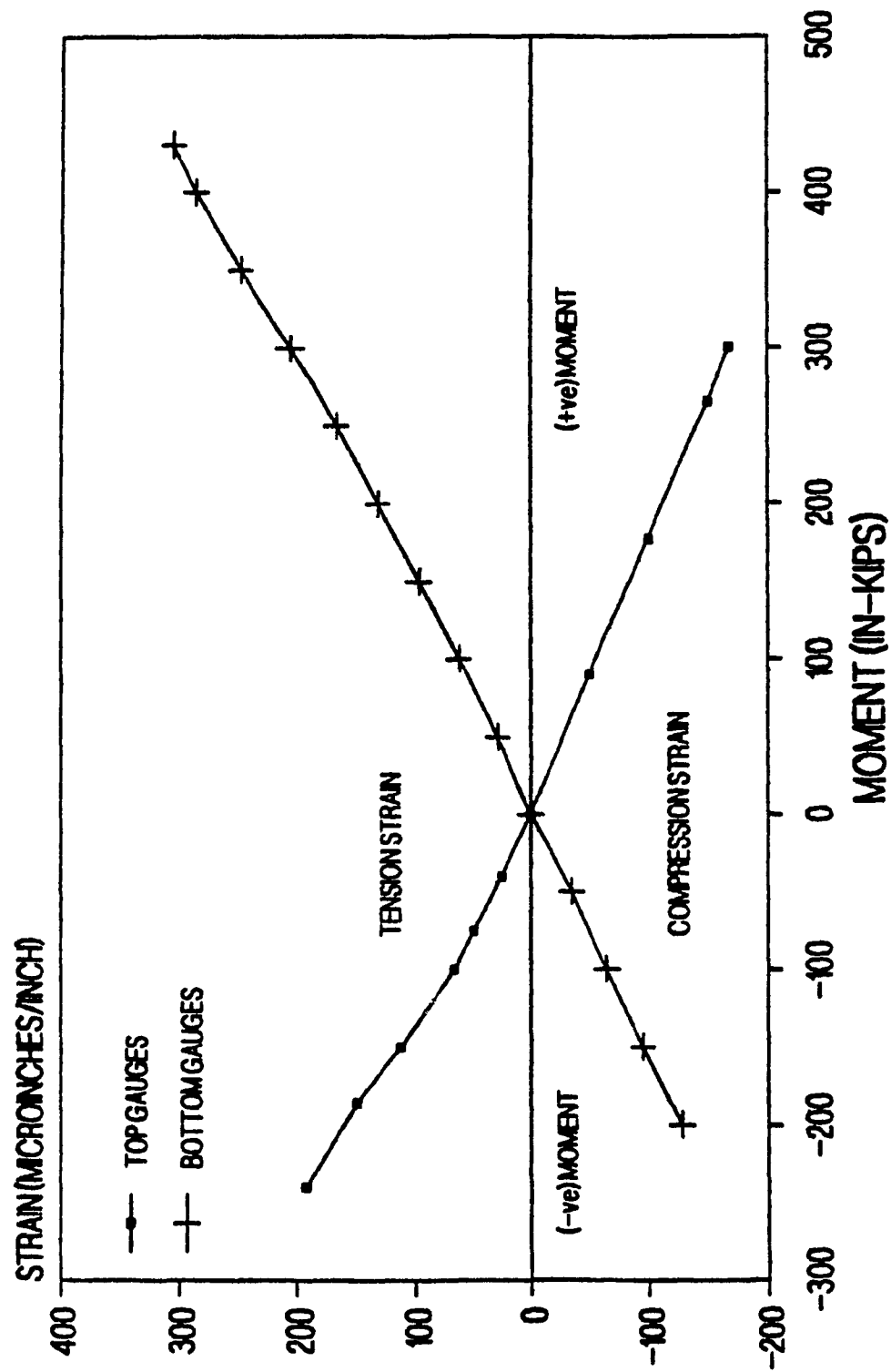
Figure 3.3 Calibration Curve for Concrete Ties

27

3.10 STRAINS OF PRESTRESSING WIRES

Strain gauges were installed on the initially unstressed prestressing wires of tie number 8 and 15 at the manufacturing plant. The strain gauge rosette readings are again expressed in terms of $\epsilon_x(1+\mu)$ where:

μ is Poisson's Ratio for steel = 0.30

and ϵ_x is the tensile strain

Each strain gauge was calibrated on its respective wire and the results are shown in Figures 3.4, 3.5, 3.6 and 3.7. The strain gauges were monitored during the pouring of the concrete, through the transfer of the prestress and up until the ties were removed from the forms. Relaxation of the wires over time is shown in Figure 3.8 and 3.9.

3.11 INSTRUMENTATION

All data recorded was in the form of bending strains. The circuits were temperature compensated by placing rosette gauges in a wheatstone bridge, with the signals amplified and transmitted by means of cables to a tape recorder. These signals were also played out on a high speed chart recorder.

The strain gauges were 2" (51 mm) long and had a resistance of 120 ohms. At each measurement location two strain gauges were stacked perpendicular to each other and connected in a rosette configuration to compensate for any temperature variations. But the temperature compensating gauges, placed perpendic-

28

STRAIN GAUGED REINFORCING WIRE
BRIDGE TIE CALIBRATION TESTS

APPLIED LOAD – KIPS

WIRE No.1

STRAIN – MICROINCHES/INCH x 1000
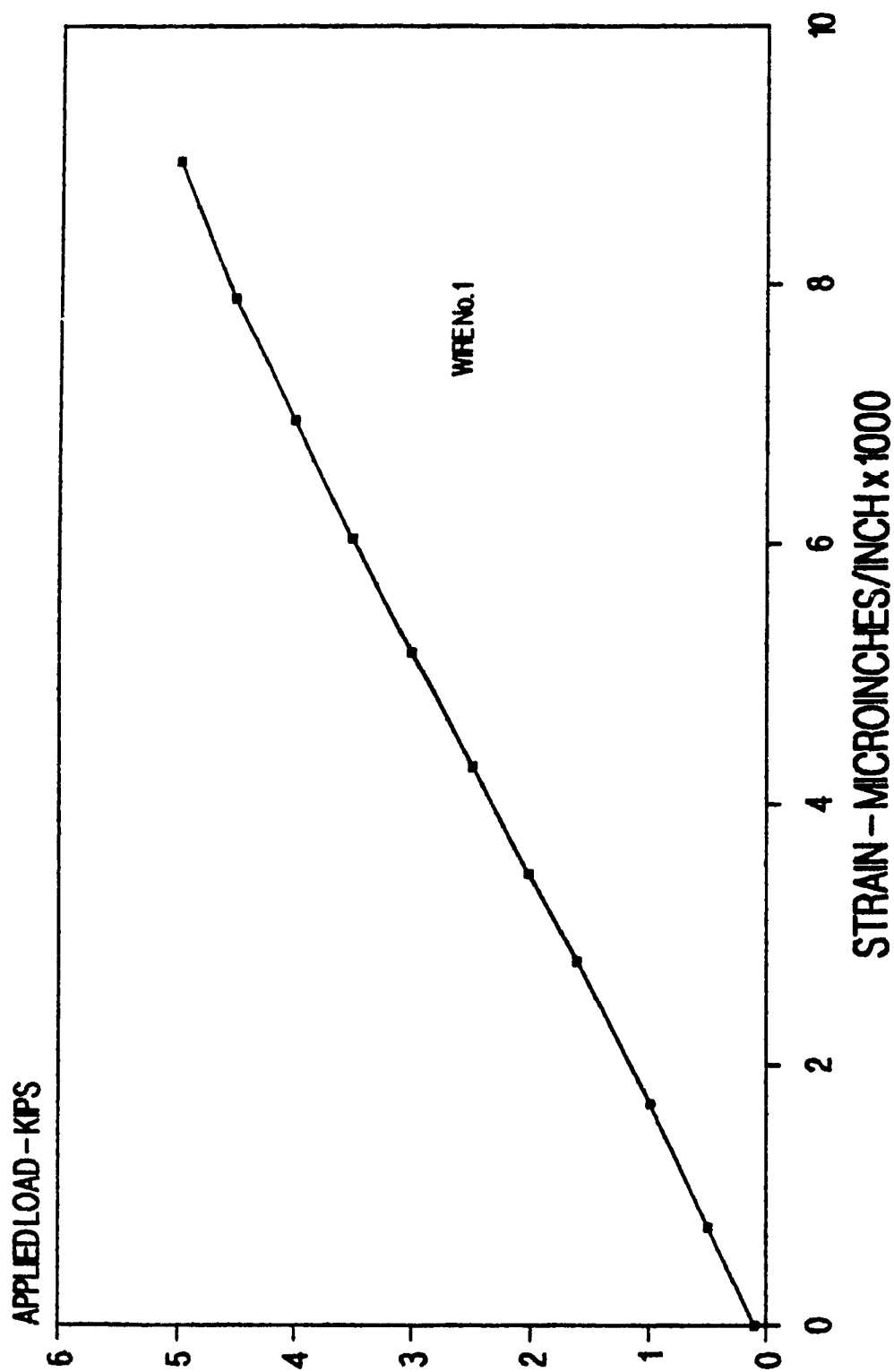
Figure 3.4 Calibration Curve for Wire 1

29
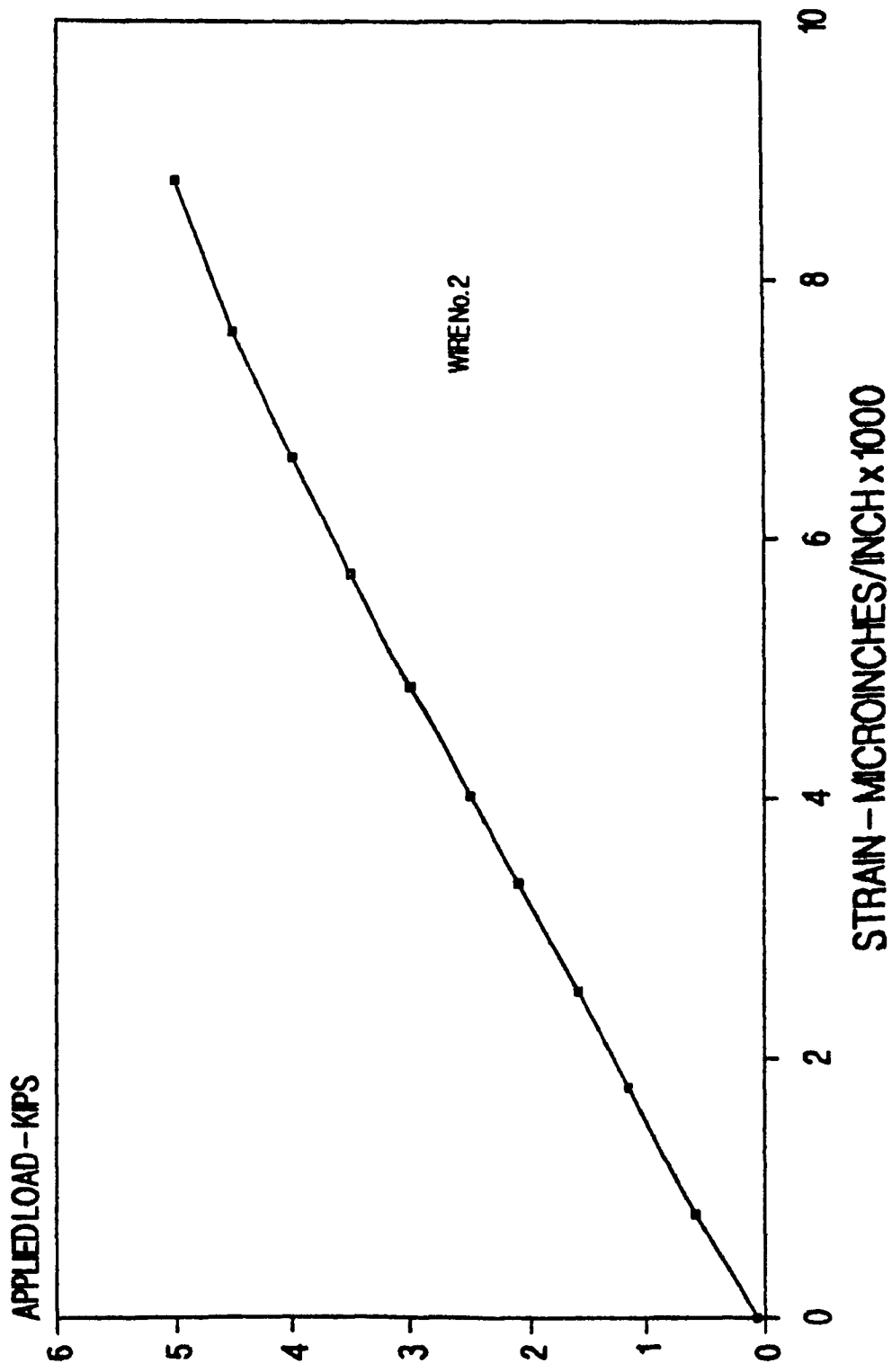
Figure 3.5   Calibration Curve for Wire 2

STRAIN GAUGED REINFORCING WIRE
BRIDGE TIE CALIBRATION TESTS

APPLIED LOAD – KIPS

WIRE No. 3

STRAIN – MICROINCHES/INCH x 1000
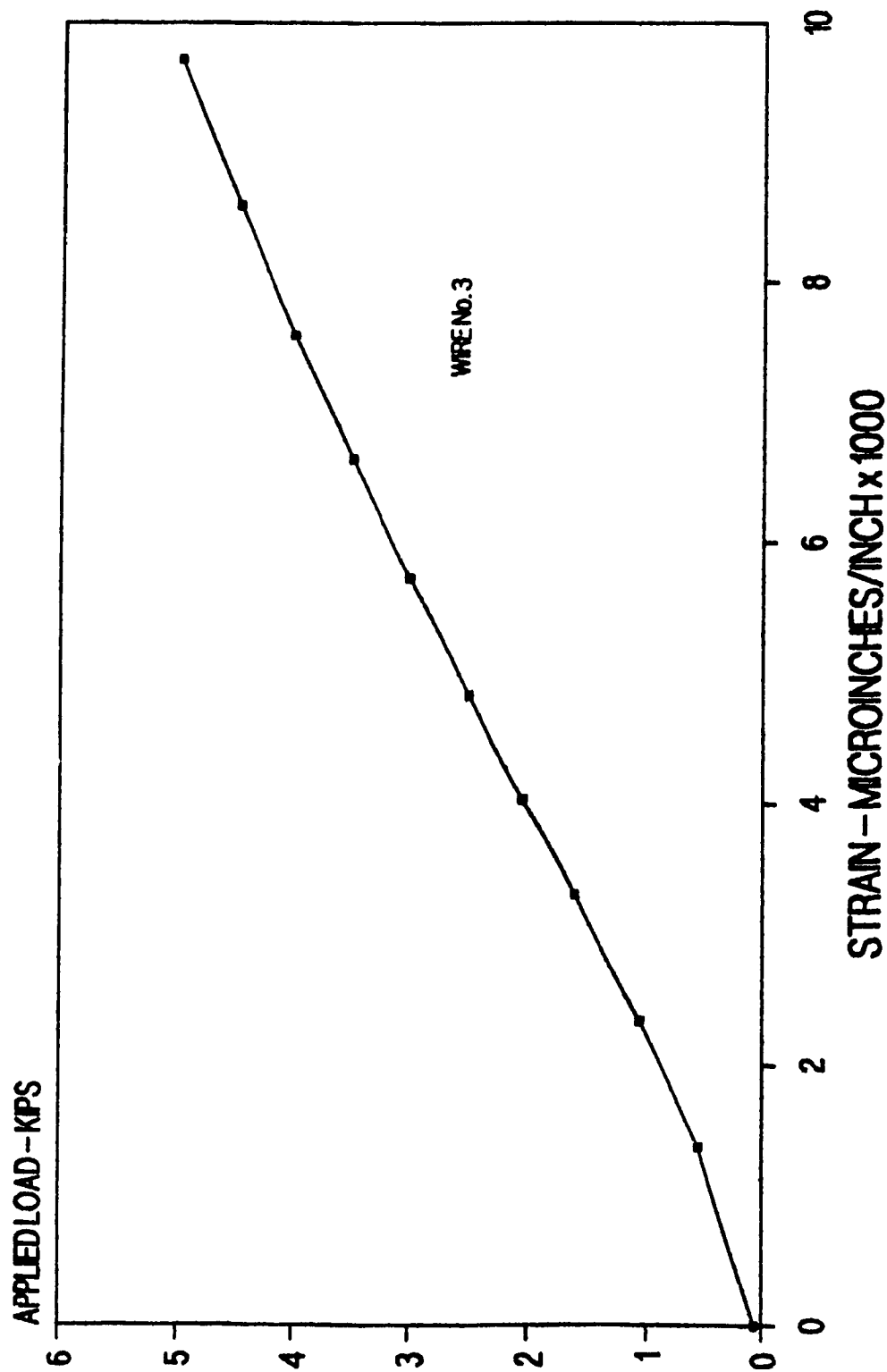
Figure 3.6 Calibration Curve for Wire 3

31

STRAIN GAUGED REINFORCING WIRE
BRIDGE TIE CALIBRATION TESTS
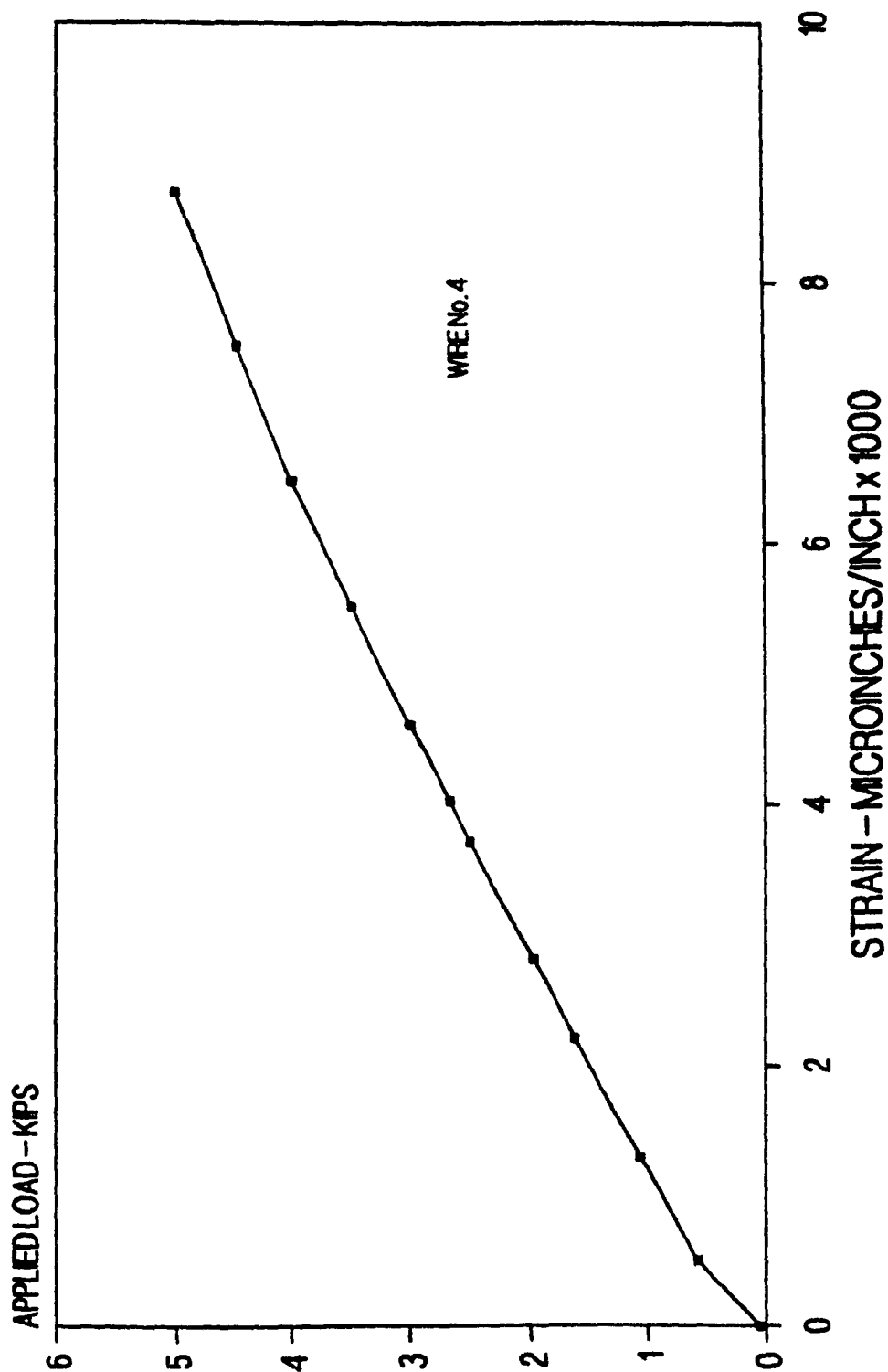
Figure 3.7 Calibration Curve for Wire 4

STRAIN GAUGED REINFORCING WIRES
INSTALLATION IN BRIDGE CONCRETE TIES
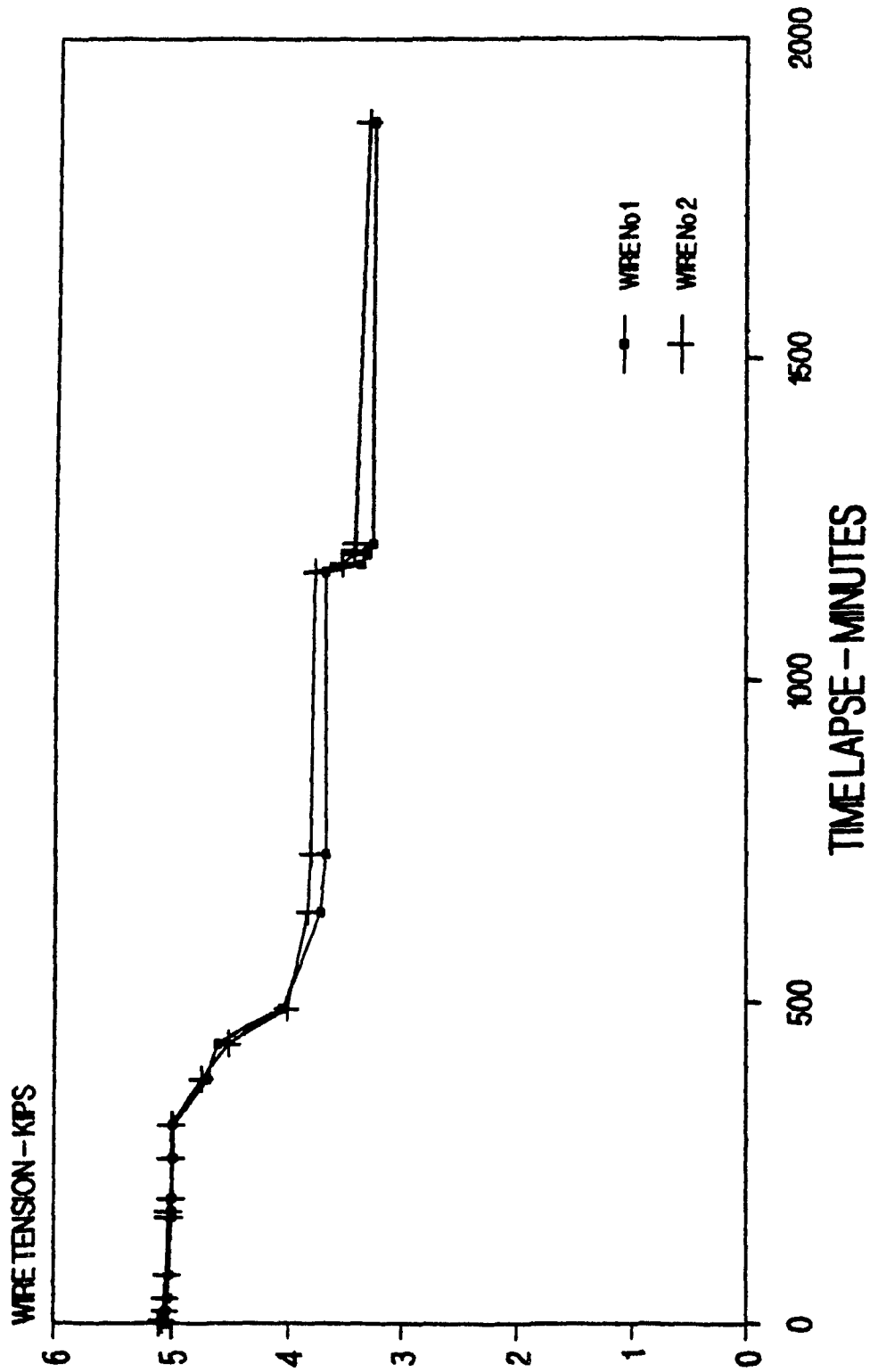
Figure 3.8 Relaxation of Wires 1 and 2 Over Time
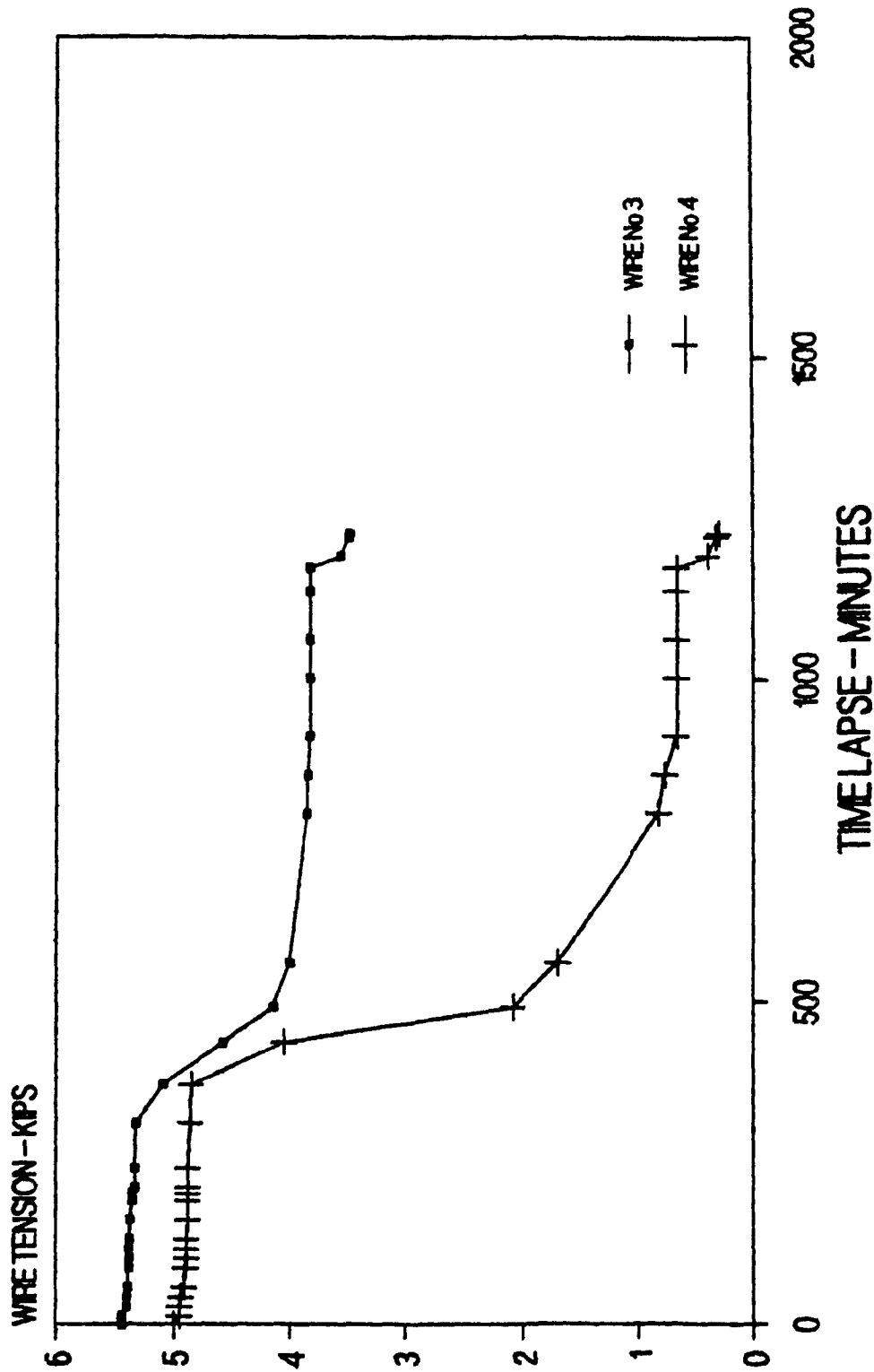
Figure 3.9 Relaxation of Wires 3 and 4 Over Time

ularly to the direction of principle strain, measure the Poisson's effect of strain $\mu\epsilon_b$. Therefore, the total strain output of each rosette is $(1+\mu)\epsilon_b$, where ϵ_b is the bending strain.

The two strain gauges of the rosette were connected inside a two wire transmitter box (or T.W.T.), in series to the left branch of a wheatstone bridge. It was configured to form a half bridge with two 350 ohm dummy resistors placed in the opposite branch. The two wire transmitter box provides the wheatstone bridge with voltage excitation of the bridge, and an amplification of 500 of the bridge voltage output with a conversion of the voltage into a current signal. The mathematical expression of voltage change for this system (22) is presented in Appendix A.

This current signal is transmitted directly to a receiver box along data cables across a constant differential voltage but with floating reference voltage. In this manner the measurements do not suffer voltage drops or noise pick up along the length of the cables.

The receiver box converts the current signal back into a voltage signal. Also, it permits the balancing of the wheatstone bridge and the setting of a variable gain.

The two wire transmitter and receiver system provides an amplitude resolution of the micro volts. The frequency response was flat to 2,000 Hz and the circuits were calibrated through an internal calibration system.

The receiver output from each measurement location was recorded onto a tape recorder and simultaneously played on a chart recorder. There were 52 strain gauge circuits and data was taken in stages with 3 tape recorders being used in parallel. As a reference in time, the three tape recorders recorded in parallel with a common signal to each.

The three tape recorders were FM type recorders made by Kyowa. One was a 14 channel RT-600B, while the other two were 6 channel RTP-501A's. Their basic characteristics were a tape speed of 3.75 in/s (95.2 mm/s), a signal to noise ratio of 46 decibels and a frequency response which was flat up to 2,500 Hz.

The chart recorder was a Datagraph model HR2000 made by Bell and Howell. It is a light sensitive chart recorder with a flat frequency response up to 5,000 Hz.

3.12 THE 1984 AND 1986 TEST PROCEDURE

The measurements taken in 1984 were undertaken in three stages which are shown in Table 3.3. The first stage was set up to

evaluate the rail-tie and tie-girder pad combinations at each
end of the bridge. These are as follows:

EVA and SA-47 for ties numbered 1 to 4

SBR-60A and AASHTO for ties numbered 19 to 22

The second set up was to evaluate the following combination of
rail-tie and tie-girder pads:

SBR-60A and SA-47 for ties numbered 5 to 11

EVA and AASHTO for ties numbered 12 to 18

The third set up was to evaluate the following combination of
rail-tie and tie-girder pads:

EVA and SA-47 for ties numbered 1 to 4

SBR-60A and SA-47 for ties numbered 5 to 11

EVA and AASHTO for ties numbered 12 to 18

SBR-60A and AASHTO for ties numbered 19 to 22

The data obtained in 1986 was undertaken in one set up and
consisted mainly of measuring strains at the rail seat bottom
of tie location as this is the location of maximum strains.
In this set up the 5 mm EVA pads were replaced by 6.5 mm
Hytrel pads and the ties over the abutments (ties 1 and 22)
were replaced. In addition, 50 concrete track ties were
installed on each approach of the bridge, replacing timber
ties. The set up is also shown in Table 3.3.

CONCRETE BRIDGE TIE TESTS – STRAIN GAUGE SETUP FOR 1984

TIE #	1	3	7	8	9	14	15	16	20	22	TRAINS
SET UP NO. 1	GB/GT RB/RT CB/CT	GB/GT RB/BT CB/CT							RB/RT CB/CT	RB/RT CB/CT	12
SET UP NO. 2			CB/CT	GB/GT RB/RT CB/CT W1/W2	CB/CT	CB/CT	GB/GT RB/RT CB/CT	CB/CT		RB/RT	7
SET UP NO. 3	RB/RT CB		CB	RB/RT CB	CB	CB	RB/RT CB	CB	CB	GT RB/RT CB/CT	16

CONCRETE BRIDGE TIE TESTS – STRAIN GAUGE SETUP FOR 1986

	3	7	8	9	14	15	16	20	22	TRAINS
SET UP NO. 1	RB				RB	RB/RT RC	RB	RB	RB/RT	12

TABLE 3.3 Concrete Bridge Tie Tests – Strain Gauge Setup for 1984 and 1986

CHAPTER 4

ANALYSIS OF THE C.N. FIELD TEST DATA

4.1 GENERAL

The strains measured at the rail seat top and rail seat bottom locations were obtained from the chartgraph printout of the results. These strains were statistically analyzed and the percent occurrence of strains and the percent exceeding of strains have been summarized and plotted with the resulting graphs included in Appendix B. Some of the graphs however, have been included in this chapter for completeness.

4.2 1984 RESULTS FOR POSITIVE BENDING

From a review of summary graphs 3RB, 8RB, 15RB, and 20RB for positive bending in 1984, Figure 4.1, 4.2, 4.3 and 4.4 respectively, it can be seen that in each graph two distinct regions are present. The left hand portion of each graph clearly indicates the strains due to quasi static loading with little or no impact. However, the right hand portion of each graph is clearly the combination of both. Each graph contains two distinct peaks at the left portion of the graph. These peaks are due to the static strains caused by empty cars and loaded cars with normal wheels. Thereafter, the graphs drop off to the right and indicate the small percentage of wheels which cause the high impacts.

It is evident from the summary graph of tie 20RB that the soft rail-tie pad and soft tie-girder pad combination gave the

%OCCURRENCE vs STRAIN
SUMMARY 3RB – POSITIVE BENDING 1984

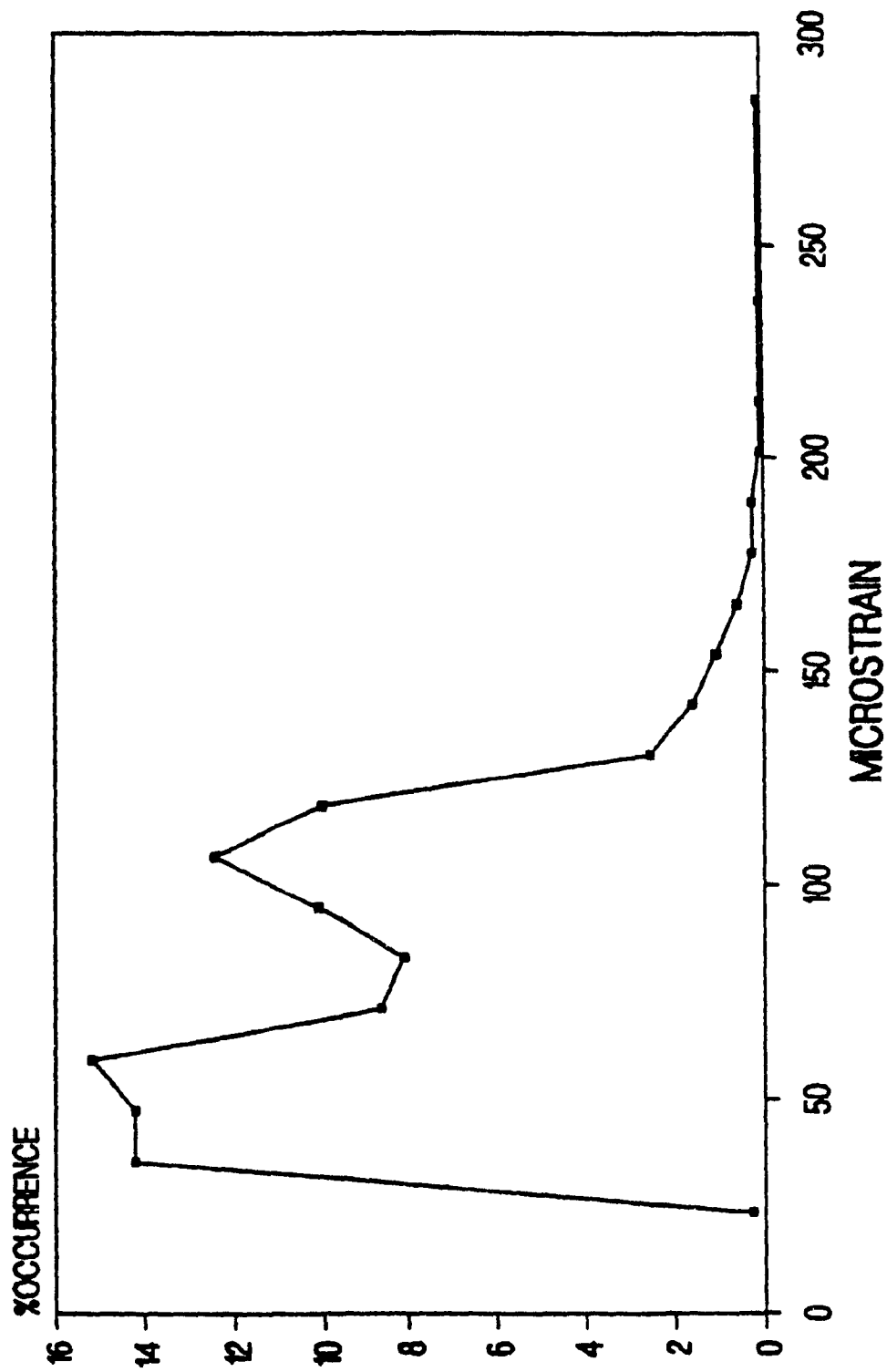Figure 4.1 Summary Graph 3RB for 1984

%OCCURRENCE vs STRAIN
SUMMARY 8RB – POSITIVE BENDING 1984

Figure 4.2 Summary Graph 8RB for 1984

%OCCURRENCE vs STRAIN
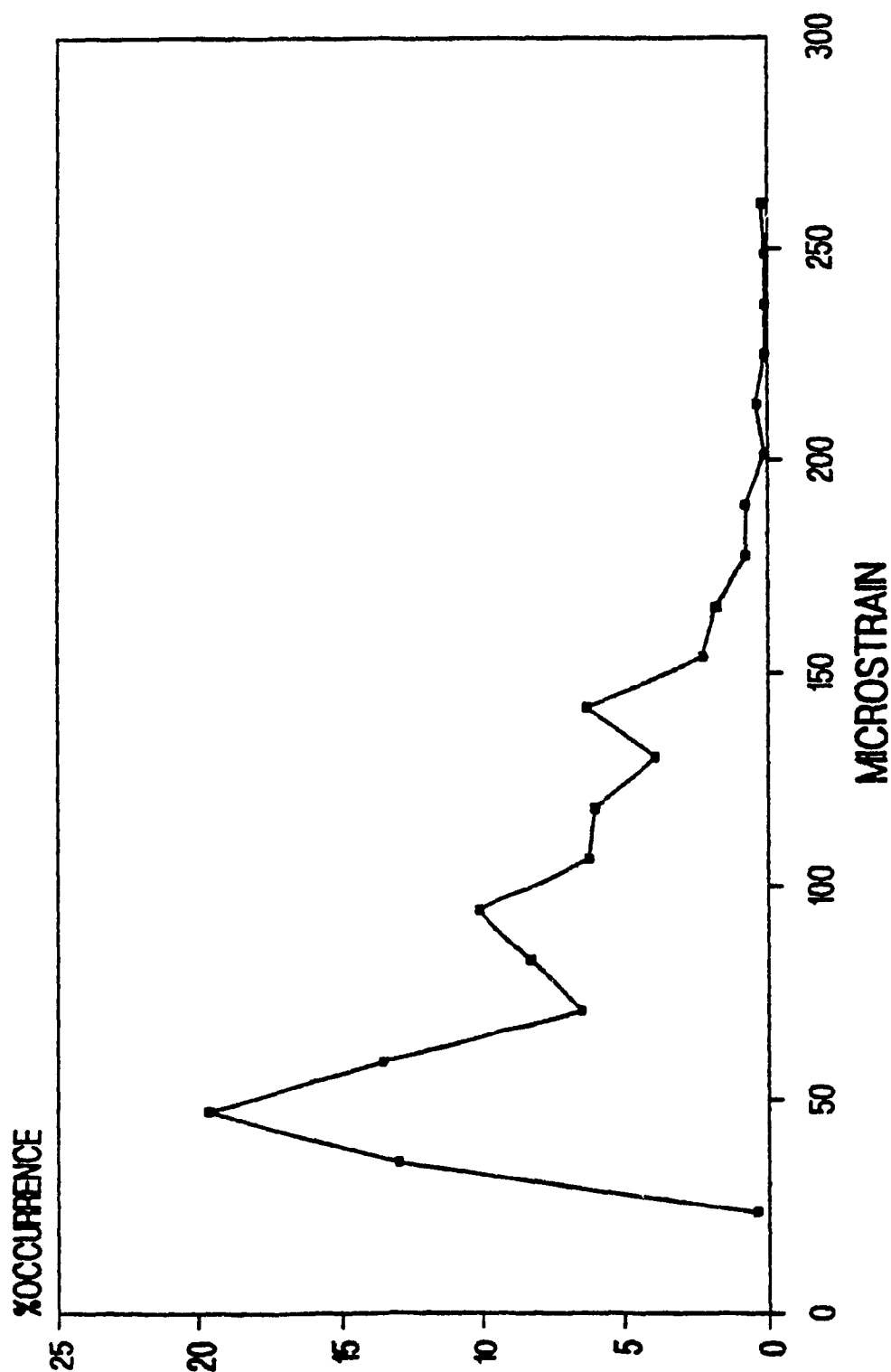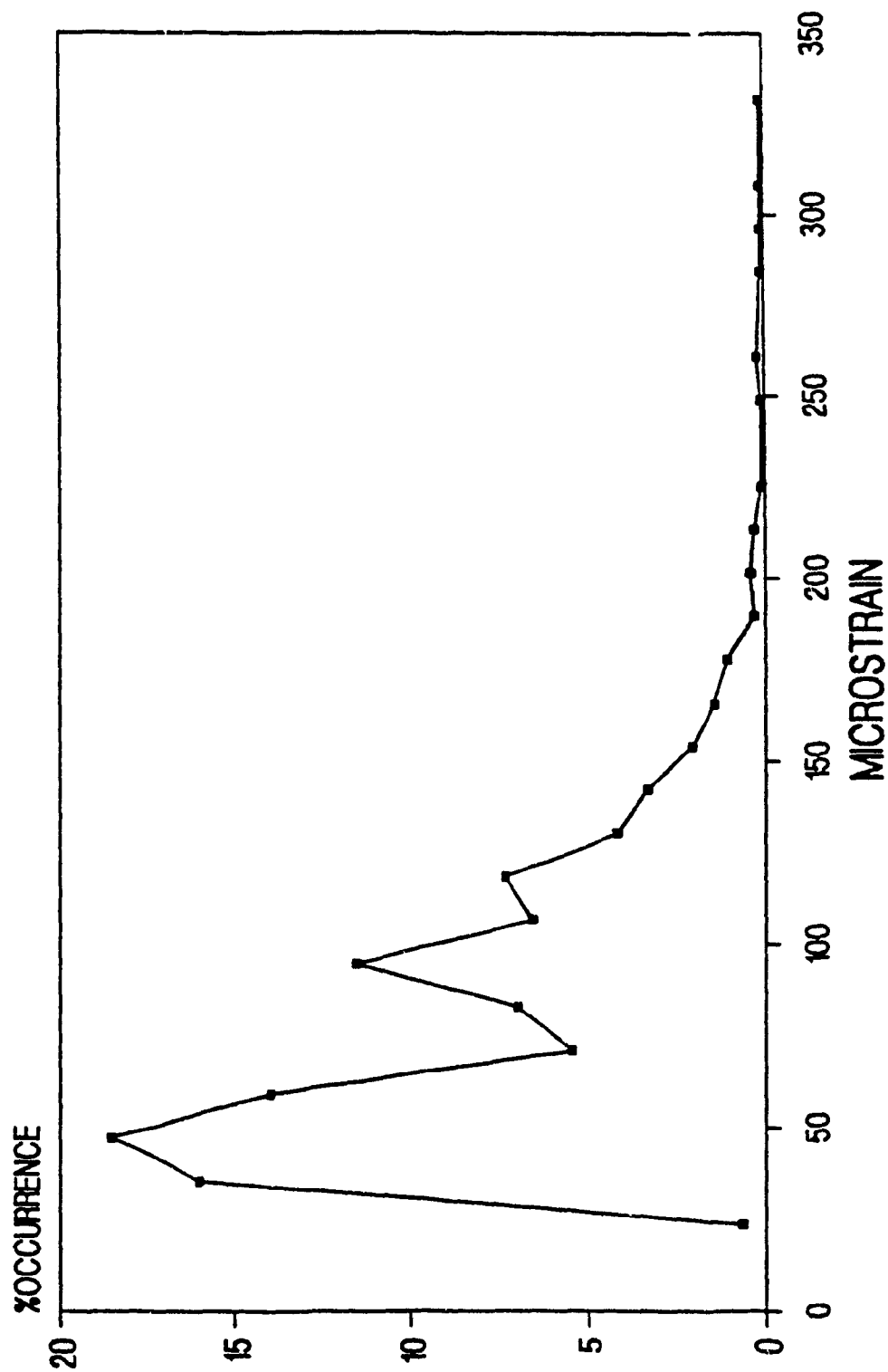## SUMMARY 15RB – POSITIVE BENDING 1984

%OCCURRENCE

MICROSTRAIN

Figure 4.3 Summary Graph 15RB for 1984

42

%OCCURRENCE vs STRAIN

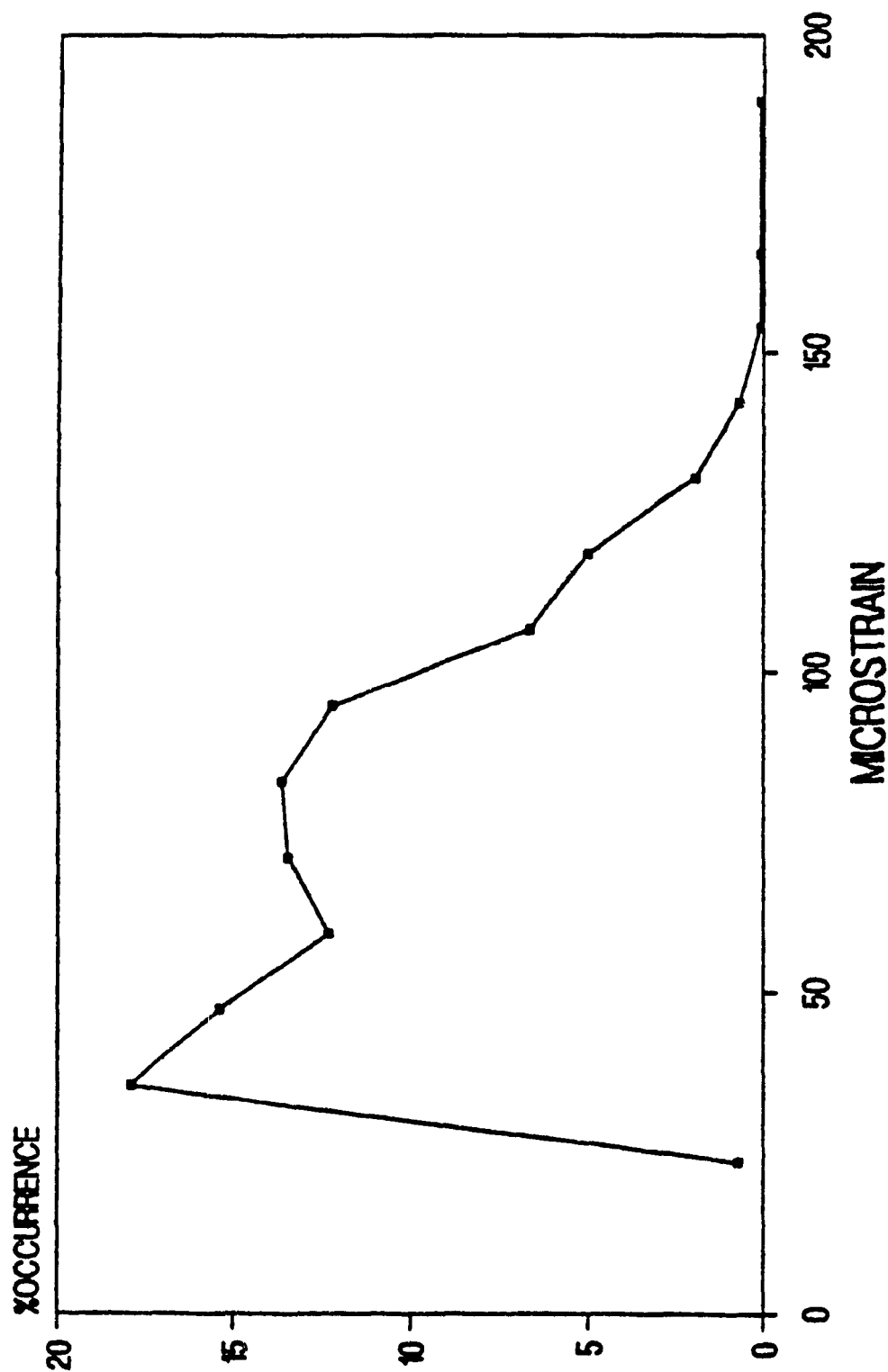SUMMARY 20RB – POSITIVE BENDING 1984

%OCCURRENCE

MICROSTRAIN

Figure 4.4   Summary Graph 20RB for 1984

43

lowest total strains. This indicates that the softer rail-tie pad attenuates more impact than a hard pad.

The largest total strains occurred when a hard rail-tie pad and hard tie-girder pad combination were used. This is indicated in summary graph 3RB, Figure 4.1. It should be noted that there were 50 percent higher strain values recorded for this combination as compared to the soft rail-tie pad and soft tie-girder pad combination.

In comparing the summary graphs 3RB, Figure 4.1 with 15RB, Figure 4.3, hard rail-tie pad with hard tie-girder pad and hard rail-tie pad with soft tie-girder pad respectively, it can be seen that there is no difference in the largest strains recorded. This therefore indicates that the strain attenuation in the system is influenced the greatest by the rail-tie pad and very little by the tie-girder pad. This is consistent with recent laboratory findings (9, 10), which concluded that the tie-girder pad had an insignificant effect on the dynamic strains experienced by the tie.

By comparing summary graphs 15RB, Figure 4.3 and 20RB, Figure 4.4, the same conclusion as above can be reached as both these ties had the soft tie-girder pads.

From summary graphs 8RB, Figure 4.2 and 20RB, Figure 4.4 it

can be seen that these ties had the lowest recorded total strains, which is directly attributed to the use of the soft rail-tie pad.

It is worth noting that the use of the soft rail-tie pads causes a small redistribution of the static wheel load to occur. This can be seen in the shifting of the peaks to the left on summary graphs 8RB Figure 4.2 and 20RB, Figure 4.4. This redistribution is attributed to the combination of rail-tie and tie-girder pads used, but is greatest when a soft rail-tie and soft tie-girder pad combination is used.

The dynamically loaded area of the graphs is cont. olled mainly by the type of rail-tie pad used.

4.3 THE 1984 RESULTS FOR NEGATIVE BENDING

The s rains from the 1984 negative bending results have been plotted in Figure 4.5, 4.6 and 4.7. The results indicate that the maximum negative bending strains vary between 103×10^{-6} to 129.9×10^{-6}. These strains are caused by impact and are purely dynamic strains.

In comparing Figures 4.5, 4.6 and 4.7 it can been seen that summary graph 15RT, Figure 4.6, which had the hard rail-tie pad and soft tie-girder pad experienced the lowest negative bending strains and that summary graphs 8RT, Figure 4.5 and

45

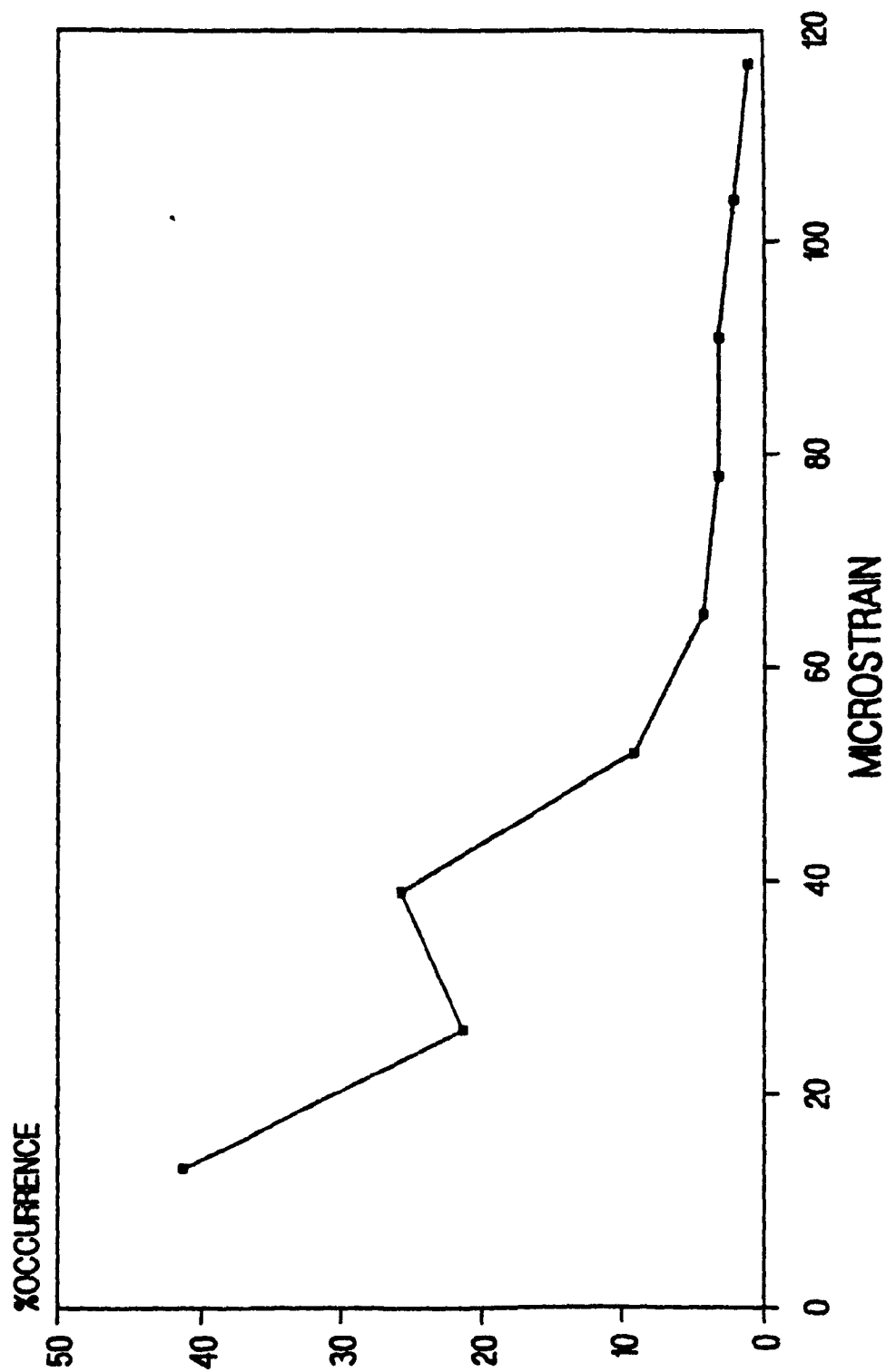# %OCCURRENCE vs STRAIN
SUMMARY 8RT – REVERSE BENDING 1984

Figure 4.5 Summary Graph 8RT for 1984

%OCCURRENCE vs STRAIN
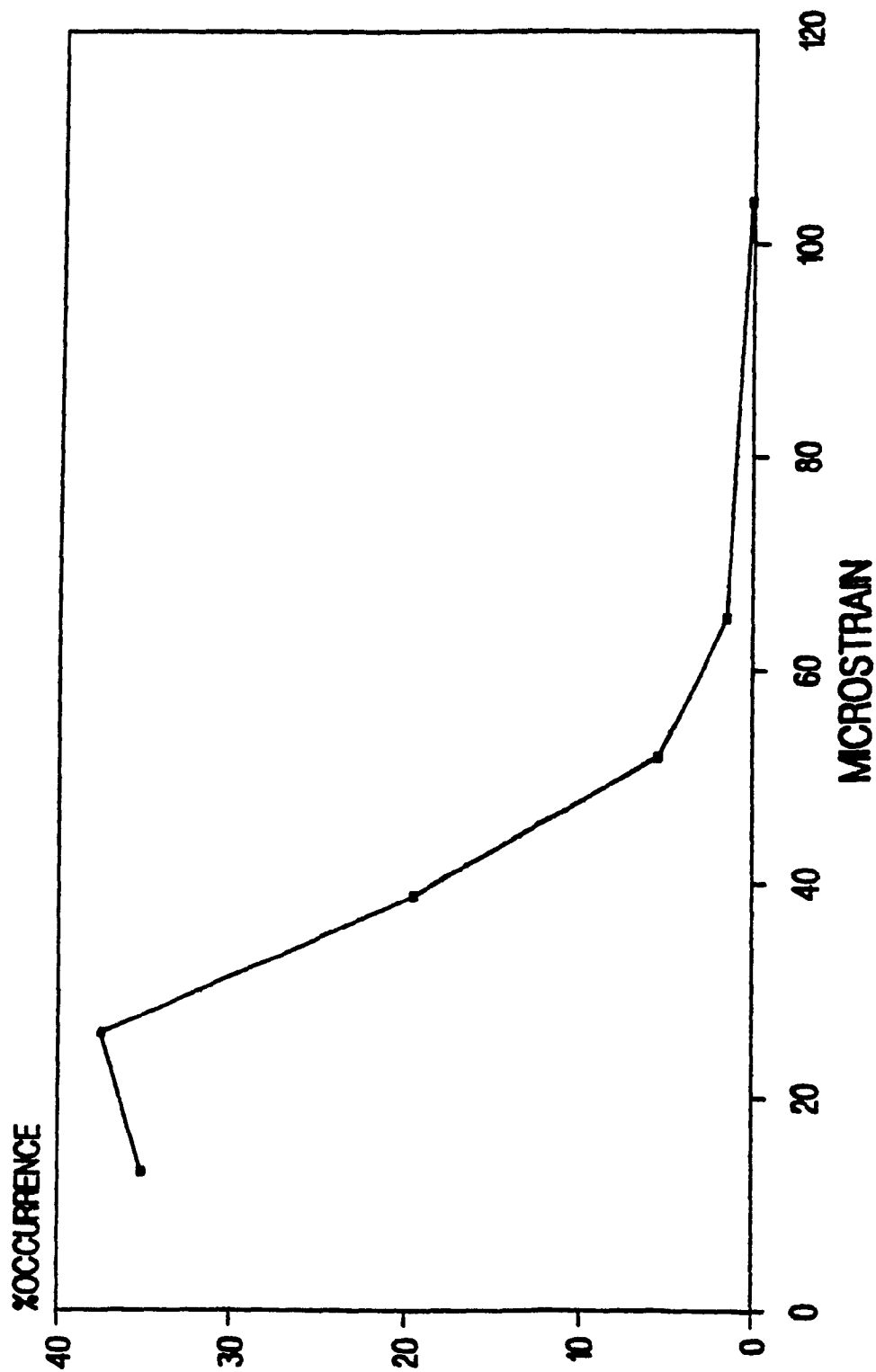## SUMMARY 15RT – REVERSE BENDING 1984

%OCCURRENCE

MICROSTRAIN

Figure 4.6 Summary Graph 15RT for 1984

%OCCURRENCE vs STRAIN
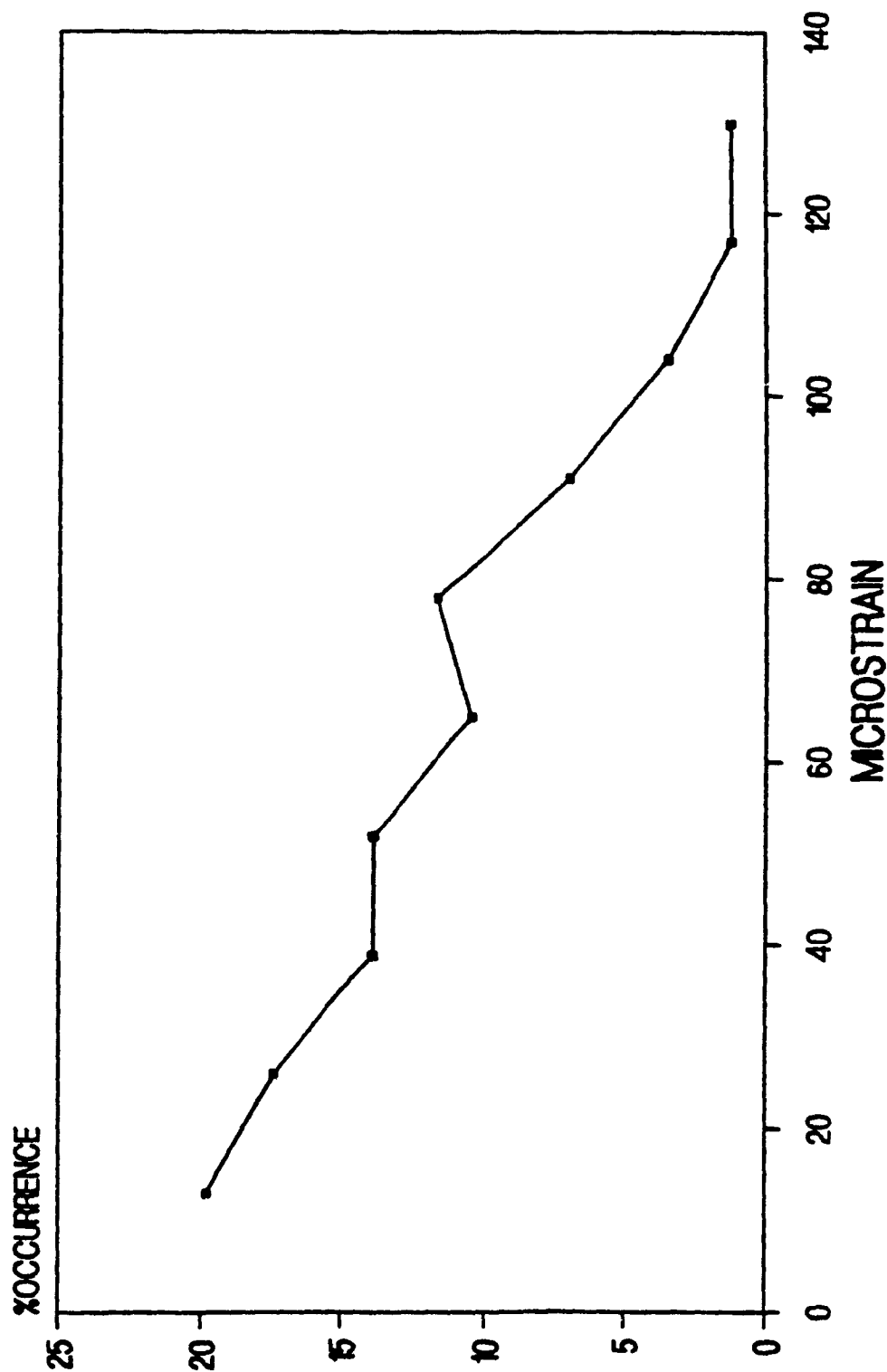SUMMARY 20RT – REVERSE BENDING 1984

Figure 4.7   Summary Graph 20RT for 1984

2ORT, Figure 4.7, which had soft rail tie-pads experienced the largest strains.

The observation here is that soft rail-tie pads apparently provide for greater negative bending strains. However, the statistics may not be meaningful in this regard, as the graph that could have clarified this could not be drawn because of a malfunctioning gauge which was subsequently disconnected. Therefore, the data for the hard rail-tie pad and hard tie-girder pad is not available.

What can be said with certainty is that the maximum strain experienced in negative bending was 129.9×10^{-6}. The C.N. Rail tie was designed for 210 psi (1.5 MPa) compressive tie stress, which is equivalent to a strain of 47.5×10^{-6}. Therefore, the C.N. Rail tie is under designed by 129.9×10^{-6} - $47.5 \times 10^{-6} = 82.4 \times 10^{-6}$.

4.4 1986 RESULTS FOR POSITIVE BENDING

The results of the 1986 positive bending strains have been plotted in Figure 4.8 and 4.9. Again, as in the 1984 positive bending results, there are two distinct regions to the graphs. The left hand portion of each graph indicates the strains due to quasi static loading with little or no impact present. The right hand portion of the graphs indicate a combination of both quasi static and dynamic strain. In addition each graph

49
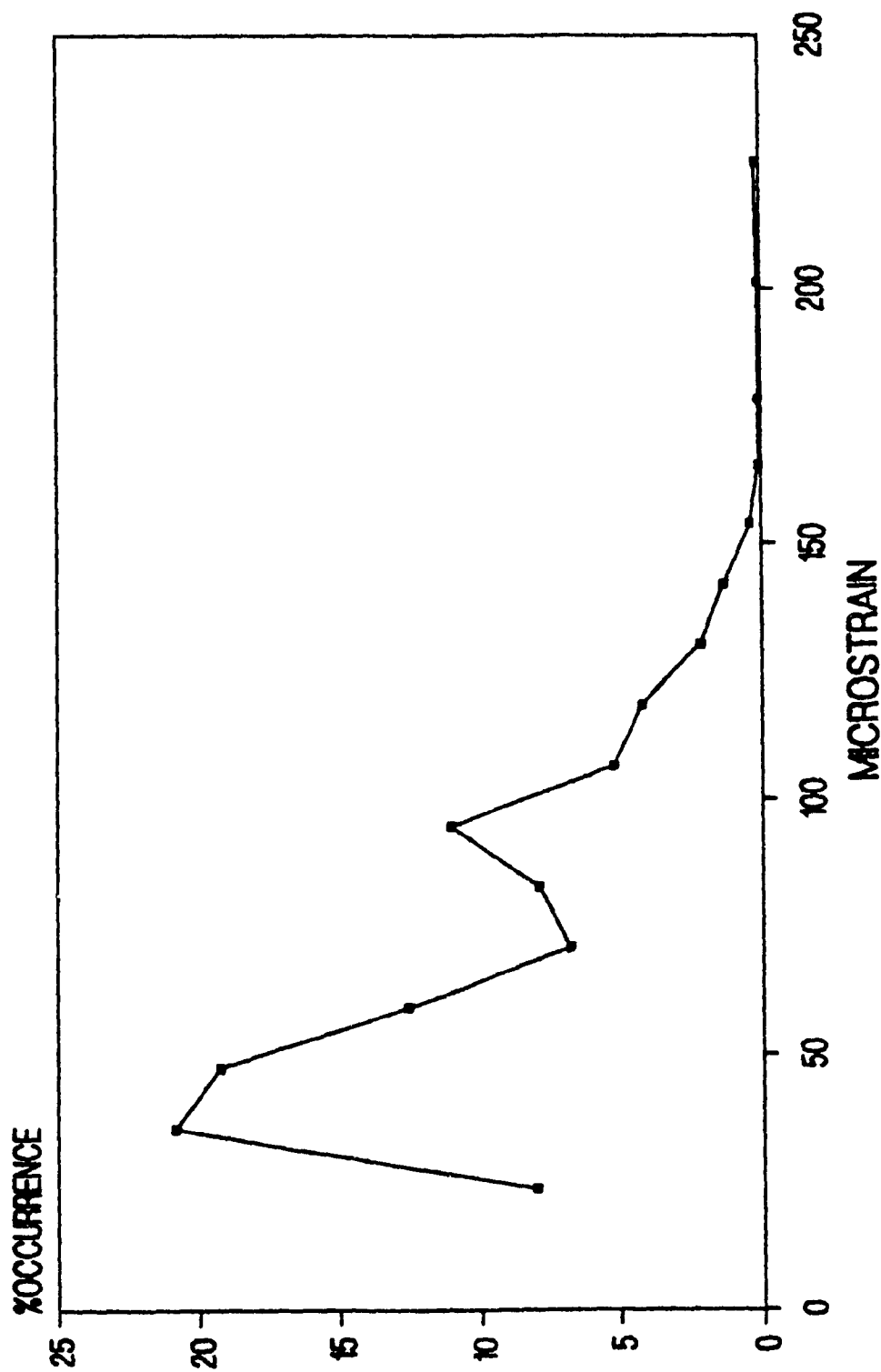
Figure 4.8 Summary Graph 3RB for 1986

%OCCURRENCE vs STRAIN
SUMMARY 15RB – POSITIVE BENDING 1986
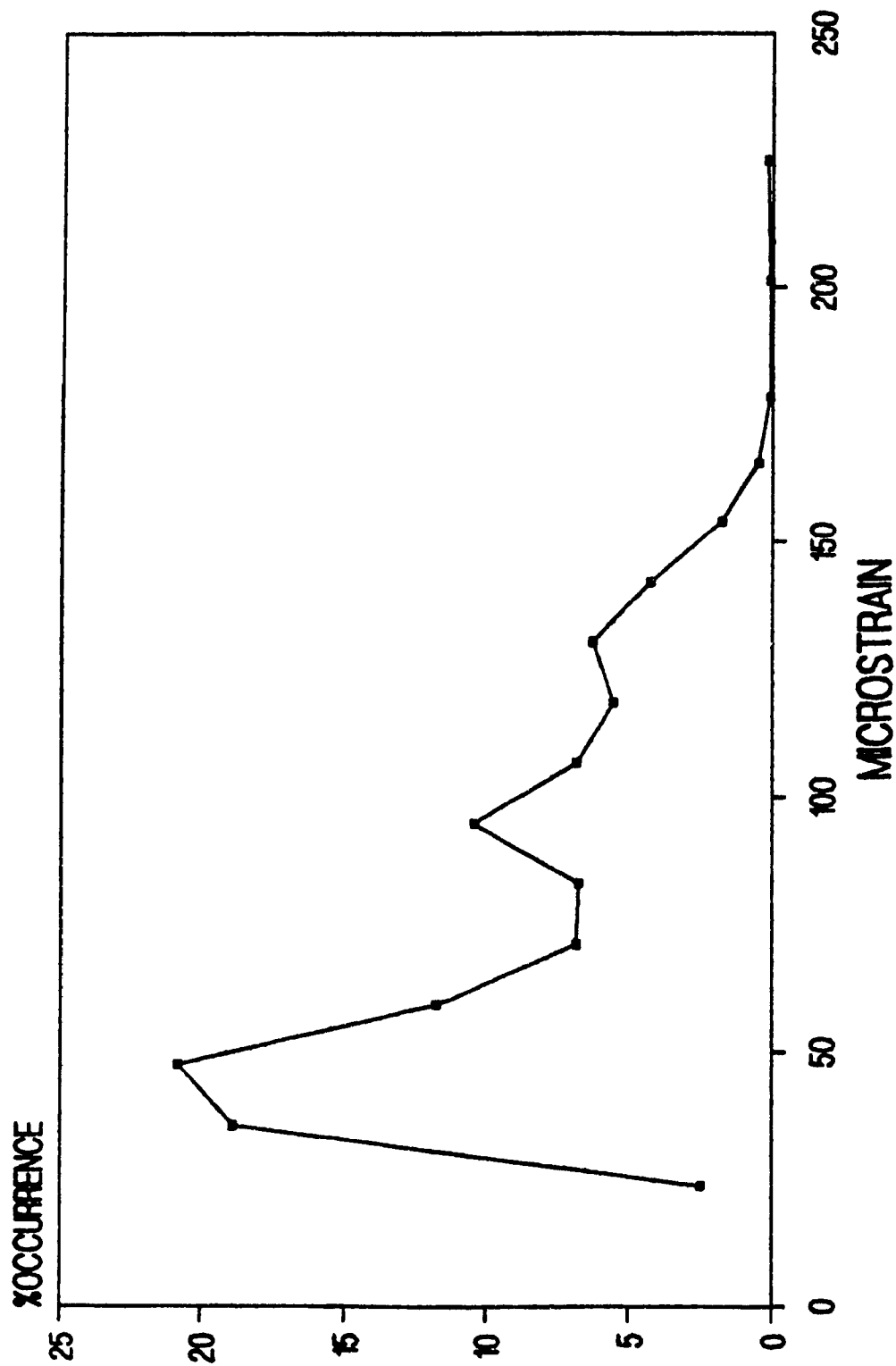
%OCCURRENCE

MICROSTRAIN

Figure 4.9 Summary Graph 15RB for 1986

contains two distinct peaks. These peaks are due to the static strains caused by the empty rail vehicles (cars) and loaded railway vehicles with normal wheels. The graphs then drop off to the right and indicate the small percentage of defective wheels that cause the high impacts.

A comparison of the 1984 graphs for positive bending indicates that the attenuation capability of the Hytrel rail-tie pads is greater than that of the SBR rail-tie pads. This indicates that the 6.5 mm studded Hytrel pad performs approximately 20 percent better in attenuating the high impacts than the SBR pads as the highest strain recorded is 225×10^{-6} in./in.

4.5 COMPARISON OF 1984 AND 1986 RESULTS FOR TIES 1 AND 22

The data for 1984 and 1986 for ties 1 and 22 (end ties) has been plotted and is shown in Figures 4.10, 4.11, 4.12 and 4.13.

A comparison of the graphs for 22RB, Figures 4.12 and 4.13 in positive bending indicates an 18 percent reduction in the strains from 1984 to 1986. This reduction of strains is due to the combination of the installation of 50 concrete approach ties and the installation of the Hytrel pads.

It should be noted that there was no appreciable reduction in the strains in tie number 1. The reason for this is unknown.

52

Figure 4.10 Summary Graph 1RB for 1984

Figure 4.11 Summary Graph 1RB for 1986

%OCCURRENCE vs STRAIN
SUMMARY 22RB – POSITIVE BENDING 1984
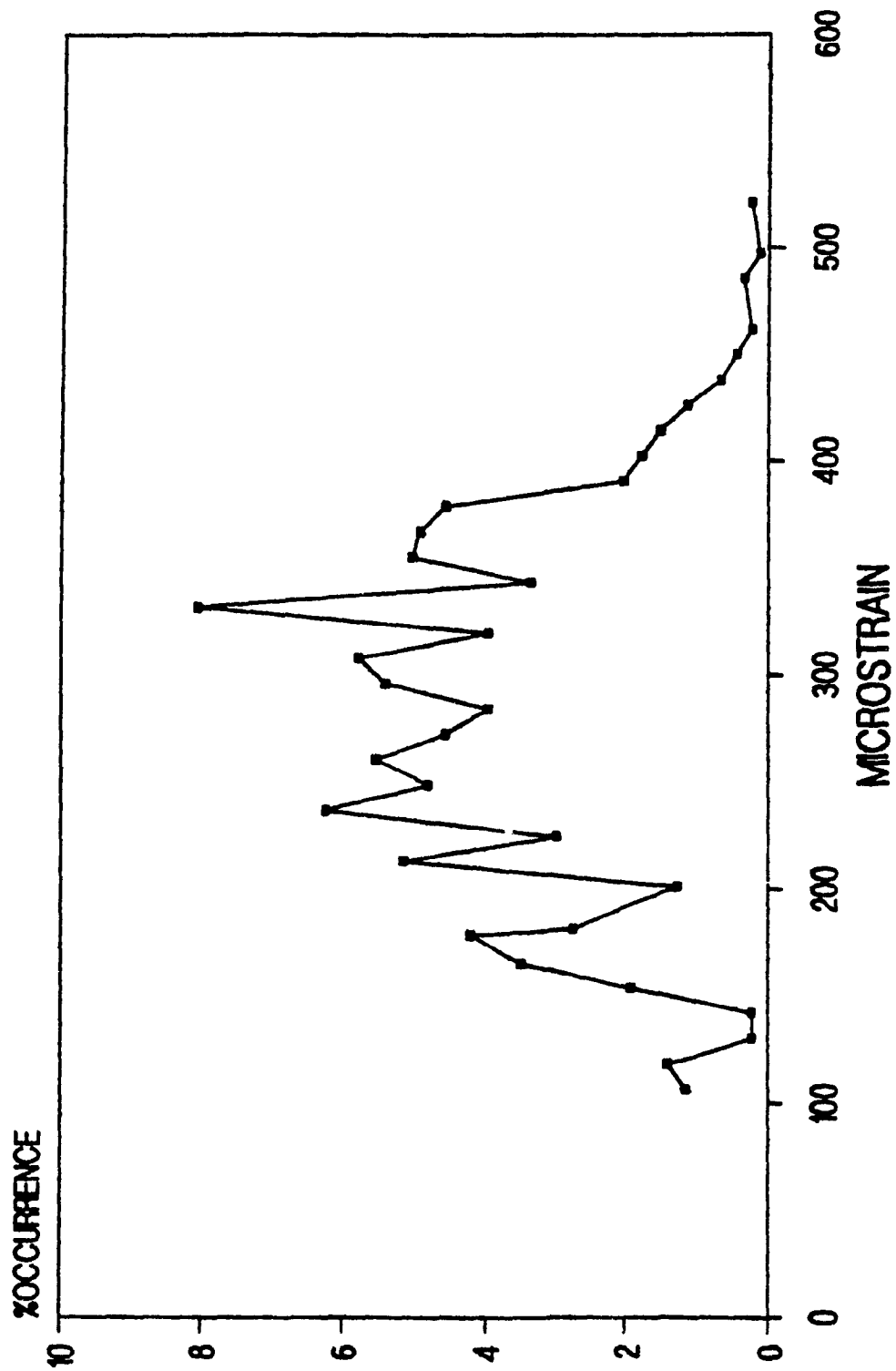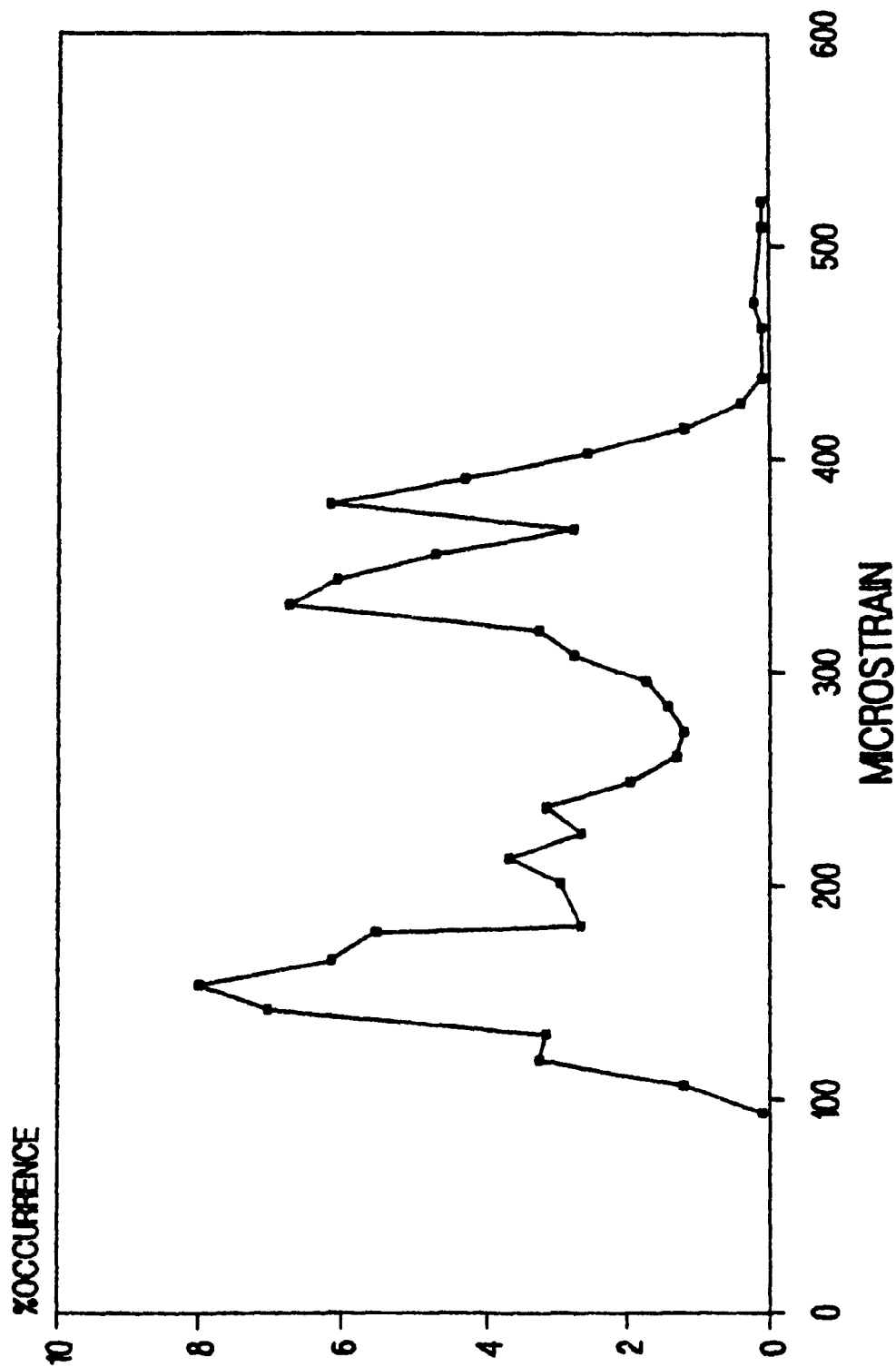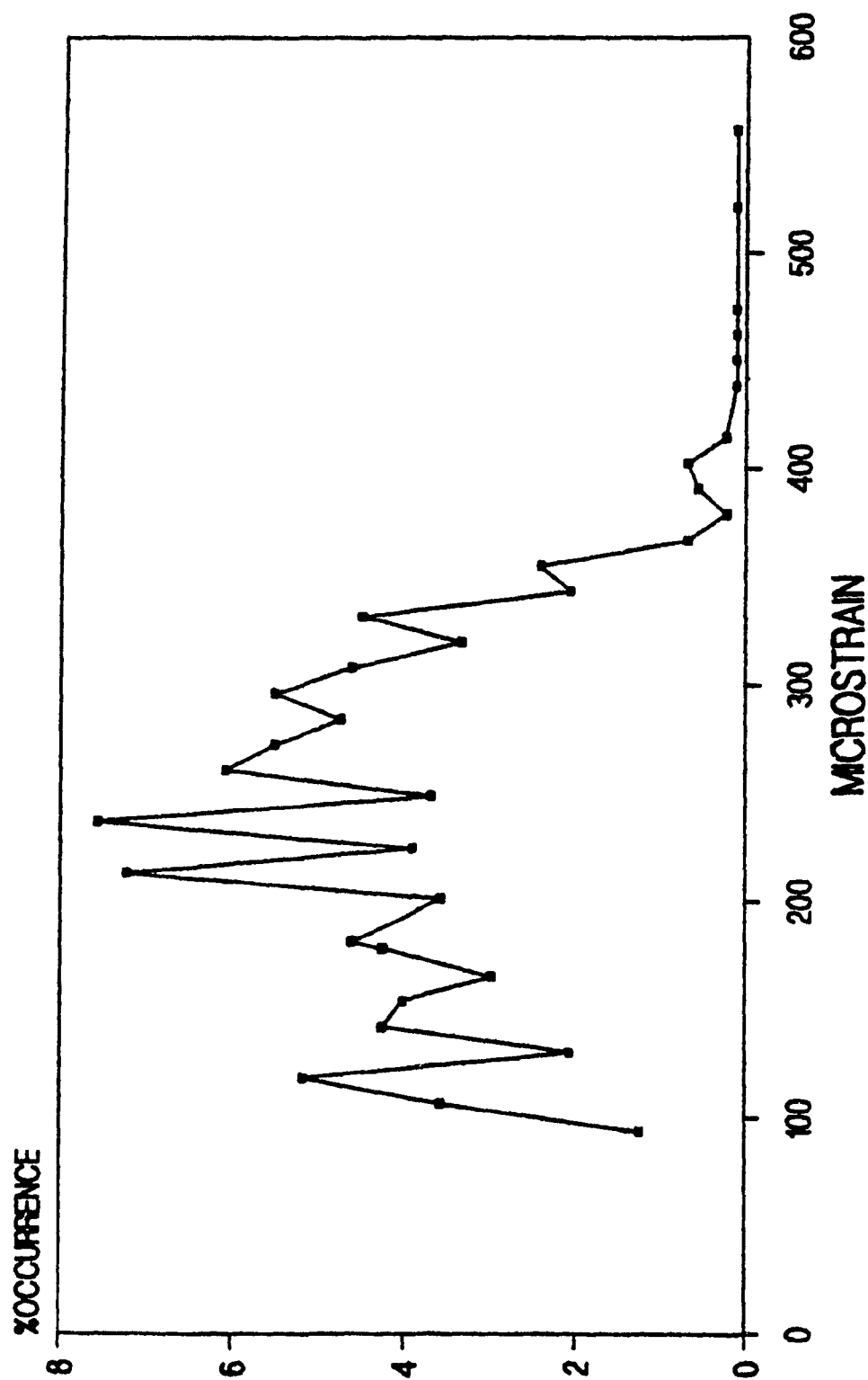
Figure 4.12   Summary Graph 22RB for 1984

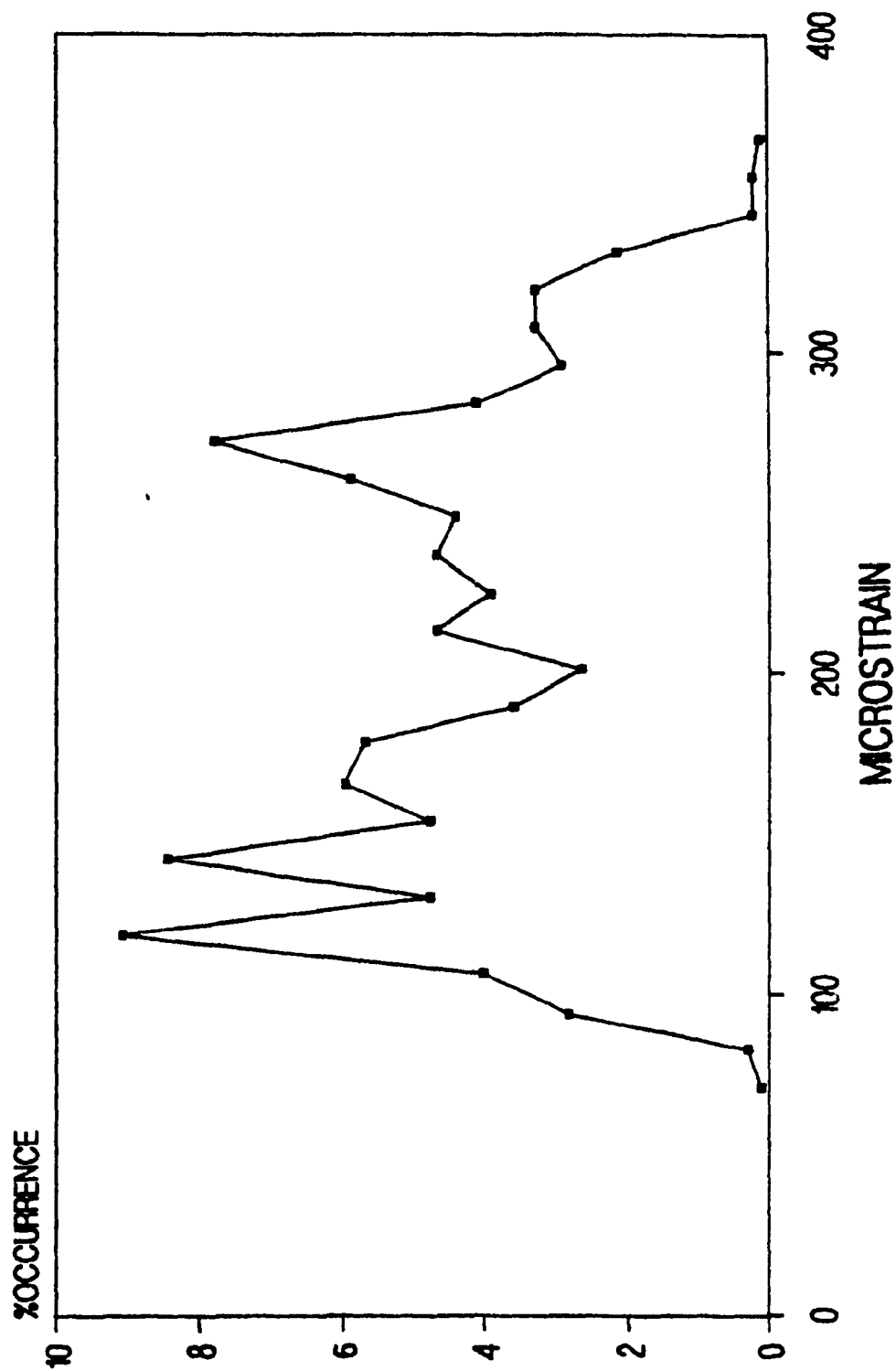## %OCCURRENCE vs STRAIN
SUMMARY 22RB – POSITIVE BENDING 1986

Figure 4.13   Summary Graph 22RB for 1986

4.6 EVALUATION OF IMPACT FACTORS

In the evaluation of the data, it is apparent that the impacts being experienced were generated by both lightly loaded as well as heavily loaded cars. Figures 4.14 and 4.15 indicate the relationship between speed and average strains, comprised of static and dynamic strain. From these two graphs come some important observations.

For lightly loaded vehicles:

1) The lightly loaded vehicles exhibit large dynamic strains in relation to the static strains. This in turn means that they display large impact factors.

2) The total strains increase with increasing speed, and then decrease after about 52 mph (85.3 km/hr).

3) The dynamic strains start at approximately 26 mph (42.6 km/hr) and increase up to approximately 52 mph (85.3 km/hr), where after they decrease.

For heavily loaded vehicles:

1) The heavily loaded vehicles exhibit larger overall strains than the lightly loaded vehicles, but smaller dynamic strains in relation to the static strains. This means that the impact factor under heavily loaded cars is smaller than lightly loaded cars.

2) The total strains generally increase up to approximately 52 mph (85.3 km/hr) whereafter they decrease.

3) The dynamic strains start at approximately 32 mph (52.5 km/hr) reaching a maximum at 52 mph (85.3 km/hr)

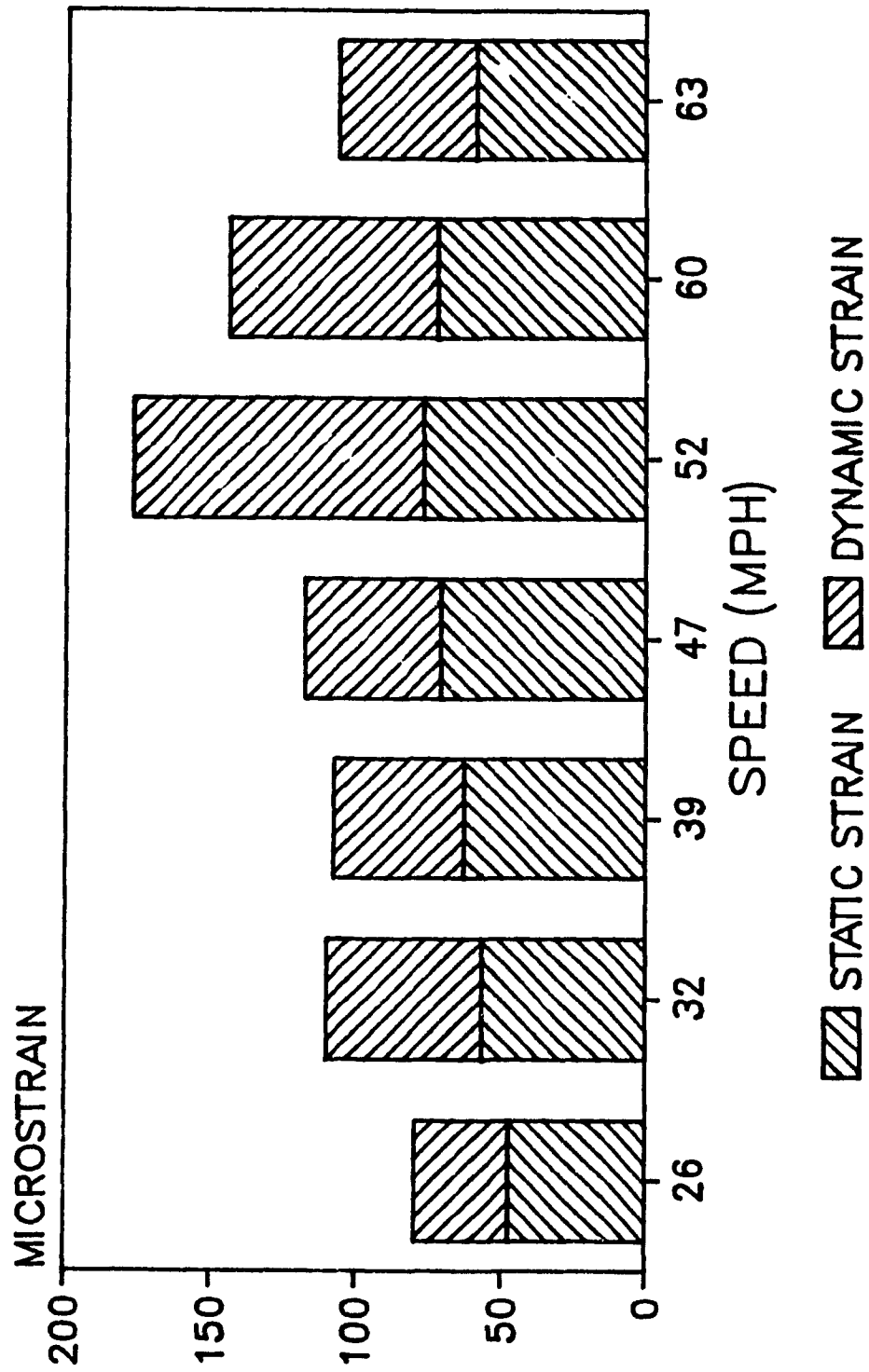57

AVERAGE STRAINS vs SPEED
LIGHT WHEEL LOADS

Figure 4.14 Average Strain Versus Speed for Light Wheel Loads
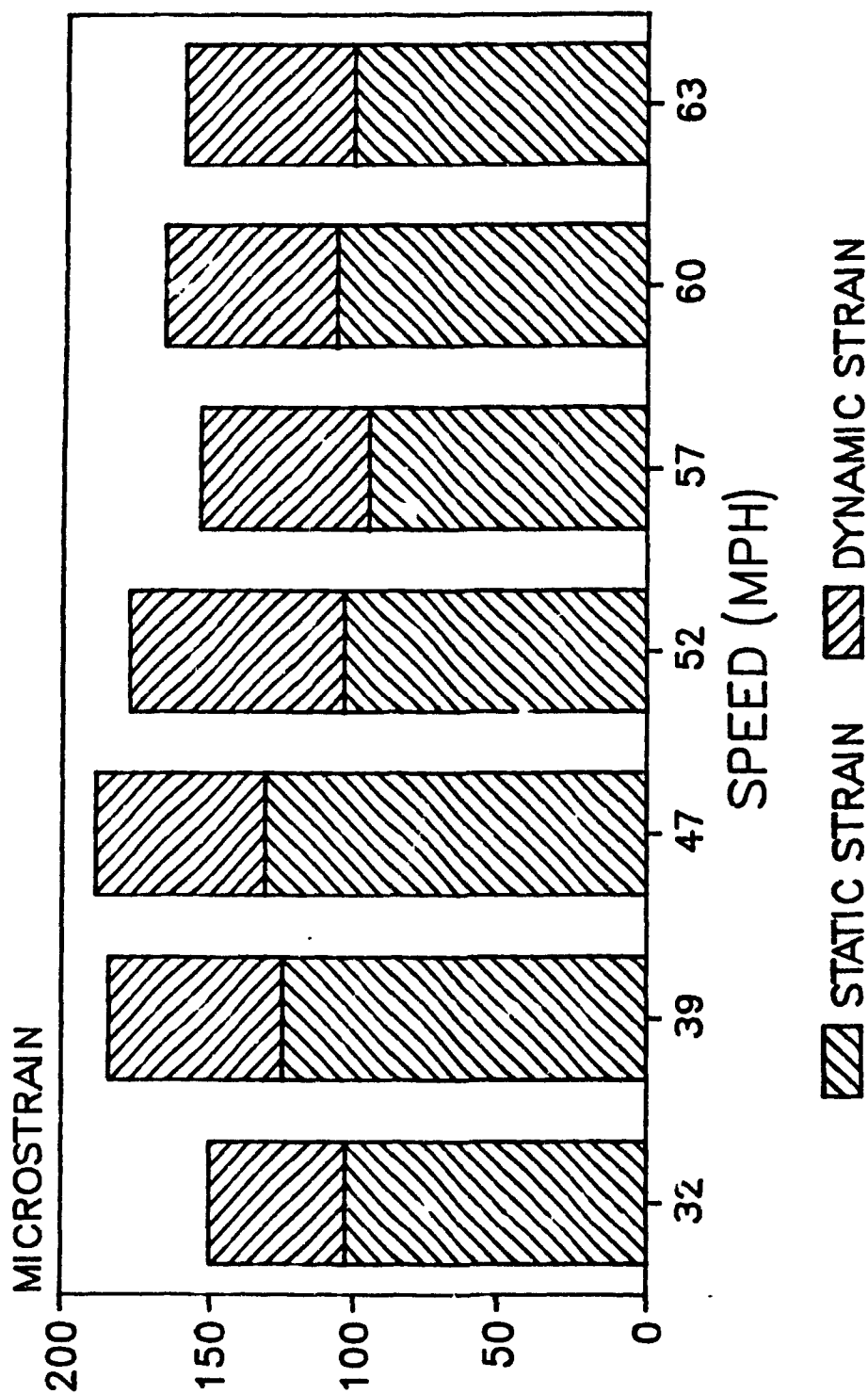
Figure 4.15   Average Strain Versus Speed for Heavy Wheel Loads

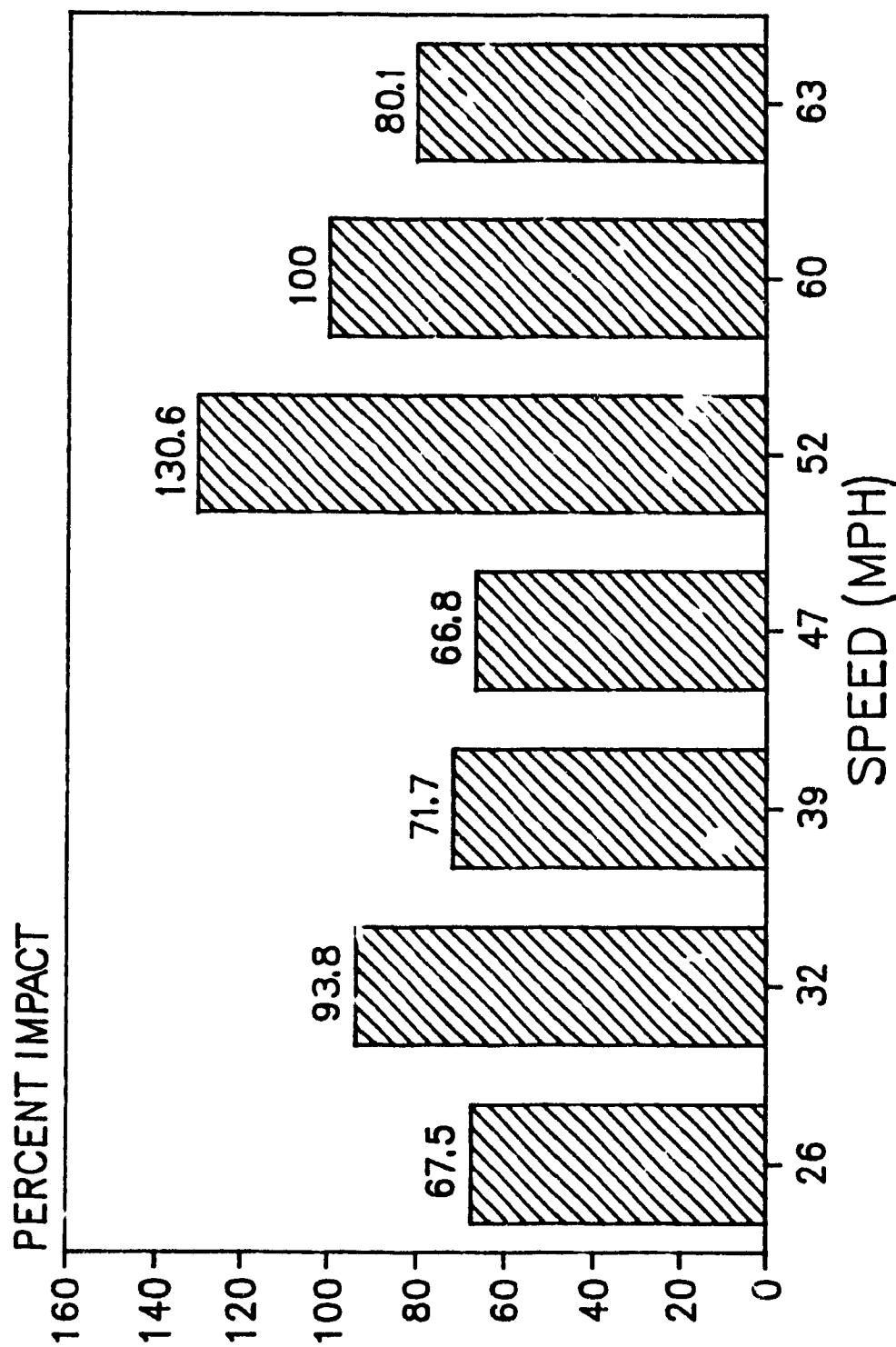# AVE IMPACT FACTORS FOR VARIOUS SPEEDS
LIGHT WHEEL LOADS

Figure 4.16 Average Impact Factors Versus Speed for Light Wheel Loads

AVE. IMPACT FACTORS FOR VARIOUS SPEEDS
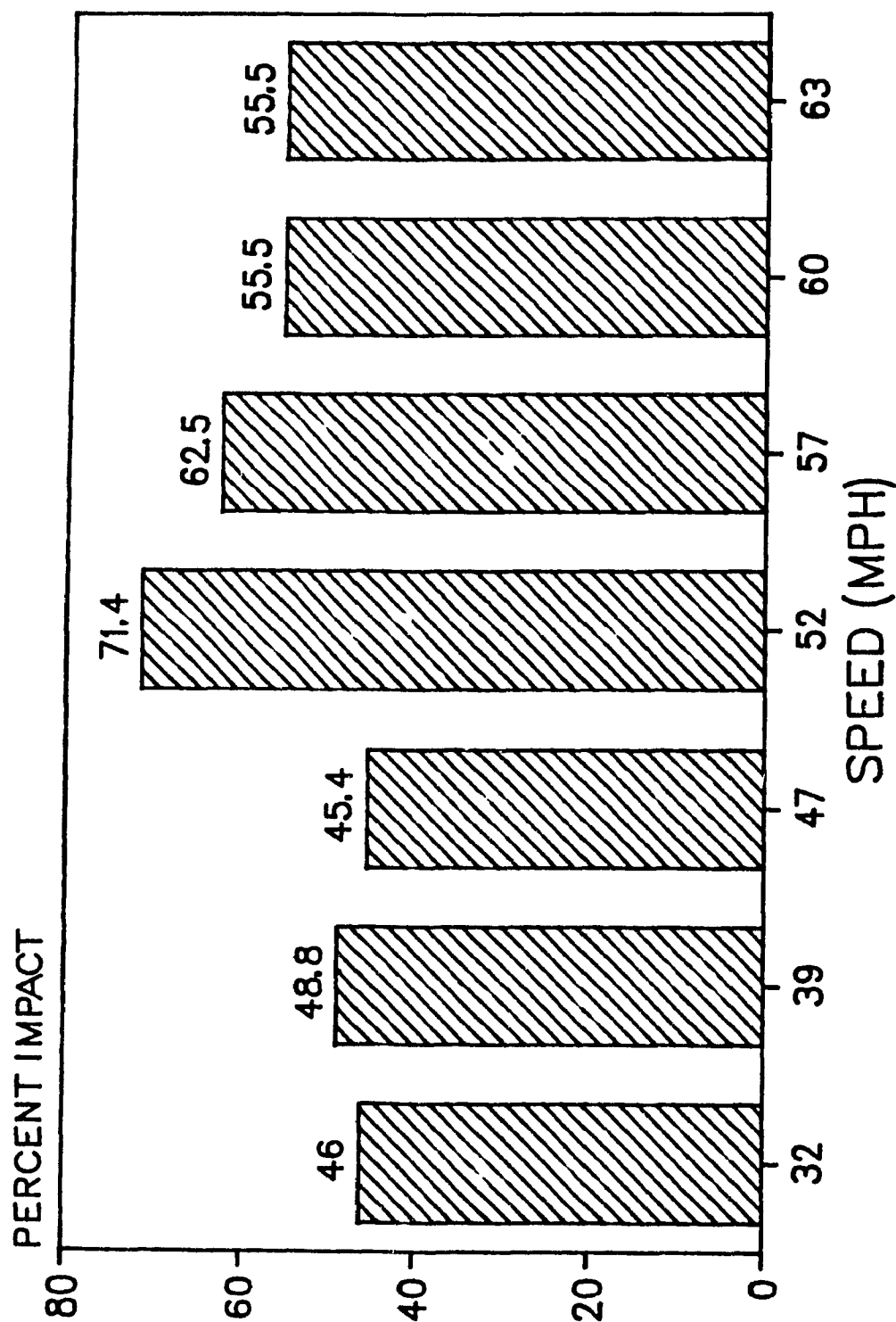## HEAVY WHEEL LOADS

PERCENT IMPACT

Figure 4.17 Average Impact Factors Versus Speed for Heavy Wheel Loads

whereafter they decrease.

Figures 4.16 and 4.17 indicate the average impact factors for light wheel loads and heavy wheel loads. What is immediately evident on comparison of these graphs is that the lighter wheel loads exhibit greater impact factors than heavier wheel loads. This would indicate that larger impacts are more a function of both the unsprung mass of the railway vehicles and of the vehicle speed, rather than that of the total vehicle mass.

A comparison of the graphs in Figures 4.14 and 4.15 indicate the dynamic strains for light wheel loads and heavy wheel loads are comparable in magnitude. This is because the unsprung mass of the heavily loaded vehicles is the same as that of the lightly loaded vehicle and would, therefore, generate the same dynamic strains for similar wheel defects or rail irregularities at comparable velocities.

4.7 INCREASED STRENGTH OF CONCRETE UNDER IMPACT

It can be seen from the impact factors measured during the 1984 field test, that the majority are greater than the design factor of 60 percent. However, the concrete ties have not cracked in positive bending due to the large impacts. There are two main reasons for this phenomena which are outlined below:

1) The rate at which the ties are loaded is so fast, approximately 3 milliseconds, and because of the ties' mass and inertia, the tie does not have a chance to respond completely as the force which caused the impact has disappeared.

The energy of the impact is, therefore, dissipated in a number of ways as follows:

a) through the rail (longitudinally)

b) by deflection of the pad

c) by deflection of the tie

d) by heat, and

e) by noise

Impact load application rates of 7 to 20 milliseconds are considered the most damaging as the load duration interval increases the ties response to the load.

2) Concrete is considered to be a stress-rate sensitive material. Recent work (2) concluded that, in general, concrete is stronger and more energy absorbing under impact than under static loading. Studies (18, 20) have shown that strain values observed at or near failure in dynamic tests for high rates of loading were significantly larger than corresponding values in the static tests. In addition, the resistance to impact (measured by the ability to absorb strain energy)

63

increased significantly with the rate of loading. It has also been noted that weaker strength concretes will show greater strength improvement than higher strength concretes.

4.8 A.R.E.A. SPECIFIED IMPACT FACTORS

The American Railway Engineering Association (A.R.E.A.) specifies the use of an assumed 200 percent impact factor (I) to account for the dynamic effect of wheel and rail irregularities. Due to premature structural failures of concrete ties (6), the bending strength specifications of the A.R.E.A. have steadily increased in response to these failures. The manual does not specifically address bridge ties and the assumed impact factor of 200 percent does not assist in the design of ties subjected to rebound effects.

4.9 FREQUENCY RESPONSE OF THE BRIDGE TIES

The flexural resonant frequency response of a prestressed concrete bridge tie is dependent on four physical parameters. These are:

1)   I, the moment of inertia of the tie

2)   L, the length of the tie

3)   W, the weight per unit length of the tie

4) A_n, the mode coefficient representing the mode shape and axle loading (or the mode coefficient for the nth mode.

The flexural resonant frequency expression commonly used (19) is given by:

$$F = \frac{A_n}{2\pi} \sqrt{\frac{g \, E \, I}{L^4 W}} \sqrt{A_n^2 + \frac{L^2 P}{EI}}$$

However, for all practical purposes, in the frequency response of the bridge ties:

$$\frac{L^2 P}{EI} \ll A_n^2$$

such that the frequency response of the tie can be approximated by:

$$F = \frac{A_n^2}{2\pi} \sqrt{\frac{g \, E \, I}{L^4 W}}$$

Table 4.18 illustrates the theoretical modes and the corresponding frequency response for the bridge ties.

From the 1984 test data, power spectra frequency analysis was performed (19) which indicated two predominant crests, the first at 88 Hz and the second at 468 Hz.

Frequency response of the bridge ties which have very close agreement with the first and third resonant modes. This indicates that these modes are present at these frequencies.

The power spectra analysis also indicated a sharp valley at 223 Hz. This point is termed a point of anti-resonance and indicates a nodal point, A nodal point is a point of no

RESONANT MODES	FREQUENCY	MODE SHAPES
1st Symmetric	86 Hz	
2nd Symmetric	240 Hz	
3rd Symmetric	472 Hz	
4th Symmetric	781 Hz	

Figure 4.18   Theoretical Resonant Modes and Frequency Response for the C.N. Rail Prestressed Concrete Bridge Tie

motion. This frequency is also close to the theoretical
second resonant frequency of 240 Hz, which indicates the
presence of the second resonant frequency mode.

CHAPTER 5

PROPOSED DESIGN MODEL

5.1 SYSTEM DYNAMICS

In most cases designers of prestressed concrete bridge ties
will not have direct access to field measured strains. As
such it may be difficult for the designer to determine the
level of strength and magnitude of prestress required for a
properly designed tie. See for instance chapter 10 of (1).

The current method employed by most designers is to specify an
impact loading by which the wheel loading is factored and
increased. The main disadvantages in this method are that it
is difficult to determine the correct impact factor and the
chosen impact factor does not help in determining the amount
of reverse bending to which the ties are subjected. There are
other disadvantages in the use of impact factors which have
been identified by others (20).

In order to assist designers in the design of prestressed
concrete bridge ties two mathematical models which predict the
strain levels under any desired loading, have been developed.
The first model predicts the strains due to positive bending
of the tie, while the second model predicts the strains due to
rebound of the tie.

Before presenting the models, an explanation of the
interaction of the rail vehicles and the track system is

perhaps in order to provide a better understanding of the mechanics behind the models. The models are based on the principal of conservation of energy and momentum. These methods are less complex and easier to use than equations of a time dependant nature.

The impact imparted to the track structure is generally caused by irregularities in the running surface of the rail, such as crushed heads, corrugation or such defects and by the wheels of the vehicles themselves. Wheel defects such as out-of-round wheels, ovate wheels, built-up-treads or skid flats tend to cause the greatest impacts to the track structure. Therefore a railway which keeps its vehicle wheels in generally good condition would be able to use a lower impact factor and design a more economical tie.

Vehicles with normal wheels would cause the ties and rail to deflect an amount proportional to the vehicle loading as if under static loading, in actuality the deflection would be quasi-static. However, if the vehicle has a wheel defect, the deflection is now two part. There is a deflection due to the static loading of the vehicle with an additional deflection due to the impact loading.

As the rail is impacted by the wheel, the tie deflects downwards beyond its static deflection point to a maximum

deflection whereupon it moves upwards and striking the wheel set of the vehicle at the statically loaded deflection point. This is because the frequency response of the vehicle is between 5 to 10 Hz, whereas the frequency response of the bridge ties is 88 Hz (in the first mode). Therefore the car and wheel set do not move and can be considered motionless or stationary in the vertical plane.

After the track has contacted the wheel set it forces the wheels and axles upward against the springs of the vehicle. This continues until the tie reaches its maximum upward deflection whereupon it is acted upon by the vehicle's sprung mass which forces the tie down to its statically deflected position. The deflection of the tie upward (rebound) is currently causing the CN type A modified ties to crack at their top centres.

5.2 MATHEMATICAL MODEL OF THE CONCRETE BRIDGE TIE RESPONSE IN POSITIVE BENDING

There are three possibilities of wheel rail impact modes from a skid flat wheel. These possibilities are illustrated in Figure 5.1.

In all three impact cases shown, the dynamic forces involved are described in Figure 5.2 below:
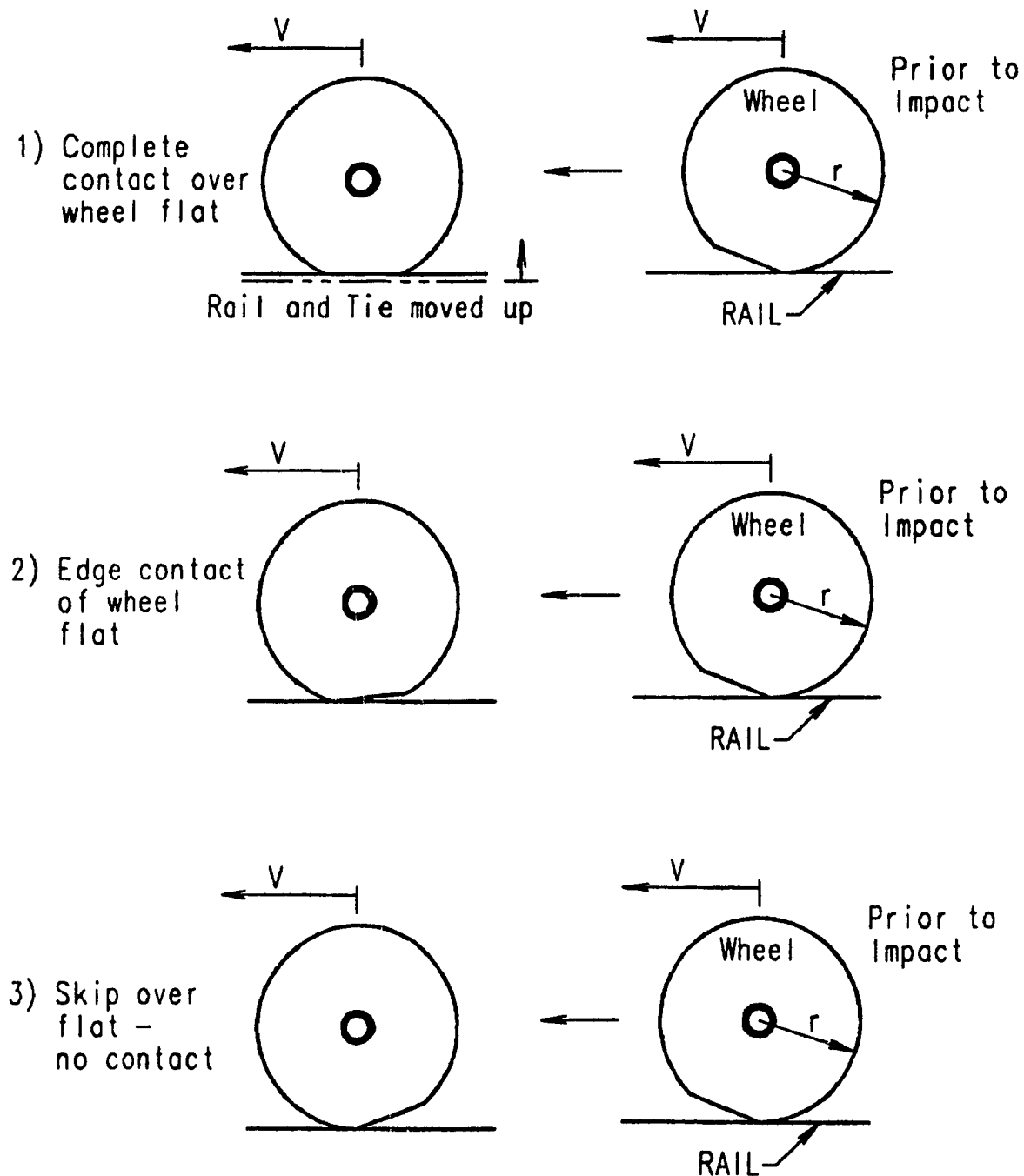
Figure 5.1   Schematic of Wheel Impacts

71
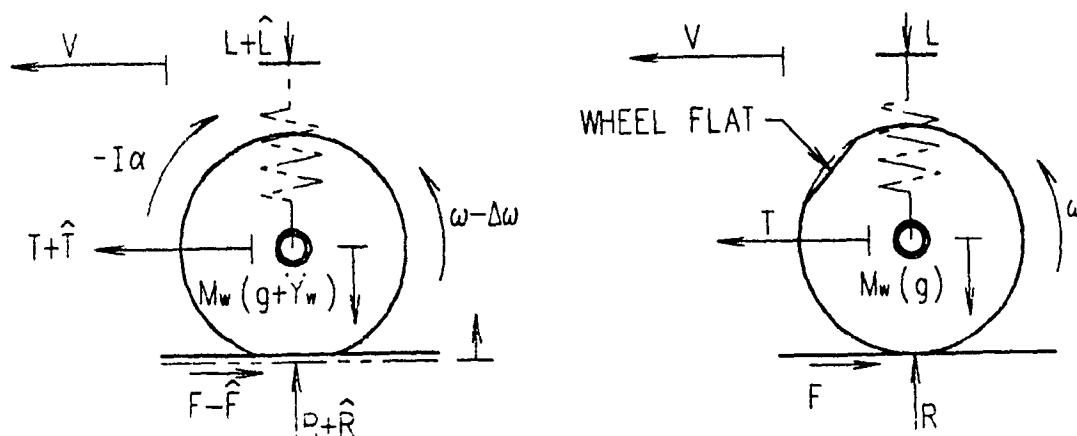
Figure 5.2   Dynamic Forces During Impact

Where:

V = linear velocity of the wheel

ω = angular velocity of rotation of the wheel

R = reaction of rail beneath the wheel

T = traction force of coupler

$\hat{F}$ = dynamic impulse loading: $\hat{F} = \int^{T} F_D(t)dt$, where T is the

period of impact and F_D is the dynamic load

α = the angular deceleration of axle due to impact

Δ = the change in angular velocity due to the impact, such

that $\Delta\omega = {}_0\int^{T}\alpha(t)dt$

This mathematical model for the impact response of concrete

bridge ties is based on a set of assumptions which are

presented in the Appendix C.   This model also relies on the

previous work and findings of (4), which determined the

fraction of the impact force on the main tie beneath the wheel

to be relatively constant at 50 percent.

72

Before presenting the model, an outline of the assumptions that have been made are presented as follows:

Basic Set of Assumptions

1) The axle and wheel's horizontal velocity is constant, ie: the railcar does not change in velocity with a flat wheel.

2) The impact occurs directly over a tie.

3) The impact occurs completely, as the wheel is over the tie and the dynamic deflection takes place about the statically deflected position of the track. This was shown in time traces of tie strains obtained in the CN field tests.

4) The axle and wheel has little to drop, before the impact occurs; (see Appendix C); a period for the wheel flat to rotate past is 6 times greater than that of the wheel to fall.

5) The impact occurs simultaneously on both rails.

6) The rail and tie are rigidly connected.

7) That linear superposition of dynamic and static deformation of tie holds.

8) Consider the worst cause scenario (for design purposes), ie: the wheel flat impacts the rail with the two surfaces parallel; there is always contact between wheel and rail which is the case for heavily loaded vehicles running up to 40 mph (see Appendix C).

9) The upward velocity of rail prior to impact, is

negligible.

10) For design purposes in calculating positive and negative bending strains at tie center, the first flexural mode of the tie in bending is used in the mathematical development.

11) The impact vertical velocities of wheel, rails and ties prior to impact are assumed negligible compared to their velocities after impact.

12) The change in wheel angular velocity $\Delta\omega$ is small compared to ω, due to impact couple and slipping.

Kinematic Mechanism Of Wheel - Rail Impacts:
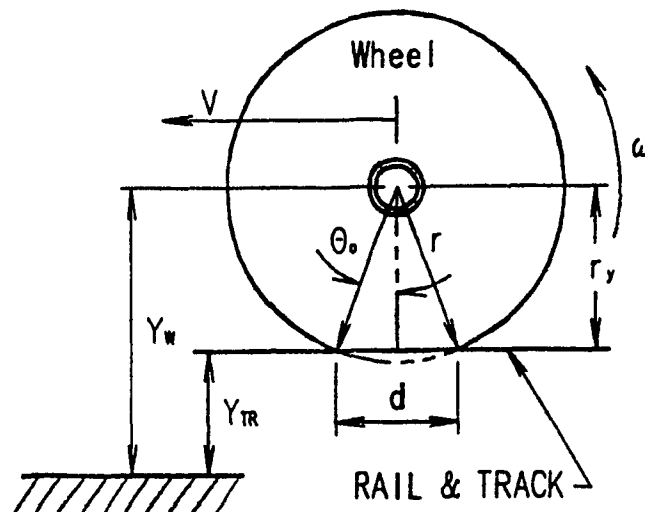
Figure 5.3   Kinematic Mechanism of Wheel - Rail Impact

Description of mechanism in wheel - rail kinematics during

74

impact and up to the moment of separation.

displacement: $Y_w = -Y_{TR} + r_Y$ (1)

velocity: $\dot{Y}_w = -\dot{Y}_{TR} + \dot{r}_Y$ (2)

Where:

v = velocity of wheel and axle

ω = angular velocity of wheel

r = radius of wheel

v = $\omega . r$

d = length of skid flat

Y_w = vertical displacement of wheel

Y_{TR} = vertical displacement of the tie at the rail seat

r_Y = vertical displacement between axle and rail

r_Y = $r \cos \theta_0 - \omega t$ (3)

$\dot{r}_Y$ = $r\omega \sin \theta_0 - \omega t$ (4)

$\dot{Y}w$ = $-\dot{Y}_{TR} + \dot{r}_y = r\omega \sin (\theta_0 - \omega t) - \dot{Y}_{TR}$ (5)

Dynamic Analysis Using Conservation of Momentum and Impulsive Forces
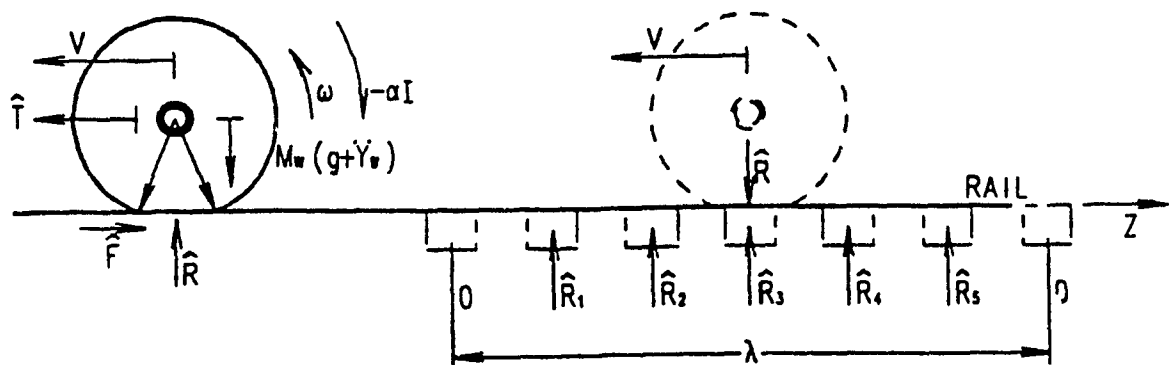
Figure 5.4   Distribution of Impact Forces

75

$$\hat{R} = \int_0^T R(t)\,dt = \left[\dot{Y}_W^{II} - \dot{Y}_W^I\right] M_W \tag{6}$$

where superscript "I" and "II" denote before and after impact, respectively.

$$\hat{R} = \sum_{n=1}^5 \hat{R}_n + \int_0^\lambda \left[\dot{Y}_R^{II} - \dot{Y}_R^I\right] M_R\, d_z \tag{7}$$

where Y_R is the deflection of rail and λ is the centre to centre line of 7 ties, and M_R is the mass of rail per unit length.

$$\hat{R} = \int_{-a}^{l+a} \left[\dot{Y}_{Tn}^{II} - \dot{Y}_{Tn}^I\right] M_T\, dx \tag{8}$$

Where M_T is the mass of tie per unit length and $\dot{Y}_{Tn}$ is the vertical velocity of tie n^{th} as a function of position x.

$$\left[\dot{Y}_W^{II} - \dot{Y}_W^I\right] M_W = \sum_{n=1}^5 \int_{-a}^{l+a} \left[\dot{Y}_{Tn}^{II} - \dot{Y}_{Tn}^I\right] M_T\, d_x + \int_0^\lambda \left[\dot{Y}_R^{II} - \dot{Y}_R^I\right] M_R\, d_z \tag{9}$$

$$\dot{Y}_W^{II}\cdot M_W = \sum_{n=1}^5 \int_{-a}^{l+a} \dot{Y}_{Tn}^{II}\cdot M_T\, d_x + \int_0^\lambda \dot{Y}_R^{II} M_R\, d_z \tag{10}$$

Simplifying yields:

$$\dot{Y}_W\cdot M_W = \sum_{n=1}^5 \int_{-a}^{l+a} \dot{Y}_{Tn}\cdot M_T\, dx + \int_0^\lambda \dot{Y}_R\cdot M_R\, dz \tag{11}$$

The same impact period for all ties is assumed and only vertical linear motion is considered. Therefore, from (4), upon impact, 50 percent of the impulse force is on the center tie.

76
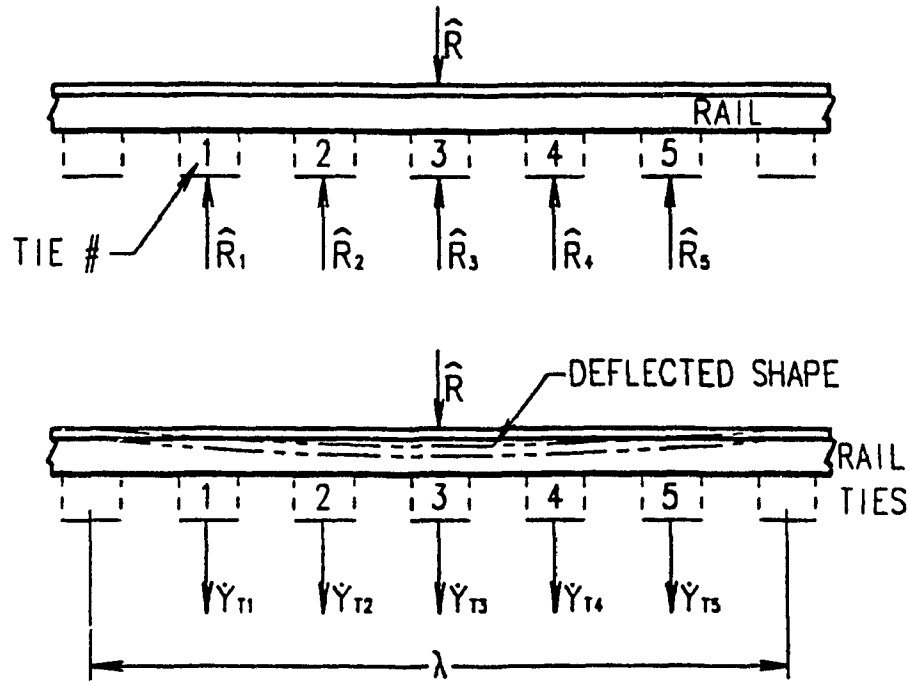
Figure 5.5   Assumed Deflected Shape of Rail After Impact

$$\hat{F} = \int_0^T F(t)\, dt = \sum_{n=1}^{5} \int_{-a}^{l+a} \left[\dot{Y}_{Tn}^{II} - \dot{Y}_{Tn}^{I}\right] M_{tie(n)}\, dx + \int_0^{\lambda} \left[\dot{Y}_R^{II} - \dot{Y}_R^{I}\right] M_R\, dx \qquad (12)$$

$$but \quad \hat{R}_n = \int_0^T R_n(t)\, dt = \int_0^{l+a} \left[\dot{Y}_{Tn}^{II} - \dot{Y}_{Tn}^{I}\right] M_{tie(n)}\, dx \qquad (13)$$

where $\dot{Y}_R = \dot{Y}_{rail}$ and $\dot{Y}_{Tn} = \dot{Y}_{tie\,\#}$, where $n = 1,2,3,4,5$.

The equation can be simplified knowing that:

$\dot{Y}_{Tn} = 0$ for ties 1 to 5 and $\dot{Y}_R^{I} = \dot{Y}_N^{I} = 0$

and: $\quad \hat{R} = \left(\dot{Y}_W^{II} \right) M_W$

$$\hat{R} = \sum_{n=1}^{5} \int_{-a}^{l+a} \dot{Y}_{Tn}^{II} M_T dx + 2 \int_{0}^{\lambda} \dot{Y}_R^{II} M_R \, dr \tag{14}$$

For the sake of clarity the superscript "II" can be omitted.

$$\dot{Y}_W M_W = \sum_{n=}^{5} \int_{-a}^{l+a} \left(\dot{Y}_{Tn} M_T \right) dx + 2 \int_{0}^{\lambda} \left(\dot{Y}_R M_R \right) dr \tag{15}$$

Note that for a given tie the summation is the same as that of the static condition:

$$2 \left[\hat{R}_3 + 2 R_{2,4} + 2 R_{1,5} \right] = \sum_{n=1}^{5} \int_{-a}^{l+a} \left(\dot{Y}_{Tn} M_T \right) dx \tag{16}$$

Therefore:

$$\dot{Y}_W M_W = 2 \left[\hat{R}_3 + 2 R_{3,4} + 2 R_{1,5} \right] + 2 \int_{0}^{\lambda} \left(Y_R M_R \right) \, dr \tag{17}$$

From (9), for 132 lb. rail and 136 lb. rail, with tie spacings from 16" (406 mm) to 24" (610 mm), it can be determined that:

$$\frac{R_2}{R_3} = \frac{R_4}{R_3} = \frac{36}{86.36} = 0.42$$

so that $R_2 = R_4 = 0.42 R_3$

$$\frac{R_1}{R_3} = \frac{R_5}{R_3} = \frac{5.68}{86.36} = 0.06$$

so that $R_1 = R_5 = 0.6 R_3$

Therefore from the above:

$$\hat{R}_3 = 0.5 \hat{R}$$

$$\hat{R}_2 = \hat{R}_4 = 0.42 \; \hat{R}_3 = 0.42\,(0.5)\,\hat{R} = 0.21 \; \hat{R}$$

$$\hat{R}_1 = \hat{R}_5 = 0.06 \; \hat{R}_3 = 0.06\,(0.5) \; \hat{R} = 0.03 \; \hat{R}$$

Substituting these values into equation 17 we obtain:

$$\dot{Y}_W M_W = 2\hat{R}_3 \,[1 + 2\,(0.42) + 2\,(0.06)] + 2\int_0^\lambda (Y_R M_R)\,dr \qquad (18)$$

$$\dot{Y}_W M_W = 2\hat{R}_3 \,(1.96) + 2\int_0^\lambda (Y_R M_R)\,dr \qquad (19)$$

In general terms and in the case of tie number 3:

$$2\,\hat{R}_3 = (Y_T M_T)\,dx \quad , \text{ for each tie including the central tie.}$$
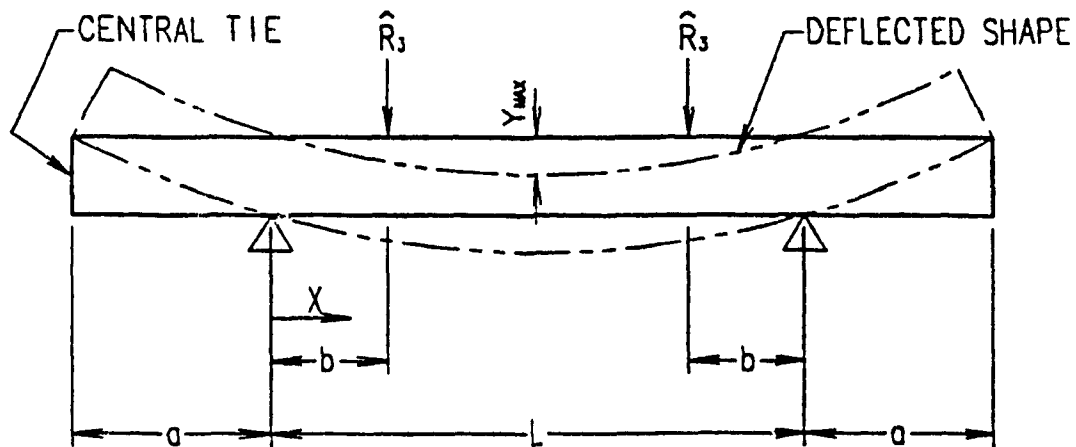
Figure 5.6   Assumed Deflected Shape of the Tie
in the First Mode

The above diagram represents the deflected shape of the tie in the first mode. The frequency of the tie in the first

mode is 88 Hz (from field measurements). The first mode

gives the largest impact deflection.

The assumed displacement is given by:

$$Y_T = Y_{max} \sin\left(\frac{\pi x}{L}\right) \sin 2\pi Ft \qquad (20)$$

The velocity is given by:

$$\dot{Y}_T = Y_{max} 2\pi F \sin\left(\frac{\pi x}{L}\right) \cos 2\pi Ft \qquad (21)$$

at t = 0, the velocity is a maximum.

For conservation of momentum for a tie with zero initial

velocity:

$$\hat{R}_3 = \int_{-a}^{l+a} \rho_c A Y_{max} 2\pi F \sin\left(\frac{\pi x}{L}\right) \cos(2\pi Ft)\, dx \qquad (22)$$

Where:

ρ_c = mass density of concrete

A = cross-sectional area of the bridge tie

F = frequency of the tie in the first mode = 88 Hz

now let: $\overline{Y}_T = 2\pi F\, y_{max}$

substituting into equation 22 yields.

$$2\,\hat{R}_3 = \rho_c A \overline{Y}_T \cos 2\pi Ft \int_{-a}^{l+a} \sin \frac{\pi x}{L}\, dx \qquad (23)$$

$$2\,\hat{R}_3 = \rho_c A \overline{Y}_T (\cos 2\pi Ft)\left(\frac{-L}{\pi} \cos \frac{\pi x}{L}\right)\Big|_{-a}^{l+a} \qquad (24)$$

evaluating by parts yields:

$$-\frac{L}{\pi} \cos \frac{\pi x}{L} = -(21.6 + 21.6) = -43.21$$

80

$\rho_c A = 0.029$ *slugs*

$2 \hat{R}_3 = (0.029) (43.21) (\cos 2 \pi Ft) \overline{Y}_T$

$2 \hat{R}_3 = 1.25 \cos 2 \pi Ft \overline{Y}_T$

at the point of impact t = 0

therefore:

$2 \hat{R}_3 = 1.25 \overline{Y}_T$,

so $2 \hat{R}_3 = 1.25 \overline{Y}_T$ for the central tie.

To obtain the deflection at the rail seat, the following

expression must be used:

$\dot{Y}_{TR} = \overline{Y}_T \sin \frac{\pi b}{L}$ (at rail seat)   (25)

$2 \hat{R}_3 = \dfrac{1.25 \dot{Y}_{TR}}{\sin(\frac{\pi b}{L})}$ *where:* $\sin \left(\frac{\pi b}{L} \right) = 0.555$

$2 \hat{R}_3 = 2.25 \dot{Y}_{TR}$ (26)

$\dot{Y}_W M_W = 2.25 \dot{Y}_{TR} (1.96) + 2 \int\limits_0^{\lambda} \left(\dot{Y}_R M_R \right) dr$

$\dot{Y}_W M_W = 4.41 \dot{Y}_{TR} + 2 \int\limits_0^{\lambda} \left(\dot{Y}_R M_R \right) dr$ (27)

but according to kinematics (from equation 2 and 5)

$\dot{Y}_W = \dot{r}_Y - \dot{Y}_{TR}$

$\dot{Y}_W = \dot{r}_Y - \dot{Y}_{TR} = r \omega \sin \left(\Theta_0 - \omega t \right) - \dot{Y}_{TR}$

but from equation 4, $\dot{r}_y = r\omega \sin (\Theta_0 - \omega t)$

at: $t = 0$, $\dot{r}_y = r\omega \sin \Theta_0$, *where maximum velocity occurs*

$$\dot{Y}_W = r\omega \sin \Theta_0 - \dot{Y}_{TR} \tag{28}$$

$$M_W [r\omega \sin \theta_0 - \dot{Y}_{TR}] = 4.41 \, \dot{Y}_{TR} + 2 \int_0^\lambda (\dot{Y}_R \, M_R) \, dr \tag{29}$$

where $\theta_0 = 1/2$ angle of wheel flat.

The apparent linear mass (Mw) involved in the impact is:

1) mass of wheel set, plus

2) 1/3 the mass of 2 side frames

Mw = 8.67 slugs (for average 100 ton car)

$$\dot{Y}_{TR} \times 13.0 = 8.67 \, r\omega \sin \theta_0 - 2 \int_0^\lambda (\dot{Y}_R \, M_R) \, dr \tag{30}$$

Assuming that the rail and the ties deflect together at the rail seats, the following configuration is obtained:
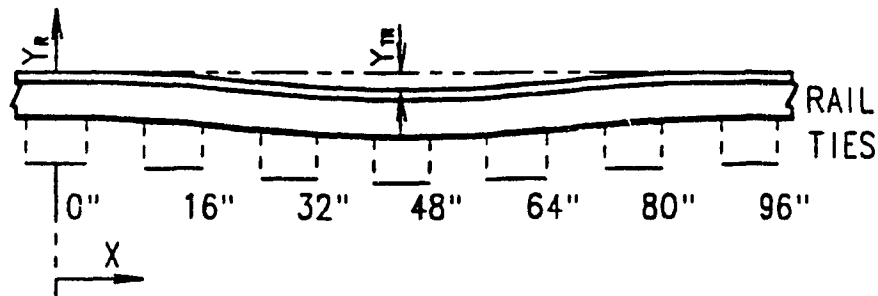
Figure 5.7   Assumed Displacement of Rail and Ties

Therefore $Y_R = Y_{TR}$

$$\text{note that: } \frac{\hat{R}_n}{\hat{R}_3} = \frac{\int\limits_{-a}^{l+a} \dot{Y}_{TN} \, M_T \, dx}{\int\limits_{-a}^{l+a} \dot{Y}_{T3} \, M_T \, dx} \qquad (31)$$

$$\text{with } \dot{Y}_{TN} \, (x, t) = Y_{max} \, (2\pi F) \, \sin \frac{\pi X}{\ell} \, \cos 2\pi F t, \qquad (32)$$

where $F = 88$ Hz.

substituting yields:

$$\frac{\hat{R}_n}{\hat{R}_3} = \frac{Y_{max_n} (2\pi F t) \, \cos 2\pi F t \int\limits_{-a}^{l+a} \sin \frac{\pi X}{\ell} \, dx}{Y_{max_3} \, (2\pi F f) \, \cos 2\pi F t \int\limits_{-a}^{l+a} \sin \frac{\pi X}{\ell} \, dx} = \frac{\overline{Y}_{TN}}{\overline{Y}_{T3}} \qquad (33)$$

$$\text{but } \dot{Y}_{TR_3} = \dot{Y}_{Tn} \, \sin \frac{\pi b}{\ell}$$

$$\text{so } \frac{\hat{R}_n}{\hat{R}_3} = \frac{\overline{Y}_T}{\overline{Y}_{TR_3}} = \frac{\dot{Y}_R \, (16,4)}{\dot{Y}_R \, (48)} \qquad (34)$$

Now, assuming the deflected rail shape is compatible with the deflection of the rail seat on the tie, the deflection of the rail is established as:

$$\overline{Y}_{TR_n} = \dot{Y}_R \, (16, n)$$

where the tie spacing = 16" (406 mm)

$$Y_R = Y_{TR_3} \, F_{(r)} \, \sin 2\pi F t, \qquad (35)$$

where $F_{(r)}$ is a function of the vertical deflection along the track

$$\dot{Y}_R = Y_{TR_3} \, (2\pi F) \, F_{(r)} \, \cos 2\pi F t \qquad (36)$$

$$\dot{Y}_R = \overline{Y}_{T_1} \sin \frac{bn}{\ell} \, F_{(r)} \cos 2\pi Ft \qquad (37)$$

Therefore:

$$\frac{\dot{Y}_R \,(16 \times n)}{Y_R \,(48)} = \frac{F(16 \times n)}{F(48)}$$

The function of $F_{(r)}$ must be chosen such that it is compatible with the tie displacement at the rail seat:

Set $F_{(r)} = \sin^6 \frac{\pi r}{\lambda}$ where $\lambda = 96''$ (2.44m)

The following is a table for the ratios:

$$\frac{\hat{R}_n}{\hat{R}_3} \text{ and } \frac{F(16 \times n)}{F(48)}$$

n r	1 16	2 32	3 48
$\hat{R}_n/\hat{R}_3$	0.06	0.42	1.00
F_n/F_3	0.02	0.42	1.00

Table 5.1 Summary of Ratios $R_n/\hat{R}_3$ and $F(16 \times n)/F(48)$

From the above table it can be seen that the chosen function $F_{(r)} = \sin^6 \frac{\pi r}{\lambda}$ is appropriate.

Therefore: $\dot{Y}_R = \overline{Y}_T \sin \frac{b\pi}{\ell} \sin^6 \frac{\pi r}{\lambda} \cos 2\pi ft \qquad (38)$

at $t = 0 \quad \dot{Y}_R = \overline{Y}_T \sin^6 \frac{\pi x}{\lambda} \qquad (39)$

$$\int_0^\lambda \sin^6 \frac{\pi x}{\lambda} \; (dx) \tag{40}$$

$$= \frac{-\sin^5\left(\frac{\pi x}{\lambda}\right)\cos\left(\frac{\pi x}{\lambda}\right)}{6 \; \pi/\lambda} + \frac{5}{6}\left(\frac{3x}{8} - \frac{\sin\left(\frac{\pi x}{\lambda}\right)}{4\pi/\lambda} + \frac{\sin\left(\frac{4\pi x}{\lambda}\right)}{32\pi/\lambda}\right)$$

where $\lambda = 96''$ (2.44 m)

solving yields

$$\int_0^\lambda \sin^6 \frac{\pi x}{\lambda} = 30 \tag{41}$$

substituting into the left hand side of equation 30 yields:

$$\int_0^\lambda \dot{Y}_R \; M_R \; dr = 30 \; M_R \; \overline{Y}_T \; \sin \frac{b\pi}{\ell} \; \cos 2\pi F t \tag{42}$$

$$\int_0^\lambda \dot{Y}_R \; M_R \; dr = 30 \; M_R \; \dot{Y}_{TR} \; \cos 2\pi F t \tag{43}$$

Therefore:

$$\int_0^\lambda M_R \; \overline{Y}_T \; \sin \frac{b\pi}{\ell} \; \sin^6 \frac{\pi r}{\lambda} \; \cos 2\pi F t \; dr \tag{44}$$

$$= 30 \; M_R \; \dot{Y}_T \; \sin \frac{b\pi}{\ell} \; \cos 2\pi F t \tag{45}$$

$$= 30 \; M_R \; \dot{Y}_{TR} \; \cos 2\pi F t \tag{46}$$

$$M_R = \rho_R \; A_R = (0.283 \; lbs/in^3 \; x \; 12.91 \; in^2)/386.4 \tag{47}$$

$M_R = 0.0095 \; slugs \qquad say \qquad M_r = 0.01 \; slugs$

$$\int_0^\lambda \dot{Y}_R M_R \, dr = 30.0 \times 0.01 \times \dot{Y}_{TR} \times \cos 2\pi Ft \tag{48}$$

At impact, the maximum momentum occurs at t = 0 therefore,

$30 \times 0.01 \times \dot{Y}_{TR}$,

therefore, from equation 30

$$\ddot{Y}_{TR} \times 13.0 = 8.67 \, r \, \omega \sin \Theta_0 - 2 \int_0^\lambda \dot{Y}_R M_R \, dr \tag{49}$$

we now obtain

$$\dot{Y}_{TR} (13.0 + 0.60) = 8.67 \, r \, \omega \sin \Theta_0 \tag{50}$$

assuming 36" (914 mm) Heuman wheels, r = 18" (457 mm)

sin Θ_0 = 0.028 for a 1" (25.4 mm) skid flat

$\omega = V/r$

$$13.60 \, \dot{Y}_{TR} = 8.67 \times 18 \times V \sin \Theta_0 \tag{51}$$

Assuming a freight train velocity of 40 mph (66 km/h), which was the average speed across the bridge (all monitored trains)

$$13.60 \, \dot{Y}_{TR} = 8.67 \times 706 \times 0.028 = 171.39 \tag{52}$$

$\dot{Y}_{TR} = 12.60$ in/sec (0.23 m/sec)

Knowing the maximum tie velocity from the wheel impact, at rail seat and therefore the tie center, the maximum strain at tie center can be computed from the assumed deflected shape. The vertical velocity along the tie is expressed as:

$$\dot{Y}_T(x, t) = \overline{Y} \frac{\sin \pi x}{\ell} \cos 2\pi Ft \tag{53}$$

Where $\overline{Y} \sin \frac{\pi b}{\ell} = \dot{Y}_{TR}$ and $\overline{Y} = Y_{max} \, 2\pi F$

To express maximum strain at the tie centre, set $30 = \ell/2$ and $t = 0$ (immediately)

$$\textit{Therefore } \dot{Y} = \frac{\dot{Y}_{TR}}{\sin\frac{\pi b}{\ell}} = \frac{12.60}{\sin\frac{\pi 18}{96}} \qquad (54)$$

$\dot{Y} = 22.68$ in/sec (0.58 m/sec) at tie centre

Maximum displacement Y_{max} at the tie center

$$Y_{max} = \frac{\dot{Y}}{2\pi F} = \frac{22.68}{2\pi 85} = 0.042'' \ (1.1 \ mm) \ \textit{at tie centre.} \qquad (55)$$

The expression of vertical tie displacement along its length is expressed as:

$$Y_T \ (x, t) = Y_{max} \sin\left(\frac{\pi x}{\ell}\right) \sin 2\pi F t \qquad (56)$$

To express the bending strain in terms of vertical displacement of the beam.

$$\sigma = \frac{MY}{I} \ \textit{or} \ \epsilon . E = \frac{MY}{I} \ \textit{or} \ \epsilon = \frac{MY}{EI}, \ \textit{also} \ M = EI \ \frac{d^2 Y_7}{dx^2}$$

$$\textit{so} \ \epsilon = Y \ \frac{d^2 Y_T}{dx^2} \qquad (57)$$

ϵ_{max} at the tie centre:

$$\epsilon_{max} = \frac{d^2}{dx^2}\left[Y_{max} \sin\frac{\pi x}{\ell} \sin 2\pi f t \right] \qquad (58)$$

where ϵ_{max} is taken at maximum deflection of the tie from impact.

At maximum deflection of tie, the time component "$\sin 2\pi F t$" of the assumed mode expression is:

$$t = \frac{1}{4F}$$

Therefore:

$$\sin 2\pi Ft = 1$$

$$so\ \epsilon_{max} = Y_b\ Y_{max}\ \frac{d^2}{dx^2}\left[\sin\frac{\pi x}{\ell}\right] = Y_b\ Y_{max}\left(\frac{\pi}{\ell}\right)^2\sin\frac{\pi x}{\ell} \tag{59}$$

$$for\ x = \frac{\ell}{2}$$

$$\epsilon_{max} = Y_b\ Y_{max}\left(\frac{\pi}{\ell}\right)^2,\ where\ Y_{max} = 0.042''\ (1.1mm)$$

Considering the bottom fibre tensile strain, for positive bending:

Y_{max} = 0.042" (1.1 mm)

ℓ = 96" (2.44 m)

Y_b = 5.84" (148.3 mm)

$$\epsilon = Y_b\ Y_{max}\left(\frac{\pi}{\ell}\right)^2$$

$$\epsilon_{max} = 5.84\ x\ 0.042\left(\frac{\pi}{96}\right)^2 \tag{60}$$

$\epsilon_{max} = 262\ x\ 10^{-6}$ *in./in. dynamic strain*

The static strain must now be added to this component such that:

$\epsilon_{max} = \epsilon_{max}$ (dynamic) + ϵ_{max} (static)

ϵ_{max} (static) = 153 x 10^{-6} in./in.

$\epsilon_{max} = (262\ x\ 10^{-6}) + (153\ x\ 10^{-6})$

$\epsilon_{max} = 415\ x\ 10^{-6}$ in./in.

5.3 MATHEMATICAL MODEL OF THE CONCRETE BRIDGE TIE RESPONSE IN NEGATIVE BENDING

Using the same basic assumptions as that of the preceeding mathematical model for the tie response in the positive bending, the negative bending response has been developed. This method has been based on the conservation of energy and is considered to occur in the first flexural mode.

From the energy method:

$$\sigma = \frac{MY}{I} \quad and \quad \sigma = \epsilon E$$

$$Therefore \ \epsilon E = \frac{MY}{I}$$

$$and \ \epsilon = \frac{MY}{EI} \quad ; \quad \frac{M}{EI} = \frac{\epsilon}{Y}$$

$$but \quad \frac{M}{EI} = \frac{-d^2Y}{dx^2} \quad and \quad \frac{\epsilon}{Y} = \frac{-d^2y}{dx^2}$$

The assumed mode of deflection is given by:

$$Y = Y_0 \sin\left(\frac{\pi x}{L}\right) \tag{1}$$

$$\frac{d^2y}{dx^2} = -\left(\frac{\pi}{L}\right)^2 Y_0 \sin\left(\frac{\pi x}{L}\right) \tag{2}$$

$$Now \ setting \ \left(\frac{\pi}{L}\right)^2 Y_0 = A$$

$$Yields \ \frac{d^2y}{dx^2} = -A \sin\left(\frac{\pi x}{L}\right) \tag{3}$$

89
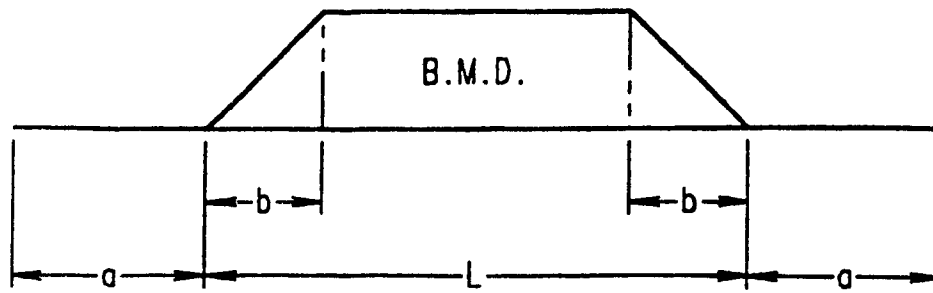
Figure 5.8 Bending Moment Diagram for Tie

From the above bending moment diagram

a = 24" (610 mm)

b = 18" (457 mm)

ℓ = 96" (2.44 m)

From the energy method

$$u = \int \frac{M^2(x)\,dx}{2EI} \qquad (5)$$

$$U_D = U_U + W_{Y0}' + 1/2\; k\left(\frac{Y_0'}{2}\right)^2 \qquad (6)$$

Where:

U_D = energy stored in the tie due to the downward deflection.

U_U = energy stored in the tie due to the upward deflection.

W = wheel load.

Y_0' = upward deflection of tie.

k = spring constant for railway vehicles

Evaluating each term separately yields:

$$U_D = \int_{-a}^{l+a} \frac{EI}{2} \left(\frac{M}{EI}\right)^2 dx$$

$$= \int_{-a}^{l+a} \frac{EI}{2} \left[A \sin\left(\frac{\pi x}{L}\right) \right]^2 dx$$

$$= \int_{-a}^{l+a} \frac{EIA^2}{2} \sin^2\left(\frac{\pi x}{L}\right) dx$$

$$= \frac{EIA^2}{2} \int_{-a}^{l+a} \sin^2\left(\frac{\pi x}{L}\right) dx$$

Similarily:

$$U_U = \int_{-a}^{l+a} \frac{EI}{2} \left(\frac{M}{EI}\right)^2 dx$$

$$= \int_{-a}^{l+a} \frac{EI}{2} \left[B \sin\left(\frac{\pi x}{\ell}\right)^2 \right] dx$$

$$= \int_{-a}^{l+a} \frac{EIB^2}{2} \sin^2\left(\frac{\pi x}{\ell}\right) dx$$

$$= \frac{EIB^2}{2} \int_{-a}^{l+a} \sin^2\left(\frac{\pi x}{\ell}\right) dx$$

Where: $B = \left(\frac{\pi}{\ell}\right)^2 Y_0'$

$$WY = 2 \, WY_0' \sin\left(\frac{b\pi}{\ell}\right)$$

91

$$\text{and } 1/2 \ K \ Y_s^2 = 1/2 \ K \left(B \ \frac{\ell^2}{2\pi^2} \right)^2 \tag{11}$$

$$1/2 \ K \ Y_s^2 = 1/2 \ K \ B^2 \left(\frac{\ell}{2\pi} \right)^2$$

Where Y_s = Compression of the vehicle springs. Taking the above terms and evaluating yields:

$$U_D = \frac{EIA^2}{2} \left[\left(\frac{1}{2} \ (120) - \frac{96}{4\pi} \ \sin \left(\frac{240\pi}{96} \right) \right) \right] -$$

$$\left[\left(\frac{1}{2} \ (-24) - \frac{96}{\pi} \ \sin \left(\frac{-48\pi}{96} \right) \right) \right] \tag{12}$$

$$U_D = \frac{EIA^2}{2} \left[\left(60 - \frac{24}{\pi} \ \sin 2.5\pi \right) - \left(-12 - \frac{96}{\pi} \ \sin \left(\frac{-\pi}{2} \right) \right) \right] \tag{13}$$

$$U_D = \frac{EIA^2}{2} \left[\left(60 - \frac{24}{\pi} \ \sin 7.854 \right) - \left(-12 - \frac{24}{\pi} \ \sin - 1.571 \right) \right] \tag{14}$$

$$U_D = \frac{EIA^2}{2} \left[(60 - 7.6394) - (-12 + 7.6394) \right] \tag{15}$$

$$U_D = \frac{EIA^2}{2} \left[52.3606 + 4.3606 \right] \tag{16}$$

$$U_D = \frac{EIA^2}{2} \ (56.7212) \tag{17}$$

Similarily:

$$U_U = \frac{EIA^2}{2} \ (56.7212) \tag{18}$$

$$2 \ WY_0' \ \sin \left(\frac{b\pi}{\ell} \right) = 2 \ WY_0' \ \sin \left(\frac{18\pi}{96} \right) \tag{19}$$

$$= 2\ WY_0'\ (0.5336) \tag{20}$$

$$\text{but } Y_0' = B\left(\frac{\ell}{\pi}\right)^2 \tag{21}$$

Therefore, substituting equation 21 into equation 10 yields:

$$2\ W\ B\left(\frac{\ell}{\pi}\right)^2 \sin\left(\frac{b\pi}{\ell}\right) \tag{22}$$

Where w = Weight of wheel loading. Normal 100 ton (890 kN) car vehicle bogie (truck) weighs 8,000 lbs. (35.6 kN). Under impact the central tie receives 50 percent of the load. Only 1 wheel set is being considered.

$$\text{So: } W = 8,000 \times \frac{1}{2} \times \frac{1}{2} = 2,000\ lbs.\ (8.9\ kN)$$

Therefore:

$$2\ WY_0'\ \sin\left(\frac{b\pi}{\ell}\right) = 2\ (2,000)\ B\left(\frac{96}{\pi}\right)^2 \sin\left(\frac{18\pi}{96}\right) \tag{23}$$

$$2\ WY_0'\ \sin\left(\frac{b\pi}{\ell}\right) = 2.075 \times 10^6\ B \tag{24}$$

The term $1/2\ k\ (Y_s')^2$ considers the compression of the bogie (truck) springs after the ties have been impacted by the rebounding tie.

k = 37,000 lbs/in (6,479 N/mm)

$Y_0' = 2\ Y_s$ where Y_s is the compression of the springs.

$$\frac{1}{2}\ K\left(\frac{Y_0'}{2}\right)^2 = \frac{1}{8}\ K\ Y_0'^2 \tag{25}$$

$$\text{but } Y_0' = B\left(\frac{\ell}{\pi}\right)^2 \tag{26}$$

$$\text{therefore } Y_0'^2 = B^2 \left(\frac{\ell}{\pi}\right)^4 \qquad . \qquad (27)$$

Substituting equation 27 into 25 and evaluating yields:

$$\frac{1}{8} k B^2 \left(\frac{\ell}{\pi}\right)^4 = \frac{1}{8} \times 37,000 \times \left(\frac{96}{\pi}\right)^4 B^2 \qquad (28)$$

$$= 4,032.711 \times 10^6 \ B^2$$

$$A = \frac{\epsilon}{Y \sin\left(\frac{\pi x}{\ell}\right)} \quad \text{where} \quad x = \frac{\ell}{2} \qquad (29)$$

Therefore: $A = \frac{\epsilon}{Y}$ when $Y = 5.84$" (148 mm)

The maximum positive strain (from the model for the ties response in positive bending) is 262×10^{-6}.

$$\text{Therefore } A = \frac{\epsilon}{Y} = \frac{262 \times 10^{-6}}{5.84} \qquad (30)$$

$A = 44.86 \times 10^{-6}$.

Substituting this value for A into the equation for U_D and evaluating for B yields:

$$U_D = \frac{(4.15 \times 10^6) \ (1560) \ (44.86 \times 10^{-6})^2 \ (56.7212)}{2} \qquad (31)$$

$$U_D = 369.5 \qquad (32)$$

Similarily:

$$U_U = \frac{(4.15 \times 10^6) \ (1,560) \ (56.7212) \ B^2}{2} \qquad (33)$$

$$U_U = 1.8361 \times 10^{11} \ B^2 \qquad (34)$$

$$1/2 \ K \left(\frac{Y_0'}{2}\right)^2 = 4,032.71 \times 10^6 \ B^2 \qquad (35)$$

$$2 \; W \; B \; Y_0' \; \sin\left(\frac{b\pi}{\ell}\right) = 2.075 \; x \; 10^6 \; B \qquad\qquad (36)$$

Therefore:

$$369.5 = 1.8361 \; x \; 10^{11} \; B^2 + 4,032.71 \; x \; 10^6 \; B^2 + 2.075 \; x \; 10^6 \; B$$

$$369.5 = 1.87639 \; x \; 10^{11} \; B^2 + 2.075 \; x \; 10^6 \; B \qquad\qquad (37)$$

Using the quadratic equation and solving yields.

$$B = 41.5 \; x \; 10^{-6} \; \text{in.}^{-1} \qquad\qquad (38)$$

$$but \; B = \frac{\epsilon}{Y_t} \qquad where \; Y_T = 6.16" \; (157 \; mm)$$

$$\epsilon = B \; Y \; \lambda = (42 \; x \; 10^{-6}) \; (6.16) \qquad\qquad (39)$$

$$\epsilon = 259 \; x \; 10^{-6} \; \text{in./in.}$$

The maximum static strain $= 153 \; x \; 10^{-6}$. Therefore the

dynamic strain in negative bending is:

$$(259 \; x \; 10^{-6}) - (153 \; x \; 10^{-6}) = 106 \; x \; 10^{-6}. \; \text{in./in.} \qquad\qquad (40)$$

5.4   DISCUSSION ON THE MODELS

From the above models the strain levels can be determined in

the tie for both positive and negative bending.

The model for the positive bending tie response predicts the

maximum positive strain (static and dynamic) for the bottom

fibre of the tie.

The tie can be designed using the strain levels as:

$\sigma_b = \epsilon_b \; E_c$ (for positive bending)

$\sigma_t = \epsilon_t \; E_c$ (for negative bending)

CHAPTER 6

DESIGN OF THE CONCORDIA TEST TIES

6.1 CONVERSION OF MODEL STRAINS TO STRESSES

Using the mathematical model of the preceding chapter, full
scale ties for experimental laboratory testing were designed.
Three separate tie designs using the original C.N.R. tie
envelope were undertaken.

The design of the ties is based on using the maximum strains
calculated in the previous chapter and converting them to
design stress levels at the outer fibres of the tie. The
maximum strain (combined static and dynamic) at the bottom of
the tie due to positive bending is 415×10^{-6}.

The corresponding stress level can be calculated from:

$$\sigma_b = \epsilon_b \, E_c \text{ and } \sigma_t = \epsilon_t \, E_c$$

Where

$$E_c = 57,000 \sqrt{f_c'}$$

and f_c' is specified as 6,000 psi (41.4 MPa)

Therefore: $E_c = 4.42 \times 10^6$ Psi (3,048 MPa)

$$\sigma_b = 4.42 \times 10^6 \times 4.15 \times 10^{-6}$$

$$\sigma_b = 1,835 \text{ psi (12.7 MPa)}$$

Use 1,850 psi (12.8 MPa) compression

The tie is subject to negative bending (reverse bending)
caused by dynamic impact. Therefore, the tie does not feel
the effects of static loading when subjected to negative

bending and the top fibre stress level can be calculated from the maximum dynamic strain value.

$\sigma_t = \epsilon_t \, E_c$

$\sigma_t = 106 \times 10^{-6} \times 4.42 \times 10^6$

$\sigma_t = 469$ psi (3.3 MPa)

Use $\sigma_t = 500$ psi (3.4 MPa) compression

It was decided to design two tie types with eccentric prestress (Type 1 and Type 2) and one type with uniform prestress (Type 3). For the Type 2 tie an arbitrary value of $\sigma_t = 1,000$ psi (6.90 Mpa) was chosen because $\sigma_t \approx \frac{1}{2} \sigma_b$.

Summarizing the stress value for each type of tie:

	TYPE 1	TYPE 2	TYPE 3
σ_t	500 psi	1,000 psi	1,850 psi
	3.4 MPa	6.9 MPa	12.8 MPa
σ_b	1,850 psi	1,850 psi	1,850 psi
	12.8 MPa	12.8 MPa	12.8 MPa

In practice, it is best to design the tie such that when it is subjected to maximum service loading, the concrete within the tie remains in compression even though the concrete can carry tension, usually limited to approximately 0.1 f_c' in uniaxial tension.

As the original C.N.R. tie envelope was maintained, the

97

properties of the tie can now be summarized.

A = 130.28 in.^{2} (84,057 mm^2)

I = 1,560 in.^{4} (6.49 x 10^8 mm^4)

Y_t = 6.16 in. (156.6 mm)

Y_b = 5.84 in. (148.3 mm)

6.2 DESIGN OF THE TYPE 1 TIE

By knowing the desired design stresses σ_t = 500 psi (3.4 MPa)

and σ_b = 1,850 psi(12.8 MPa), and by using the following well

known formulas (3, 5):

$$\sigma_t = \frac{P}{A} - \frac{P\,e\,Y_t}{I}$$

$$\sigma_b = \frac{P}{A} + \frac{P\,e\,Y_b}{I}$$

the required prestressing force, P, and the eccentricity, e,

can be determined. Substituting the above values into the two

equations and solving yields:

P = 155,420 lbs. (691.3 KN)

Back - substitution yields:

e = 1.13" (28.7 mm)

An assumed loss in prestressing force due to relaxation of

wires, creep and shrink of concrete, was taken as 27 percent.

This value is based on the C.N.R. experience with concrete

track ties, whose values ranged from 25 to 30 percent.

Therefore P_i = $\dfrac{P}{1 - 0.27}$ = $\dfrac{P}{0.73}$

$$P_i = \frac{155,420}{0.73} = 212,900 \ lbs \quad (947\,kN)$$

The use of 3/8" (9.55 mm) diameter prestressing strand with a tensile strength, f_{pu}, of 270 ksi (1,860 MPa) was selected.

The normal range of prestressing force initially applied to each strand is in the order of 0.7 f_{pu} A_s to 0.8 f_{pu} A_s. The value of 0.7 f_{pu} A_s = 16,100 lbs (71.6 kN) is chosen as the initial prestressing force.

Therefore the number of strands required is:

212,900 / 16,100 = 13.22 strands.

Use 14 - 3/8" (9.55 mm) diameter strands. Therefore, the initial prestressing force applied to each strand is:

212,900 / 14 = 15,210 lbs (67.6 kN)

15,210 lbs (67.6 kN) = 0.66 f_{pu} A_s

The final prestressing force after losses in each strand is:

15,210 x 0.73 = 11,103 lbs (49.4 kN)

Through a trial and error process, the arrangement of 14 strands as shown in Figure 6.1, was chosen.

6.3 DESIGN OF THE TYPE 2 AND TYPE 3 TIES

The Type 2 and Type 3 test ties were designed using the same general procedure as for the Type 1 ties. Table 6.1 indicates

the tabulated values for all 3 tie designs. Again a trial and error process is used in order to arrive at an acceptable arrangement of prestressing strands. The Type 2 and Type 3 ties are shown in Figures 6.2 and 6.3 respectively.

Figure 6.4 indicates the comparison of the various tie cross sections. A comparison of the effective prestress levels in these various tie designs is shown in Figure 6.5.

6.4 ULTIMATE MOMENT CAPACITY CHECK OF THE TYPE 1 TIE

In order to check the ultimate moment capacity of the ties, the stress - strain compatibility method has been used. This method more accurately predicts the ultimate moment capacity of the tie. This was useful in determining the required strength of the load frame and capacity of the jacks for laboratory testing.
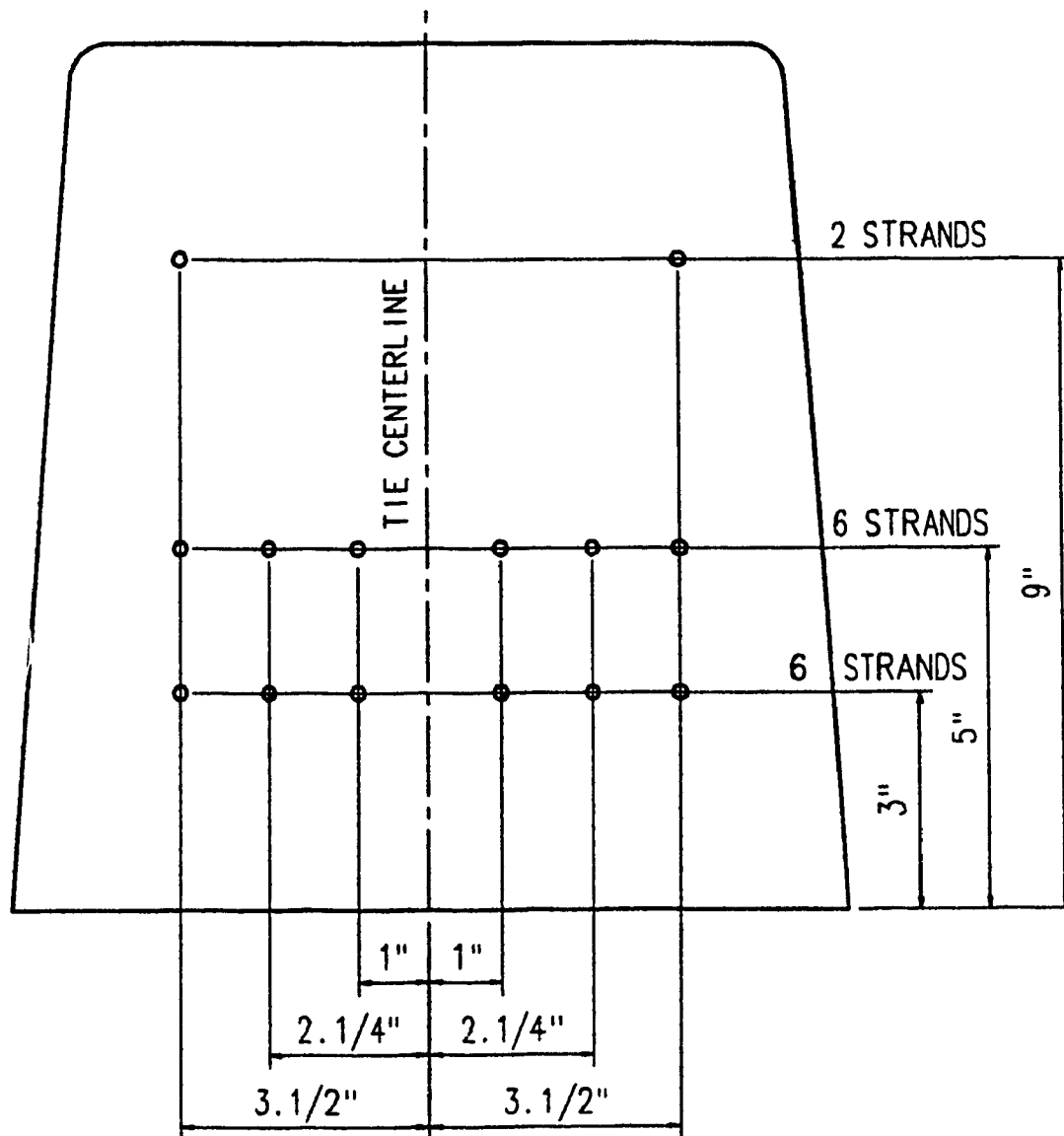
TIE TYPE No.1   (ECCENTRIC PRESTRESS)

1) 14 x 3/8" (9.5mm) DIA. − 7 WIRE STRAND WITH PRESTRESSING FORCE OF 15,210 lbs. (67.7 kN) EACH.

2) 15,210 lbs. (67.7 kN) = 0.66 fpu As

3) TOTAL PRESTRESSING FORCE = 212,940 lbs. (947.2 kN).

4) EFFECTIVE PRESTRESSING FORCE = 155,445 lbs. (691.4 kN).

5) STRESSES IN CONCRETE AFTER TRANSFER:

f_t = 500 psi (3.4 MPa) COMPRESSION

f_b = 1850 psi (12.8 MPa) COMPRESSION

6) ECCENTRICITY (e) = 1.13 in. (28.7mm)

Figure 6.1   Strand Arrangement of the Type 1 Tie

Labels within the figure:
- 4 STRANDS
- 6 STRANDS
- 6 STRANDS
- TIE CENTERLINE
- 9"
- 5"
- 2"
- 1" 1"
- 2.1/4" 2.1/4"
- 3.1/2" 3.1/2"
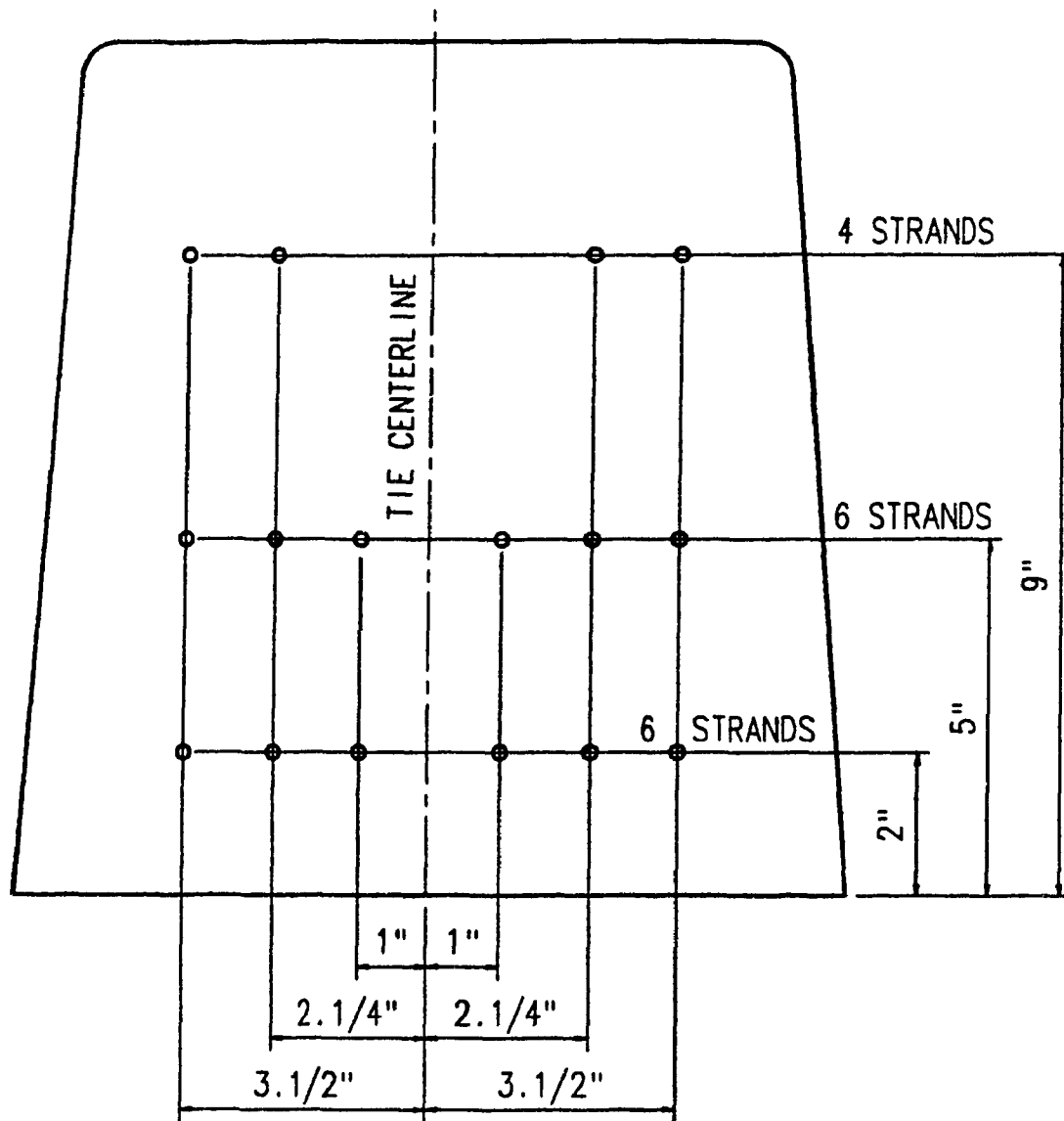
TIE TYPE No.2   (ECCENTRIC PRESTRESS)

1) 16 x 3/8" DIA. (9.5mm) – 7 WIRE STRAND WITH PRESTRESSING FORCE OF 16,021 lbs. (71.3 kN) EACH.
2) 16,021 lbs. (71.3 kN) = 0.7 f_{pu} A_s
3) TOTAL PRESTRESSING FORCE = 256,337 lbs. (1140.2 kN).
4) EFFECTIVE PRESTRESSING FORCE = 187,126 lbs. (832.3 kN).
5) STRESSES IN CONCRETE AFTER TRANSFER:
   f_t = 1000 psi (6.9 MPa) COMPRESSION
   f_b = 1850 psi (12.8 MPa) COMPRESSION
6) ECCENTRICITY (e) = 0.59 in. (15.0mm)

Figure 6.2   Strand Arrangement of the Type 2 Tie

CENTER LINE

TIE

4 STRANDS

4 STRANDS

4 STRANDS

4 STRANDS

4 STRANDS

9.1/2"

7.3/4"

5.1/2"

4"

2.1/2"

1" 1"

3" 3"
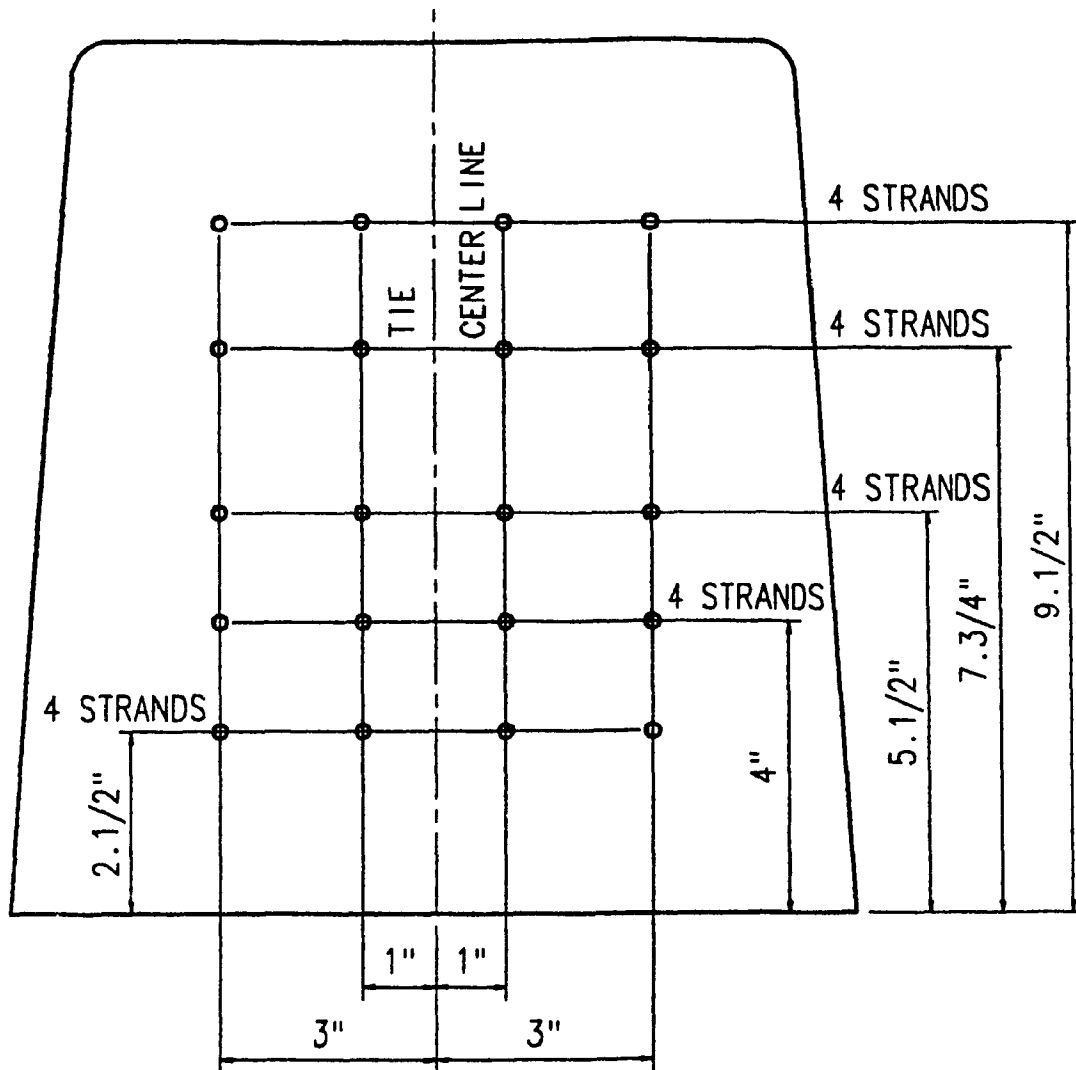
TIE TYPE No.3   (UNIFORM PRESTRESS)

1) 20 x 3/8" DIA. (9.5mm) — 7 WIRE STRAND WITH PRESTRESSING FORCE OF 16,510 lbs. (73.4 kN) EACH.

2) 16,510 lbs. (73.4 kN) = 0.72 fpu As

3) TOTAL PRESTRESSING FORCE = 330,162 lbs. (1468.6 kN).

4) EFFECTIVE PRESTRESSING FORCE = 241,046 lbs. (1072.7 kN).

5) STRESSES IN CONCRETE AFTER TRANSFER:

   f_t = 1850 psi (12.8 MPa) COMPRESSION

   f_b = 1850 psi (12.8 MPa) COMPRESSION

6) ECCENTRICITY (e) = 0

Figure 6.3   Strand Arrangement of the Type 3 Tie

103

TYPE	1	2	3
A	130.28 in^2 84,057 mm^2	130.28 in^2 84,057 mm^2	130.28 in^2 84,057 mm^2
I	1560. in^2 6.49 x 10^{4}m^4	1560 in^4 6.49 x 10^{-4}m^4	1560 in^4 6.49 x 10^{4}m^4
Y_t	6.16 in 156.5 mm	6.16 in 156.5 mm	6.16 in 156.5 mm
Y_b	5.84 in 148.3 mm	5.84 in 148.3 mm	5.84 in 148.3 mm
NO. STRANDS	14	16	20
% LOSSES	27	27	27
σ_t	500 psi 3.45 MPa	1,000 psi 690 MPa	1,850 psi 12.75 MPa
σ_b	1,850 psi 12.75 MPa	1,850 psi 12.75 MPa	1,850 psi 12.75 MPa
e	1.13 in 28.70 mm	0.59 in 14.99 mm	0 0
P_i	212,940 lbs 947.2 kN	256,337 lbs 1,140 kN	330,162 lbs 1,469 kN
P_{eff}	155,440 lbs 691.4 kN	187,126 lbs 832 kN	241,018 lbs 1,072 kN

Table 6.1 Characteristics of Tie Designs
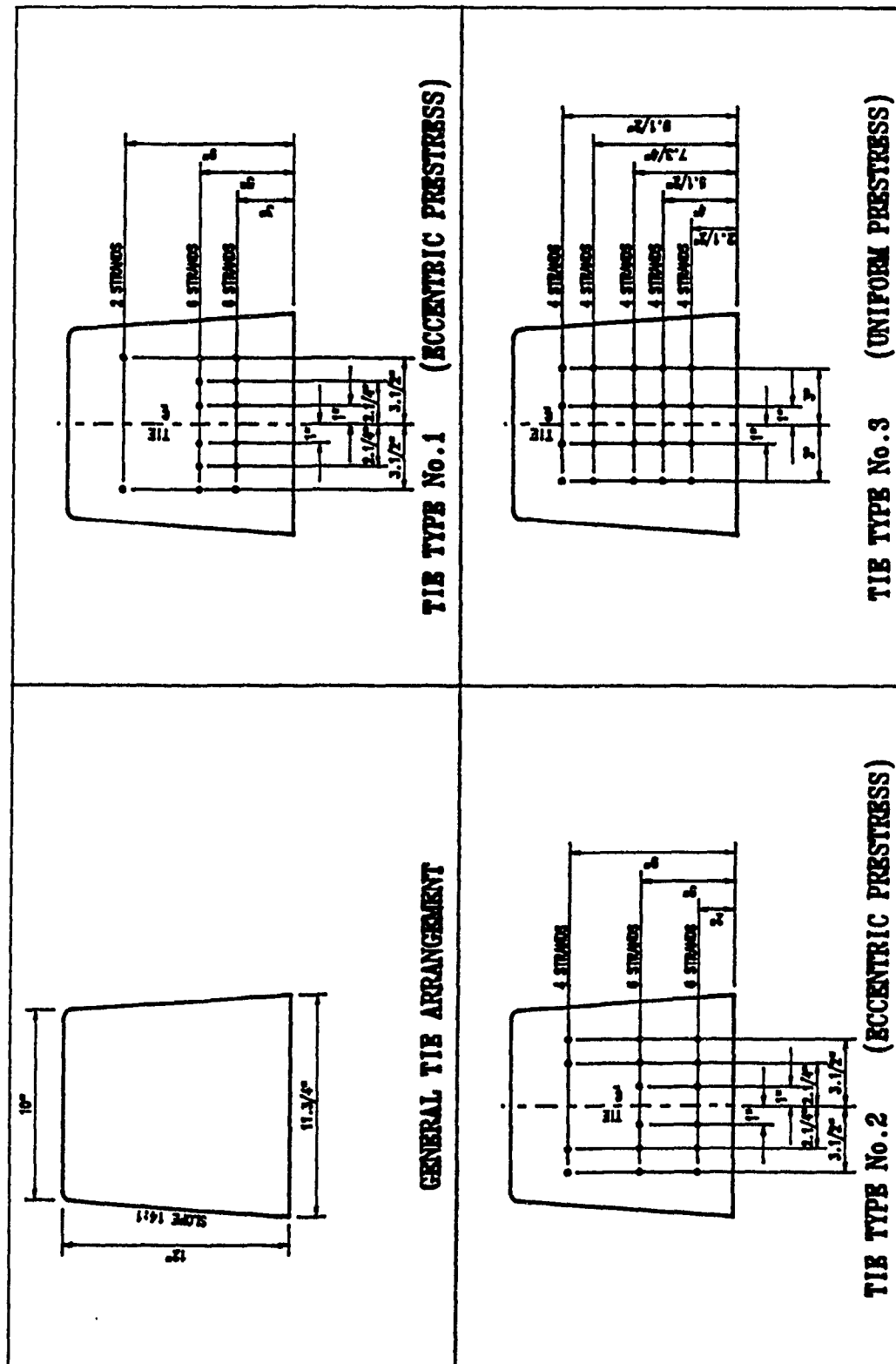
Figure 6.4 Comparison of Various Tie Cross Sections
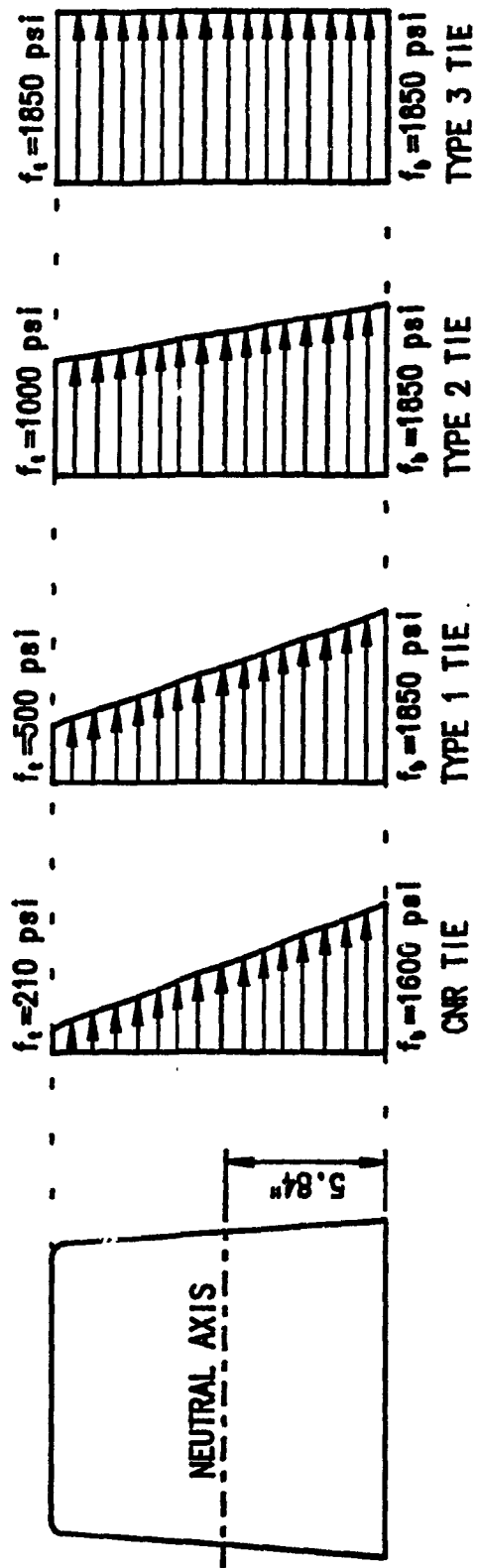
Figure 6.5 Comparison of Effective Prestress Levels in Various Ties
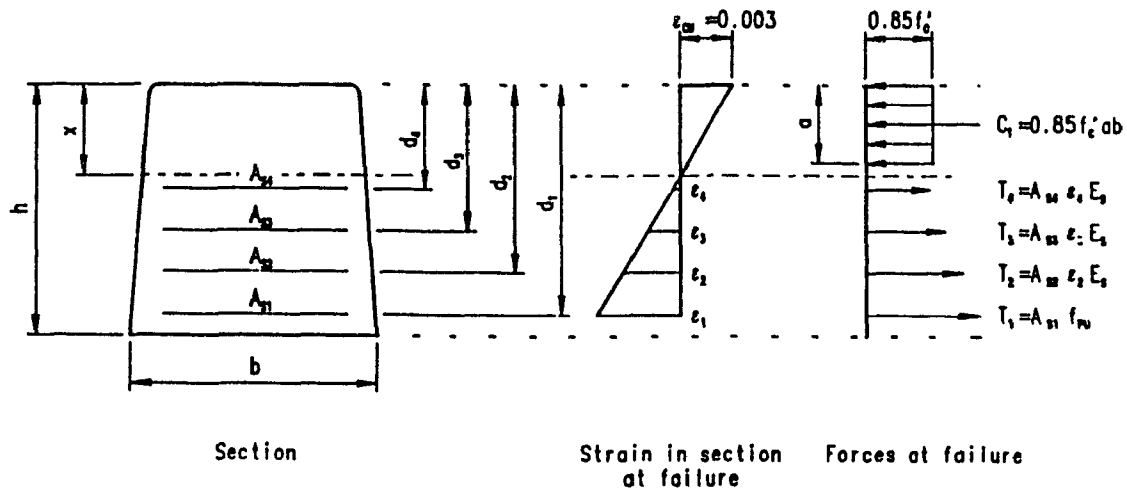
Figure 6.6 Stress - Strain Compatability Diagram

From the above diagram the following is obtained:

f_{se} = effective prestress in steel after losses

f_{se} = 155,440 / 14 x 0.085 = 130,622 psi (900.6 MPa)

$$e_{se} = \frac{f_{se}}{E_s} = \frac{130,622}{29,000,000} = 0.0045$$

$$e_{su} = \frac{f_{pu}}{E_s} = \frac{270,000}{29,000,000} = 0.0093$$

From the placement of strand within the tie the following can be determined:

d_1 = 9" (229 mm), d_2 = 7" (178 mm) and d_3 = 3" (76 mm)

Assume the balanced case where concrete ruptures as the steel yields, and solve for X_{max}, where:

$$a = 0.80\ X_{max}$$

$$X_{max} = \frac{e_{cu}\ d_1}{e_1 + e_{cu}}$$

Where: $\epsilon_1 = \epsilon_{psi} - \epsilon_{se} = 0.0093 - 0.0045 = 0.0048$

and $\epsilon_{cu} = 0.003$

$$X_{max} = \frac{(0.003)(9)}{0.0048 + 0.003}$$

$$X_{max} = \frac{(0.003)(9)}{0.0048 + 0.003}$$

$$X_{max} = 3.46"\ (87.9\ mm)$$

Now assume that the steel fails first:

$$\epsilon_2 = \frac{e_2\ (d_2 - x)}{(d_1 - x)} = 0.0048\ \frac{(7 - x)}{(9 - x)}$$

$$\epsilon_3 = \frac{-e_1\ (d-3 - x)}{(d_1 - x)} = -0.0048\ \frac{(3 - x)}{(9 - x)}$$

$$T_1 = A_{s_1}\ f_{pu} = (6\ x\ 0.085)\ x\ 270,000 = 137,700\ lbs\ (612.5\ kN)$$

$$T_2 = A_{s_2}\ f_{pu}\ (\epsilon_2/\epsilon_1) = 6\ x\ 0.085\ x\ 270,000\ \left(\frac{7 - x}{9 - x}\right)$$

$$T_2 = 137,700\ \left(\frac{7 - x}{9 - x}\right)$$

$$C_1 = 0.085\ f_c'\ a\ b$$

set $a = 0.8x$ and $b = 10"\ (25\ mm)$

$$C_1 = 0.85\ x\ 6,000\ x\ (0.8x)\ x\ 10$$

$$C_1 = 40,800\ x$$

(

$$C_2 = A_{s_3} (-\epsilon_3/\epsilon_1) = 2 (0.085) \, 270{,}000 \left(\frac{3 - x}{9 - x} \right)$$

$$C_2 = -45{,}900 \left(\frac{3 - x}{9 - x} \right)$$

Collecting terms yields:

$$T_1 + T_2 = C_1 + C_2$$

Therefore:

$$137{,}700 + 137{,}700 \left(\frac{7 - x}{9 - x} \right) = 40{,}800x - 45{,}900 \left(\frac{3 - x}{9 - x} \right)$$

Solving the above by use of the quadratic equation yields:

x = 4.29" (109.0 mm)

but $x > X_{max}$ (ie 4.29" > 3.46")

Therefore use $x = X_{max} = 3.46$" (87.9 mm)

Now substitute $X_{max} = 3.46$ (87.9 mm) to obtain:

$$\epsilon_2 = \epsilon_1 \left(\frac{d_2 - X_{max}}{d_1 - X_{max}} \right) = \epsilon_1 \left(\frac{7 - 3.46}{9 - 3.46} \right)$$

$$\epsilon_2 = 0.639 \epsilon_1$$

$$\epsilon_3 = \epsilon_1 \left(\frac{d_3 - X_{max}}{d_1 - X_{max}} \right) = \epsilon_1 \left(\frac{3 - 3.46}{9 - 3.46} \right)$$

$$\epsilon_3 = -0.083 \epsilon_1$$

Solving for T_1, T_2, C_1 and C_2 in terms of f_{s1} yields:

$T_1 = A_{s1} \, f_{s1} = 6 \, (0.085) \, f_{s1} = 0.510 \, f_{s1}$

$T_2 = A_{s2} \, f_{s1} \, (\epsilon_2/\epsilon_1) = 6 \, (0.085) \, (0.639) \, f_{s1} = 0.326 \, f_{s1}$

$C_1 = 0.85 \, f_c' \, a \, b$

$C_1 = 0.85 \, (6{,}000) \, (0.80 \times 3.46) \, (10.0) = 141{,}168 \text{ lbs } (627.9 \text{ kN})$

$C_2 = A_{s3} \, f_{s1} \, (\epsilon_3/\epsilon_1) = 2 \, (0.085) \, (0.083) \, f_{s1}$

$C_2 = 0.014 \, f_{s1}$

Collecting terms and solving for f_{si} yields:

$T_1 + T_2 = C_1 + C_2$

$0.510 \, f_{s1} + 0.326 \, f_{s1} = 141,168 + 0.014 \, f_{s1}$

$f_{s1} = 171,737$ lbs (763.9 kN)

Therefore:

$T_1 = 87,586$ lbs (389.6 kN)

$T_2 = 55,986$ lbs (249.0 kN)

$C_1 = 141,168$ lbs (627.9 kN)

$C_2 = 2,404$ lbs (10.7 kN)

Now by taking moments about T_1 the ultimate capacity of the tie can be obtained.

$\Sigma \, M_{T1} - 0$

$M_u - C_1 \, (d_1 - a/2) + C_2 \, (d_1 - d_3) - T_2 \, (d_1 - d_2)$

$M_u - 141,168 \left(9 - \left(\dfrac{2.77}{2}\right)\right) + 2,404 \, (9 - 3) - 55,986 \, (9 - 7)$

$M_u - 977,446 \; in - lbs$ (110.5 kN-m)

But $M_u = 18 \, P_u$

Therefore: $P_u = 54.3$ kips (241.5 kN)

6.5 ULTIMATE MOMENT CAPACITY OF THE TYPE 2 AND TYPE 3 TIES

The ultimate moment capacity of the Type 2 and Type 3 ties was calculated in a similar manner to that of the Type 1 tie. In addition the ultimate moment capacity of the ties was also calculated for the ties in the inverted position (subjected to rebound). The ultimate moment capacity of all three tie types

in both the right-side up and inverted positions is summarized in Table 6.2.

6.6 CRACKING MOMENT OF THE TYPE 1 TIE

In order to determine the cracking moment of the tie, it is necessary to convert the prestressing strand to an equivalent concrete area, such that:

$A_T = A_c + A_s (n - 1)$

Where: n = modular ratio = E_s/E_c and

$E_c = 57,000 \sqrt{f_c'}$

$E_s = 29 \times 10^6 \; Psi$ (200 kPa)

$A_T = 130.5 + 14(0.085) \left(\dfrac{29 \times 10^6}{4.42 \times 10^6} - 1 \right)$

$A_T = 130.5 + 6.62$

$A_T = 137.12 \; in^2 \; (88,470 \; mm^2)$

$A_i = 137.12 - \dfrac{d \, (b + b_1)}{2}$

Assume that the height of the tie remains constant at 12" (304.8 mm) and that the effect of the steel is uniformly distributed over the width of the tie.

Therefore:

$137.12 = 12 \left(\dfrac{b + b_1}{2} \right)$

so b + b$_1$ = 22.85" (580 mm)

111

22.85 - 21.75 = 1.10" (28 mm)

1.10/2 = 0.55" (14 mm) top and bottom

b = 10 + 0.53 = 10.53" (268 mm)

substituting and solving for I_T yields:

$$I_T = d^3 \; \frac{(b^2 + 4bb_1 + b_1^2)}{36 \; (b + b_1)}$$

I_T = 1,642 in^4 (683.45 x 10^6 mm^4)

Volume of tie $= \dfrac{130.50}{144} \; x \; 12 = 10.88 \; ft^3 \; (0.31 \; m^3)$

weight of concrete = 150 lbs / ft^3 (2,400 kg/m^3)

Therefore, the tie weighs 1,632 lbs (7.3 Kn)

M_{self} = 816 ft - lbs (1.1 kN-m) (for tie supported on a 8 ft

(2.44 m) span)

Top fibre stress due to prestress and self weight only is:

$$f_{t_{self}} = \frac{155,440}{130.50} - \frac{155,446 \; (1.13) \; (6.16)}{1,642} + \frac{(816 \; x \; 12) \; (6.16)}{1,642}$$

$f_{t_{self}}$ = 569 *psi* (3.9 *MPa*) *compression*

Bottom fibre stress due to prestress and self weight only is:

$$f_{b_{self}} = \frac{155,440}{130.50} + \frac{155,400 \; (1.13) \; (5.84)}{1,642} - \frac{(816 \; x \; 12) \; (5.84)}{1,642}$$

$f_{b_{self}}$ = 1781 *psi* (12.3 *MPa*)

The modulus of rupture for concrete is given as:

$f_r = 7.5 \; \sqrt{f_c'}$

f_r = 580 psi (2.58 MPa)

The cracking moment for both the upright and the inverted

tie (supported on a 8 ft (2.44 m) span and loaded on a 5 ft

(1.52 m) span) can now be calculated from the following:

$$M_{cr_{pos}} = \left(\frac{f_r + f_b}{Y_b} \right) I_T$$

$$M_{cr_{pos}} = \frac{(580 + 1,781)}{5.84} \; 1,642$$

$$M_{cr_{pos}} = 663,829 \; in - lbs \; (75.0 \; kN\text{-}m)$$

$$M_{cr_{pos}} = 18 \; P_{cr}$$

$$P_{cr} = 36,879 \; lbs \; (164.0 \; kN)$$

$$P_{cr} = 36.8 \; kips \; (164.0 \; kN)$$

$$M_{cr_{neg}} = \left(\frac{f_r + f_t}{Y_t} \right) I_T$$

$$M_{cr_{neg}} = \left(\frac{580 + 569}{6.16} \right) 1642$$

$$M_{cr_{neg}} = 306,276 \; in - lbs \; (34.6 \; kN\text{-}m)$$

$$M_{cr_{neg}} = 18 \; P_{cr}$$

$$P_{cr} = 17,015 \; lbs \; (75.7 \; kN)$$

$$P_c = 17.0 \; kips \; (75.7 \; kN)$$

6.7 CRACKING MOMENTS FOR THE TYPE 2 AND 3 TIES

The cracking moment for both the Type 2 and the Type 3 tie were calculated in a similar manner as the Type 1 tie. The values have been summarized in Table 6.2.

TIE TYPE	1	2	3
$M_{cr\ pos}$ (in.k)	663.8	780.2	966.0
$P_{cr\ pos}$ (kips)	36.8	43.3	53.7
$M_{cr\ neg}$ (in.k)	306.3	333.5	391.5
$P_{cr\ neg}$ (kips)	17.0	18.5	21.7
$M_{u\ pos}$ (in.k)	977.5	1267.6	1156.5
$P_{u\ pos}$ (kips)	54.3	70.4	64.3
$M_{u\ neg}$ (in.k)	622.0	782.9	956.0
$P_{u\ neg}$ (kips)	34.6	43.5	53.1

TABLE 6.2 CRACKING AND ULTIMATE CAPACITY FOR TIE TYPES

6.8 CALCULATION OF SPLITTING FORCE

In order to determine the shear strength of the ties the method outlined in Figure 6.7 has been used. This method will be used to determine if the ties will fail in flexure or shear.

TYPE 1 TIES

$$f_{tc} = \frac{V}{ba} = \frac{54,300}{10.88 \times 18} = 277\ psi\ (1.91\ MPa)$$

$$f_{ct} = \frac{Va}{bh^2} = \frac{54,300}{10.88 \times (12)^2} = 624\ psi\ (4.30\ MPa)$$

114
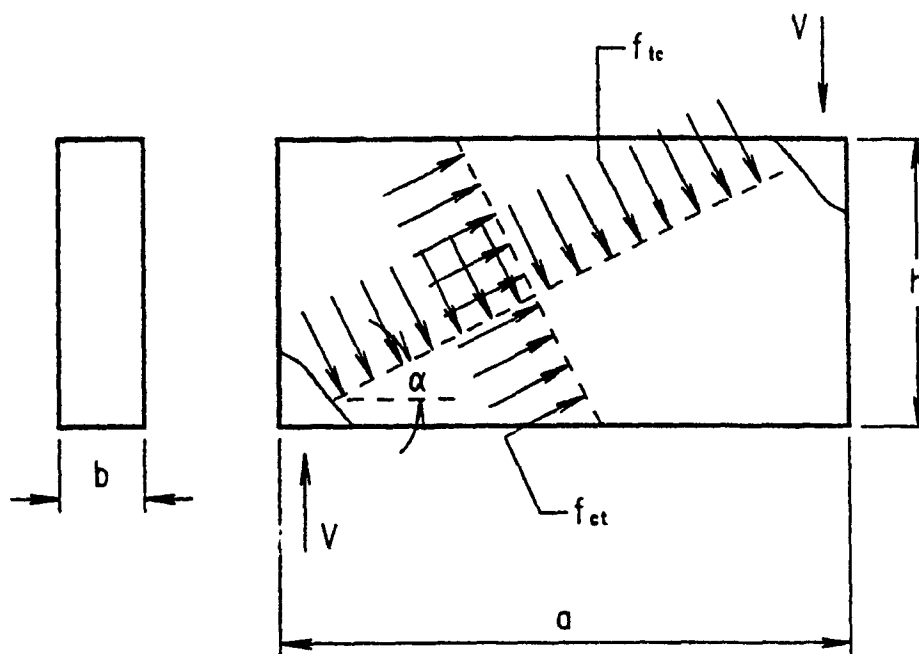
$$TAN \ \alpha = h/a$$

$$f_{tc} = \frac{V}{ba}$$

$$f_{ct} = \frac{Va}{bh^2}$$

$$\frac{f_{ct}}{f_{tc}} = \frac{a^2}{h^2}$$
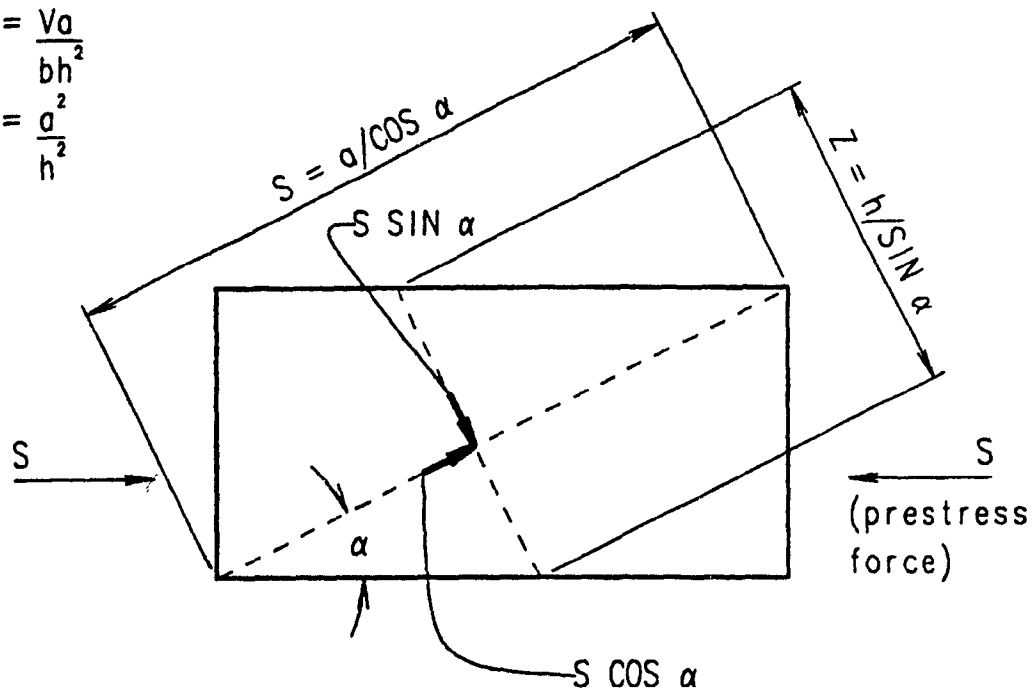
Figure 6.7   Diagram of Splitting Forces

115

$$P_{eff} = 155,420 \ lbs \ (691.3 \ kN)$$

$$S = a^2 + h^2 = 18^2 + 12^2 = 468 \ psi \ (3.2 \ MPa)$$

$$f_{cts} = P_{eff} \frac{a}{S^2 \ h} = \frac{155,420 \times 18}{468 \times 12} = 498 \ psi \ (3.5 \ MPa)$$

$$f_{tcs} = \frac{P_{eff} \ h}{b \ S^2} = \frac{155,420 \times 12}{10.88 \times 468} = 366 \ psi \ (2.5 \ MPa)$$

$$f_c = f_{ct} + f_{cts} = 624 + 498 = 1,122 \ psi \ (7.7 \ MPa) \ tension$$

$$f_t = f_{tc} - f_{tcs} = 277 - 366 = -89 \ psi \ (0.6 \ MPa) \ compression$$

$$f_{to} = 0.08 \ f_c' = 480 \ psi \ (3.3 \ MPa)$$

$$f_c = f_c'\left(1 - \frac{f_t}{f_{to}}\right)$$

$$f_c = 6,000 \left(1 - \frac{-89}{480}\right) = 7,112.5 \ (49.0 \ MPa)$$

use the lessor of f_c' or f_c

$f_c' < f_c$ therefore   use f_c'

$V_{split} = f_c' \ hb$

$V_{split} = 6,000 \ (12) \ (10.88)$

$V_{split} = 783 \ kips \ (3,484 \ kN)$

TYPE 2 TIES

$$P_{eff} = 187,126 \ lbs \ (8.32 \ kN)$$

$$f_{tc} = \frac{V}{ba} = \frac{70,400}{(10.88) \ (144)} = 809 \ psi \ (2.5 \ MPa)$$

$$f_{ct} = \frac{Va}{bh^2} = \frac{70,400 \times 18}{(10.88)\ (144)} = 809\ psi\ (5.6\ MPa)$$

$$s = A^2 + h^2 = 468\ in^2\ (0.30\ m^2)$$

$$f_{cts} = P_{eff}\ \frac{a}{s^2\ h} = \frac{187,126 \times 18}{468 \times 12} = 600\ psi\ (4.1\ MPa)$$

$$f_{tcs} = \frac{P_{eff} \times h}{b\ s^2} = \frac{187,126 \times 12}{10.88 \times 468} = 441\ psi\ (3.0\ MPa)$$

$f_c = f_{ct} + f_{cts} = 809 + 600 = 1,409\ psi\ (9.7\ MPa)$ (tension)

$f_t = f_{tc} - f_{tcs} = 360 - 441 = -81\ psi\ (0.6\ MPa)$ (compression)

$f_{to} = 480\ psi\ (3.3\ MPa)$

$$f_c = f_c'\left(1 - \frac{f_t}{f_{to}}\right) = 6000\left(1 - \left(\frac{-81}{480}\right)\right)$$

$f_c = 7,012.5\ psi\ (48.3\ MPa)$.

$f_c > f_c'$ therefore use f_c '

$V_{split} = f_c'\ h\ b$

$V_{split} = 6,000\ (12)\ (10.88) = 783,360\ (3,484\ kN)$

$V_{split} = 783\ kips\ (3,484\ kN)$

TYPE 3 TIES

$P_{eff} = 241,046\ lbs\ (1,072.1\ kN)$

$$f_{tc} = \frac{V}{ba} = 64, \frac{300}{(10.88 \times 18)} = 328\ psi\ (2.3\ MPa)$$

$$f_{ct} = \frac{Va}{bh^2} = \frac{64,300 \times 18}{(10.88)\ (144)} = 739\ psi\ (5.1\ MPa)$$

$$s = 468\ in^2\ (0.30\ m^2)$$

117

$$f_{cts} = \frac{P_{eff}\ a}{s^2\ h} = \frac{241,046\ x\ 18}{(468)\ (12)} = 773\ psi\ (5.3\ MPa)$$

$$f_{tcs} = \frac{P_{eff}\ x\ h}{b\ s^2} = \frac{241,046\ x\ 12}{(10.88)\ (468)}$$

$f_{tcs} = 568\ psi\ (3.9\ MPa)$

$f_c = f_{ct} + f_{cts} = 739 + 773 = 1,512\ psi\ (10.4\ MPa)$

$f_t = f_{tc} - f_{tcs} = 328 - 568 = -240\ psi\ (1.7\ MPa)$

$f_{to} = 480\ psi\ (3.3\ MPa)$

$$f_c = f_c'\left(1 - \frac{f_t}{f_{to}}\right) = 6,000\left(1 - \frac{240}{480}\right)$$

$f_c = 9,000\ psi\ (62.0\ MPa)$

use $f_c' = 6,000\ psi\ (62.0\ MPa)$ as $f_c' < f_c$

$V_{split} = f_c'\ hb$

$V_{split} = 6,000\ (12)\ (10.88)$

$V_{split} = 783\ kips\ (3,484\ kN)$

6.9 CALCULATION OF EQUIVALENT IMPACT FACTOR

In order to compare the relative strength of this tie in terms of an impact factor a calculation of the equivalent impact factor has been undertaken.

Knowing that the bottom stress of the tie is 1,850 psi (12.8 MPa), the total applied moment was calculated from:

$$M_{total} = \frac{\sigma_b\ I}{Y_b}$$

$$M_{total} = \frac{1,850 \; x \; 1,560}{5.84}$$

M_{total} = 494,178 in-lbs (55.8 kN.m)

M_{total} = 494.18 in-k (55.8 kN.m)

M_{total} = M_{self} + M_{LL} + M_{sDl}

M_{self} = 9,792 in-lbs (1.1 kN.m)

M_{sDl} = 3,000 in-lbs (0.3 kN.m)

M_{sDl} + M_{self} = 9.79 + 3.0 = 12.79 in-k (1.4 kN.m)

494.18 - 12.79 = 481.39 in-k (54.4 kN.m)

but M_{LL} = 18 P_{LL}

P_{LL} = 26.74 kips (118.9 kN)

Consider a 263,000 lb (1,170 kN) railcar on 4 axles, which is equivalent to a 65,750 lb (301.4 kN) axle loading. The load is spread over 3 ties.

Therefore:

$$\frac{65,750}{2 \; x \; 3} = 10,958 \; lbs \; (48.7 \; kN)$$

26.74 = (10.96) (1 + I)

2.44 = (I + 1)

I = 144 percent

In terms of Cooper's E-80 loading:

M_{LL} = 13.33

26.73 - 13.33 (I + 1)

I = 100 percent

6.10 FATIGUE CRACKING MOMENT

The fatigue cracking moment of the concrete ties is

119

calculated in a similar manner to that given in section 2.9. The fatigue cracking moment (both positive and negative) for each type of tie is given as follows:

TYPE 1 TIE

Positive fatigue cracking moment:

$$M_f = \frac{f_b \times I}{Y_b} = \frac{1,850 \times 1,560}{5.84}$$

$M_f = 494.2$ in.K (55.8 kN.m)

Negative fatigue cracking moment:

$$M_f = \frac{f_t \times I}{Y_t} = \frac{500 \times 1,560}{6.16}$$

$M_f = 126.6$ in.K (14.3 kN.m)

TYPE 2 TIE

Positive fatigue cracking moment:

$$M_f = \frac{f_b \times I}{Y_b} = \frac{1,850 \times 1,560}{5.84}$$

$M_f = 494.2$ in.K (55.8 kN.m)

Negative fatigue cracking moment:

$$M_f = \frac{f_t \times I}{Y_t} = \frac{1,000 \times 1,560}{6.16}$$

$M_f = 253.3$ in.K (28.6 kN.m)

TYPE 3 TIE

Positive fatigue cracking moment:

$$M_f - \frac{f_b \times I}{Y_b} - \frac{1,850 \times 1,560}{5.84}$$

$M_f = 494.2$ in.K (55.8 kN.m)

Negative fatigue cracking moment:

$$M_f - \frac{f_t \times I}{Y_t} - \frac{1,850 \times 1,560}{6.16}$$

$M_f = 468.5$ in.K (52.9 kN.m)

6.11 ANALYSIS FOR DISTURBED REGIONS (END BLOCK ANALYSIS)

Analysis for the ties for several concentrated forces acting on a prismatic member indicated that the resultant tension splitting forces in the ties did not require application of stirrups.

However, to account for weaker than specified concrete or too early a release of the prestressing strand, it was decided to apply stirrups to the ties. This was done primarily to decrease the probability of bursting the ends of the ties and keep rejected ties to a minimum, especially since all ties were donated.

CHAPTER 7

TEST PROCEDURE FOR THE CONCORDIA TIES

7.1 TIE SPECIMENS

The prestressed concrete ties designed in Chapter 6 were fabricated in a single form at a precasting plant in Laval, Quebec. Six (6) full scale ties of each type were fabricated, for a total of 18 ties.

The tie specimens have been given designations in order to aid in their identification during the testing procedure and in the presentation of the results. The Type 1 ties have been designated by T1, while the six samples of this type have been sequentually numbered from B1 to B6. Therefore, the Type 1 ties have been designated T1B1 to T1B6.

Similarly, the Type 2 ties have been designated T2B1 to T2B6 and the Type 3 ties have been designated T3B1 to T3B6.

7.2 LOADING SYSTEM

The loading system consisted of simply supporting one end of the tie and roller supporting the other end at 8'- 0" (2.44 m) centre to centre and placing 2 - 0.2 in. (5mm) EVA tie pads and 2 - 132 lb. RE profile rails at standard railway gauge, 56.5" (1435 mm). The rails were approximately 12" (305 mm) long. Directly above the rails were two 120 kip (534 kN) ENERPAC RRH-6010 hydraulic jacks used for applying the loading. Immediately above one jack was a Strain-Sert 100 kip

(445 kN)) - 2 mv, 350 ohm compression load cell with a safety factor of 1.5, positioned below a load distribution beam. The load cell contained internal electrical resistance strain gauges connected to an Intertechnology P-3500 strain gauge box with an oscilliscope output to an HP 3852A Data Aquisition unit with an HP 310 Computer System.

The lateral movement of the ties was not prevented and the ties were allowed to rotate under the applied loading. This was because of the previously documented problems experienced by others performing like tests (8, 14) wherein the clamping systems failed under high loadings. Figure 7.1 illustrates the loading system used to test the ties.

7.3 INSTRUMENTATION

Two 125 ohm electrical resistance strain gauges were installed on the top and bottom vertical faces of the ties at midspan, in order to monitor the tie centre strains.

Three electrical linear velocity displacement transducers (LVDT's) were used to measure deflections of the ties at three locations. One gauge was placed directly above each of the supports of the ties and the third placed at the midspan of the tie.
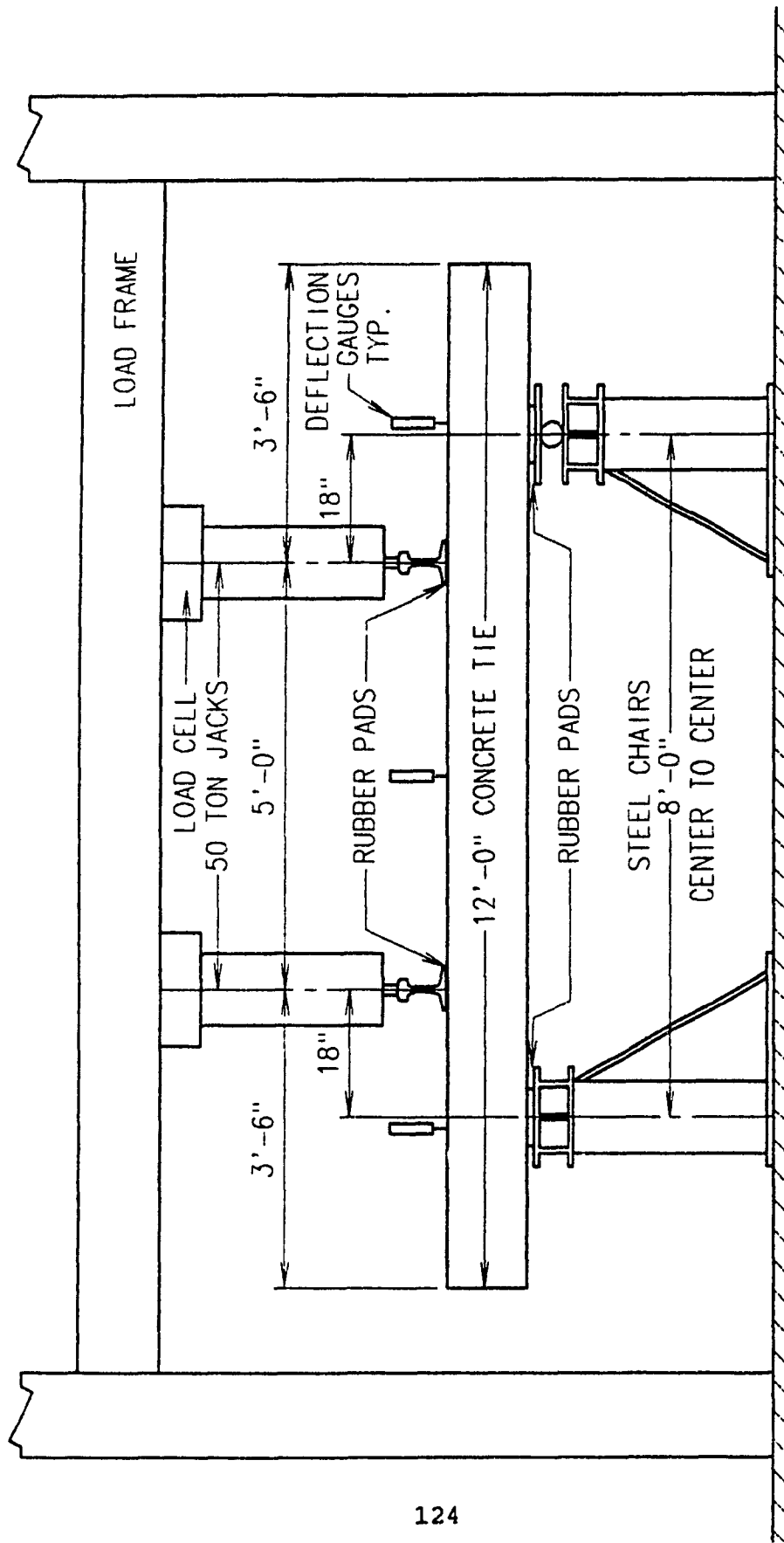
Figure 7.1 Loading System Used in Laboratory Testing of Ties

124

7.4 TESTING PROCEDURE

The ties were individually placed in the load frame as described in section 7.2 and illustrated in Figure 7.1.

The testing program consisted of subjecting the three types of ties to increasing static loading forces noting both cracking and ultimate loads. The test program was a compilation of three tests as outlined below:

TEST 1a - an inverted tie was loaded in increments approximately 5 kips (22.2 kN) until first cracking was achieved. The crack location along with the load causing cracking was clearly marked on the tie. Loading was continued. The cracks propagated approximately half way up through the tie. The propagation of the cracks was indicated on the tie at 5 kip (22.2 kN) intervals. Ties tested in this manner: T1B1, T1B4, T2B1, T3B1, T3B5 and T3B6.

TEST 1b - the tie from Test 1a was installed in the load frame right side up (in reverse from 1a) and loaded in approximately 5 kip (22.2 kN) increments until first cracking was reached. The location of first cracking and its magnitude was clearly marked on the tie. Loading continued in 5

kip (22.2 kN) intervals, with the propagation of cracks marked, until ultimate capacity was reached. Ties tested in this manner: T1B1, T1B4, T2B1, T3B1, T3B5 and T3B6.

TEST 2 –   An inverted tie was placed in the load frame and loaded in 5 kip (22.2 kN) increments until first cracking was reached. The location of first cracking and its magnitude was clearly marked on the tie. Loading continued in 5 kip (22.2 kN) intervals, with the propagation of cracks marked, until ultimate capacity was reached. Ties tested in this manner: T1B3, T2B3, T2B4 and T3B3.

TEST 3 –   a right side up tie was placed in the load frame and loaded in 5 kip (22.2 kN) increments until first cracking was reached. The location of first cracking and its magnitude was clearly marked on the tie. Loading continued in 5 kip (22.2 kN) intervals, with the propagation of cracks marked, until ultimate capacity was reached. Ties tested in this manner: T1B5, T2B2, T2B5, T3B2 and T3B4.

In total 16 of the 18 ties fabricated were tested to destruction. The remaining two have been retained for future tests.

7.5 CONCRETE STRENGTH

The specified 28 day compressive strength of the concrete to be used in the ties was set at 6,000 psi (41.4 MPa). In order to obtain the actual compressive strength of the concrete, 4" by 8" (101.6 mm by 203.2 mm) test cylinders were poured at the same time as the ties. These cylinders were tested on a Tinius Olsen compression machine.

The mean compressive strength of the concrete from cylinder testing was found to be 7,094 psi (48.9 MPa) with a standard deviation of 1,329 psi (9.2 MPa). Table 7.1 indicates the compressive cylinder strengths of the concrete for the ties tested.

TIE NO.	COMPRESSIVE STRENGTH psi	COMPRESSIVE STRENGTH MPa
T1B1	6876	47.43
T1B2	7018	48.39
T1B3	6724	46.36
T1B4	7054	48.64
T1B5	7616	52.51
T2B1	5761	39.72
T2B2	8005	55.19
T2B3	6520	44.96
T2B4	4646	32.03
T2B5	6565	45.27
T3B1	9390	64.74
T3B2	8937	61.62
T3B3	9554	65.87
T3B4	6027	41.56
T3B5	6433	44.36
T3B6	6382	44.00

Table 7.1 Summary of Concrete Compressive Strength - $f_{c'}$

7.6 PRESTRESSING STEEL

The prestressing strand used in the manufacture of the ties was seven wire strand of nominal diameter 3/8" (9.5 mm) and nominal area of 0.085 in.^{2} (55 mm^2). The ultimate tensile

strength of the strand is 270,000 psi (1,860 MPa).

The total prestressing force applied to each tie was measured at the precasting plant. Each strand was marked, pulled to the specified prestressing force with the amount of extension of each measured. Upon release of the prestressing jacks, the elongation in each strand was again measured. This last measurement was used in determining the total prestressing force applied to the ties.

The total elongation, after release of the jacks, was divided by the known jacking length (from anchoring bulkhead to anchoring bulkhead) to obtain the strain in each strand. The average strain for all the strands of a tie was taken and applied to the graph of the stress - strain curve, Figure 7.2, supplied by the tie manufacturer. From this an applied force per strand was obtained. The total applied force per tie was obtained by simply multiplying by the number of strands per tie.

The losses for creep and shrink of concrete were assumed as 15 percent. The total applied prestressing force was then multiplied by 0.85 to obtain the effective prestressing force per tie.

Table 7.2 indicates the actual prestressing force applied to

129
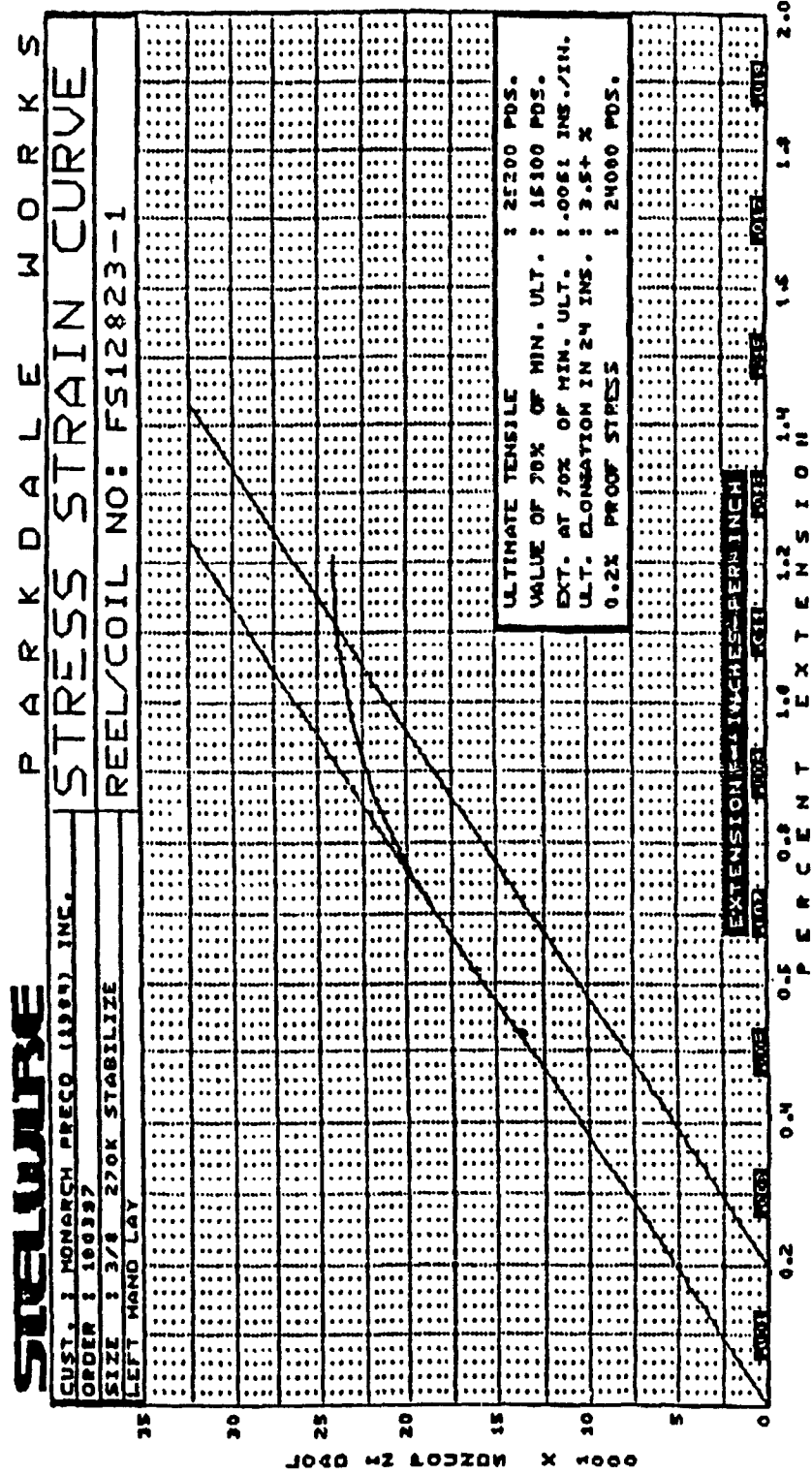
Figure 7.2   Stress - Strain Curve for 3/8" (9.5 mm) 7 Wire Strand

130

TIE NO	PRESTRESSING FORCE LBS.	PRESTRESSING FORCE kN
T1B1	160,650	714.6
T1B2	154,700	688.1
T1B3	154,700	688.1
T1B4	157,675	701.3
T1B5	164,220	730.4
T2B1	248,200	1,104.0
T2B2	248,200	1,104.0
T2B3	244,800	1,088.9
T2B4	234,600	1,043.5
T2B5	261,800	1,164.5
T3B1	289,000	1,285.5
T3B2	272,000	1,209.9
T3B3	272,000	1,209.9
T3B4	301,750	1,342.2
T3B5	280,500	1,247.7
T3B6	280,500	1,247.7

Table 7.2   Summary of Effective Prestressing Forces P_{eff}

each tie. The average effective prestressing force applied to the Type 1 ties was 158,389 lbs (704.5 kN); the Type 2 ties 247,520 lbs (1,101 kN) and the Type 3 ties 282,625 lbs (1,257.1 kN). As can be seen from Table 7.2, the effective prestressing force applied to each tie was consistent within each group.

CHAPTER 8

COMPARISON OF THEORETICAL AND
EXPERIMENTAL RESULTS FOR INDIVIDUAL TIES

8.1 GENERAL TEST OBSERVATIONS

The ties were individually loaded as outlined in Chapter 7.
As the load increased, first (flexural) cracking occurred in
all cases between the loaded rail locations. Thereafter as
the load increased new cracks began forming, which were fairly
uniformly distributed between the rails while the originally
occurring cracks propagated.

In all cases the ties cracked at a lower cracking moment, M_{cr},
than calculated. With further increase of the load, diagonal
cracks began to appear between the load point and support
(shear span). Shortly thereafter the ties failed.

Failure of the ties in all cases occurred with the crushing of
the concrete at the top of the tie in the rail seat area.
This flexural failure was brittle and tended towards being
termed explosive in nature.

All three types of ties exhibited similar cracking patterns.
Figure 8.1, 8.2 and 8.3, illustrates the cracking pattern of
the ties. The cracking pattern commenced with first cracking
which led to uniformly distributed flexural cracking,
flexural-shear cracks and finally diagonal shear cracks. In
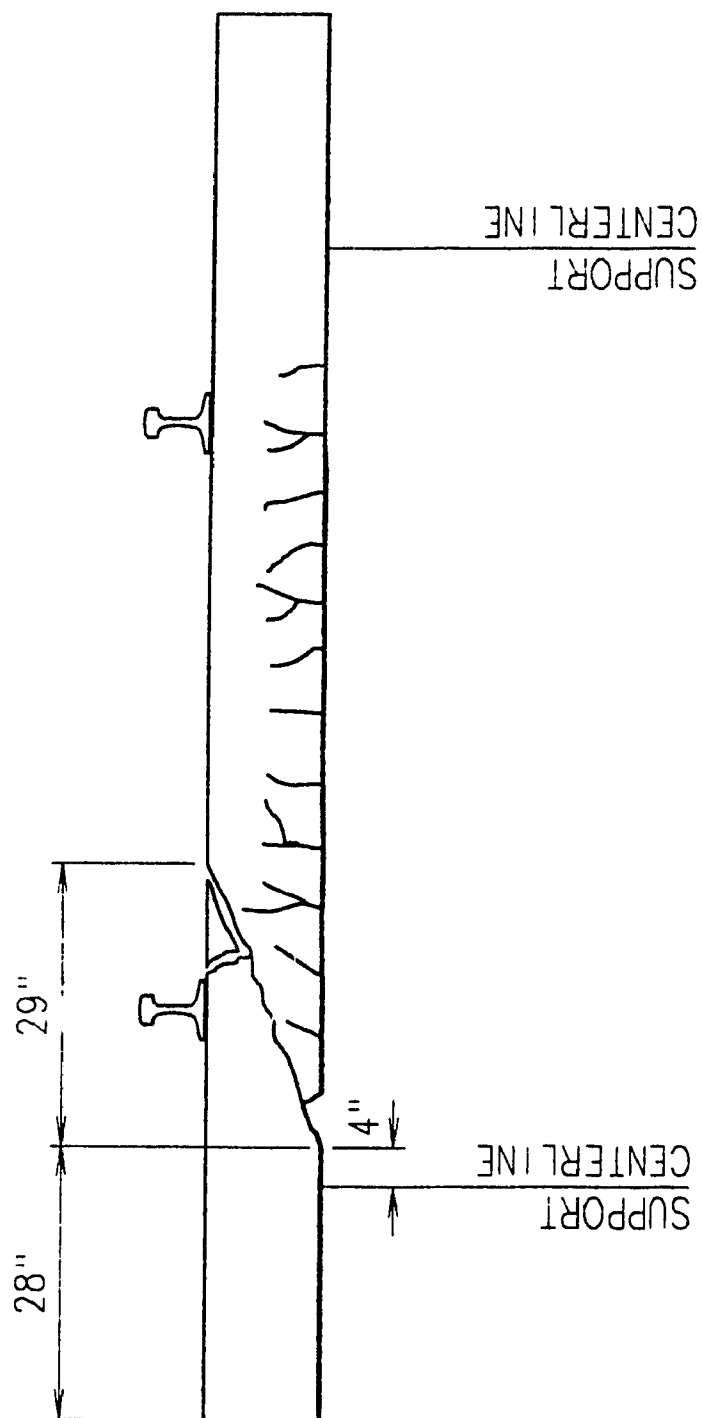
Figure 8.1 Diagram of Typical Failure Mode of a Laboratory Tested Tie
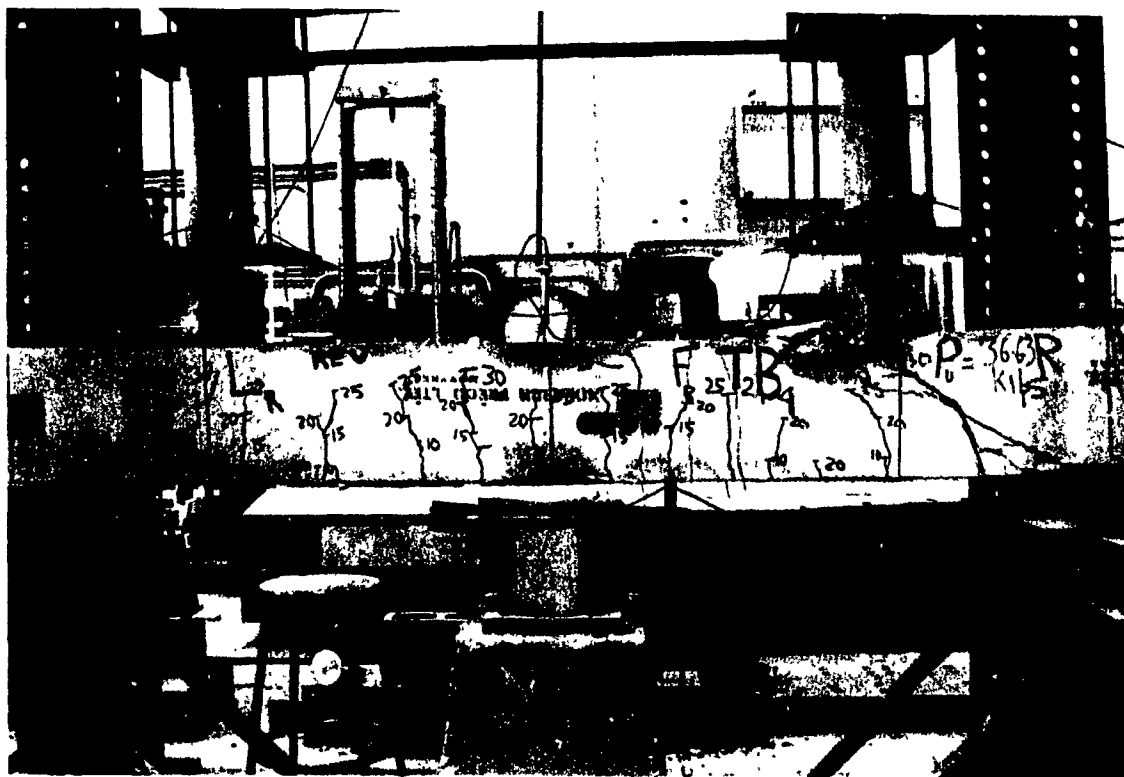
Figure 8.2   Failure Mode of Tie T2B4 Inverted Position

135
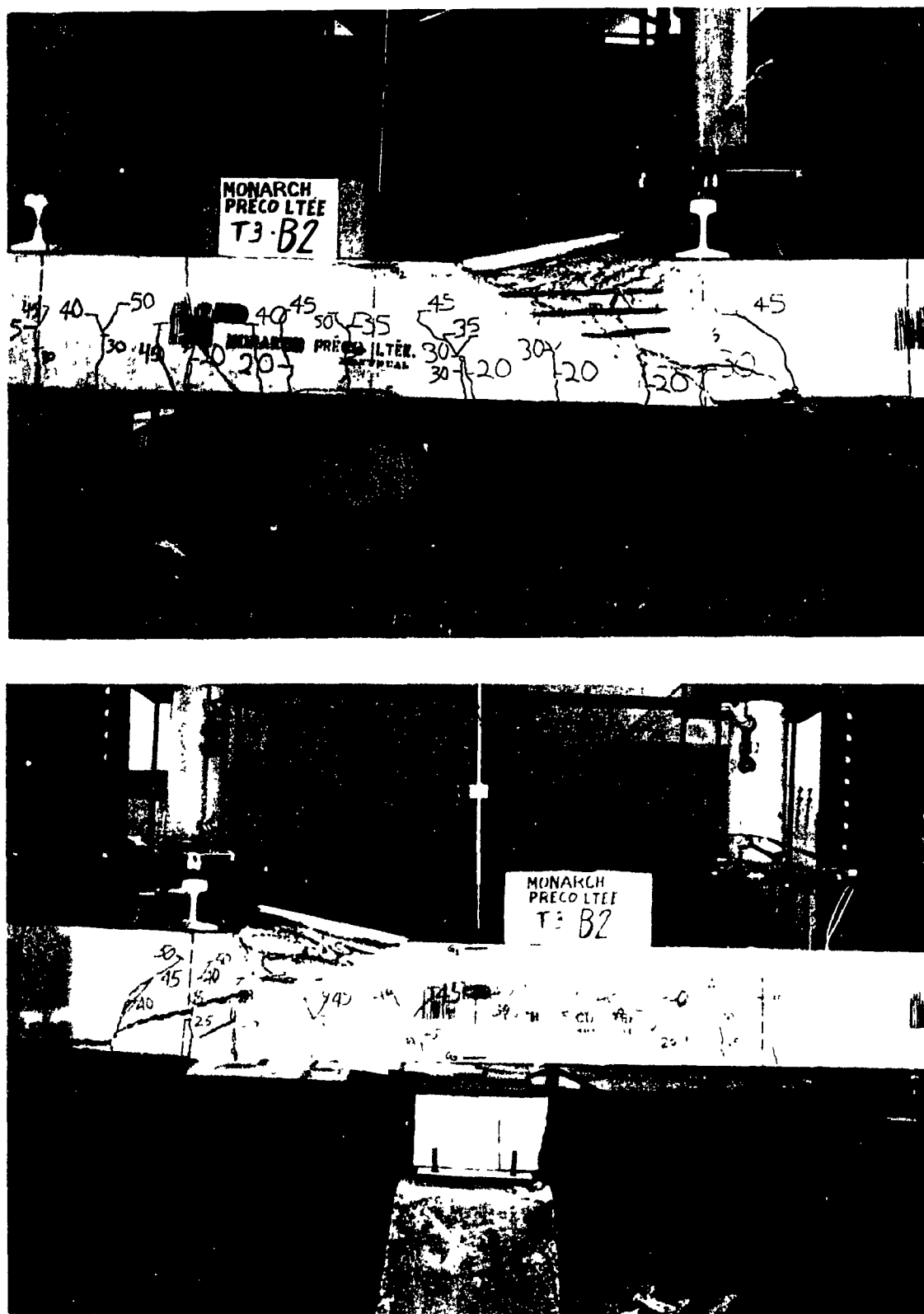
Figure 8.3   Failure Mode of Tie T3B2 Right Side up Position

136

all cases diagonal cracks appeared just prior to failure occurring.

8.2 LOAD-DEFLECTION

Load-deflection curves, for the midspan deflection, have been plotted for selected ties and are illustrated in Figures 8.4 to 8.10. From these graphs the energy absorption capacity of the individual ties can be obtained. The ability of the prestressed ties to resist impact can be measured by the amount of energy absorbed by the ties as they deflect under load. The elastic energy absorbed by the tie can be calculated by obtaining the area under the load-deflection curve up to the point of first cracking. The total energy that can be absorbed by the tie is calculated from the total area under the load-deflection curve up to the point of rupture.

According to the research studies (13), the load-deflection curves, obtained by static load tests, may be used to obtain the energy absorption capacity of the ties under dynamic loading. Therefore, load-deflection curves can be used as a measure of the impact resistance of the ties. Table 8.1 indicates both the elastic and total energy absorbed by each tie illustrated in Figures 8.4 to 8.10. The greater the ties' resilience, the greater impact resistance it will display.

137

LOAD–DEFLECTION CURVE
T1B2
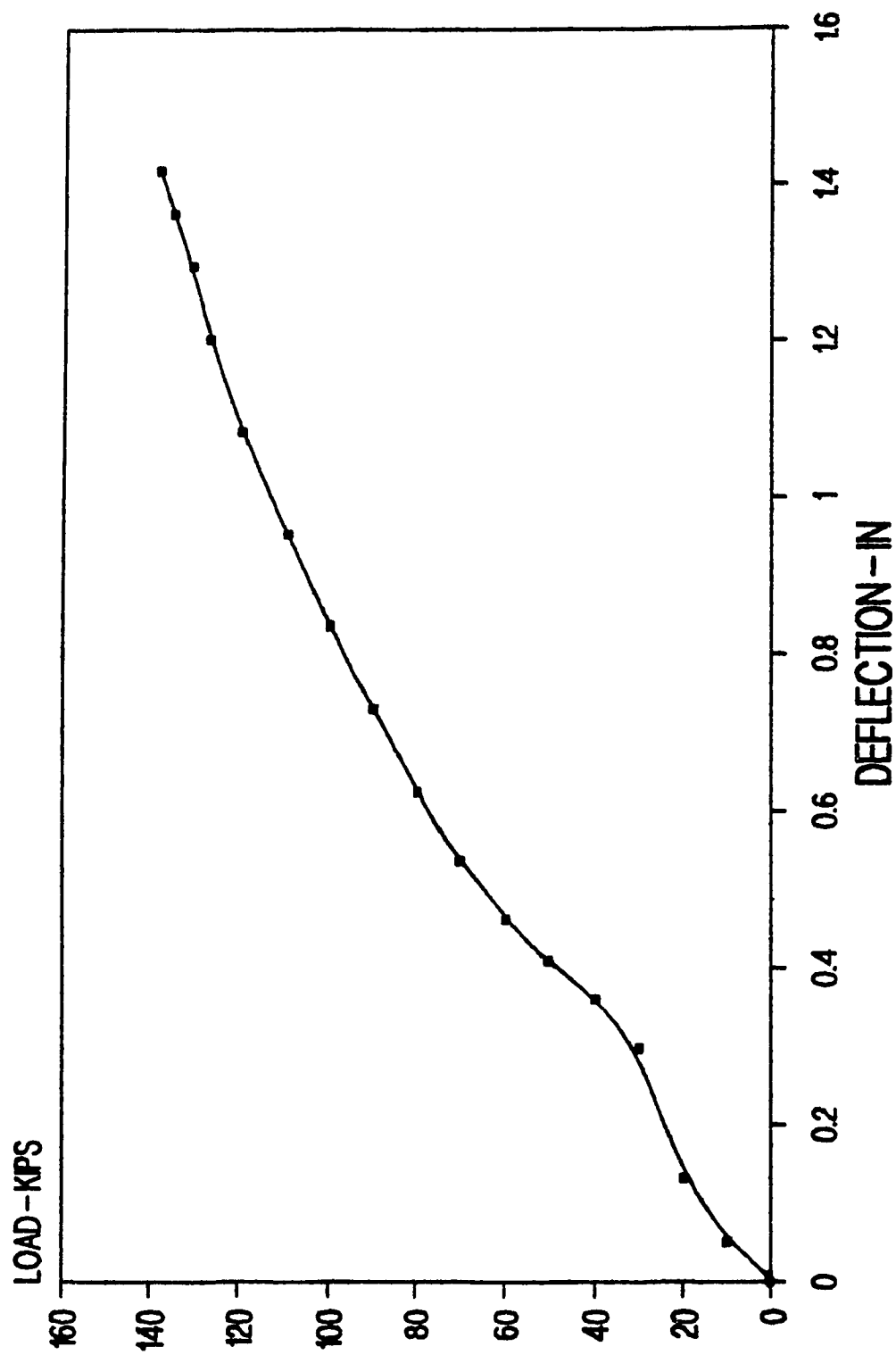
Figure 8.4 Load – Deflection Curve for Tie T1B2

LOAD-DEFLECTION CURVE
T1B3 INVERTED
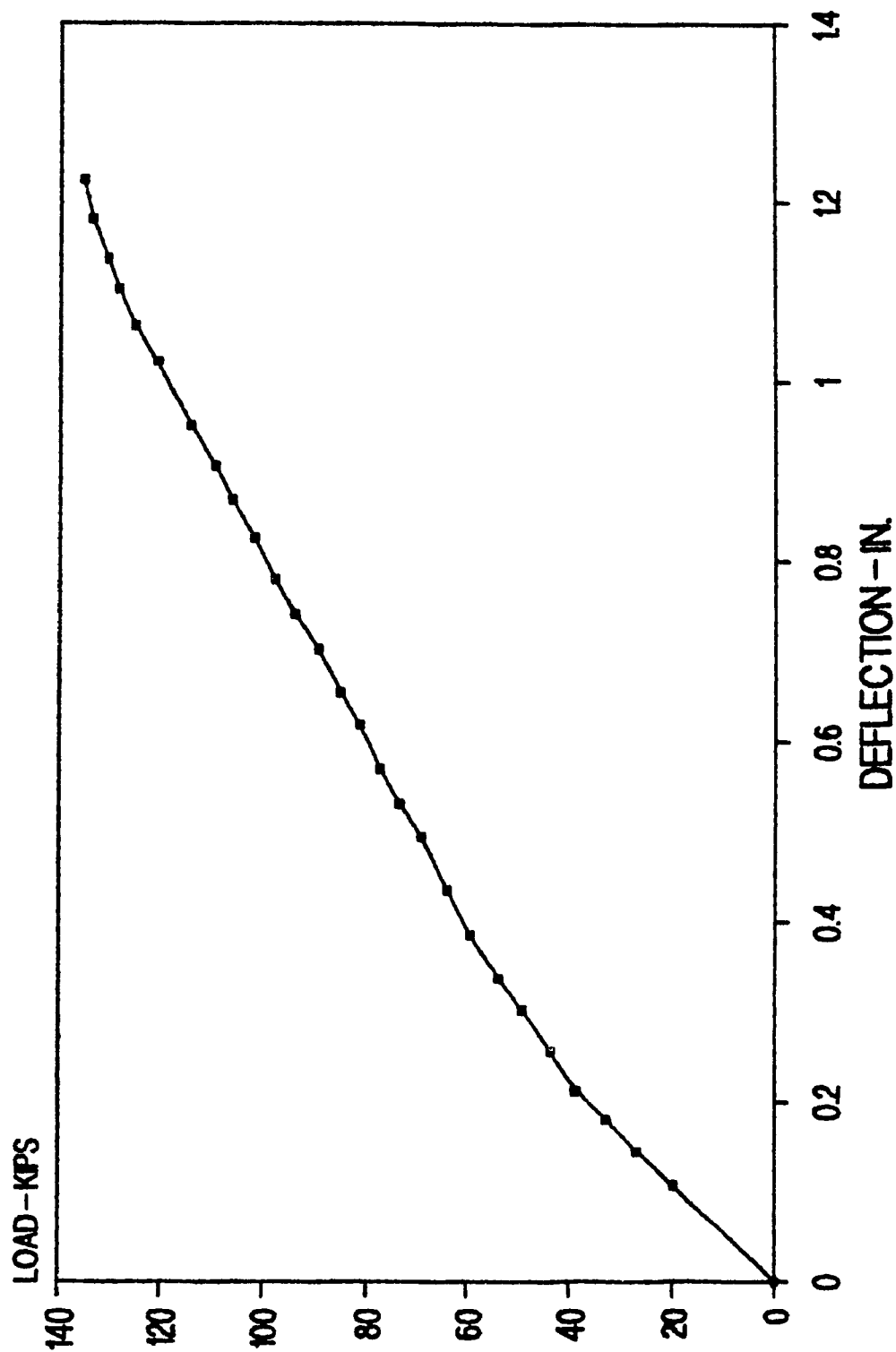
Figure 8.5 Load - Deflection Curve for Tie T1B3

LOAD-DEFLECTION CURVE
T2B1

LOAD-KIPS
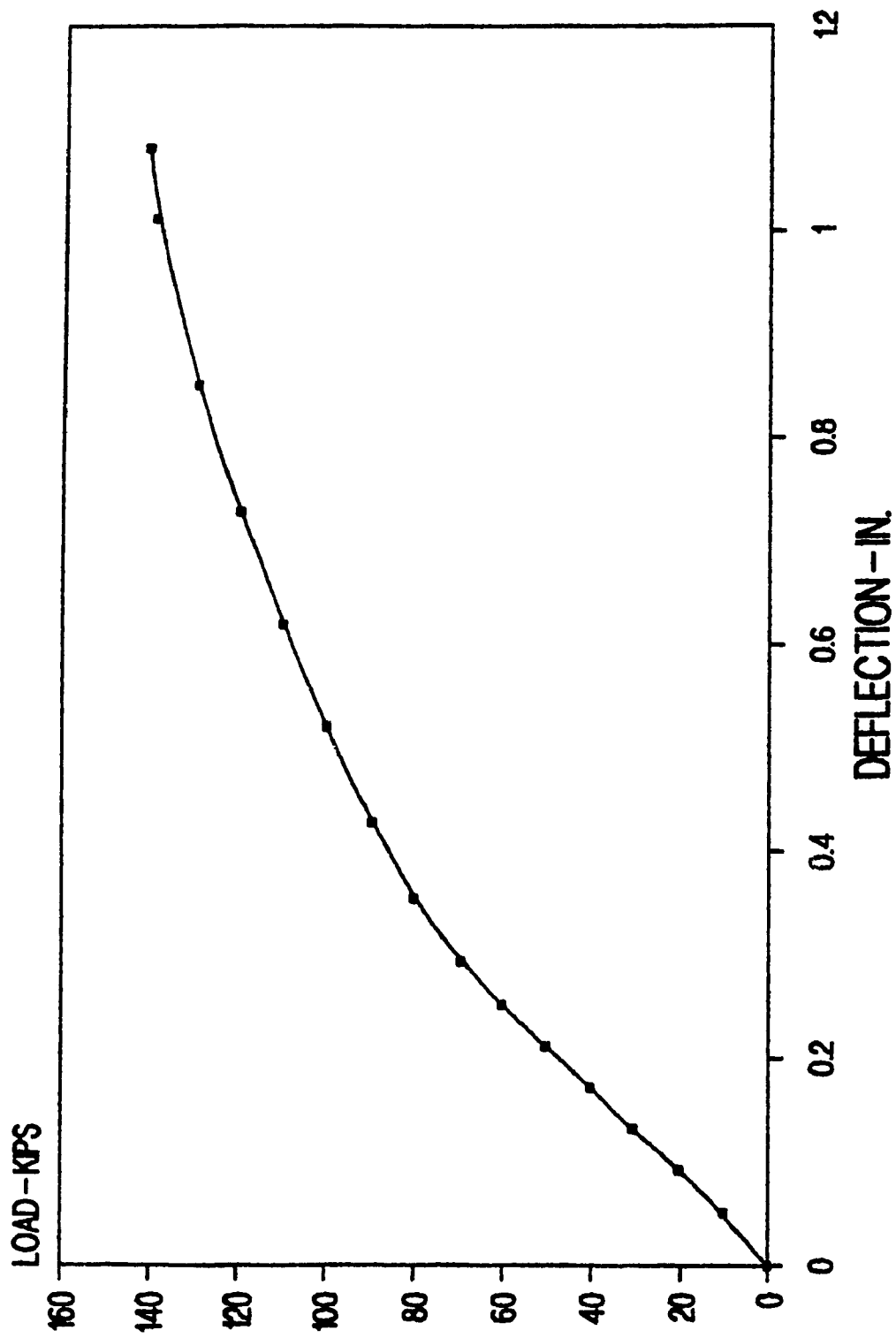
DEFLECTION-IN.

Figure 8.6 Load - Deflection Curve for Tie T2B1

LOAD-DEFLECTION CURVE
T2B2
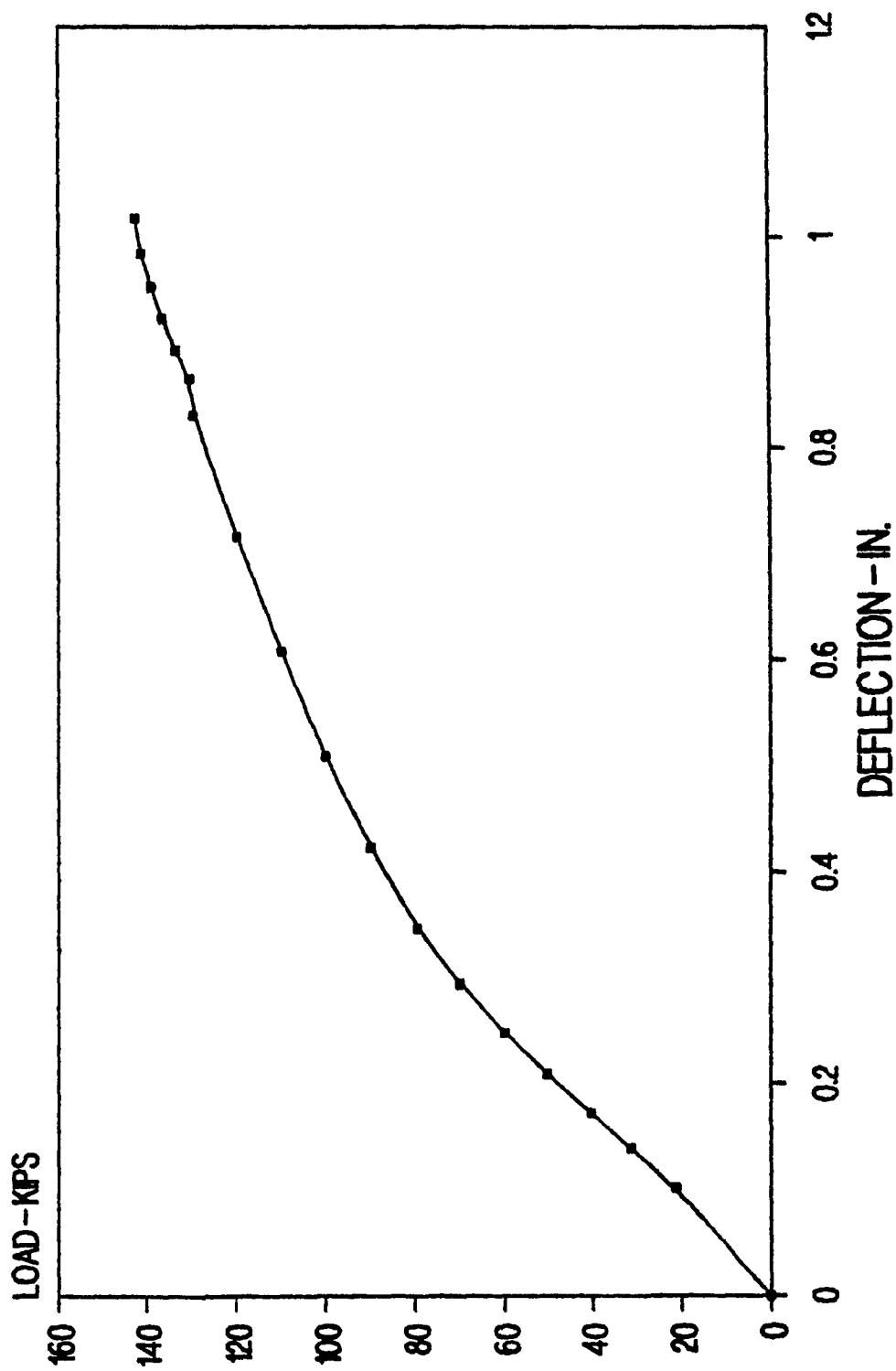
Figure 8.7 Load - Deflection Curve for Tie T2B2

LOAD-DEFLECTION CURVE
T2B3 INVERTED

LOAD-KIPS
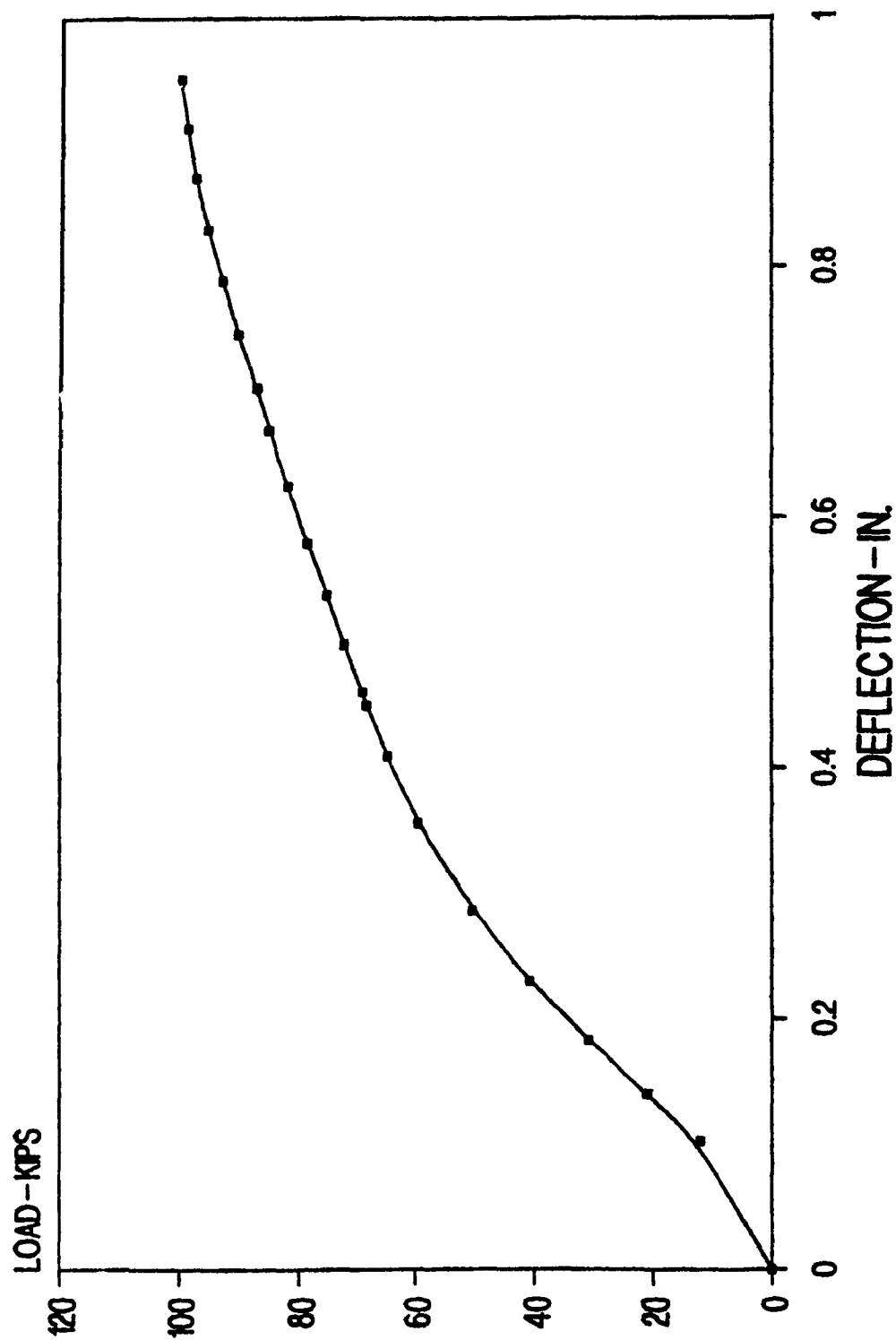
DEFLECTION-IN.

Figure 8.8 Load - Deflection Curve for Tie T2B3

142

LOAD-DEFLECTION CURVE
T3B1
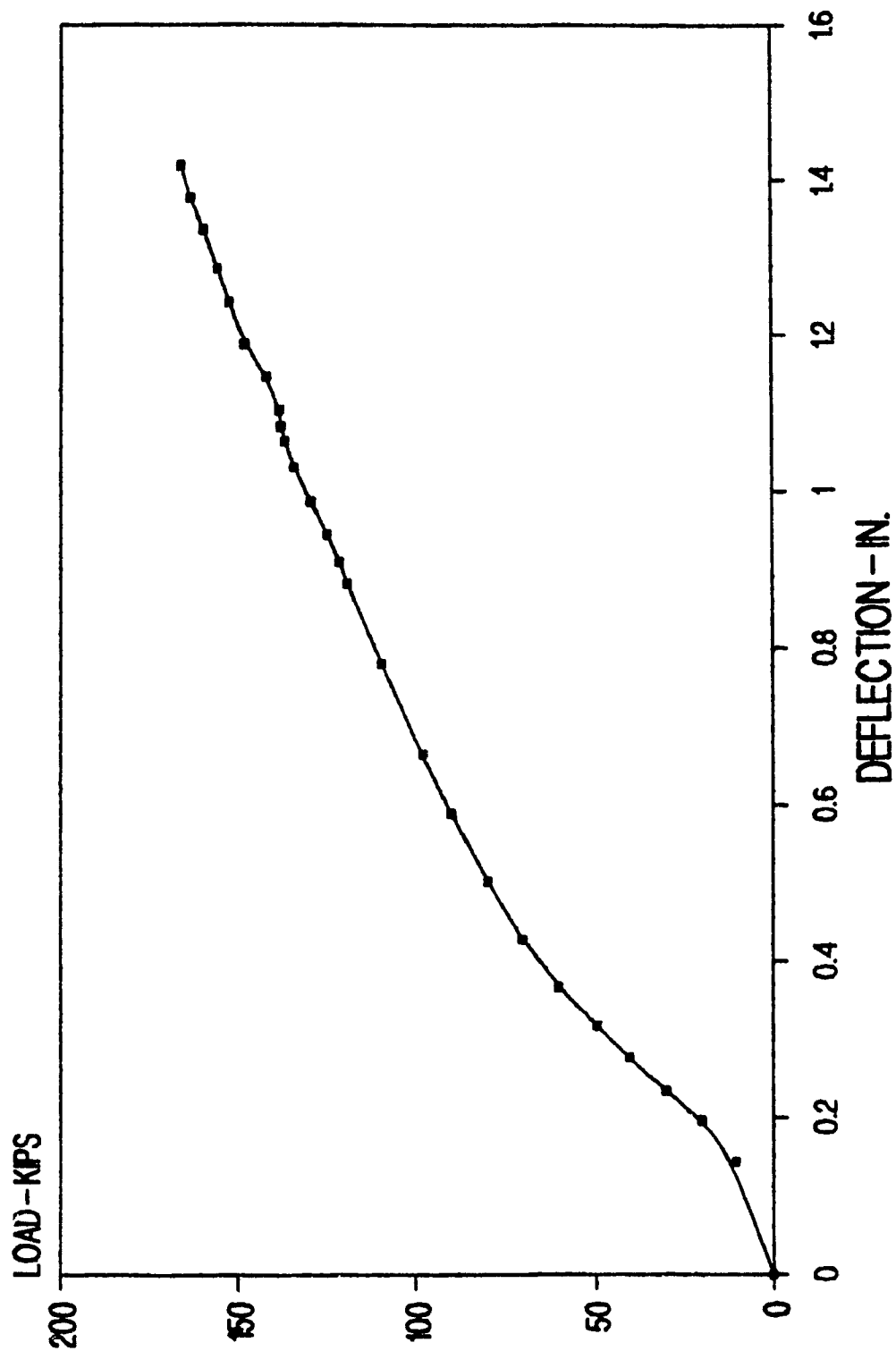
Figure 8.9 Load - Deflection Curve for Tie T3B1

LOAD–DEFLECTION CURVE
T3B2
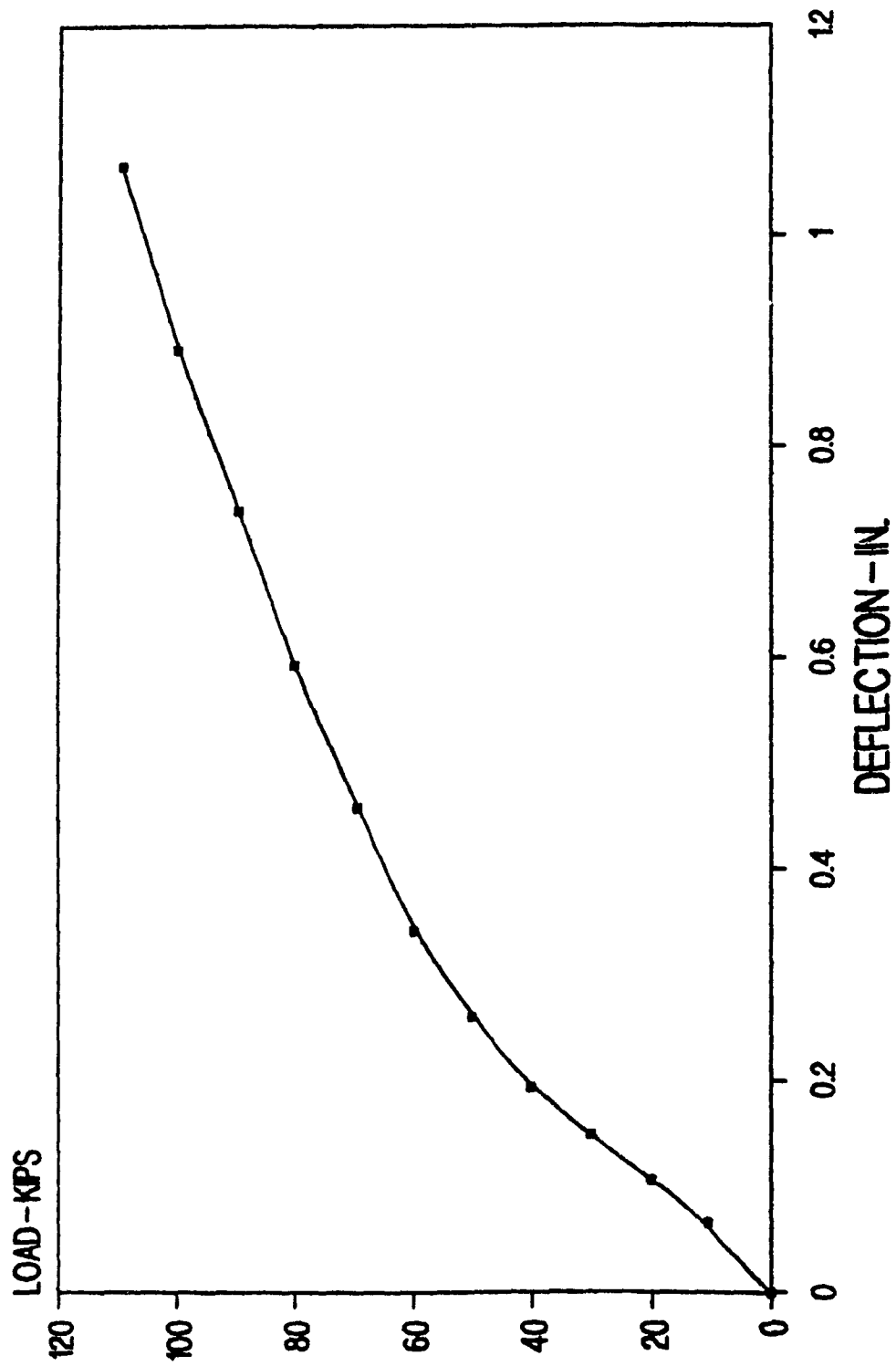
Figure 8.10 Load – Deflection Curve for Tie T3B2

144

TIE NO.	ELASTIC ENERGY		TOTAL ENERGY	
	in.-k	Kn.m	in.-k	kN.M
T1B2	8.83	1.00	62.14	7.02
T1B3	8.39	0.90	52.60	5.95
T2B1	6.58	0.75	48.18	5.44
T2B2	6.53	0.73	45.81	5.18
T2B3	1.71	0.19	30.06	3.39
T3B1	7.02	0.80	75.29	8.44
T3B2	2.47	0.28	36.96	4.18

TABLE 8.1 Elastic and Total Energy Absorption of Ties

The amount of ductility displayed in each beam was fairly consistent. The inverted ties generally showed less ductility than the ties tested in the normal position. From the results the Type 1 ties displayed the greatest energy absorbtion capability in both the inverted and normal positions.

8.3 COMPARISON OF CRACKING MOMENTS

Both the positive and negative theoretical cracking moment for each tie have been calculated by the method outlined in Chapter 6. These results have been compared to the actual cracking moments outlined by testing. Table 8.2 illustrates the comparison of the theoretical negative cracking moments with the experimental cracking moments. Table 8.3 illustrates the comparison of the theoretical positive cracking moments to

the experimental cracking moments.

The theoretical cracking moment calculation are by no means an exact figure, but rather give an estimation of the cracking moment. The cracking moment is most dependant on the stress state of the concrete, however, the cement mix, strength and size of aggregate and water cement ratio also have an influence.

TIE NO.	THEORETICAL CRACKING MOMENT		EXPERIMENTAL CRACKING MOMENT	
	in.K	kN.m	in.K	kN.m
T1B1	302	34.2	270	30.5
T1B3	296	33.4	270	30.5
T1B4	302	34.2	270	30.5
T2B1	510	57.6	270	30.5
T2B3	513	57.9	270	30.5
T2B4	478	54.0	180	20.3
T3B1	788	89.1	540	61.0
T3B3	755	85.3	450	50.9
T3B5	748	84.5	540	61.0
T3B6	747	84.4	630	71.2

TABLE 8.2 Comparison of Negative Cracking Moments

TIE NO.	THEORETICAL CRACKING MOMENT		EXPERIMENTAL CRACKING MOMENT	
	in.k	kN.m	in.k	kN.m
T1B1	682	77.1	540	61.0
T1B2	665	75.1	540	61.0
T1B4	675	76.3	360	40.7
T1B5	702	79.3	540	61.0
T2B1	819	92.6	630	71.2
T2B2	847	95.7	630	71.2
T2B5	866	97.9	720	81.4
T3B1	795	89.8	540	61.0
T3B2	755	85.3	360	40.7
T3B4	783	88.5	360	40.7
T3B5	745	84.2	540	61.0
T3B6	744	84.1	450	50.9

TABLE 8.3 Comparison of Positive Cracking Moments

Due to the variation in the compressive strength of the concrete in each tie, all experimental results have been divided by the compression strength of concrete in order to obtain comparative relative cracking data. Figure 8.11 illustrates the relationship between M_{cr}/bh^2fc' and the bottom fibre stress, f_b/f_c' for both the inverted and normal positions. These values are shown in Table 8.4.

TIE NO.	f_b/f_c'	$M_{cr}/(bh^2f_c')$
T1B1	0.2782	0.0502
T1B2	0.2623	0.0491
T1B3	0.0788	0.0244
T1B4	0.2642	0.0326
T1B5	0.2567	0.0453
T2B1	0.4258	0.0698
T2B2	0.4258	0.0502
T2B3	0.2074	0.0264
T2B4	0.2752	0.0247
T2B5	0.3942	0.0700
T3B1	0.2362	0.0367
T3B2	0.2336	0.0257
T3B3	0.2249	0.0301
T3B4	0.3844	0.0381
T3B5	0.3347	0.0536
T3B6	0.3374	0.0450

Table 8.4 Values for M_{cr}/bh^2f_c' and f_b/f_c'

As can be seen from this graph, an increase in the bottom fibre compressive prestress level leads to an increase in the cracking moment. This merely confirms what is previously known, but has been included here for completeness.
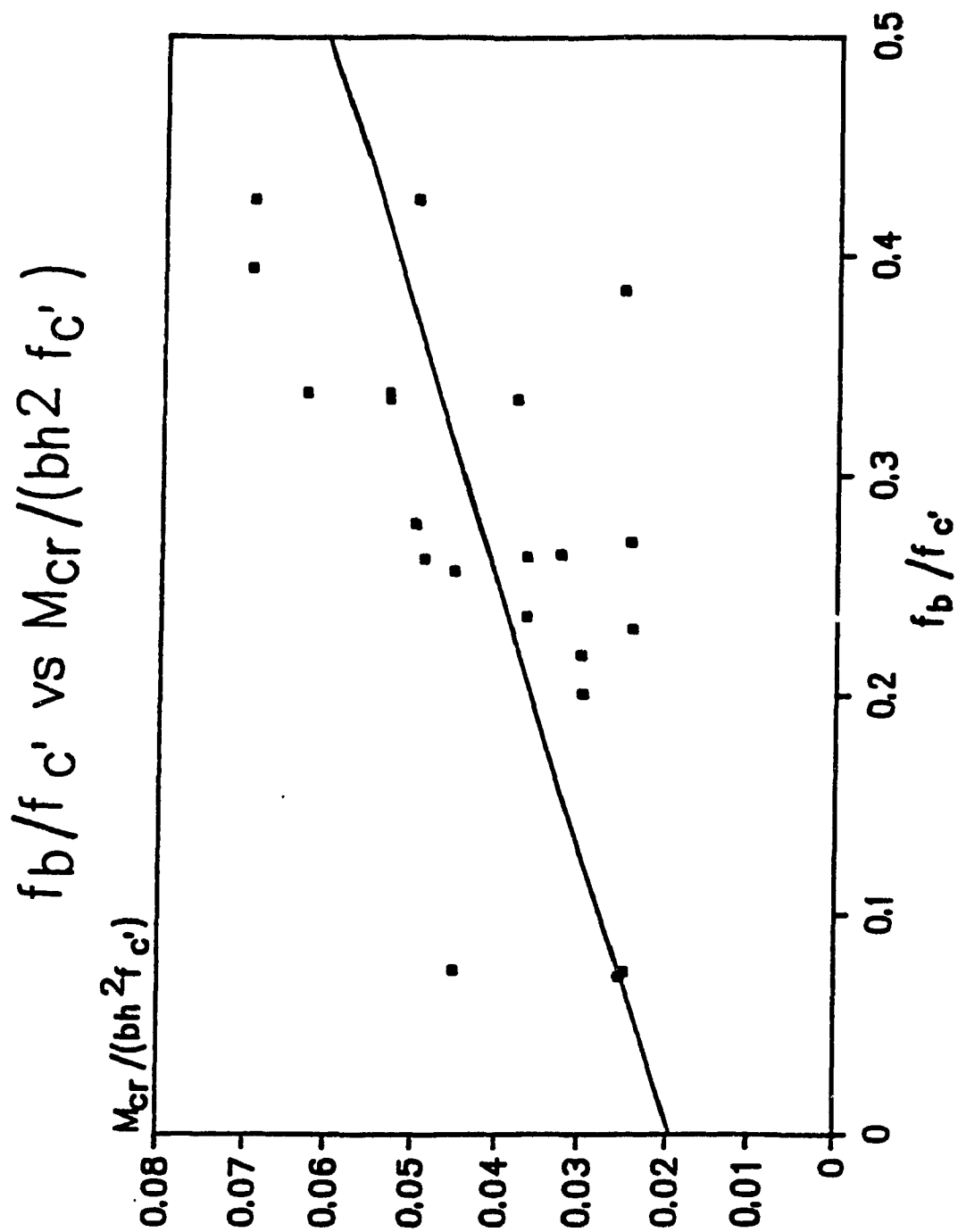
Figure 8.11 Relationship Between $M_{cr}/bh^2f_{c'}$ and $f_b/f_{c'}$

149

8.4 ULTIMATE MOMENT CAPACITY

Both the theoretical ultimate positive and ultimate negative moments for each tie have been calculated by the stress-strain compatibility method outlined in Chapter 6. Table 8.5 illustrates the comparison of the theoretical ultimate moment capacity with the experimental ultimate moment capacity for both negative and positive bending.

As can be seen from Table 8.5, the average experimental ultimate moment was 91.7 percent of the theoretical ultimate moment. This indicates that the experimental and theoretical values compare favourably.

It should be noted that no capacity reduction factor was used in the theoretical ultimate moment capacity calculations. Normal practice (4, 7) is to use a capacity reduction factor, ϕ, to allow for variations in the steel, concrete and in construction dimensions. However, had a capacity reduction factor ϕ (sometimes called ϕ factor) of 0.90 for flexure been used in the calculation, very close agreement between the theoretical and experimental values would have been obtained.

Again, due to the variation in the compressive strength of concrete in each tie, the experimental results have been divided by bh^2f_c' in order to obtain comparative relative

TIE NO.	THEORETICAL		EXPERIMENTAL		$\dfrac{Mu_{exp}}{Mu_{theo}}$
	in.K	kN.m	in.K	kN.m	
T1B1	1,148	129.7	1,221.3	138.0	1.06
T1B2	1,145	129.4	1,245.6	140.8	1.09
T1B3	646	73.0	869.4	98.2	1.35
T1B4	1,165	131.6	1,038.8	117.4	0.89
T1B5	1,289	145.7	1,422.9	160.8	1.10
T2B1	1,427	161.3	1,266.8	143.2	0.89
T2B2	1,561	176.3	1,280.3	144.7	0.82
T2B3	940	106.2	898.9	101.6	0.96
T2B4	869	98.2	672.1	75.9	0.77
T2B5	1,480	167.2	1,443.1	163.1	0.98
T3B1	1,494	168.8	1,496.5	169.1	1.00
T3B2	1,472	166.4	986.0	114.4	0.67
T3B3	1,440	162.7	1,150.0	130.0	0.80
T3B4	1,312	148.3	672.1	75.9	0.51
T3B5	1,337	151.1	1,217.9	137.6	0.91
T3B6	1,332	150.5	1,161.0	131.2	0.87

Table 8.5   Comparison of Theoretical and Experimental
Ultimate Moment Capacities

151

ultimate capacity data. Figure 8.12 indicates the graph of M_u/bh^2f_c' versus f_b/f_c'. From this graph it can be seen that increasing the bottom prestress increases the ultimate moment capacity of the tie. This is previously known and been included here for the sake of completeness. It should be noted that inverting the tie causes the top prestress to become the bottom prestress and has therefore been denoted as f_b.

TIE NO.	f_t psi	M_u iN.k	f_t/f_c'	M_u/bh^2f_c'
T1B1	516	1,221	0.0750	0.1134
T1B2	497	1,246	0.0708	0.1133
T1B3	1,851	869	0.2753	0.0826
T1B4	506	1,039	0.0717	0.0904
T1B5	527	1,423	0.0692	0.1193
T2B1	1,327	1,267	0.2303	0.1404
T2B2	1,327	1,280	0.1658	0.1021
T2B3	2,420	899	0.3712	0.0880
T2B4	2,319	672	0.4991	0.0924
T2B5	1,401	1,443	0.2134	0.1403
T3B1	2,218	1,497	0.2362	0.1018
T3B2	2,088	986	0.2336	0.0704
T3B3	2,088	1,150	0.2185	0.0769
T3B4	2,317	834	0.3844	0.0884
T3B5	2,153	1218	0.3347	0.1209
T3B6	2,153	1161	0.3374	0.1162

Table 8.6   Values for M_u/bh^2f_c, and f_t/f_c,

$f_b/f_{c'}$ vs $M_u/(bh\,2\,f_{c'})$
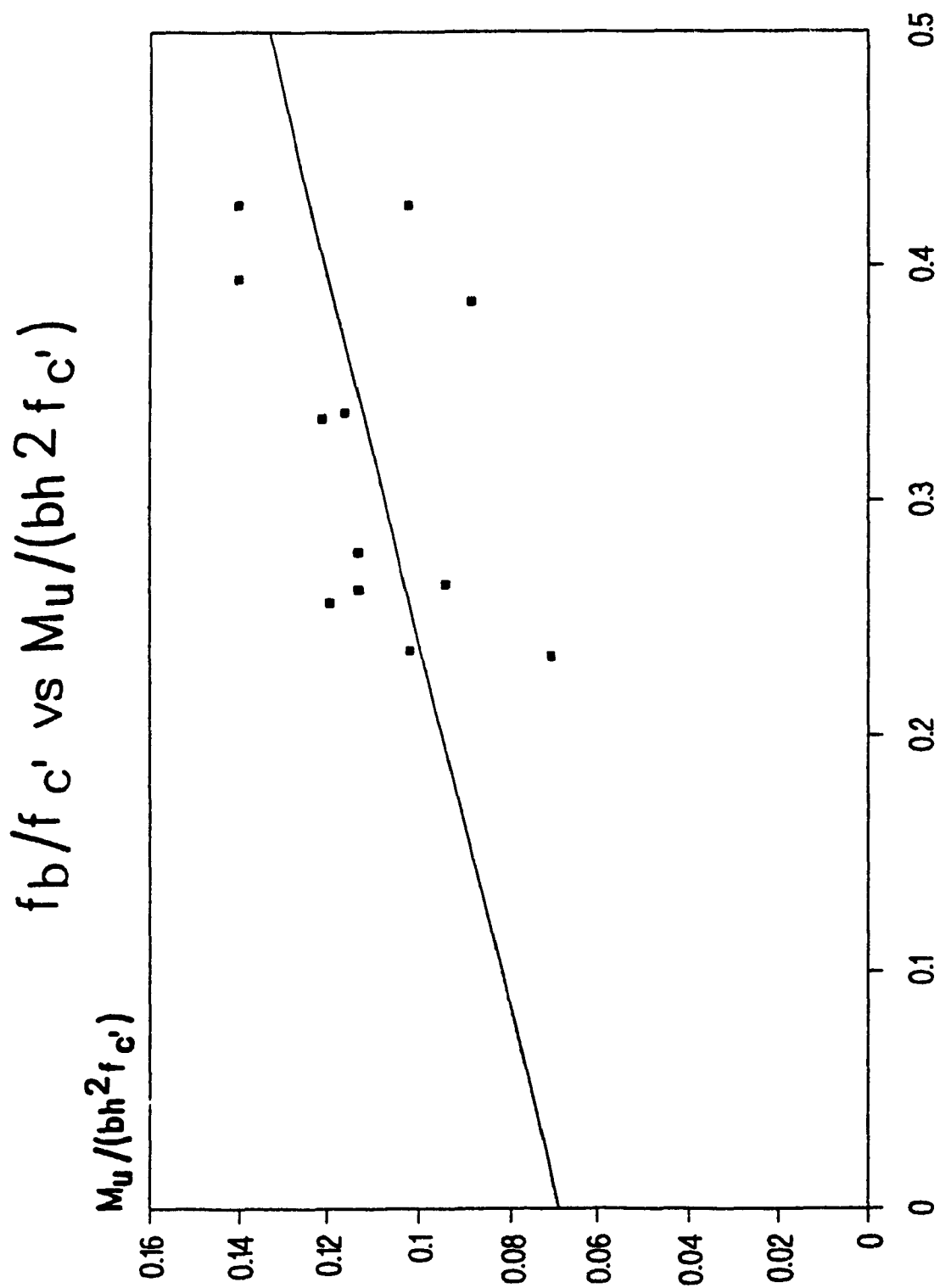
Figure 8.12 Relationship Between $M_u/bh^2f_{c'}$ and $f_b/f_{c'}$.
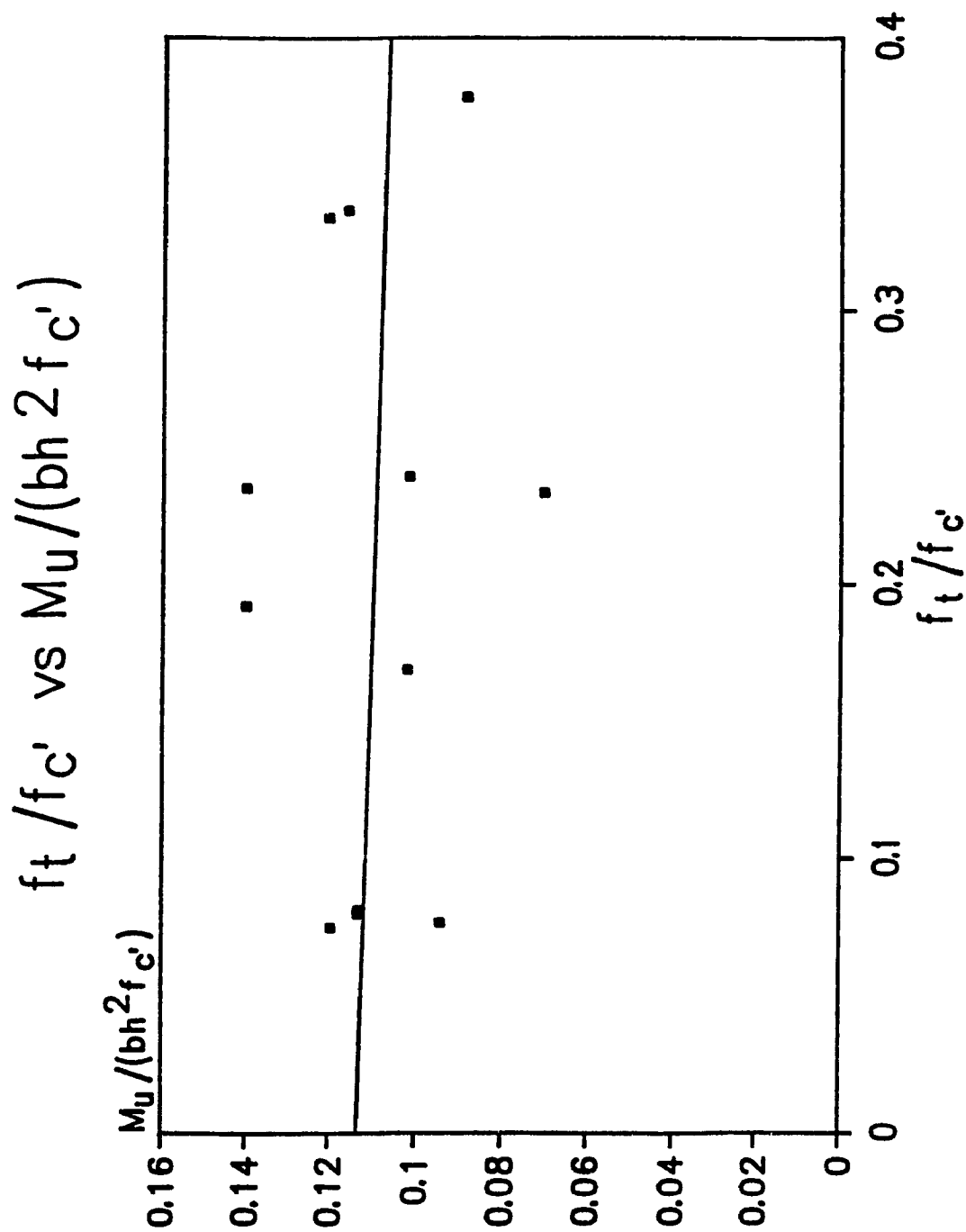
Figure 8.13 Relationship Between M_u/bh^2f_c, and f_t/f_c,

Figure 8.13 illustrates the relationship between M_u/bh^2f_c' and f_t/f_c' for positive loading only from values contained in Table 8.6. This graph indicates that increasing the level of prestress in the top of the tie, f_t, has a negligible effect on the ultimate positive moment capacity, M_u, of the tie.

This is important as it suggests that in the design of prestressed ties (or other members), subjected to reverse bending, additional prestress may be added to the tie to prevent negative cracking, without appreciably affecting the positive ultimate moment capacity.

It should be noted that the Type 3 ties, which had uniform prestress (e = o), exhibited only a 10% average decrease in positive ultimate moment capacity over the Type 2 ties.

8.5 STRAIN GAUGE READINGS

Although strain readings were recorded for the laboratory portion of the research, they could not be used in any analysis. On closer review of the measured strains, it became apparent that these strains were meaningful up to the point of first cracking and thereafter became meaningless. First cracking of the ties occurred at a loading of 15 kips (66.7 kN) to 30 kips (133.4 kN), while the ultimate load was between 60 kips (266.8 kN) to 80 kips (355.8 kN). This indicates that the strain gauges were only effective for a short period of the test performed on each tie.

CHAPTER 9

CONCLUSIONS AND RECOMMENDATIONS

9.1 CONCLUSIONS

The following conclusions may be drawn from the field testing performed in 1984 and 1986 and the laboratory testing conducted at Concordia University in 19^1:

1) The combination of soft rail-tie pad (SBR 60 durometer) with soft tie-girder pad (AASHTO 60 durometer) gave the lowest dynamic strains in the tie. This indicates that this combination of pads attenuates the most impact.

2) The combination of hard rail-tie pad (EVA) and hard tie-girder pad (SA-17) gave the largest dynamic strains in the ties.

3) The hard rail-tie and hard tie-girder pad combination gave strains 5(percent higher than that of the soft rail-tie and soft tie-girder pad combination.

4) The use of a hard rail-tie pad with a soft tie-girder pad showed negligible difference in strains in the tie when compared to the use of a hard rail-tie pad and a hard tie-girder pad. This indicates that the dynamic strains experienced by the ties are influenced the greatest by the rail-tie pad, and that the tie-girder pad has a insignificant effect on the strains.

5) The use of a soft rail-tie pad however, contributes to higher negative bending strains when the tie rebounds.

6) The maximum recorded negative strain experienced by the

C.N.R. bridge tie was 129.9×10^{-6} in/in in tension. The existing tie design is based on a compression strain of 47.5×10^{-6} in/in. Therefore, the existing C.N.R. concrete bridge tie is under designed in negative bending by at least 270 percent.

7) The use of the soft 6.5 mm Hytrel rail-tie pads gave dynamic strain readings approximately 20 percent less than the use of the soft 5 mm SBR rail-tie pads.

8) The use of the 6.5 mm Hytrel rail-tie pads and the installation of the 50 concrete track ties on the approaches to the bridge reduced the positive strains by 18 percent.

9) Both lightly and heavily loaded vehicles generated similar dynamic strain levels in the tie for the same velocity. This indicates that impacts are more a function of the unsprung mass and velocity of the vehicles.

10) Because lightly loaded and heavily loaded cars generate the same dynamic strain levels in the concrete ties, impact factors are not a practical design tool.

11) Impact factors do not assist in the design of concrete ties subjected to rebound, as they do not help predict the level of precompression required in the top of the tie.

12) The strains obtained from field testing and the strains obtained from the model for both positive and negative

bending show good correlation. For instance, the maximum negative bending strain (from rebound) obtained from the field data is 129.9 x 10^{-6} in/in and the strains obtained from the model is 106 x 10^{-6} in/in.

13) Failure of the ties in all cases was one of compression, with crushing of the concrete at the top of the tie.

14) Load-deflection curves obtained by static load tests are an indicator of the energy absorption capacity of the ties. The greater the ties' resilience, the greater its' impact resistance.

15) The experimental ultimate moment capacities compare favourably with the theoretical calculations. The average experimental ultimate moment capacity was 91.7 percent of the theoretical capacity.

16) An increase in the prestress level in the tension zone (bottom) of the tie increases the cracking strength of the tie.

17) An increase in the prestress level in the compression zone (top) of the tie has negligible effect on the positive ultimate moment capacity of the tie and greatly increases the cracking strength of the tie in rebound.

18) The Type 1 tie with a precompression level of 500 psi (3.4 MPa) in the top and 1,850 psi (12.86 MPa) in the bottom would be an ideal substitute for the current C.N.R. design.

9.2 RECOMMENDATIONS

From the research work undertaken during the course of this study, the following recommendations are presented:

1) The railway should continue to use the 6.5 mm Hytrel rail-tie pad as it attenuates the greatest impact.

2) The railway should adopt a tie design similar to the Concordia Type 1 tie with a 500 psi (3.4 MPa) precompression level in the top and a 1,850 psi (12.8 MPa) precompression level in the bottom.

3) The railway should discontinue the use of 5 mm wire as the number of wires required, from a practical viewpoint, would make jacking difficult because of interference. The use of 3/8" (9.55 mm) 7 wire strand is recommended.

4) The existing trapezoidal tie shape, 10" (254 mm) wide at the top, 11-3/4" (298 mm) wide at the bottom and 12" (305 mm) high, should be maintained.

5) Air entrained concrete of approximately 5 percent with a compression strength of 6,000 psi (41.4 MPa) minimum should be used in the manufacture of the ties to prevent the effects of freeze - thaw.

6) The use of an impact factor in design of future ties should be avoided, however, if this is not practical, the precompression level at the top of the tie should be a minimum 27 percent of the precompression level at the bottom of the tie to avoid cracking from rebound.

7) Concrete track ties should be installed on the approaches to any bridge with concrete bridge ties. This will help in the transition from ballasted track to the bridge. In addition, the track ties closest to the backwall of the bridge must be kept surfaced so as to prevent large impacts on the end bridge ties.

8) An economic analysis should be undertaken as an increased amount of prestress leads to an increase in the consumption of steel strand, which must be balanced with the improved performance and durability of the ties.

9) If the railway moves in the direction of increasing car loadings from the 100 ton car, 263,000 lbs. (1,170 kN) on 4 axles to the 125 ton car, 315,000 lbs. (1,401 kN) on 4 axles as is the trend among North American railways, then the design of the Type 1 tie should be reviewed.

10) As the statistical data available from the CN field testing is by no means complete, it is currently the best available. However, further statistical data should be obtained through cooperation with a Railway and the Concordia Type 1 tie re-evaluated in light of this data.

REFERENCES

1) American Railway Engineering Association, "Manual for Railway Engineering", Vol 2, American Railway Engineering Association, Washington, D.C.

2) Banthia, N., Mindess, S., Bentur, A., and Pigeon, M., "Impact Testing of Concrete Using a Drop Weight Impact Machine", Journal of Experimental Mechanics, March, 1989.

3) Canadian Prestressed Concrete Institute, "Metric Design Manual", Second Edition, Canadian Prestressed Concrete Institute, Ottawa, 1987.

4) Canadian Standards Association, "Code for the Design of Concrete Structures for Buildings", CAN3-A23.3-M77, Canadian Standards Association, Rexdale, 1977.

5) Collins, M. P. and Mitchell, D.,"Prestressed Concrete Basics", Canadian Prestressed Concrete Institute, Ottawa, 1987.

6) Dean, F. E., "The Effect of Service Loading on the Bending Strength of concrete Ties", U.S. Department of Transportation, Federal Railroad Administration, Report No. FRA/TTC-81/11, Washington, October, 1981.

7) Ferguson, P. M., "Reinforced Concrete Fundamentals", Third Edition, John Wiley and Sons, New York, 1973.

8) Igwe, O. R., "Precast Prestressed Ties on Bridge Girders - Experimental Response and Design Review", M.Sc. Thesis, McGill University, Montreal, November 1983.

162

REFERENCES

9) Igwemezie, J. O., "Dynamic Response and Impact Effects in Precast, Prestressed Concrete Bridge Ties", P.hD Thesis, McGill University, Montreal, September, 1987.

10) Igwemezie, J. O. and Mirza, M. S., "Impact Load Distribution in Concrete Bridge Ties", Journal of Structural Engineering, Vol. 115, No. 3, March 1989.

11) Igwemezie, J. O., Mirza, M. S. and Scott, J. F., "Field Tests of an Open Deck Railway Bridge with Concrete Ties", Canadian Journal of Civil Engineering, Vol. 16, No. 4, August, 1989.

12) Kong, W. L., "A Study on Precast Prestressed Concrete Railway Bridge Ties", M. Sc. Thesis, Queens University, Kingston, September, 1983.

13) Lin, T. Y., "Design of Prestressed Concrete Structures", Second Edition, John Wiley and Sons, New York, July 1967.

14) Mirza, M. S., Igwemezie, J. O. and Igwe, O. R., "Experimental - Analytical Study of Load Distribution Characteristics of an Open Deck Bridge System with Precast Prestressed Ties", NSERC PRAI Grant Project Report no. 8203, McGill University, Montreal, February, 1984.

15) Scott, J. F., "Assessing Concrete Ties in Bridges and Turnouts", Railway Track and Structures, Vol. 82, No. 8, 1986.

16) Scott, J. F., "Evaluation of Turnout Ties and Bridge Ties", Paper Presented to the American Railway Engineering

REFERENCES

Association Annual Conference, Chicago, March, 1986.

17) Scott, J. F., "Evaluation of Use of Strain Gauge Rosettes on Concrete Bridge Ties", Canadian National Railway Technical Research Centre, St. Laurent, July, 1986.

18) Shraddhakar, H., Shen, Z. and Darwin, D., "Strain-Rate Sensitive Behaviour of Cement Paste and Mortar in Compression", American Concrete Institute Materials Journal, Vol.87, No. 5, September - October 1990.

19) Taras, A., "Resonant Vibration Frequencies in Concrete Ties", Transport Canada - Transportation Development Centre Report No. TP 8169E, Montreal, December, 1985.

20) Wakui, H., Matsumoto, N. and Watanabe, T., "Design Impact Factor for Concrete Railway Bridges", Quarterly Report of the Railway Technical Research Institute, Vol. 30, No. 2, May, 1989.

21) Watstein, D., "Effect of Straining Rate on the Compressive Strength and Elastic Properties of Concrete", Journal of the American Concrete Institute, Detroit, Vol. 24, No. 8, April 1953.

22) Perry, C. C. and Lissner, H. R., "The Strain Gage Primer", Second Edition, McGraw Hill Book Company Inc., New York, 1962.

APPENDIX A

TWO WIRE TRANSMITTER BOX

OUTPUT VOLTAGE FORMULATION

APPENDIX A

TWO WIRE TRANSMITTER BOX OUTPUT VOLTAGE FORMULATION

1.0 GENERAL CONDITIONS OF A WHEATSTONE BRIDGE

An accurate method of measuring the resistance is by means of a circuit using a Wheatstone Bridge. The formulation for this is as outlined below. See Figures A1.1 and A1.2.

$$V_B = I_1 (R_1 + R_2) \quad \text{and} \quad e_1 = V_B - I_1 R_1$$

$$V_B = I_2 (R_3 + R_4) \quad \text{and} \quad e_2 = V_B - I_2 R_4$$

therefore:

$$e_1 - e_2 = V = (V_B - I_1 R_1) - (V_B - I_2 R_4)$$

$$e_1 - e_2 = V = I_2 R_4 - I_1 R_1$$

but: $I_1 = V_B / (R_1 + R_2)$ and $I_2 = V_B / (R_3 + R_4)$

$$e_1 - e_2 = V_B R_4 / (R_3 + R_4) - V_B R_1 / (R_1 + R_2)$$

Initially it is assumed that there is no strain on the system so that when $R_1 = R_2$ and $R_3 = R_4$, $e_1 = e_2 = 0$

This means that the output of the bridge can be set to zero.

The bridge under strain is affected by the following:

1)   forces applied to the system and Poisson's effect.

2)   temperature variations.

The strains due to stresses in three dimensions are as follows:

$$\epsilon_x = \sigma_x / E - \mu \sigma_y / E - \mu \sigma_z / E$$

$$\epsilon_y = \sigma_y / E - \mu \sigma_x / E - \mu \sigma_z / E$$

$$\epsilon_z = \sigma_z / E - \mu \sigma_x / E - \mu \sigma_y / E$$

The strains due to temperature variations are given by:

$$\epsilon_T = \alpha \Delta T$$
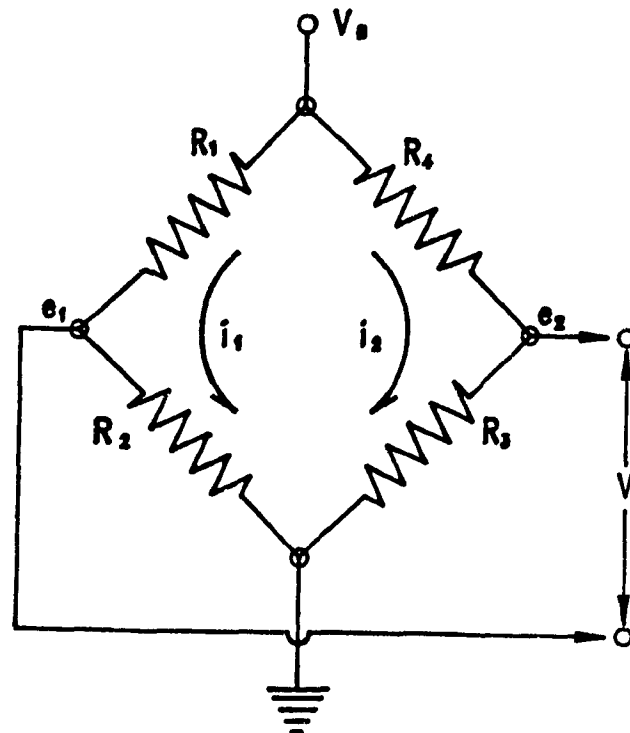
Figure A 1.0 Schematic of a Wheatstone Bridge

HEAT
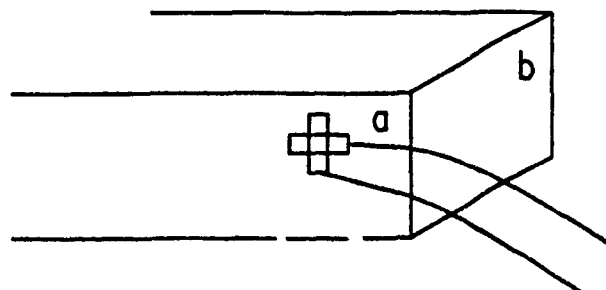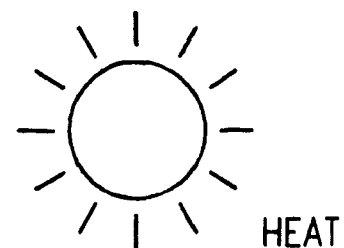
Figure A 1.1 Schematic of Strain Gauge Rosettes

If the material is homogeneous and isotropic, the strain will be the same in all directions of the system. The resistance values under the effects of strain and temperature are as outlined below:

if $R_1 = R_2 = r$ and $R_3 = R_4 = R$ (assumed when the system is initially installed) the following conditions apply:

$R_1 = r + \Delta R_F{}^a + \Delta R_T{}^a$

$R_2 = r - \Delta R_\mu{}^a + \Delta R_T{}^a$

$R_3 = R + \Delta R_F{}^b + \Delta R_T{}^b$

$R_4 = R - \Delta R_\mu{}^b + \Delta R_T{}^b$

where:

Superscripts a and b indicate the particular surface of the tie.

Subscript F indicates the strain due to applied force.

Subscript μ indicates strain due to Poisson's effect.

Subscript T indicates strain due to temperature variations.

Therefore the equation for $e_1 - e_2$ can be written as:

$$e_1 - e_2 = V_B \left[\frac{R - \Delta R_\mu{}^b + \Delta R_T{}^b}{2R + \Delta R_F{}^b - \Delta R_\mu{}^b + 2\Delta R_T{}^b} - \frac{r + \Delta R_F{}^a + \Delta R_T{}^a}{2r + \Delta R_F{}^a - \Delta R_\mu{}^a + 2\Delta R_T{}^a} \right]$$

For stresses due to forces, we have the following:

$\Delta R/R = F\epsilon_x{}^b$ and $\Delta R/r = F\epsilon_x{}^a$

$\Delta R_F{}^b = RF\epsilon_x{}^b$ and $\Delta R_F{}^a = rF\epsilon_x{}^a$

$\Delta R_\mu{}^b = RF\mu\epsilon_x{}^b$ and $\Delta R_\mu{}^a = rF\mu\epsilon_x{}^a$

therefore:

168

$$e_1 - e_2 - V_B \left[\frac{1 - F\mu e_x^b + (\Delta R_T^b/R)}{2 + Fe_x^b(1 - \mu) + (2\Delta R_T^b/R)} - \frac{1 + Fe_x^a + (\Delta R_T^a/r)}{2 + Fe_x^a(1 - \mu) + (2\Delta R_T^a/r)} \right]$$

It should be noted that in the above equation it is assumed that the initial value of $e_1 - e_2$ prior to any change in strain is zero.

2.1 THE HALF BRIDGE

In the situation where a half bridge is used, R_3 and R_4 are completion resistors and their effect on surfaces a and b are not considered.

Therefore:

$\Delta R_F{}^b = \Delta R_\mu{}^b = \Delta R_T{}^b = 0$

$\Delta R_F{}^a = \Delta R_F$

$\Delta R_\mu{}^a = \Delta R_\mu$

$\Delta R_T{}^a = \Delta R_T$

Equation $e_1 - e_2$ now becomes:

$$e_1 - e_2 - V_B \left[\frac{1}{2} - \frac{r + \Delta R_F + \Delta R_T}{2r + \Delta R_F - \Delta R_\mu + 2\Delta R_T} \right]$$

$$e_1 - e_2 - V_B \left[\frac{1}{2} - \frac{1 + Fe_x + (\Delta R_T/r)}{2 + Fe_x(1 - \mu) + (2\Delta R_T/r)} \right]$$

$$e_1 - e_2 - V_B \left[\frac{-Fe_x(1 - \mu)}{2(2 + Fe_x(1 - \mu) + (2\Delta R_T/r)} \right]$$

The following is assumed:

1)   the temperature variation during the test is small, such
     that $\Delta R_T/r = \ll 1$

2)   the maximum strain is $\epsilon_x = 500\mu\epsilon$, such that:

     $F\epsilon_x(1-\mu) = 0.04$ percent

therefore:

$$e_1 - e_2 = V_B - \left[\frac{F\epsilon_x(1 + \mu)}{4}\right]$$

The output voltage at the 25 ohm resistors of the T.W.T. is as
follows:

$$E_0 = -\frac{V_B F\epsilon_x A(1 + \mu)}{4} + V_{set}$$

where:

A is the gain of the T.W.T. = 500

V_{set} is the set voltage level, which was 2 volts

E_0 is the voltage change on a 25 ohm load resistor

F is the gauge factor,   2.055 for concrete

                          2.000 for prestressing wire

                          2.120 for the steel girders

ϵ_x is the strain in the active gauge

μ is Poisson's ratio,   0.18 for concrete

                             0.30 for steel

1.3 MODIFYING THE BRIDGE VOLTAGE

To modify the bridge voltage V_B, padding resistors designated
R_p must be added. See Figure A.1.2
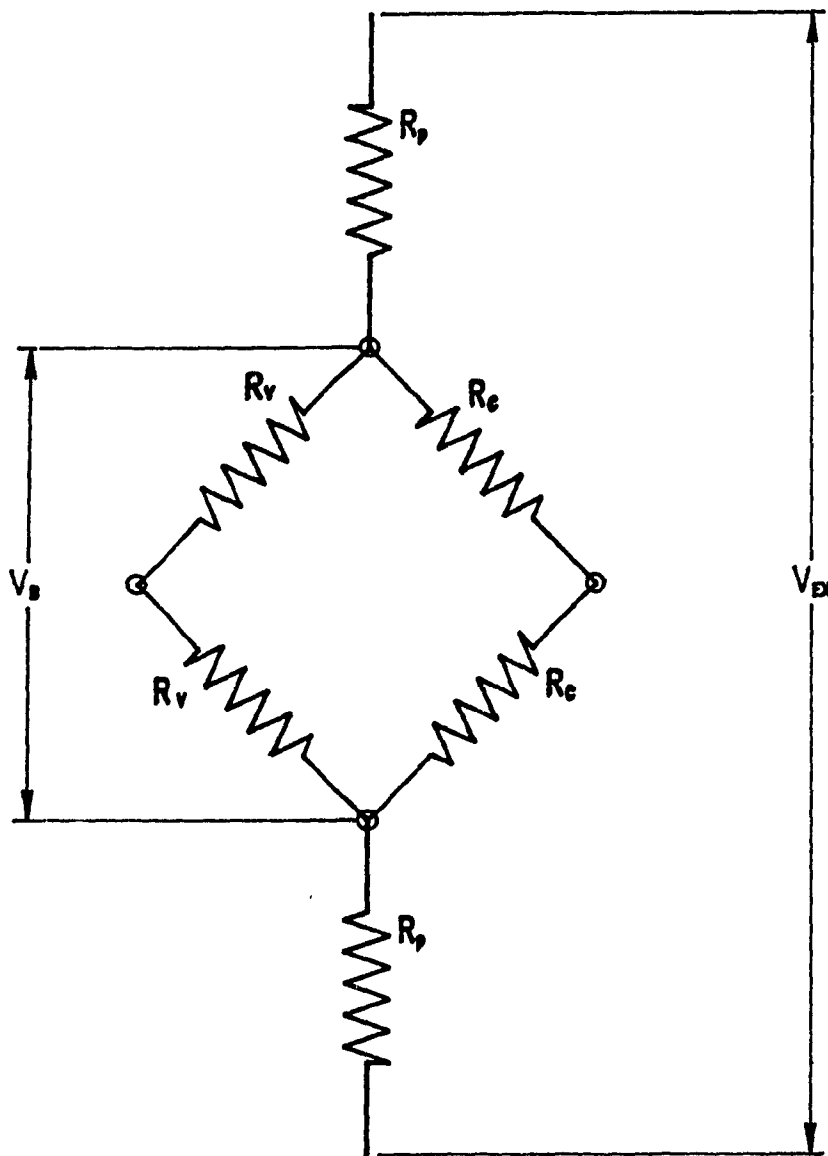
Figure A 1.2   Schematic of a Wheatstone Bridge With Padding
Resistors

171

$$\frac{1}{R_T} = \frac{1}{2R_V} + \frac{1}{2R_C}$$

$$R_T = \frac{2R_V R_C}{R_V + R_C}$$

$$V_{ex} = I \ (R_T + 2R_P)$$

$$V_{ex} = I \left[\frac{2R_V R_C + 2R_P(R_V + R_C)}{R_V + R_C} \right]$$

$$V_{ex} = 2IR_P + V_B \ and \ V_B = V_{ex} - 2IR_P$$

$$V_B = V_{ex} \left[1 - \frac{2R_P \ (R_V + R_C)}{2R_V R_C + 2R_P(R_V + R_C)} \right]$$

$$V_B = V_{ex} \left[\frac{R_V R_C}{R_V R_C + R_P(R_V + R_C)} \right]$$

Knowing the values of both V_B and V_{ex} the value of the padding resistors can be found as follows:

$$V_{ex} = V_B \left[1 + \frac{R_P(R_V + R_C)}{R_V R_C} \right]$$

$$R_P = \frac{V_{ex} - V_B}{V_B} \ x \ \frac{R_V R_C}{R_V + R_C}$$

1.4 THE EFFECT OF THE CALIBRATION SWITCH IN THE T.W.T. BOX

When the calibration switch on the receiver is in the "on" position, the resistor R_{cc} is shunted across the R_c resistor.
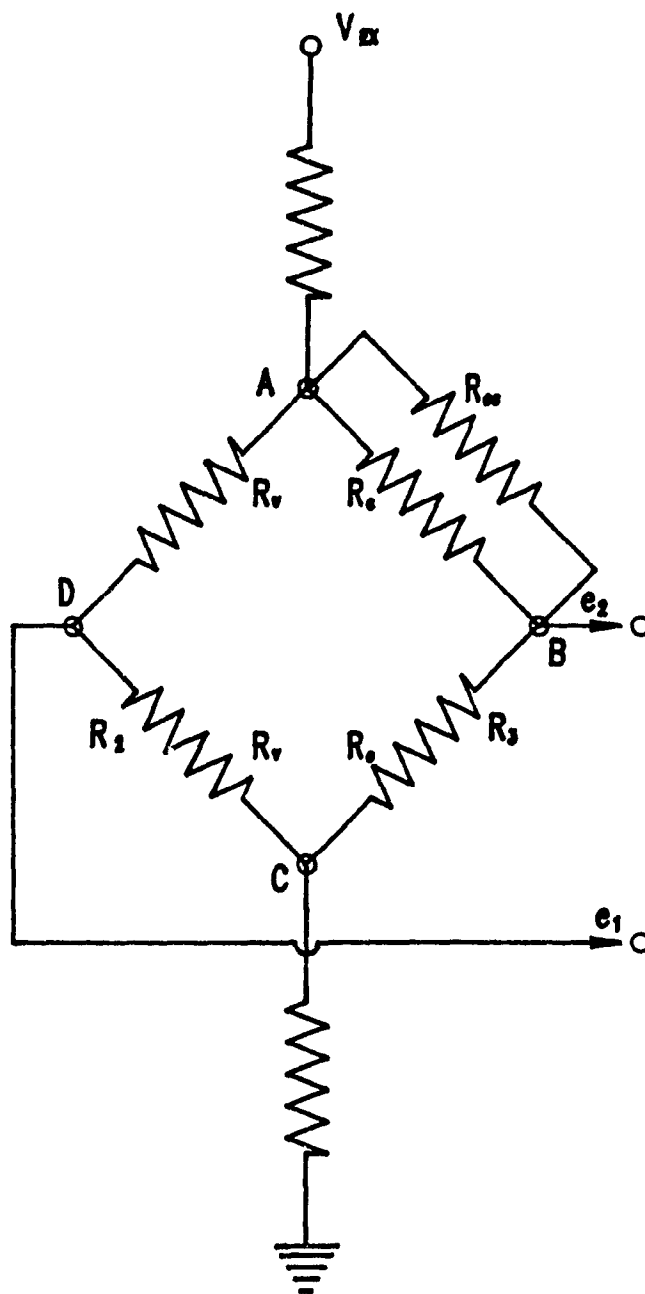
Figure A 1.3   Schematic of a Wheatstone Bridge With
Calibration Switch

See Figure A 1.3.

The new resistance of the arm AB now becomes:

$$\frac{1}{R_c'} = \frac{1}{R_c} + \frac{1}{R_{cc}}$$

$$R_c' = \frac{R_{cc}R_c}{R_{cc} + R_c}$$

therefore:

$R_c' = R_c + \Delta R_c$ where $\Delta R_c = R_c' - R_c$

$$R_c' - R_c = \frac{R_{cc}R_c}{R_{cc} + R_c} - \frac{R_c(R_{cc} + R_c)}{R_{cc} + R_c} = \frac{-R_c^2}{R_{cc} + R_c}$$

$$\Delta R_c' = \frac{-R_c^2}{R_{cc} + R_c}$$

therefore:

$R_c' = R_c + \Delta R_c = R_c(1 + \Delta R_c/R_c)$

$$R_c' = R_c \left[1 - \frac{R_c}{R_{cc} + R_c}\right]$$

It is known that,

$$\varepsilon \; x \; F = \frac{\Delta R_c}{R_c} = \frac{R_c}{R_{cc} + R_c}$$

where $\Delta R_c/R_c \ll 1$

The expression for strain, when the calibration switch at the receiver is in the on position, depends on if there was previously a test calibrating the applied exitation or load versus either:

1)   the total bridge strain , comprising of Poisson's ratio (in the case of a half bridge roseette) = $\epsilon_x(1 + \mu)$, or

174

2)	the actual longitudinal strain in the member (for example

in the x direction) = ϵ_x without Poisson's effect.

Therefore, in the case of a half bridge rosette for longitudinal stress in one direction (x) the folowing applies:

a) the total bridge strain ϵ_x^B:

$$\epsilon_x^B = \epsilon_x(1 + \mu)$$

$$\epsilon_x^B = \frac{1}{F} \times \frac{\Delta R_C}{R_C} = \frac{1}{F} \times \frac{R_C}{R_{CC} + R_C}$$

b) the actual longitudinal strain in the member ϵ_x:

$$\epsilon_x = \frac{1}{F} \times \frac{1}{(1 + \mu)} \times \frac{R_C}{(R_{CC} + R_C)}$$

where: R_{cc} = 349,650 ohms and

R_c = 350 ohms

$$E_0 = \frac{V_B \, FA \, \epsilon_x^B}{4}$$

$$E_B = \frac{-V_B \, A}{4(1 + \mu)} \left[\frac{R_C}{R_{CC} + R_C} \right]$$

175

APPENDIX B

OCCURRENCE VERSUS STRAIN

AND

CUMULATIVE PERCENT EXCEEDING GRAPHS

FOR 1984 AND 1986 C.N. FIELD TESTS
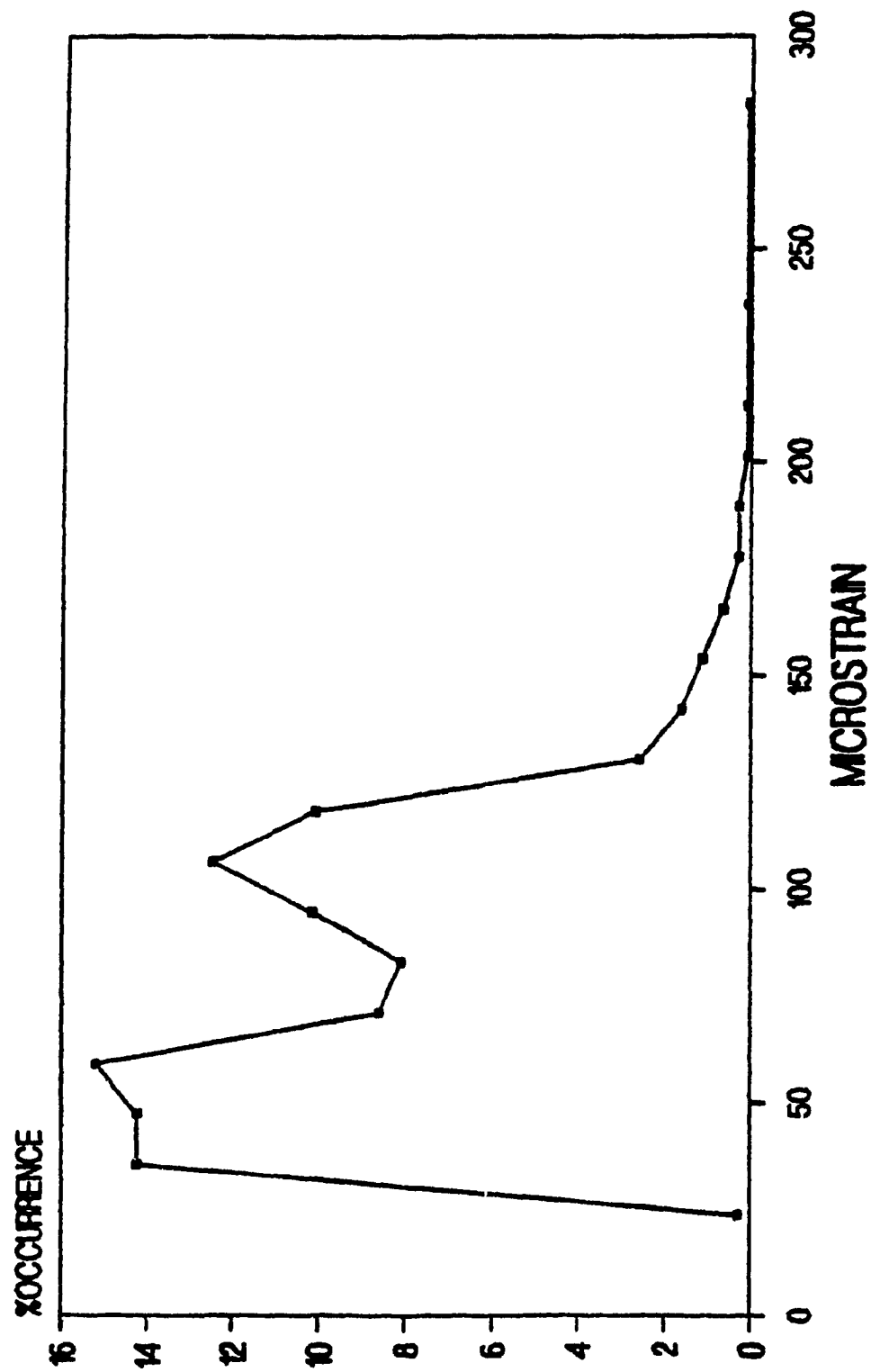
Figure B 1.0 Summary Graph 3RB for 1984
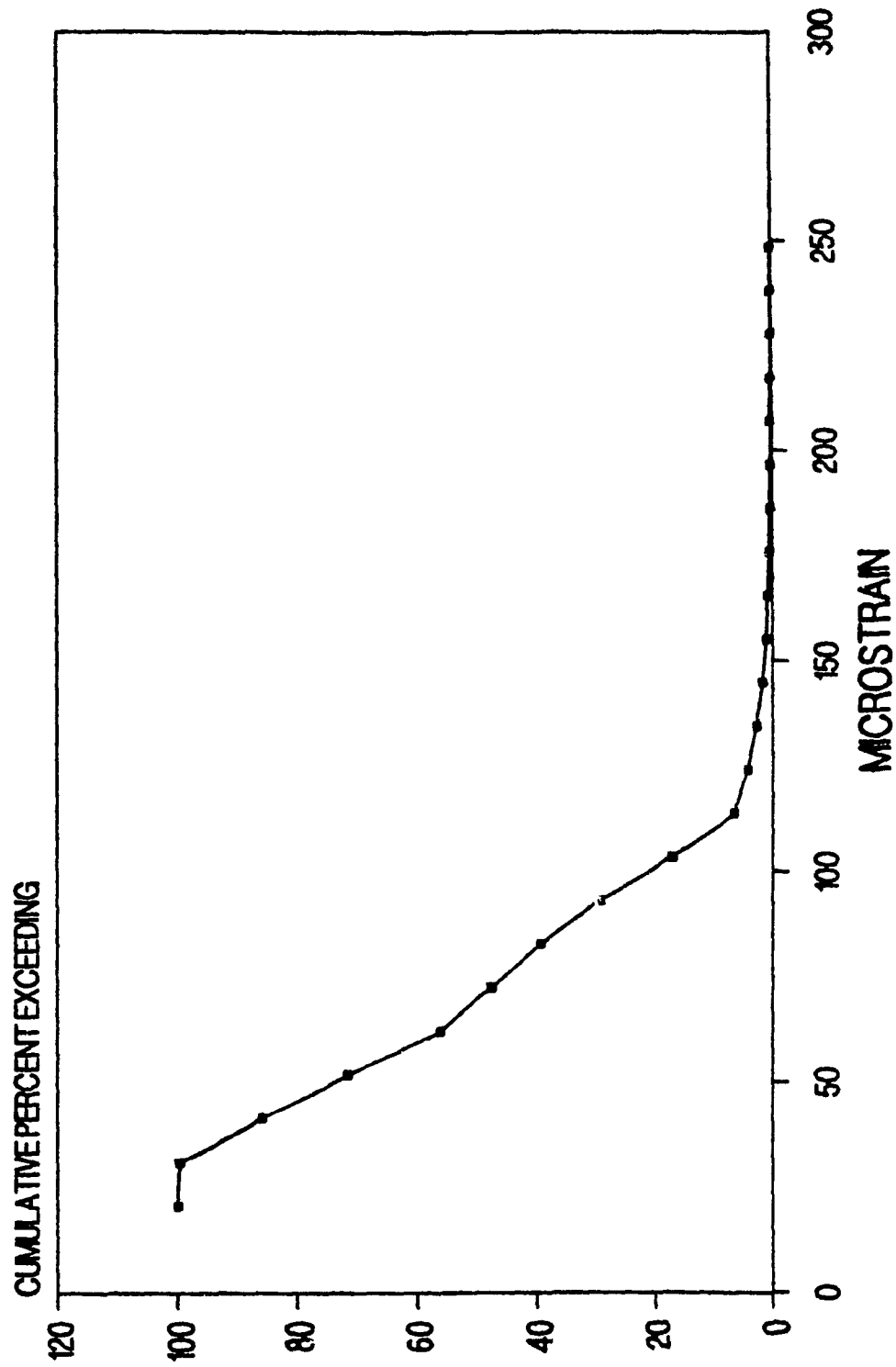
Figure B 1.1 Cumulative Exceeding Graph for 3RB, 1984

%OCCURRENCE vs STRAIN
SUMMARY 8RB – POSITIVE BENDING 1984
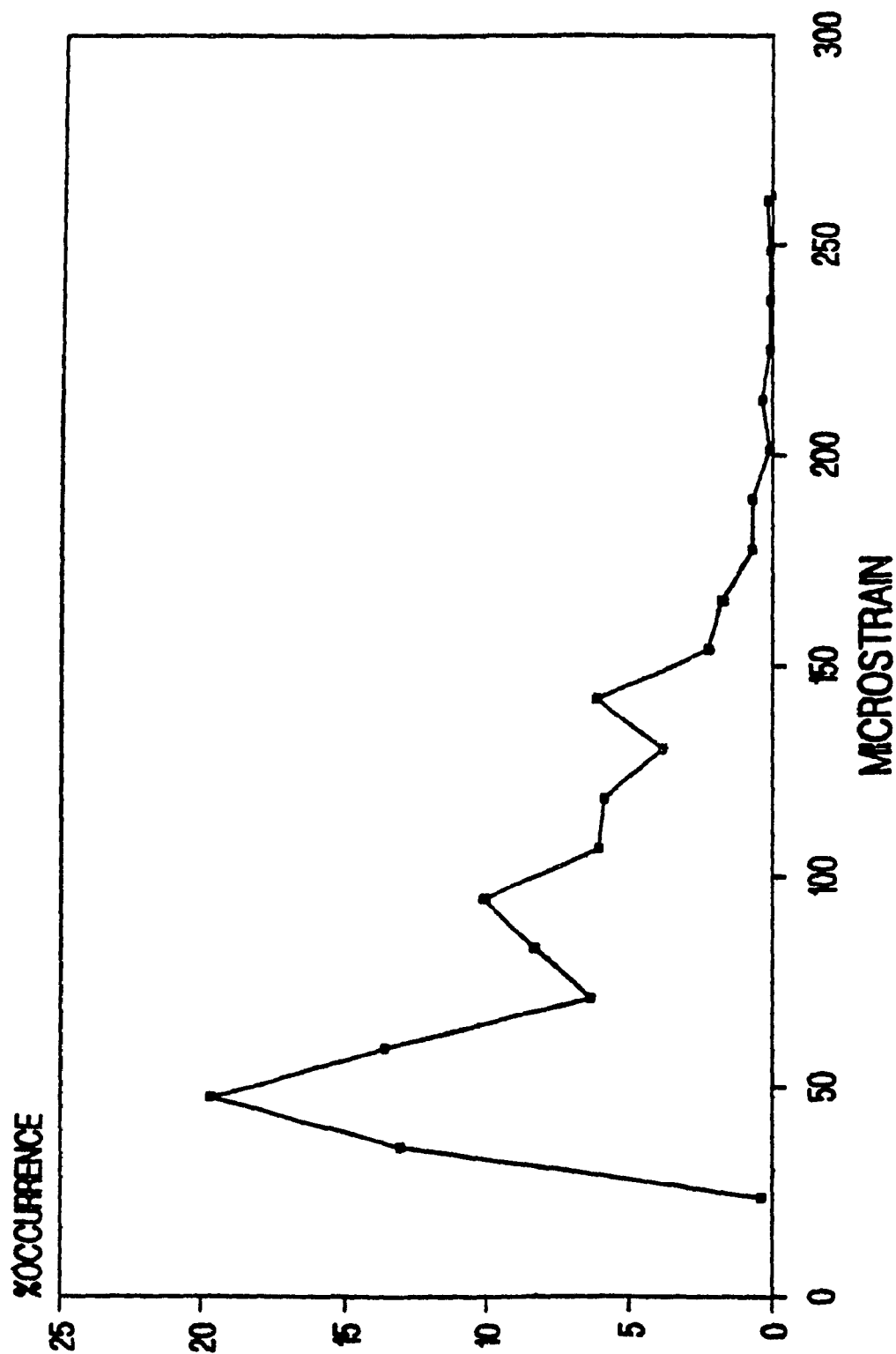
Figure B 1.2   Summary Graph 8RB for 1984

CUM. PERCENT EXCEEDING vs STRAIN
SUMMARY 8RB – POSITIVE BENDING 1984
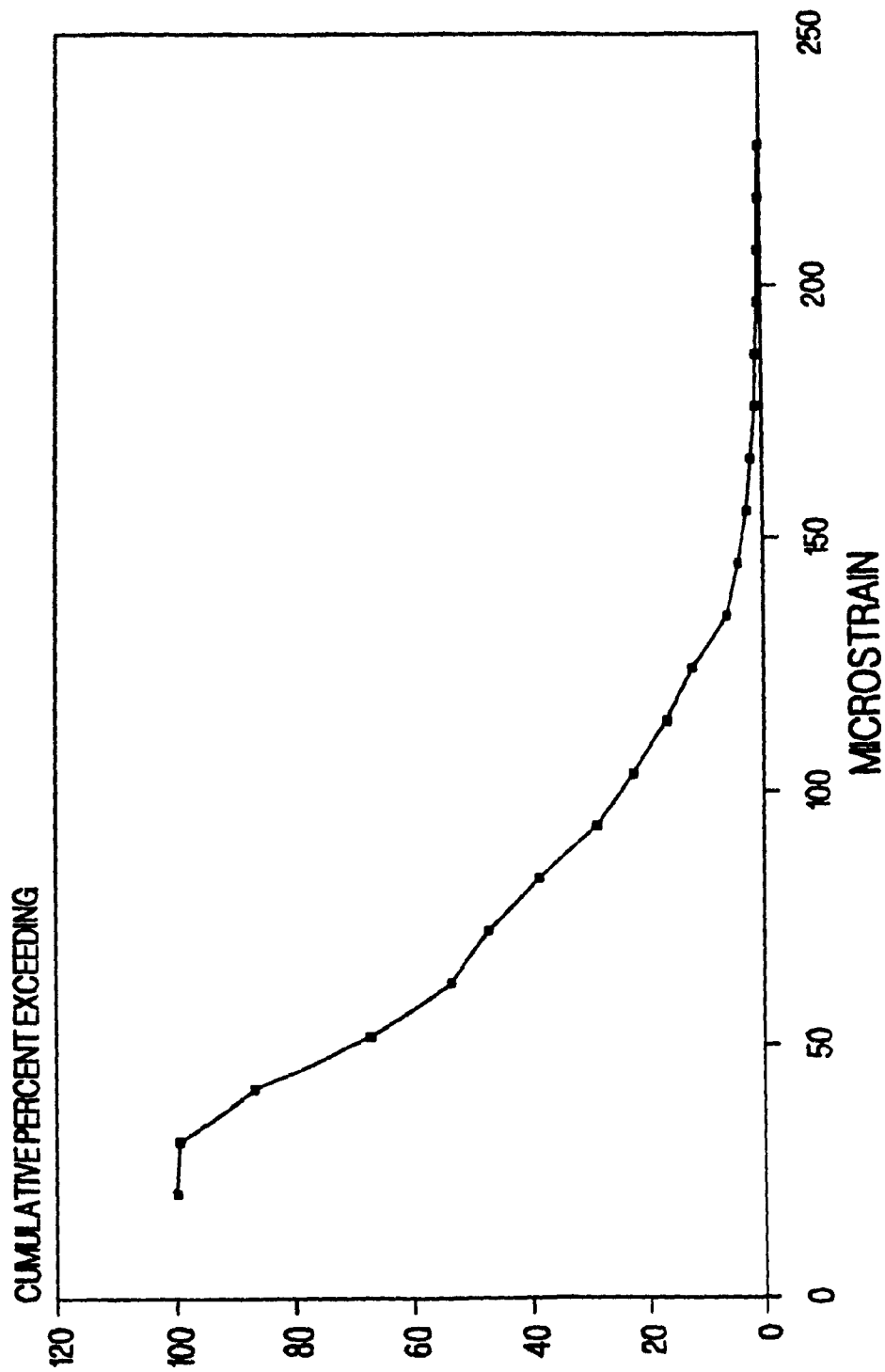
Figure B 1.3   Cumulative Exceeding Graph for 8RB, 1984
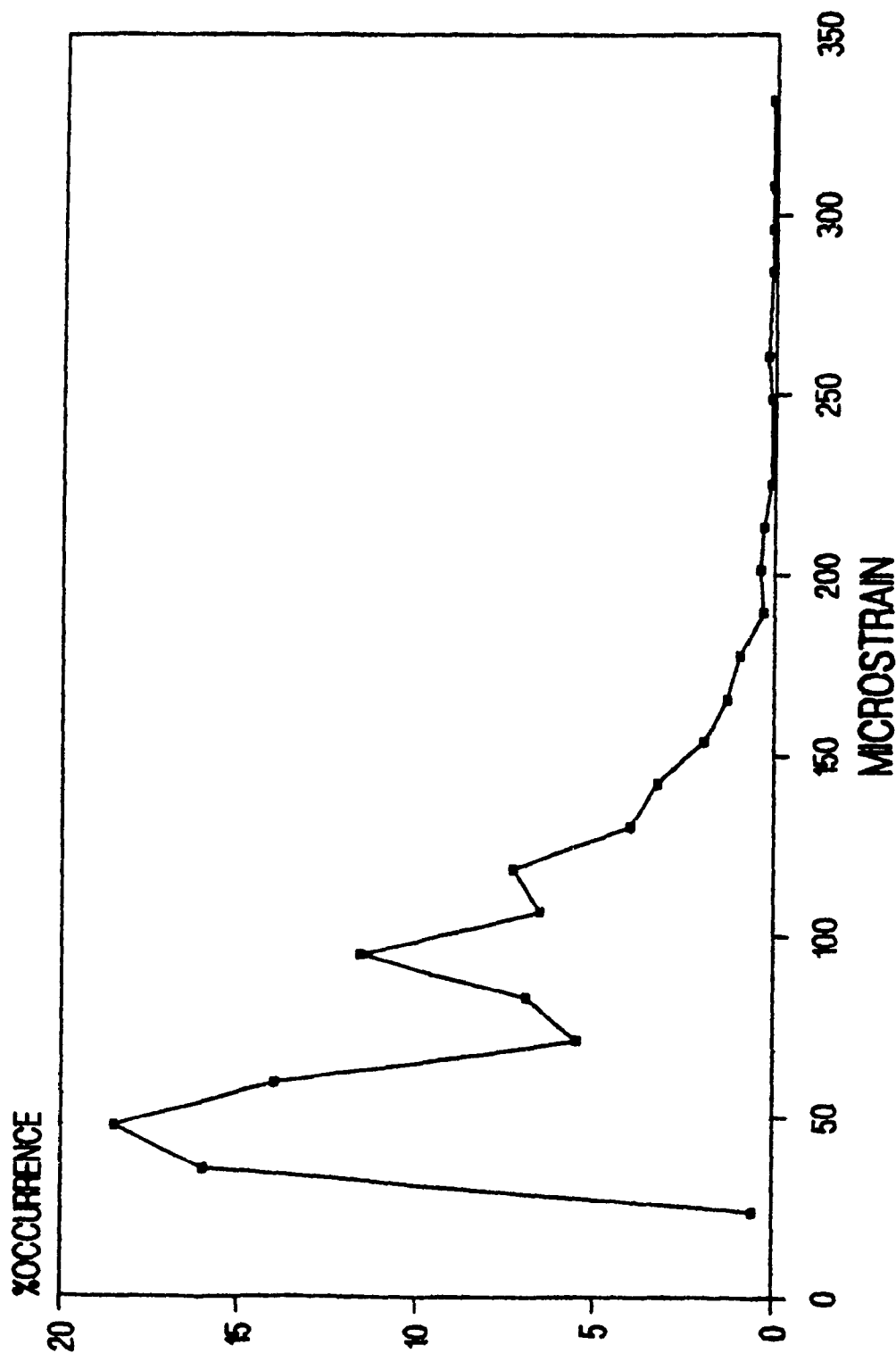
Figure B 1.4 Summary Graph 15RB for 1984

CUM. PERCENT EXCEEDING vs STRAIN
SUMMARY 15RB – POSITIVE BENDING 1984
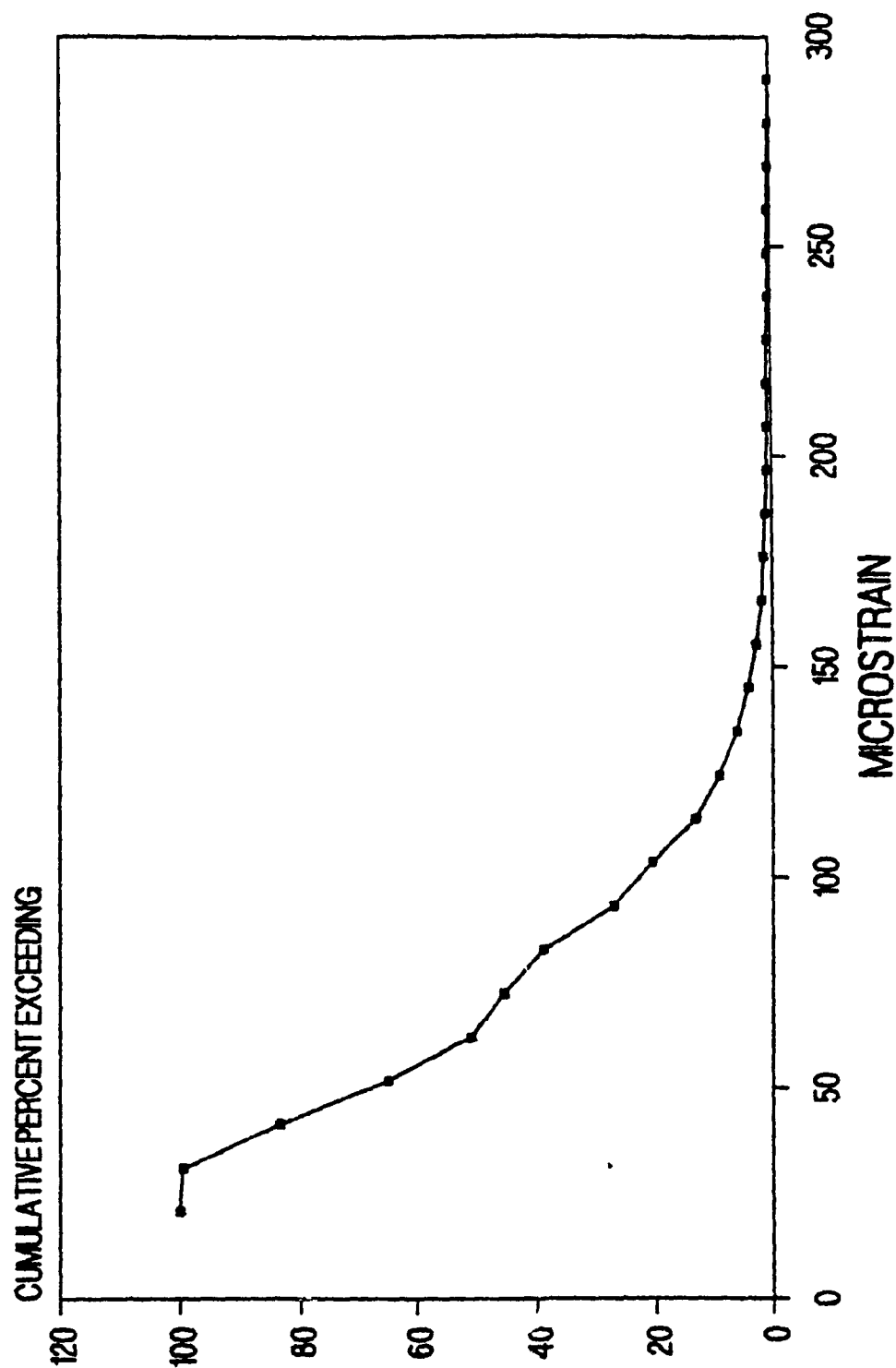
Figure B 1.5   Cumulative Exceeding Graph for 15RB, 1984
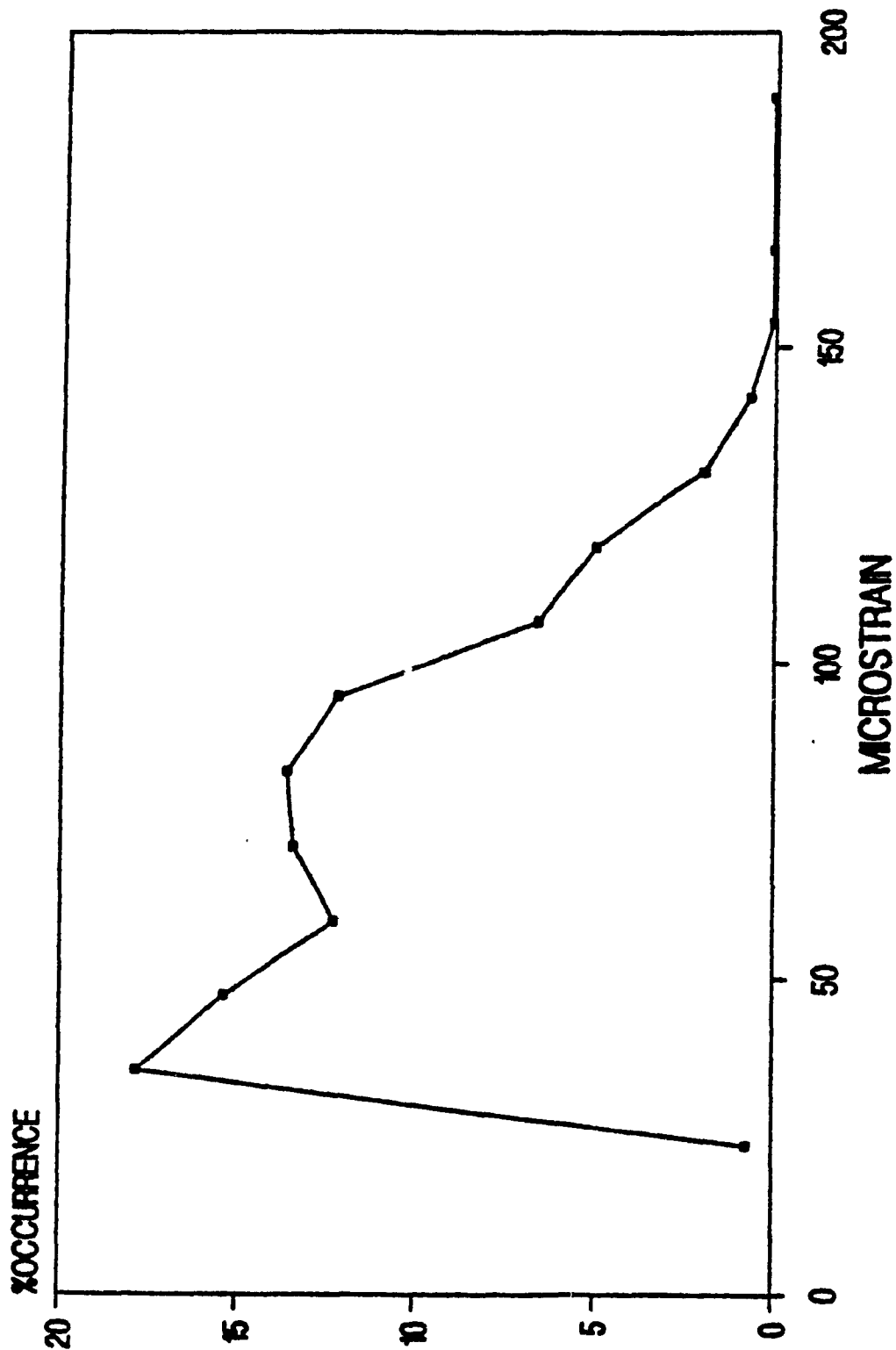
Figure B 1.6 Summary Graph 20RB for 1984

CUM. PERCENT EXCEEDING vs STRAIN
SUMMARY 20RB –POSITIVE BENDING 1984
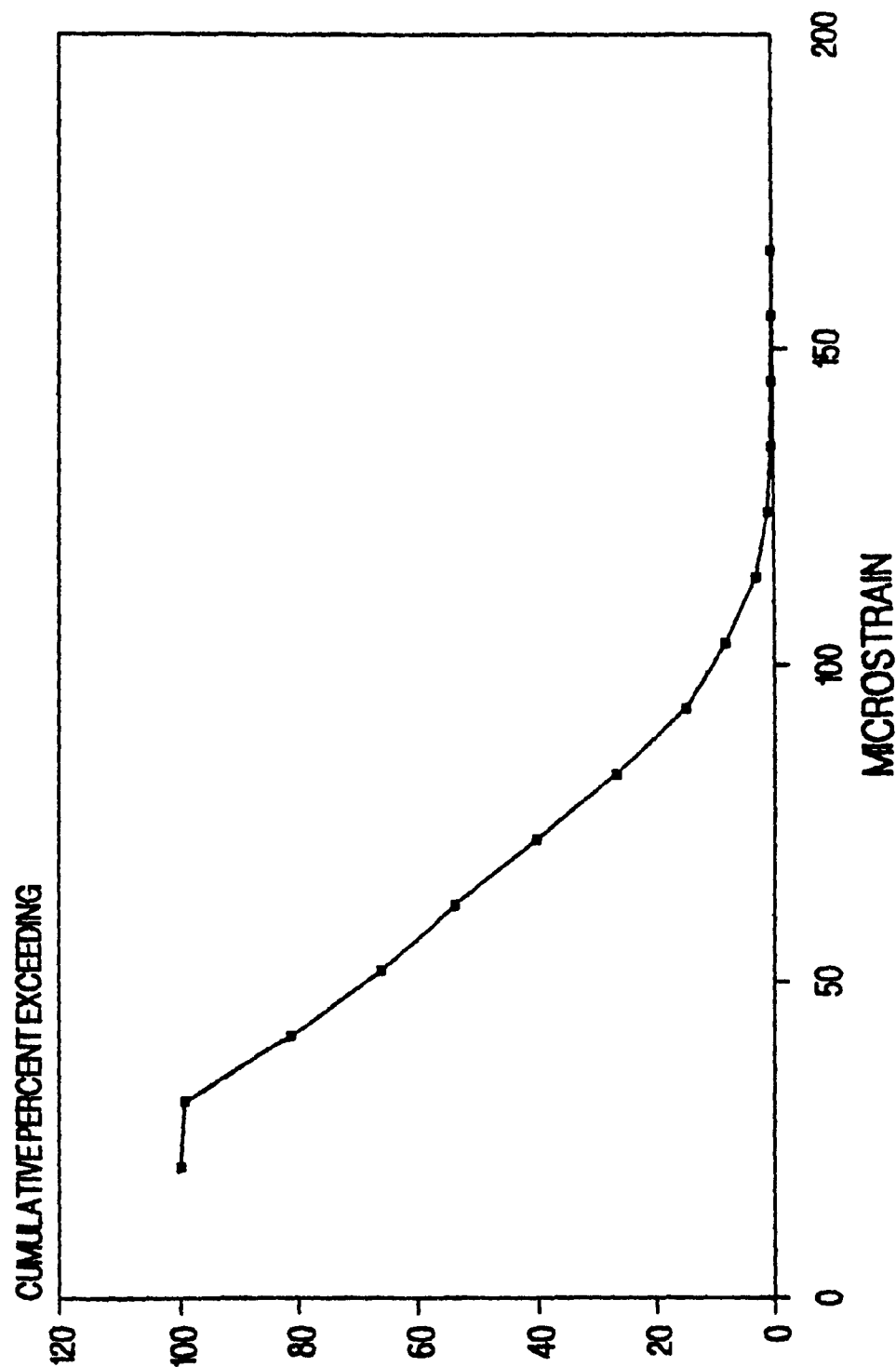
Figure B 1.7 Cumulative Exceeding Graph for 20RB, 1984

Figure B 1.8   Summary Graph 3, 8, 15, 20RB for 1984

CUM. PERCENT EXCEEDING vs STRAIN
SUMMARY 3RB, 8RB, 15RB AND 20RB 1984
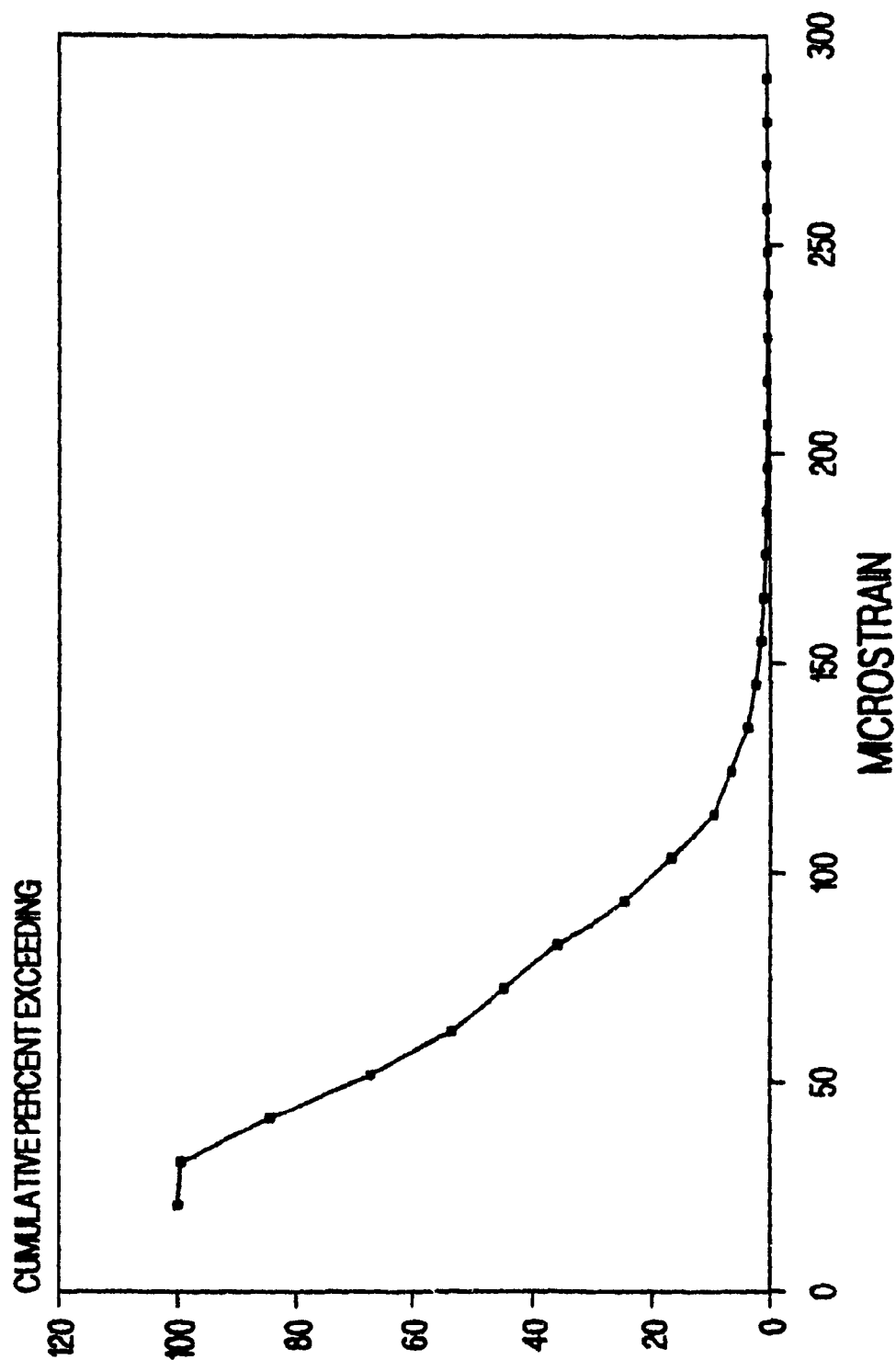
Figure B 1.9 Cumulative Exceeding Graph for 3, 8, 15, 20RB, 1984

%OCCURRENCE vs STRAIN
SUMMARY 8RT – REVERSE BENDING 1984
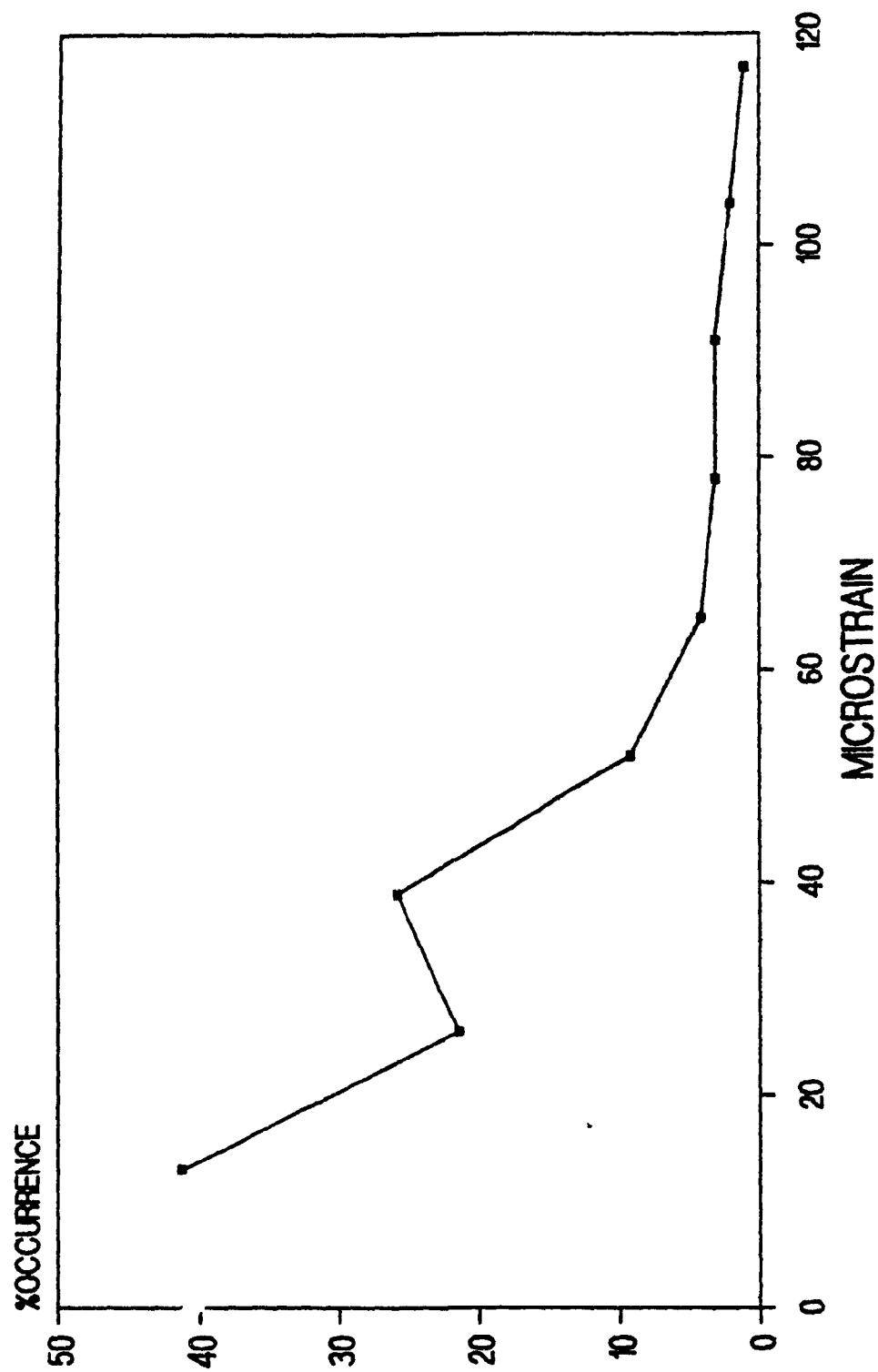
Figure B 2.0 Summary Graph 8RT for 1984

CUM. PERCENT EXCEEDING vs STRAIN
SUMMARY 8RT – REVERSE BENDING

CUMULATIVE PERCENT EXCEEDING

MICROSTRAIN
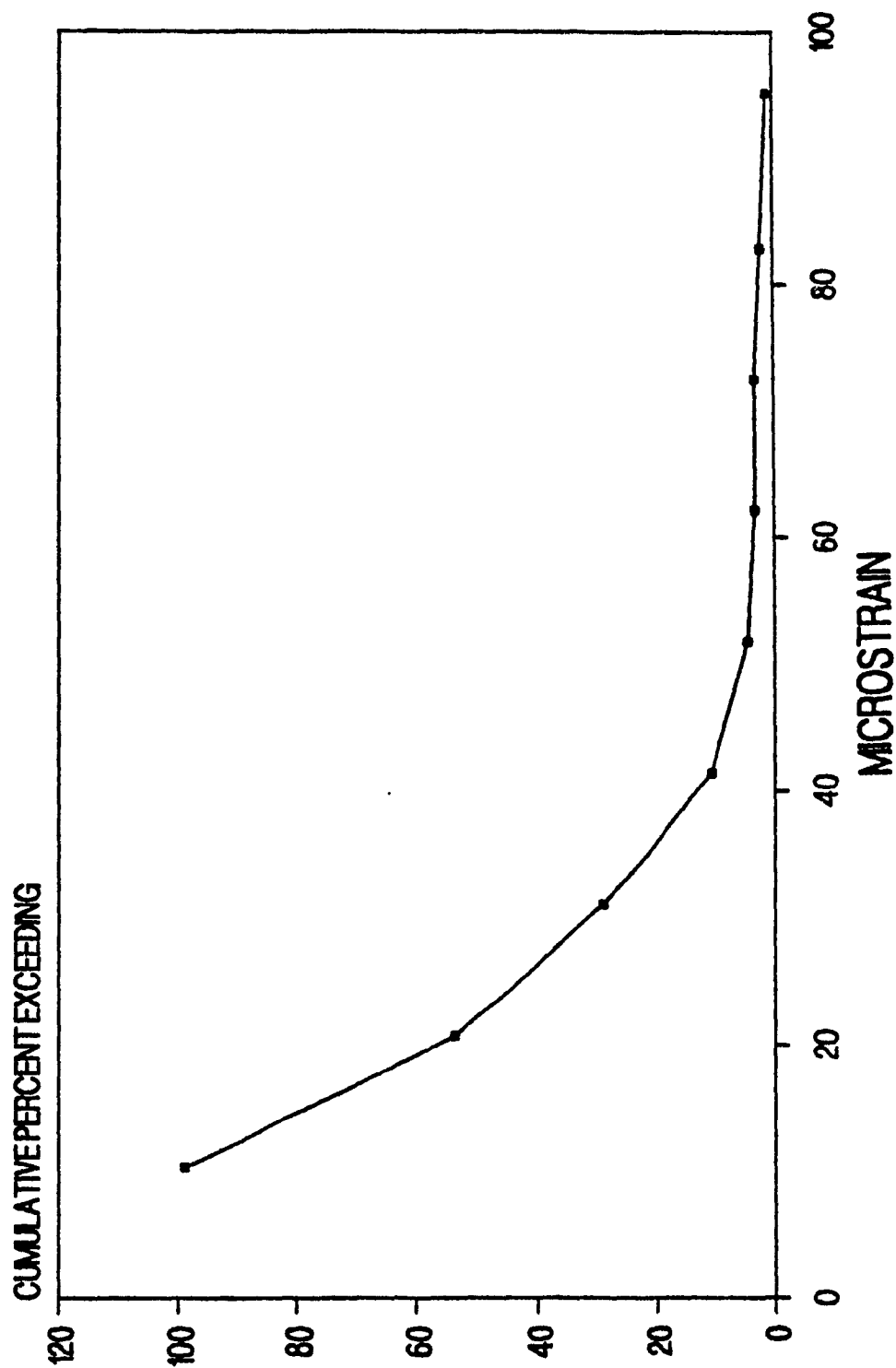
Figure B 2.1 Cumulative Exceeding Graph for 8RT, 1984

%OCCURRENCE vs STRAIN
SUMMARY 15RT – REVERSE BENDING 1984
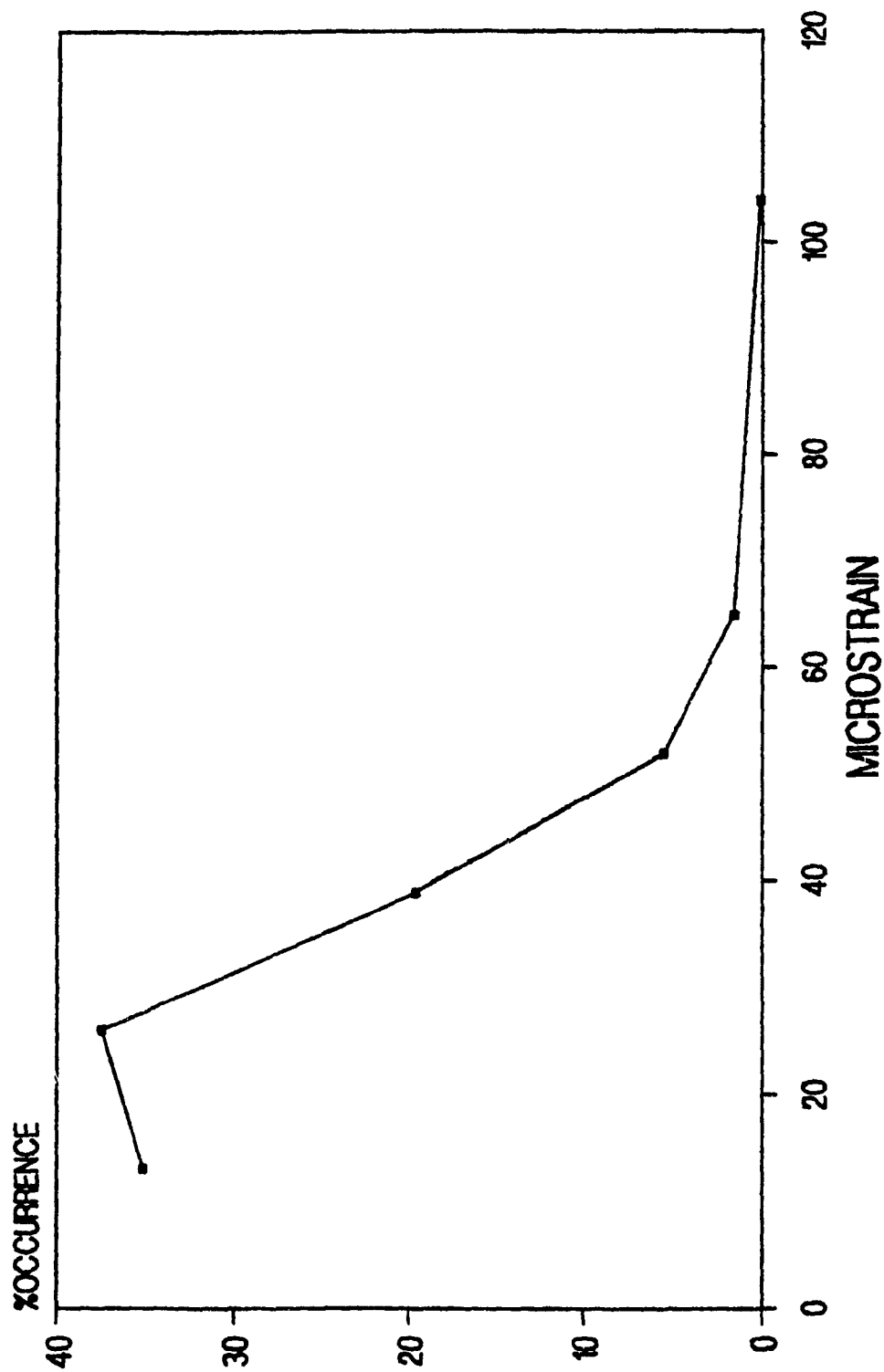
Figure B 2.2   Summary Graph 15RT for 1984

CUM. PERCENT EXCEEDING vs STRAIN
SUMMARY 15RT – REVERSE BENDING
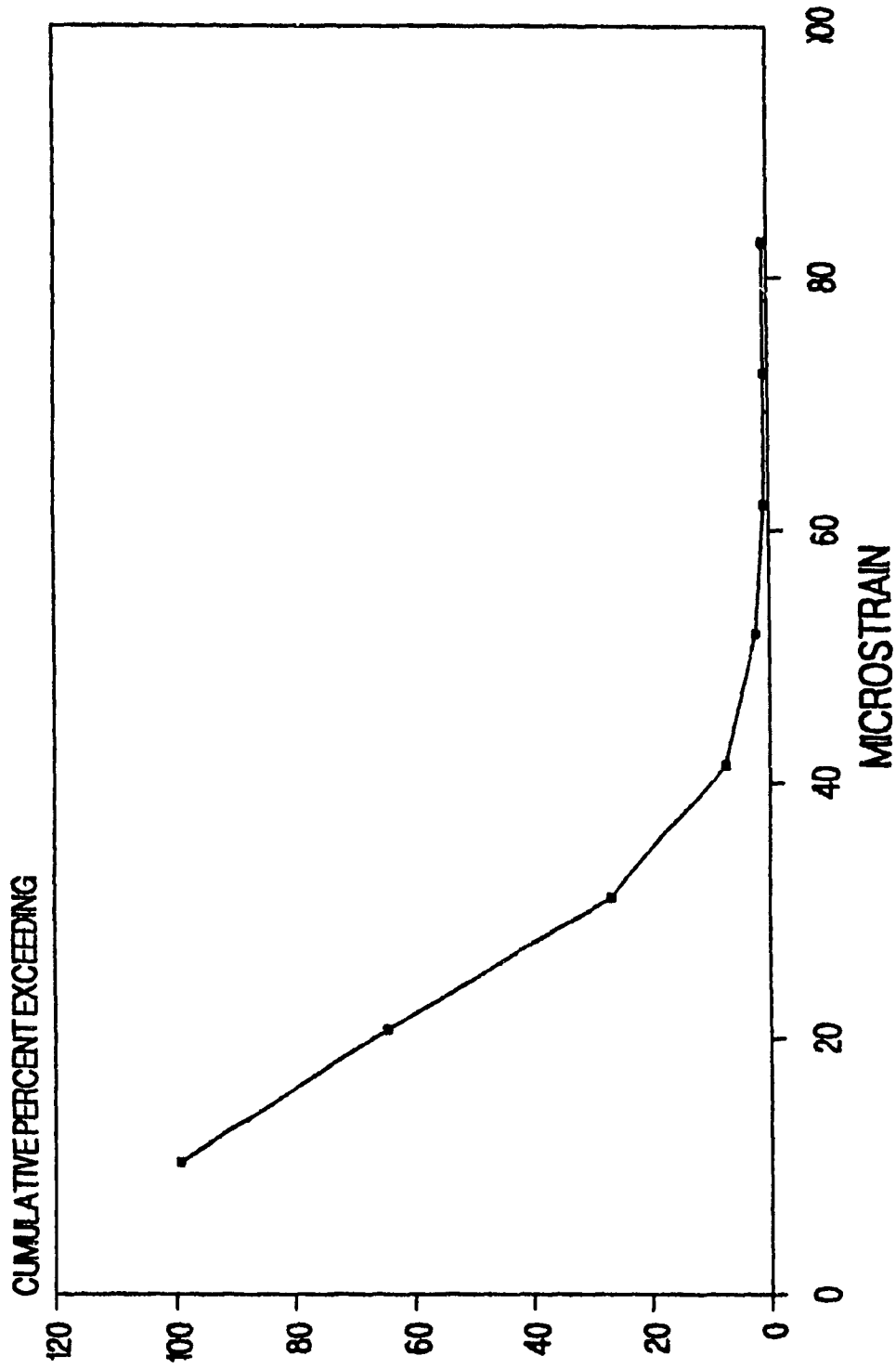
Figure B 2.3 Cumulative Exceeding Graph for 15RT, 1984

190

%OCCURRENCE vs STRAIN

SUMMARY 20RT – REVERSE BENDING 1984
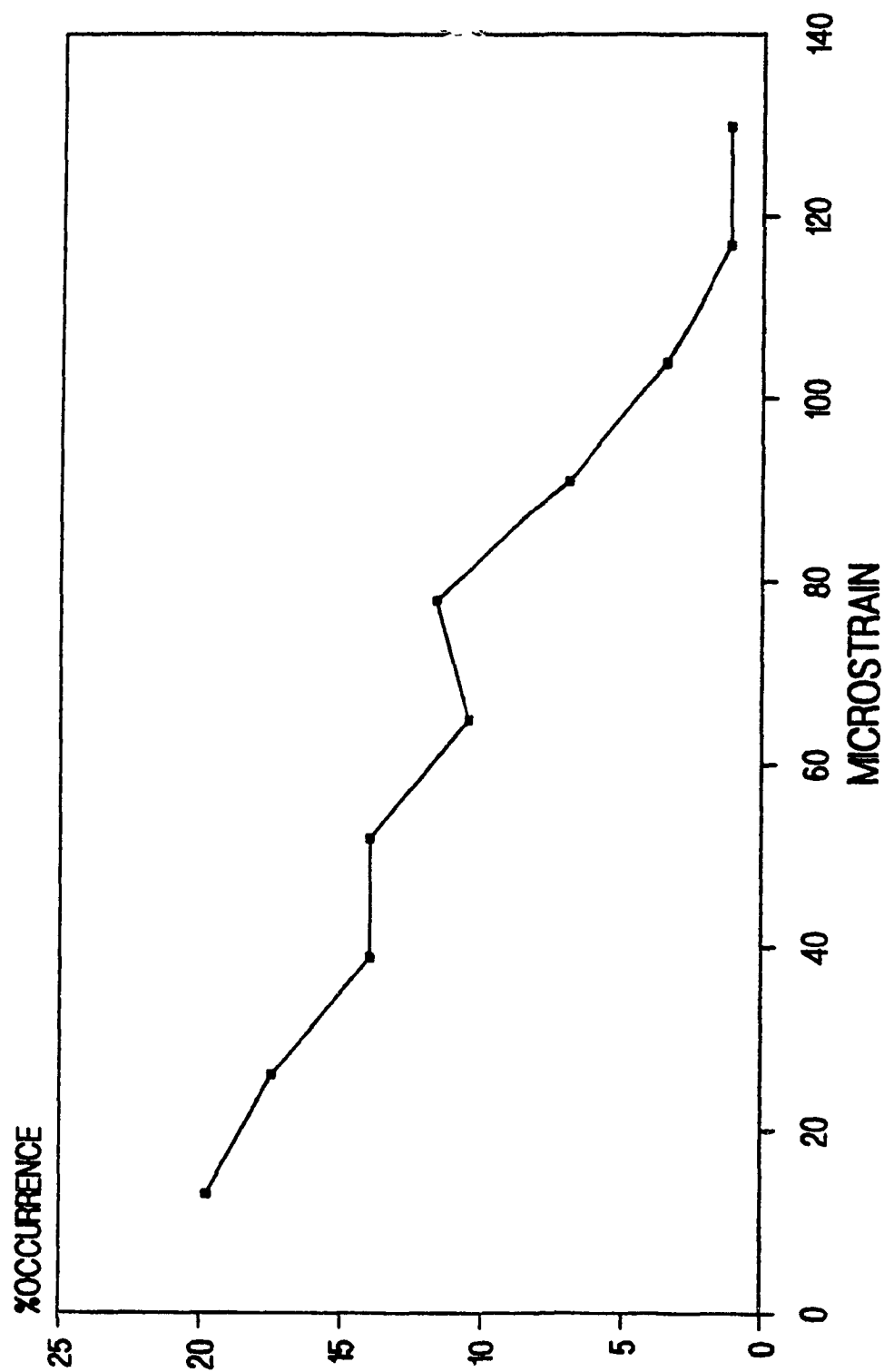
Figure B 2.4   Summary Graph 20RT for 1984

CUM. PERCENT EXCEEDING vs STRAIN
SUMMARY 20RT – REVERSE BENDING

CUMULATIVE PERCENT EXCEEDING

MICROSTRAIN
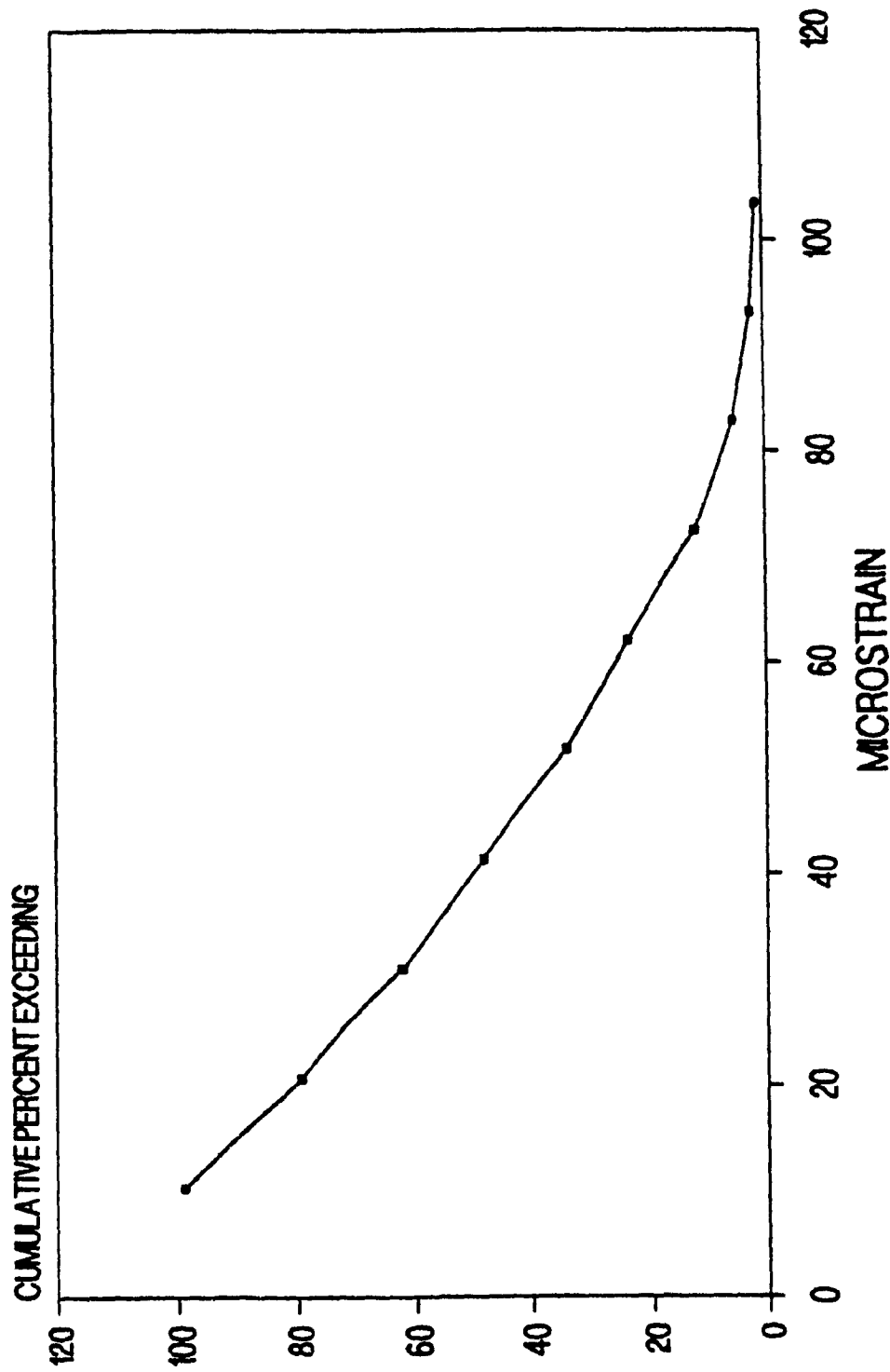
Figure B 2.5   Cumulative Exceeding Graph for 20RT, 1984

%OCCURRENCE vs STRAIN – REVERSE BENDING

SUMMARY 8RT, 15RT AND 20RT 1984

%OCCURRENCE

MICROSTRAIN
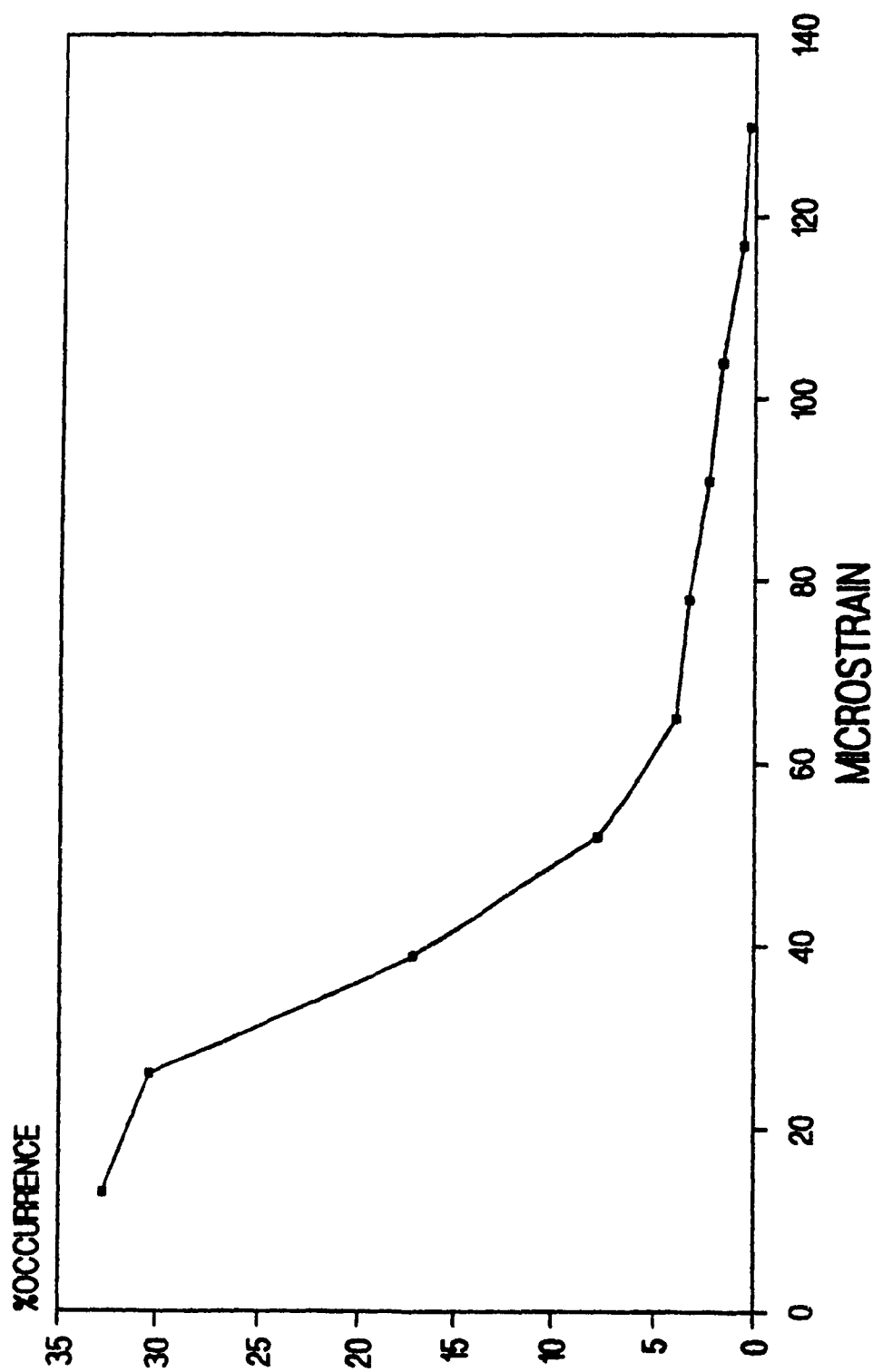
Figure B 2.6   Summary Graph 8, 15, 20RT for 1984

193

CUM. PERCENT EXCEEDING vs STRAIN
—REVERSE BENDING
SUMMARY 8RT, 15RT AND 20RT

CUMULATIVE PERCENT EXCEEDING

MICROSTRAIN
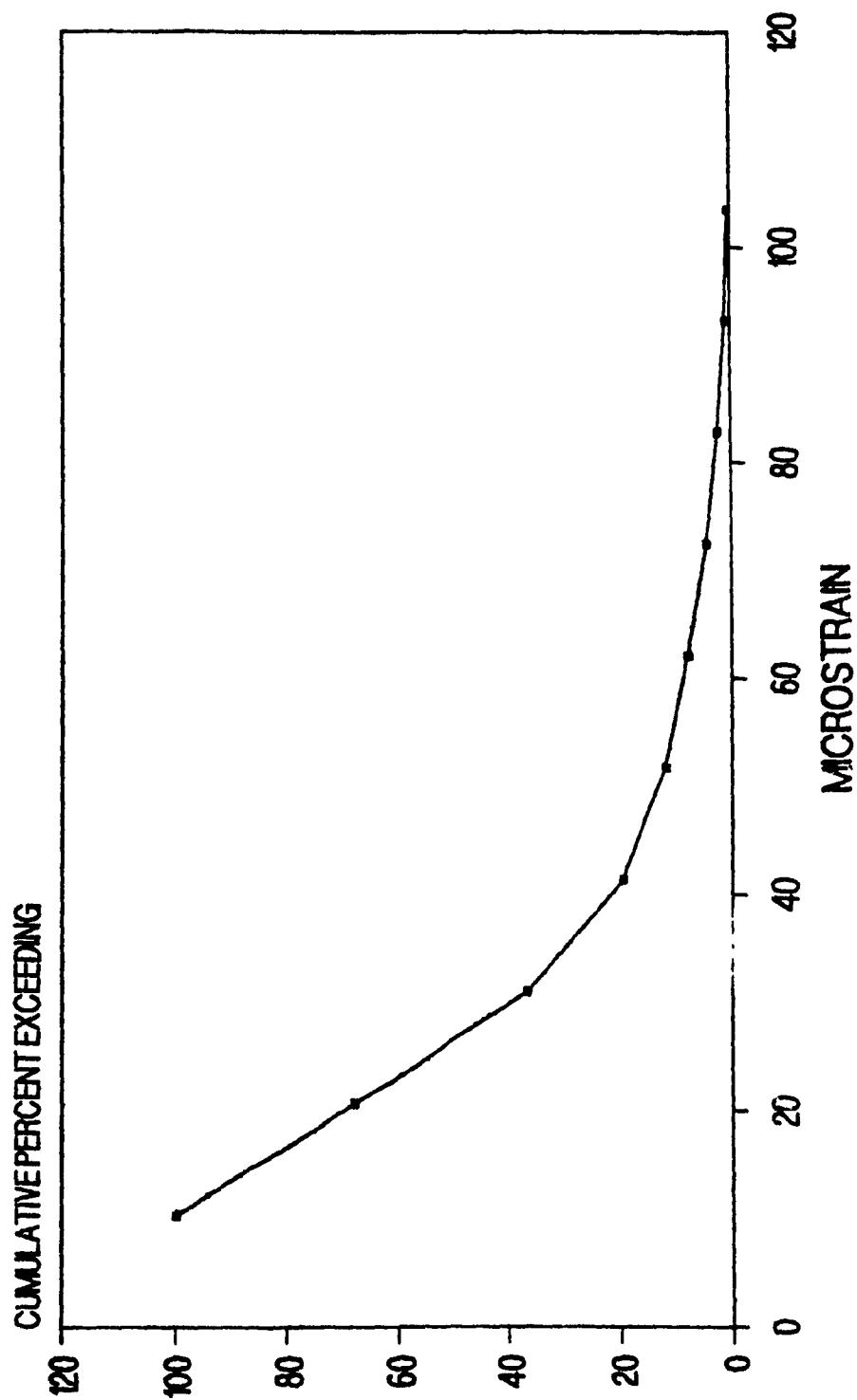
Figure B 2.7 Cumulative Exceeding Graph for 8, 15, 20RT, 1984

%OCCURRENCE vs STRAIN
SUMMARY 3RB – POSITIVE BENDING 1986

%OCCURRENCE

MICROSTRAIN
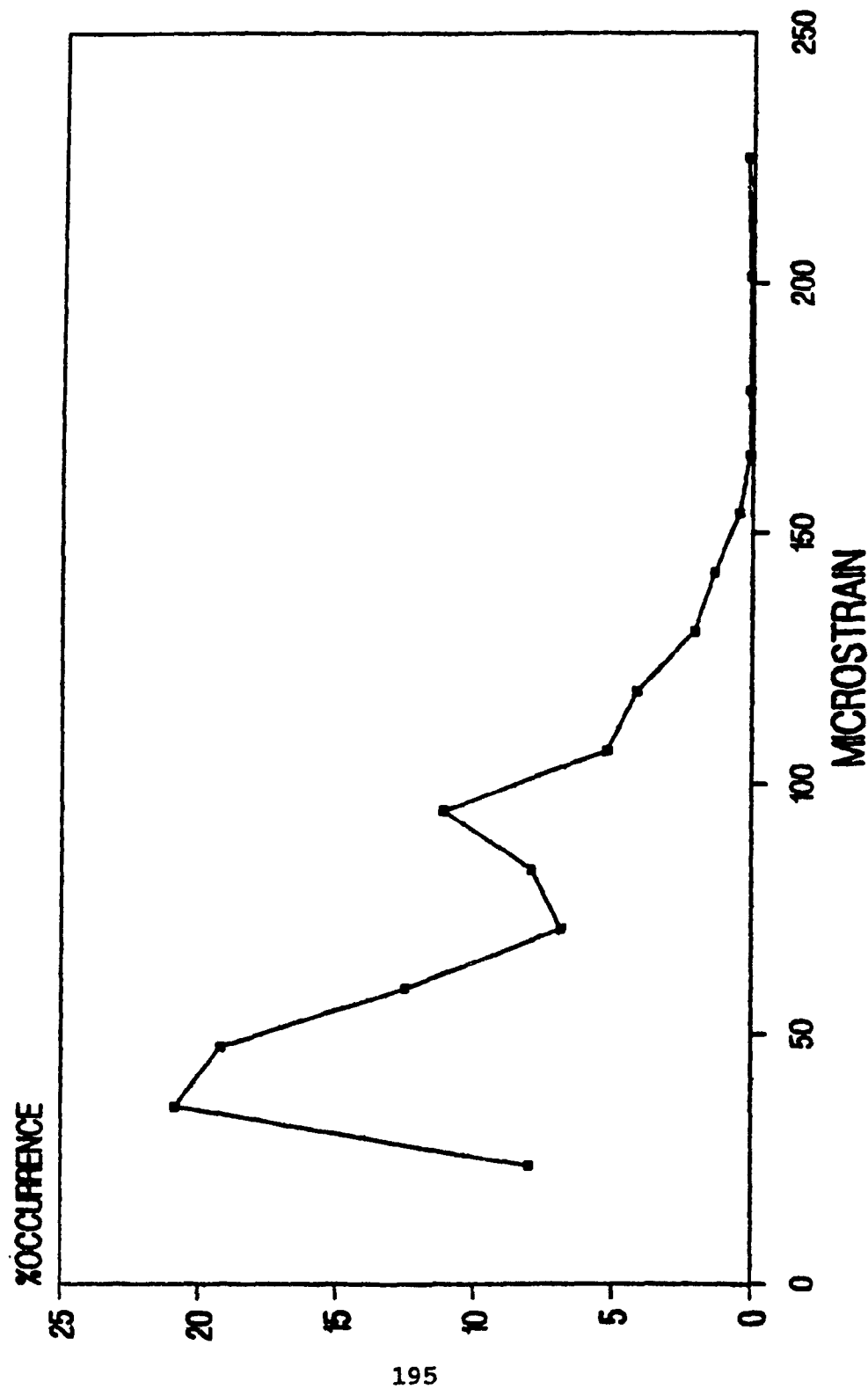
Figure B 3.0   Summary Graph 3RB for 1986

CUM. PERCENT EXCEEDING vs STRAIN
SUMMARY 3RB – POSITIVE BENDING 1986
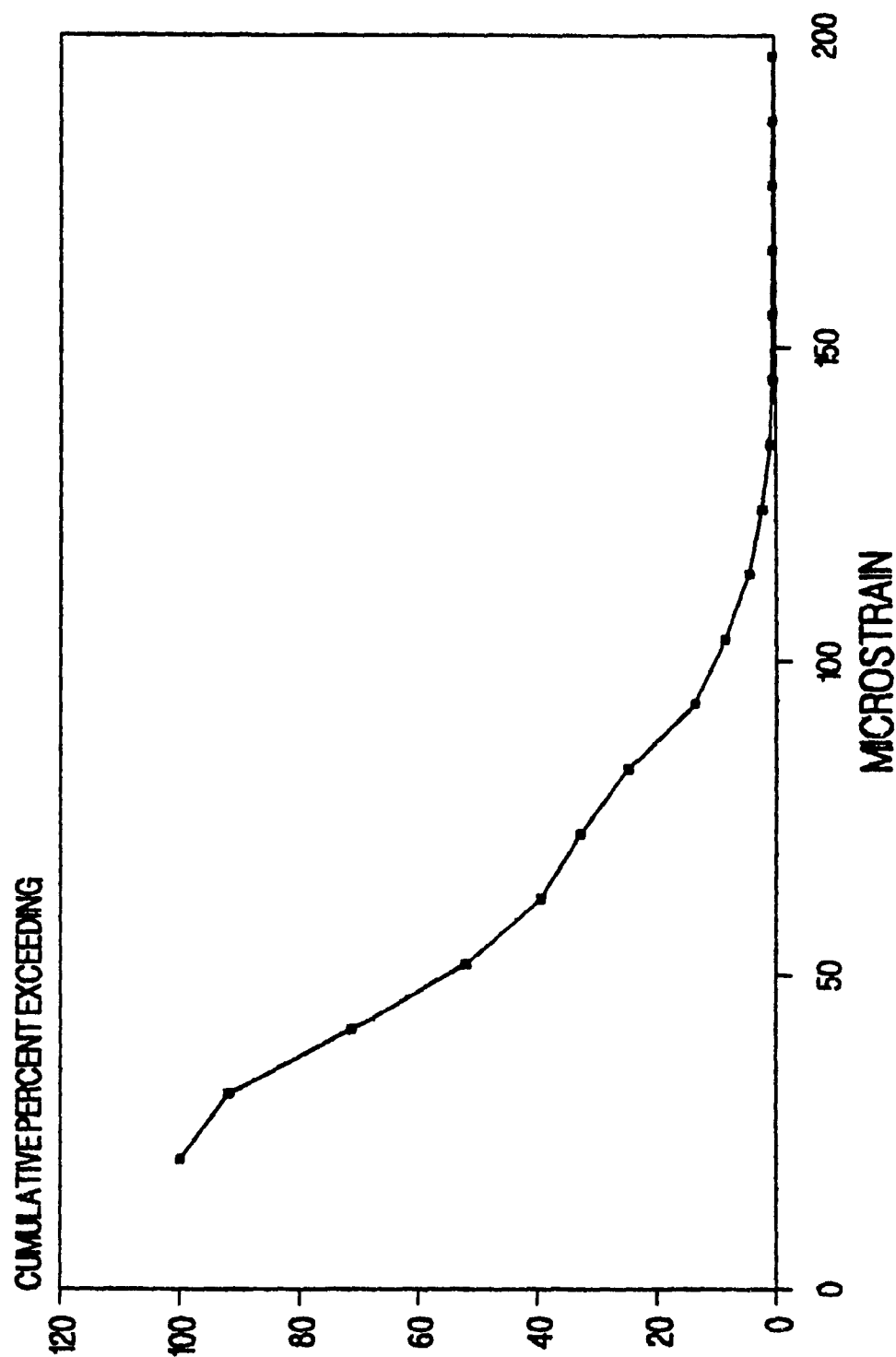
Figure B 3.1 Cumulative Exceeding Graph for 3RB, 1986

%OCCURRENCE vs STRAIN
SUMMARY 15RB – POSITIVE BENDING 1986
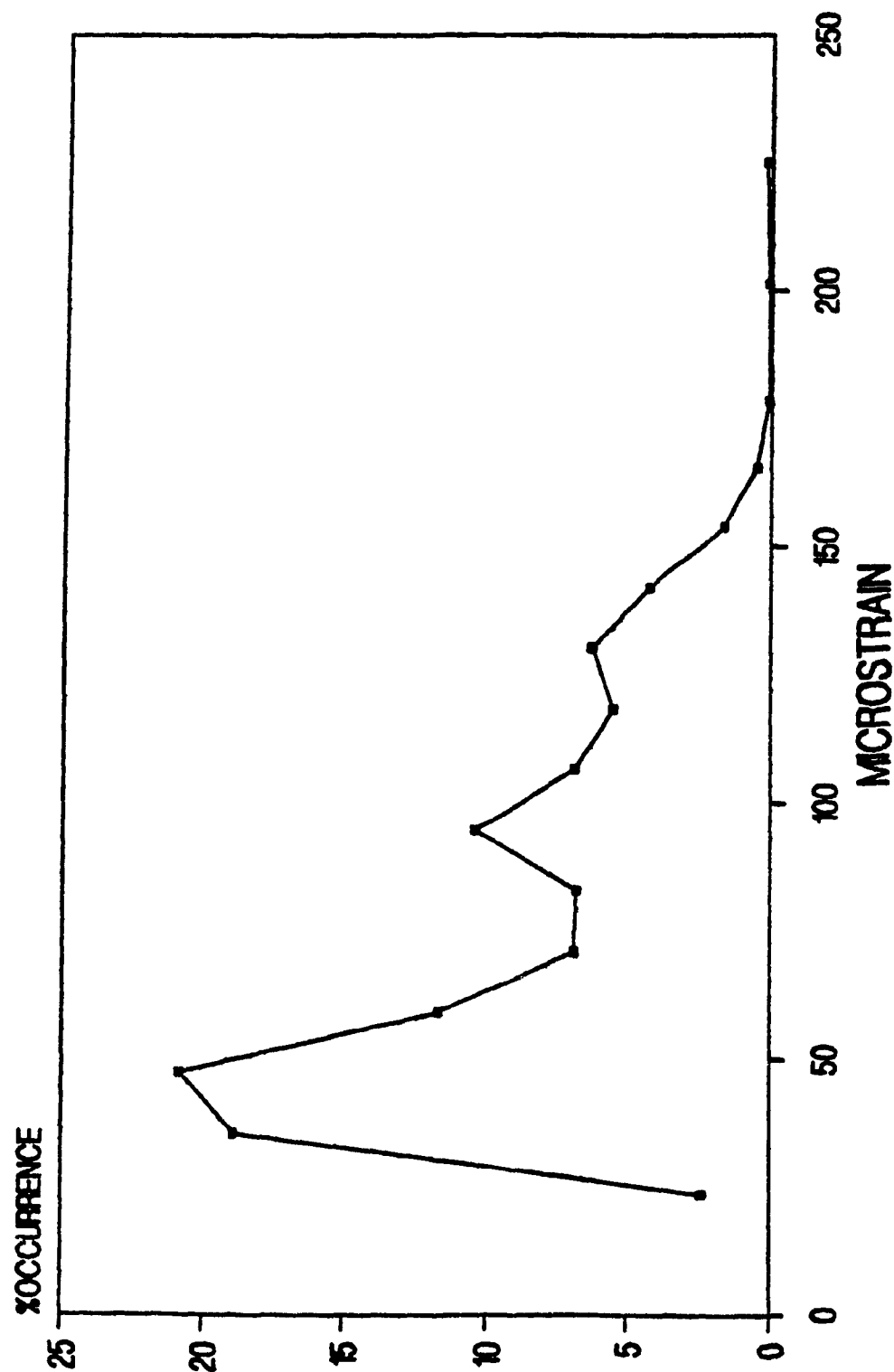
Figure B 3.2   Summary Graph 15RB for 1986

CUM. PERCENT EXCEEDING vs STRAIN
SUMMARY 15RB – POSITIVE BENDING 1986
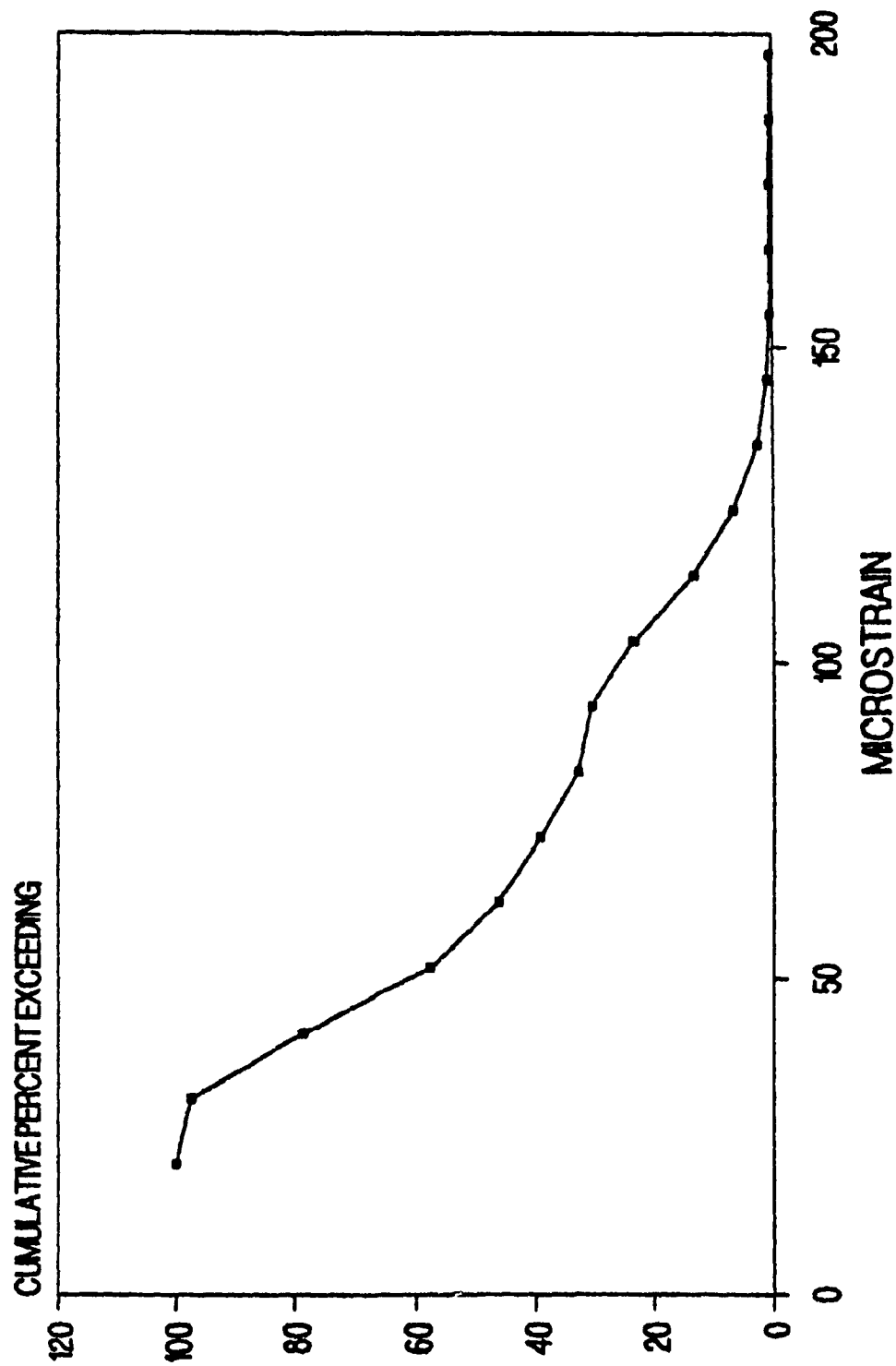
Figure B 3.3   Cumulative Exceeding Graph for 15RB, 1986

%OCCURRENCE vs STRAIN—POSITIVE BENDING
SUMMARY 3RB AND 15RB 1986
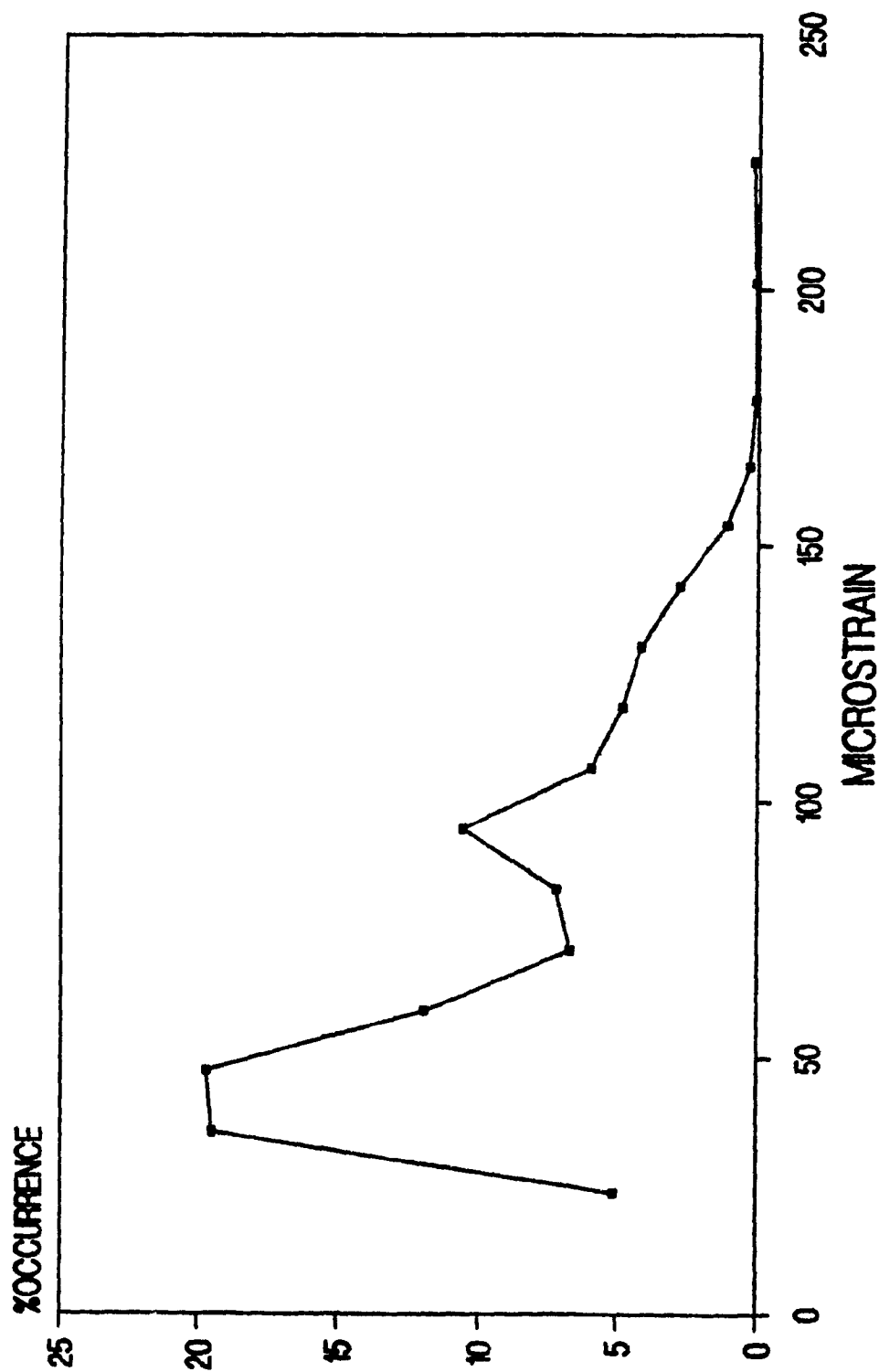
Figure B 3.4 Summary Graph 3, 15RB for 1986

CUM. PERCENT EXCEEDING vs STRAIN
SUMMARY 3RB AND 15RB 1986
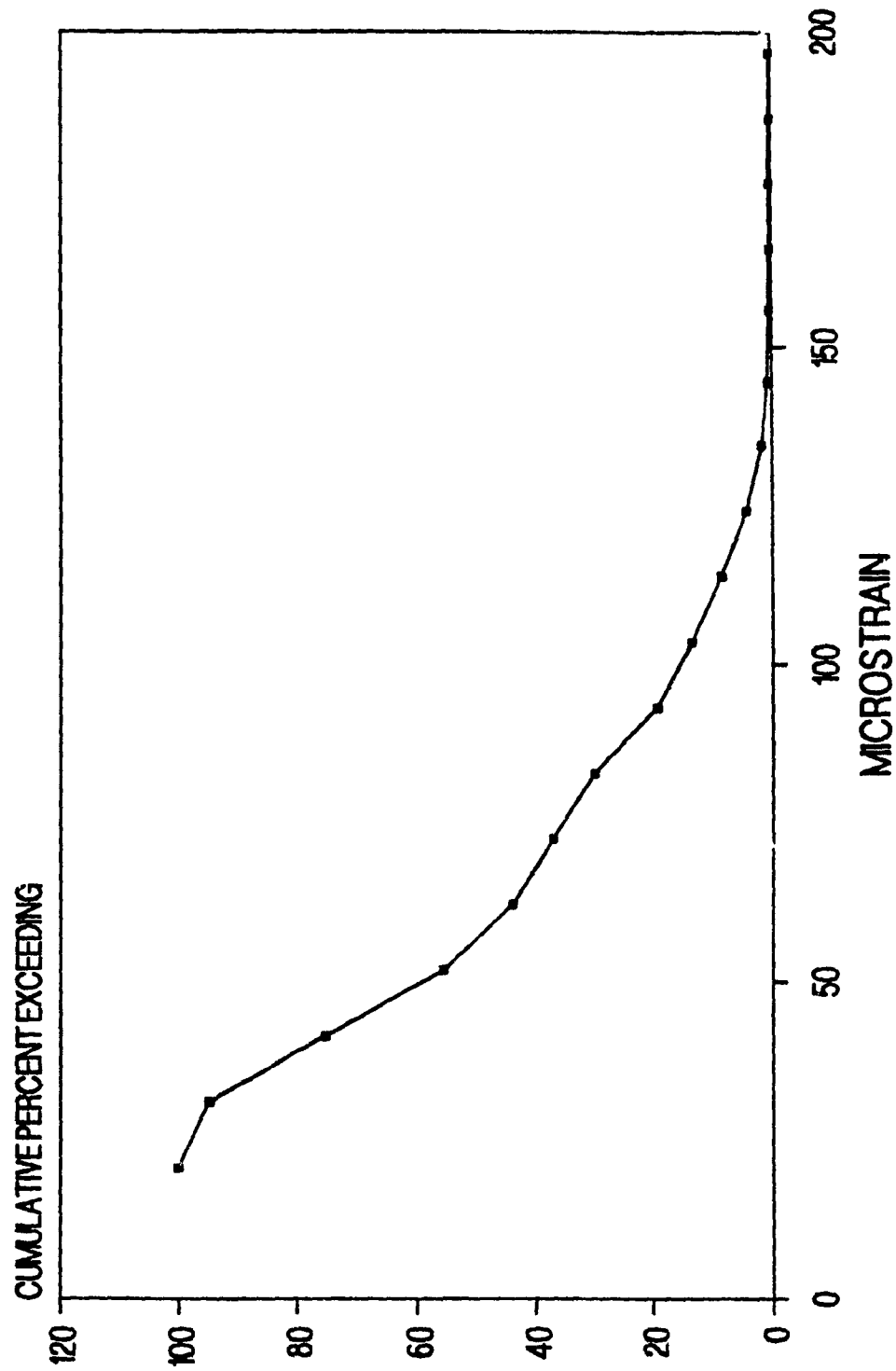
Figure B 3.5   Cumulative Exceeding Graph for 3, 15RB, 1986

%OCCURRENCE vs STRAIN
SUMMARY 1RB – POSITIVE BENDING 1984

%OCCURRENCE

MICROSTRAIN
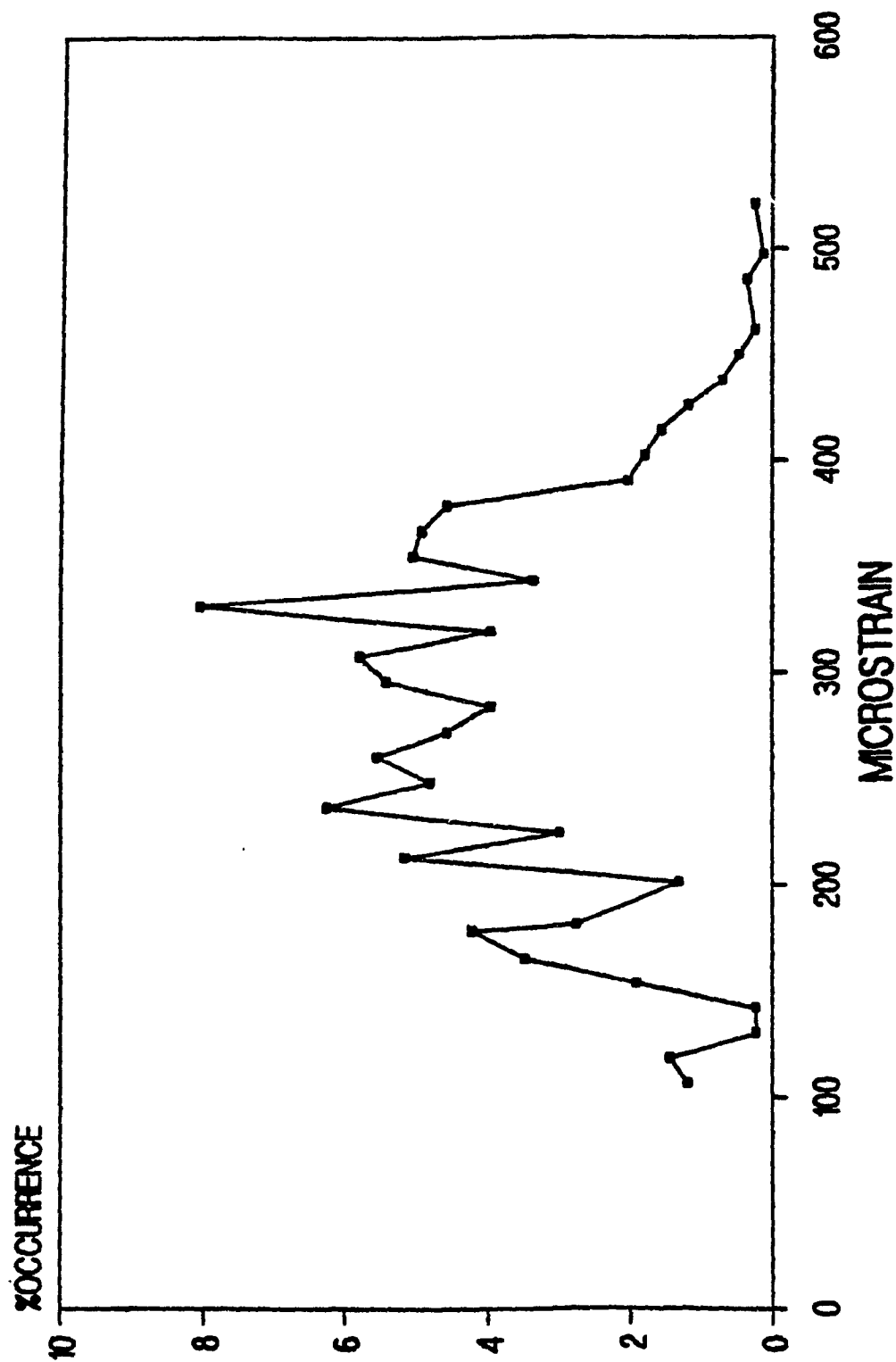
Figure B 4.0   Summary Graph 1RB for 1984

CUM. PERCENT EXCEEDING vs STRAIN
SUMMARY 1RB – POSITIVE BENDING 1984
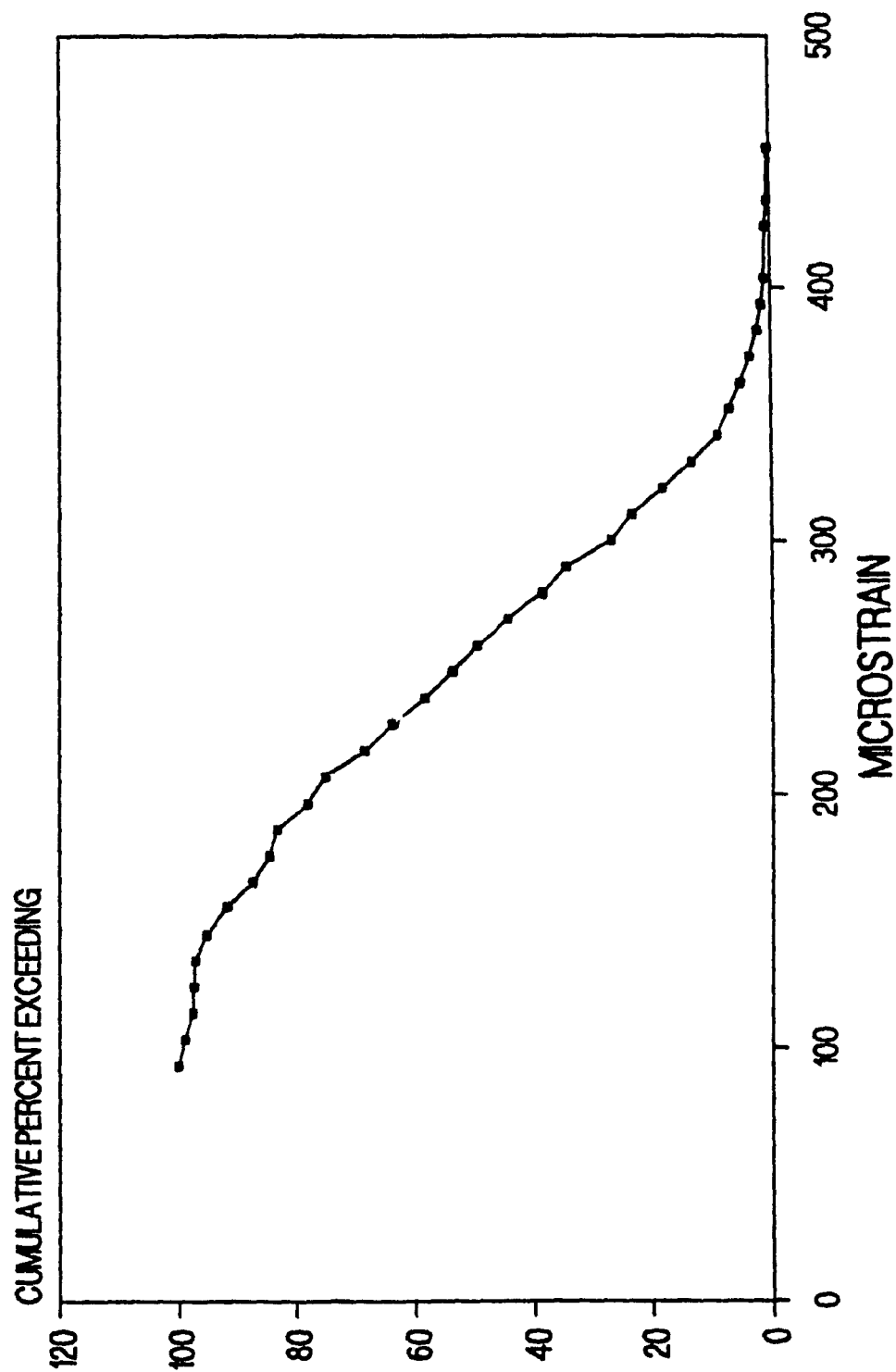
Figure B 4.1 Cumulative Exceeding Graph for 1RB, 1984

%OCCURRENCE vs STRAIN
SUMMARY 22RB – POSITIVE BENDING 1984
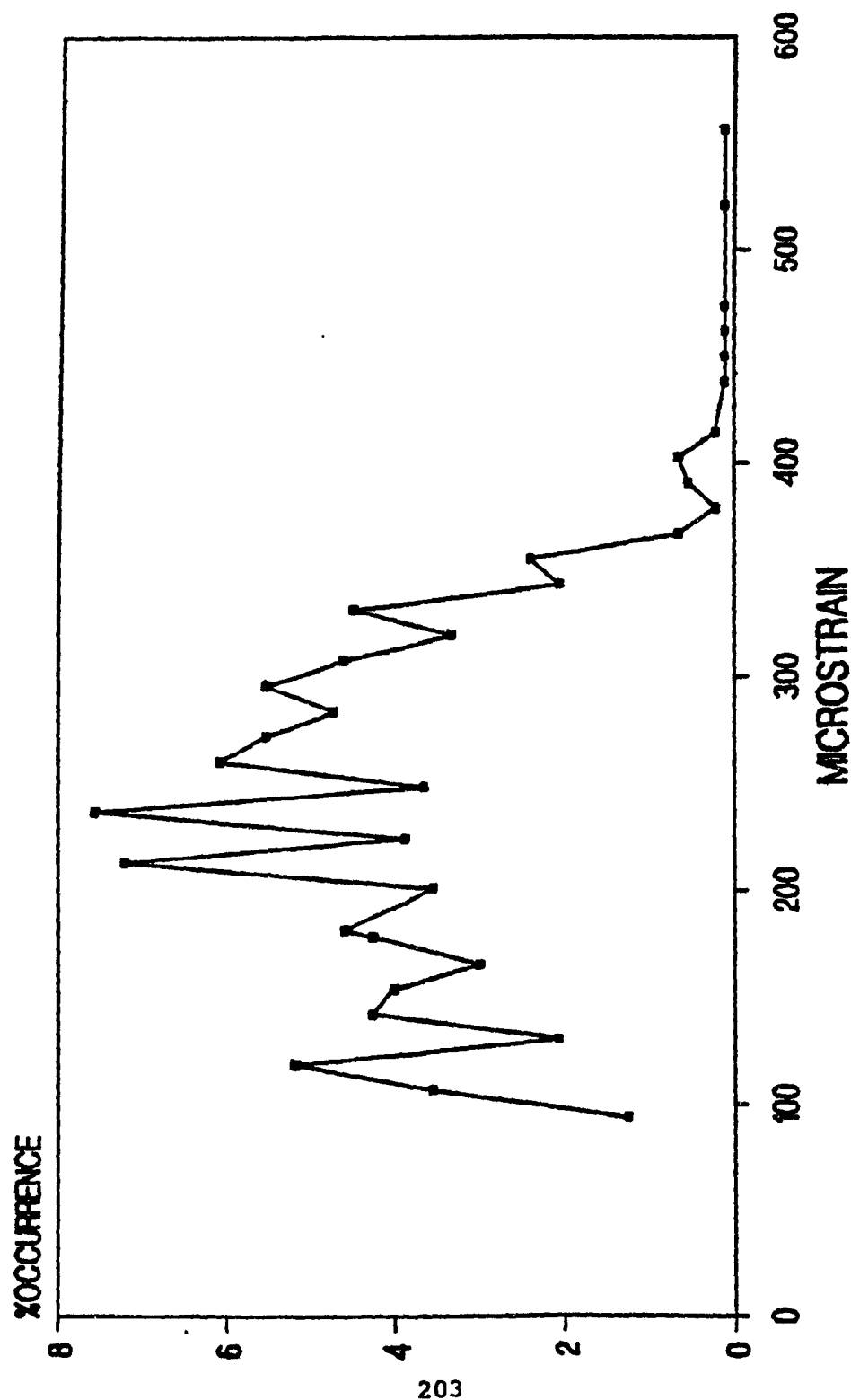
Figure B 4.2 Summary Graph 22RB for 1984

CUM. PERCENT EXCEEDING vs STRAIN
SUMMARY 22RB –POSITIVE BENDING 1984
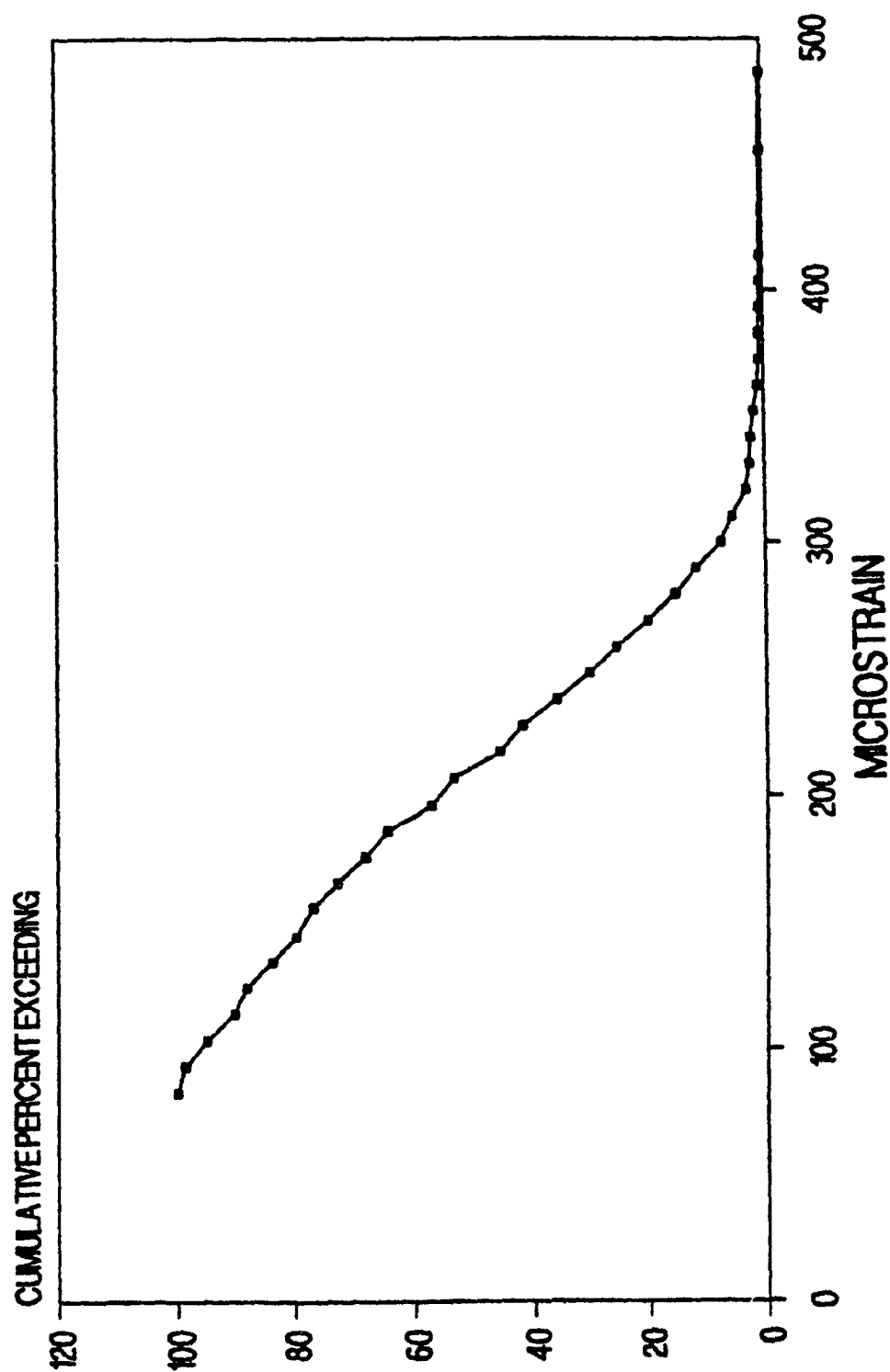
Figure B 4.3   Cumulative Exceeding Graph for 22RB, 1984

%OCCURRENCE vs STRAIN
SUMMARY 1RB –POSITIVE BENDING 1986
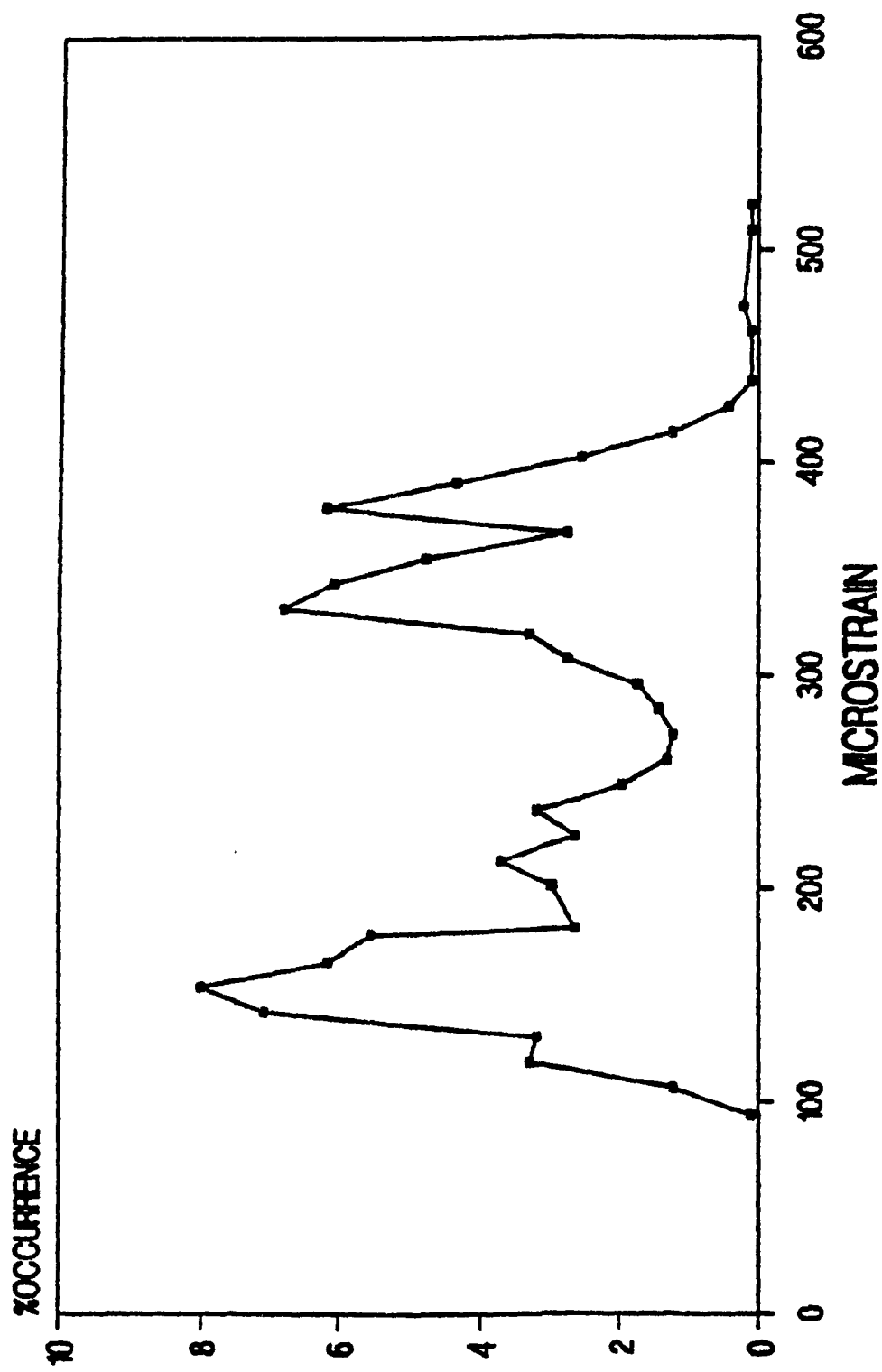
Figure B 4.4 Summary Graph 1RB for 1986

CUM. PERCENT EXCEEDING vs STRAIN
SUMMARY 1RB – POSITIVE BENDING 1986
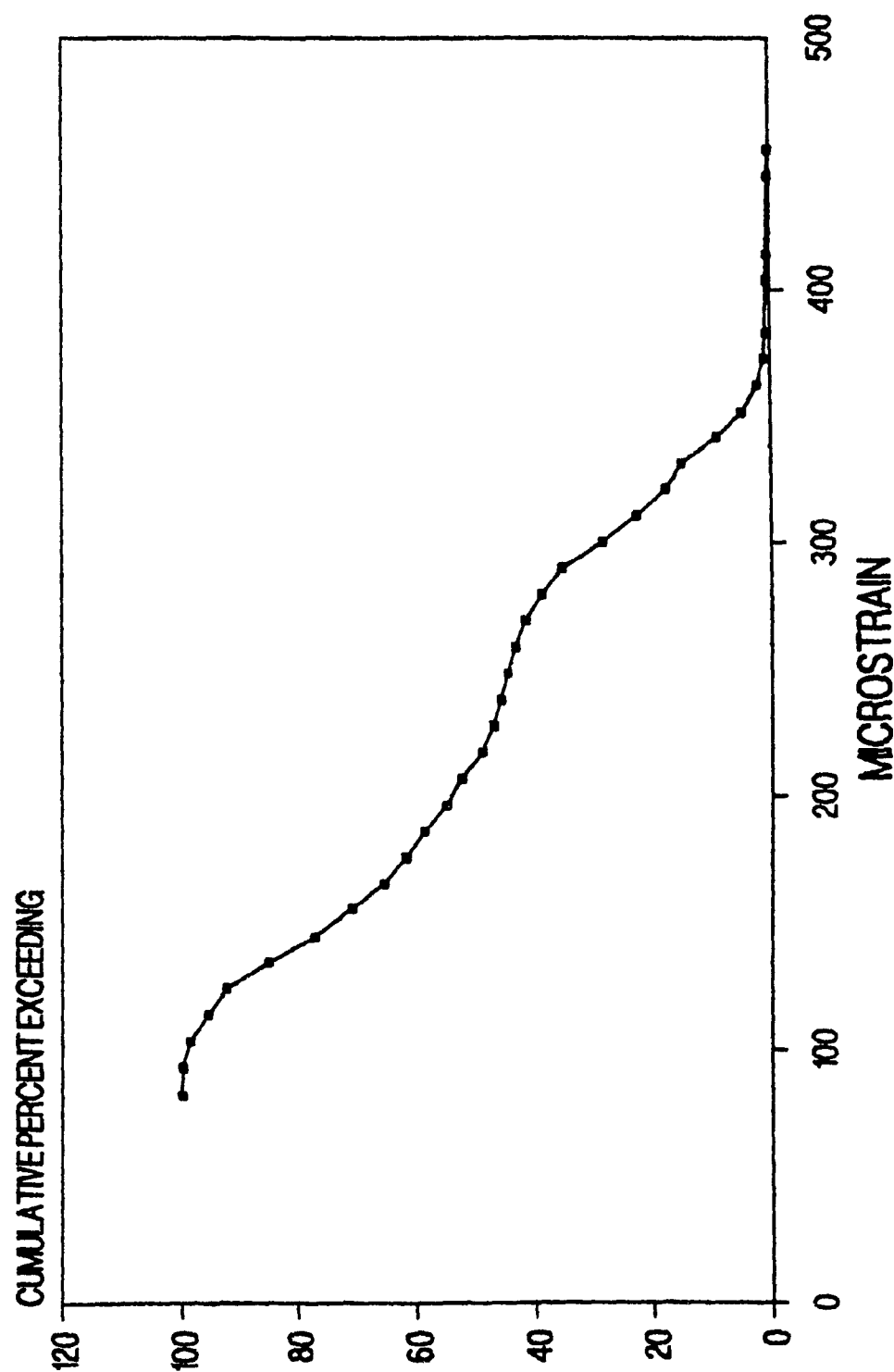
Figure B 4.5   Cumulative Exceeding Graph for 1RB, 1986

%OCCURRENCE vs STRAIN
SUMMARY 22RB – POSITIVE BENDING 1986
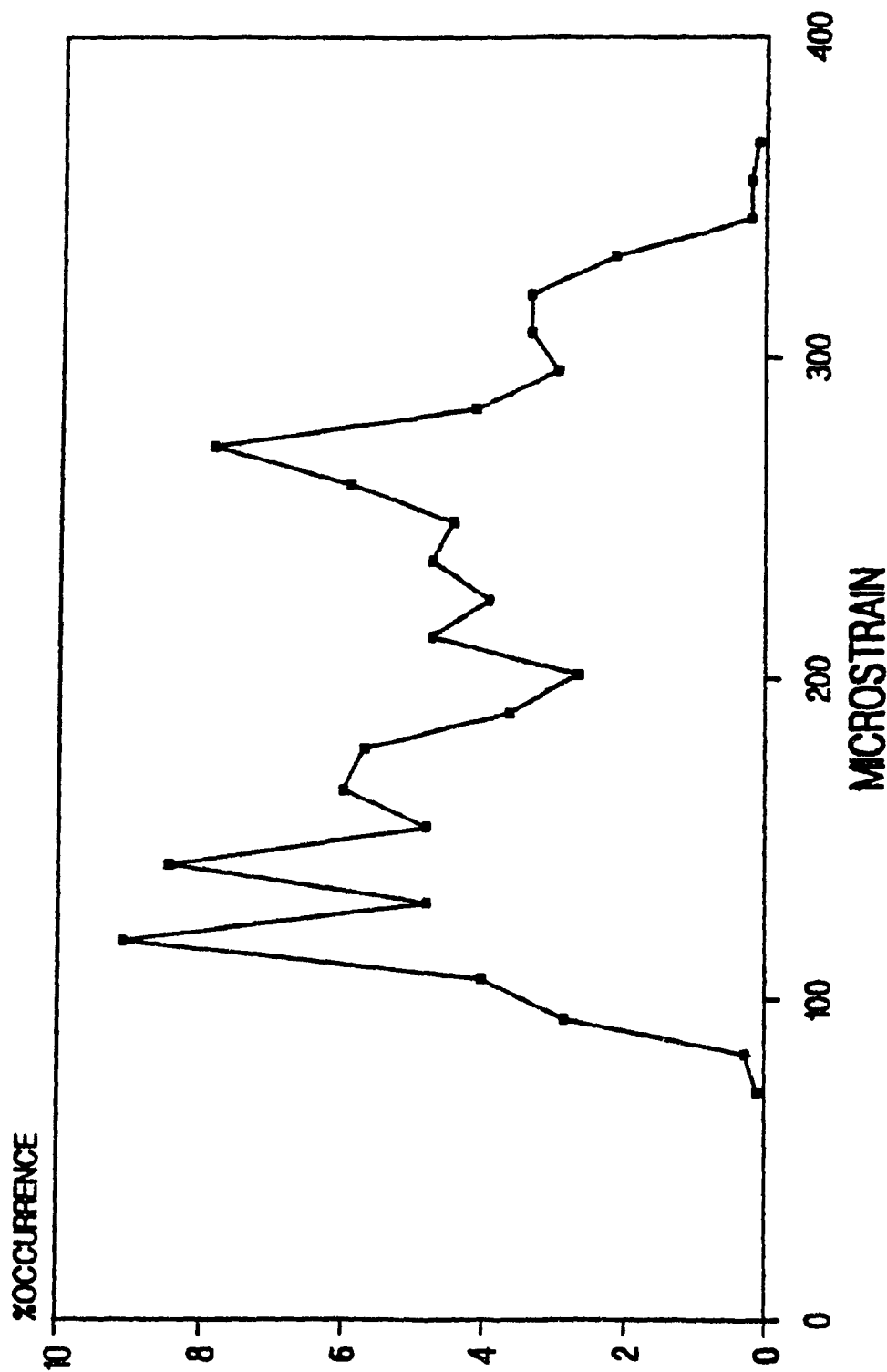
Figure B 4.6   Summary Graph 22RB for 1986

CUM. PERCENT EXCEEDING vs STRAIN
SUMMARY 22RB – POSITIVE BENDING 1986

CUMULATIVE PERCENT EXCEEDING

MICROSTRAIN
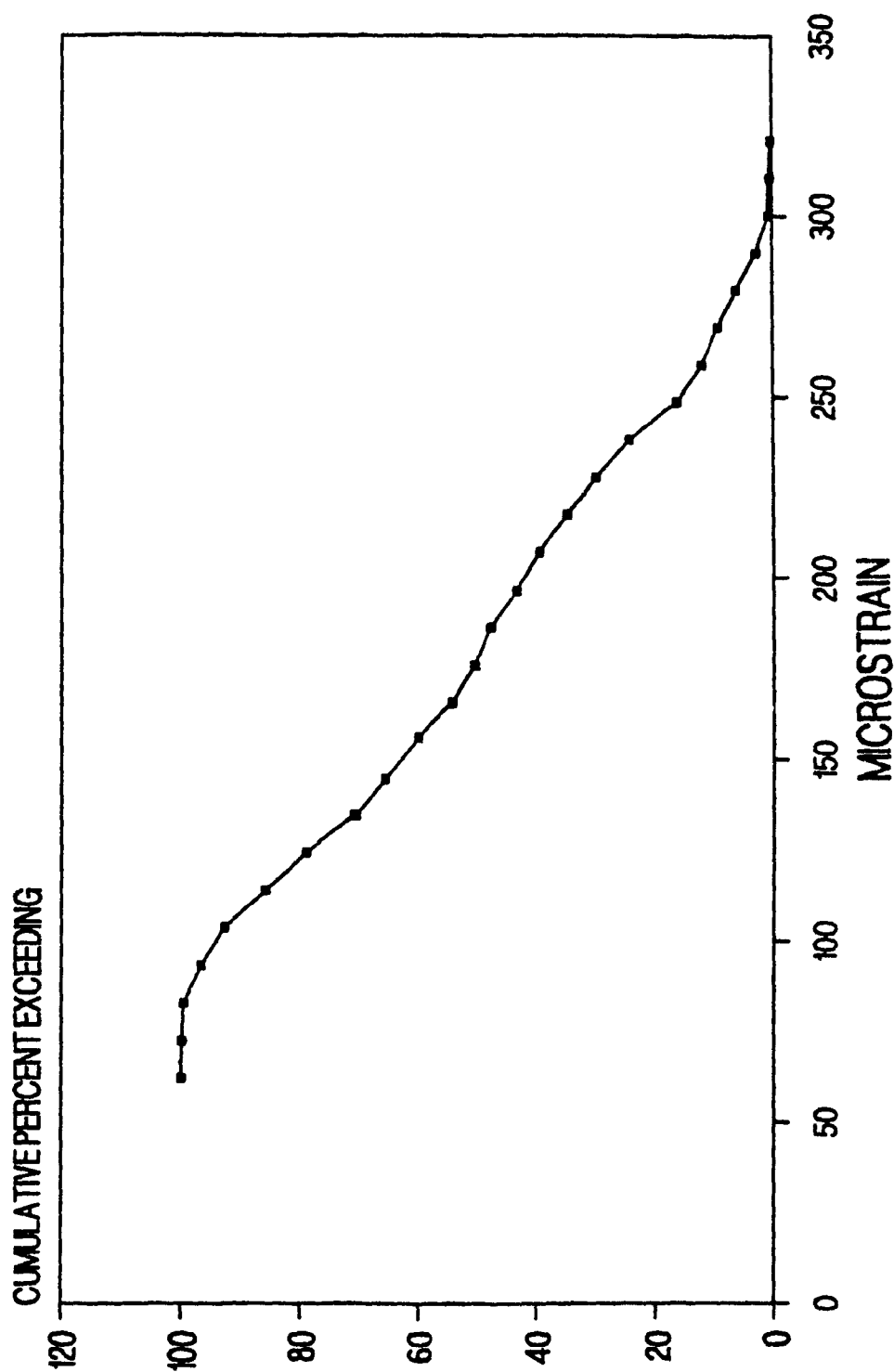
Figure B 4.7 Cumulative Exceeding Graph for 22RB, 1986

AVERAGE STRAINS vs SPEED
LIGHT WHEEL LOADS
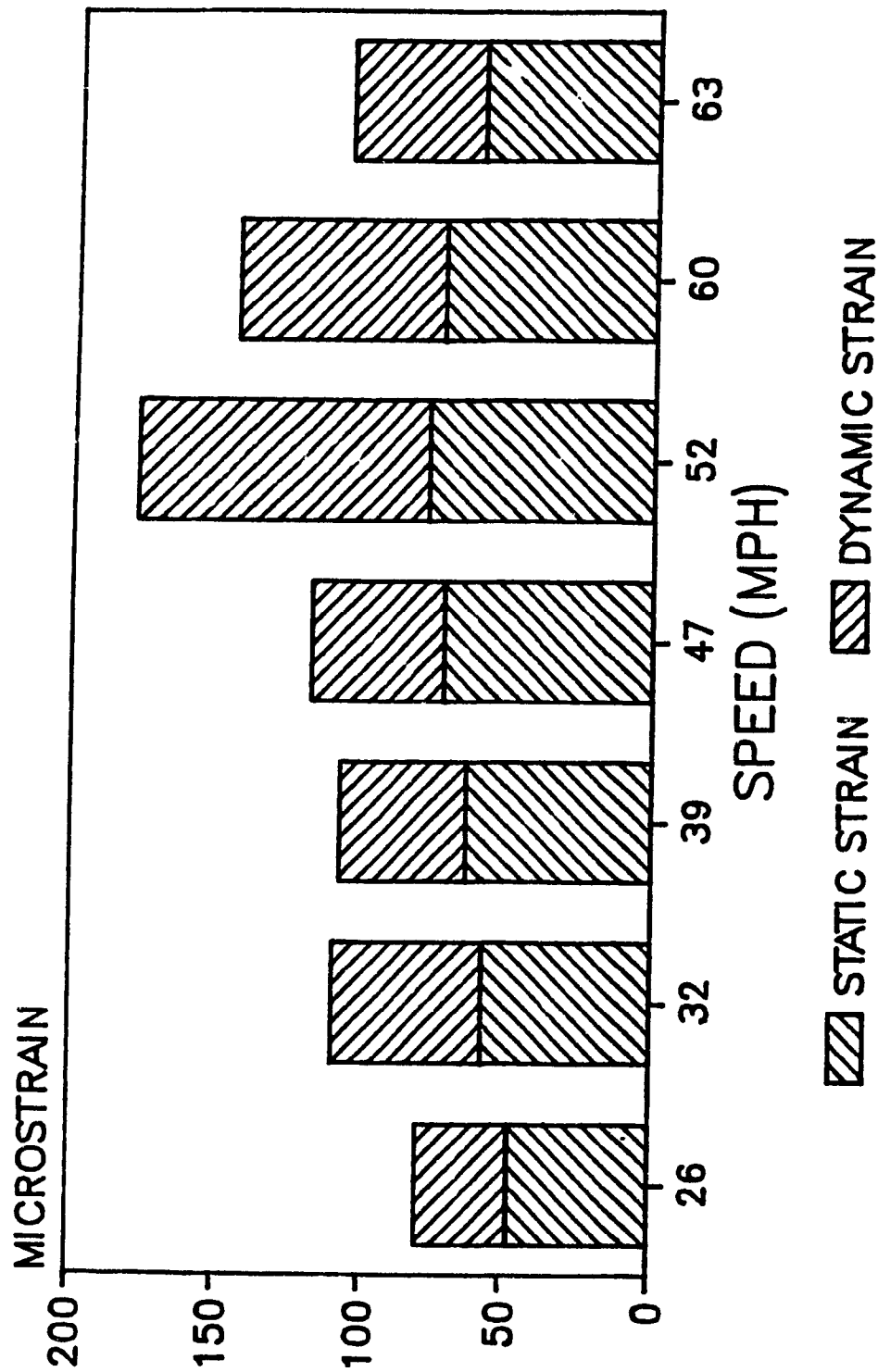
Figure B 5.0 Average Strain Versus Speed for Light Loads

209

AVERAGE STRAINS vs SPEED
HEAVY WHEEL LOADS

MICROSTRAIN

SPEED (MPH)

STATIC STRAIN   DYNAMIC STRAIN
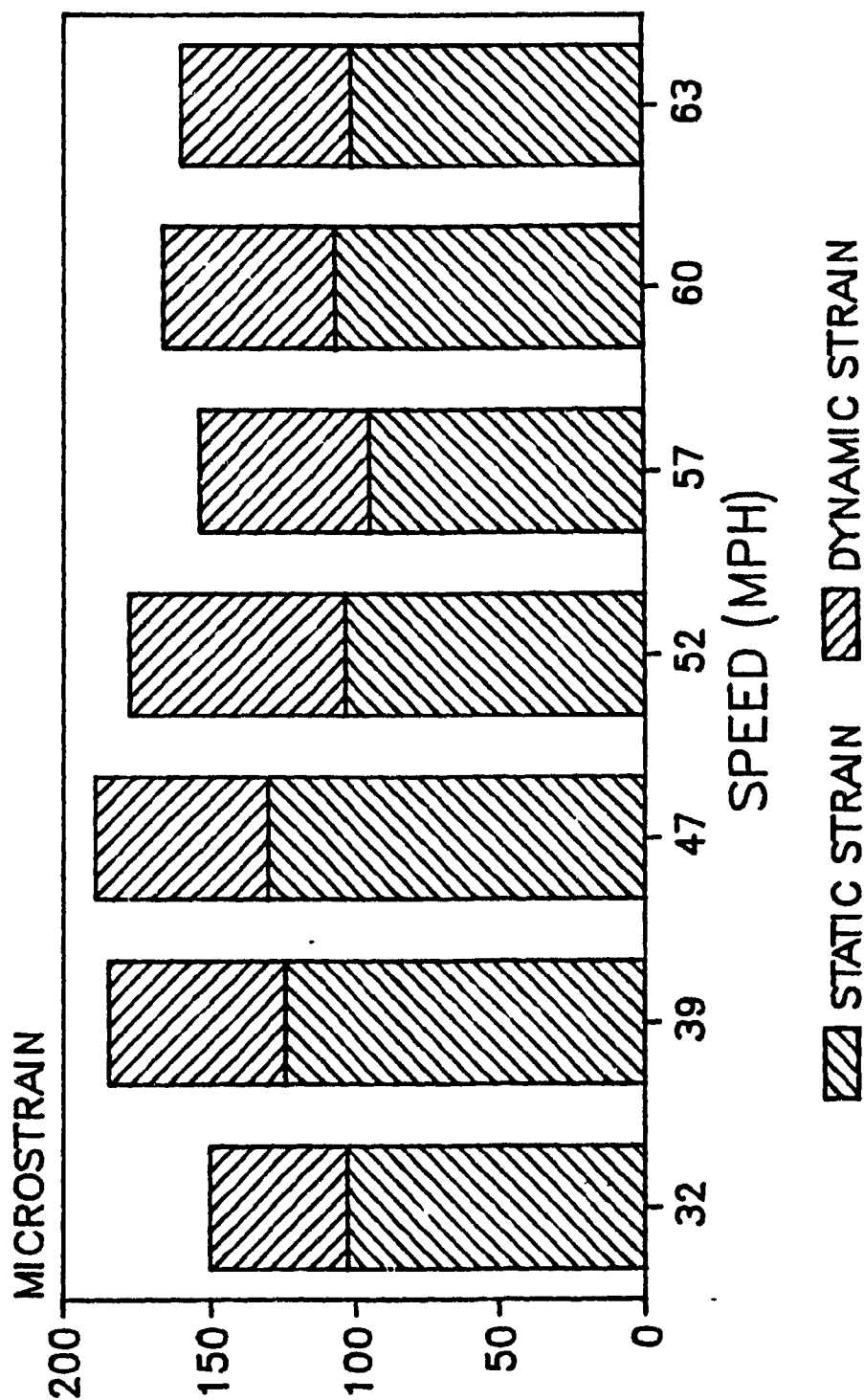
Figure B 5.1   Average Strain versus Speed for Heavy Loads

210
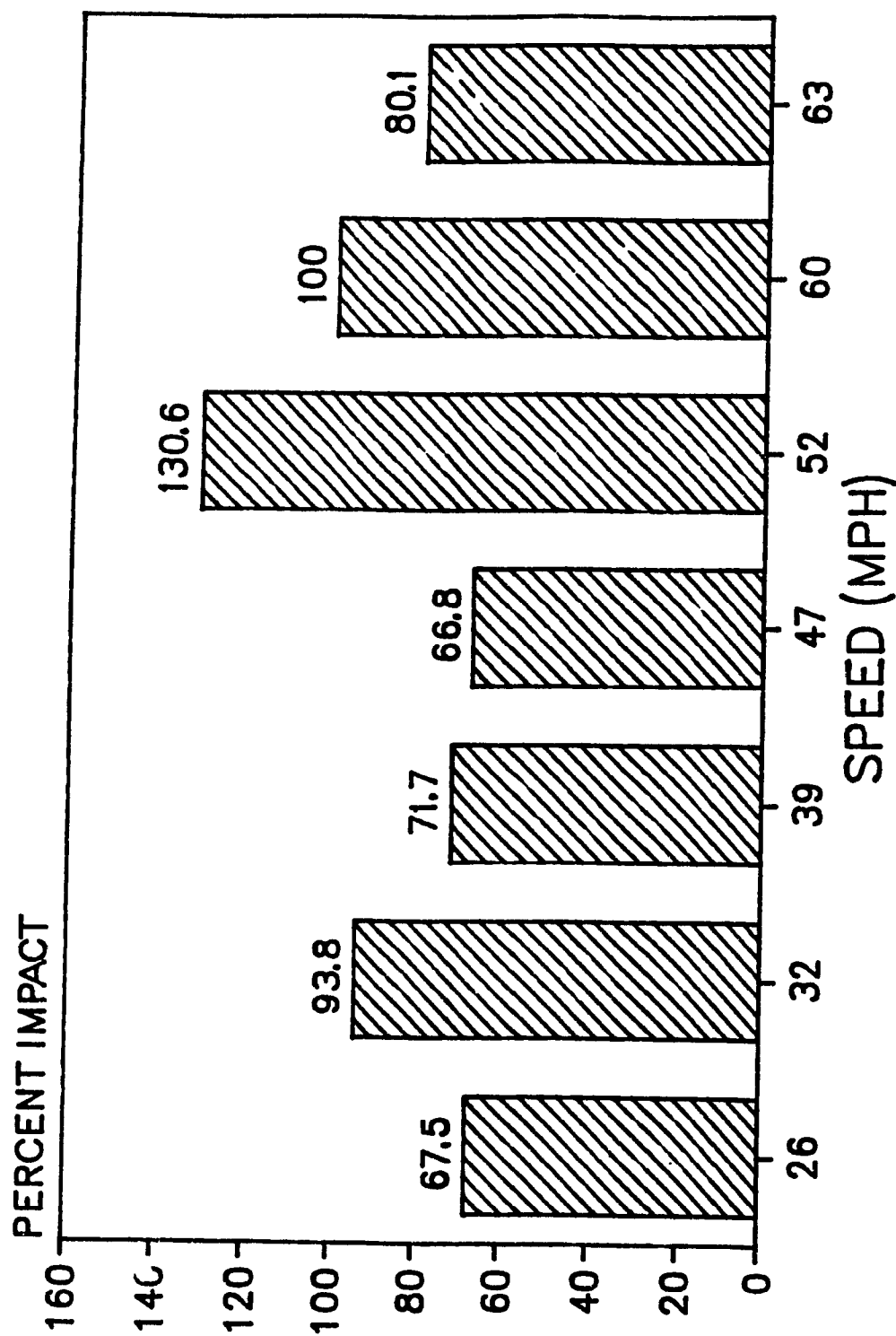
Figure B 5.2   Average Impact Factors for Light Loads

AVE. IMPACT FACTORS FOR VARIOUS SPEEDS
HEAVY WHEEL LOADS
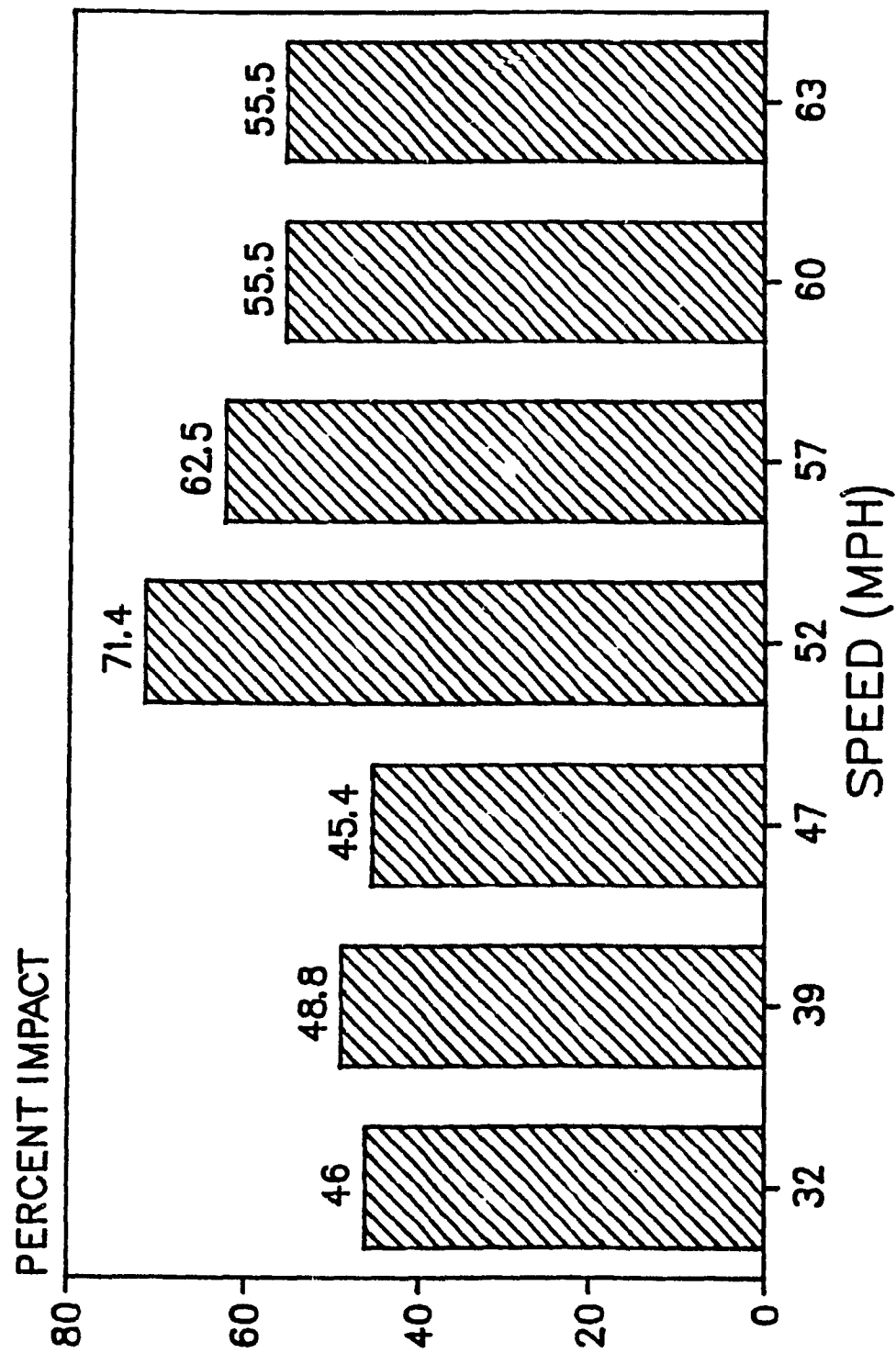
Figure B 5.3 Average Impact Factors for Heavy Loads

APPENDIX C

ANCILLARY CALCULATIONS

USED IN THE MODELS

PERIOD OF TIE TO SPRING UP AND CLOSE GAP

Consider only the central tie under wheel load:
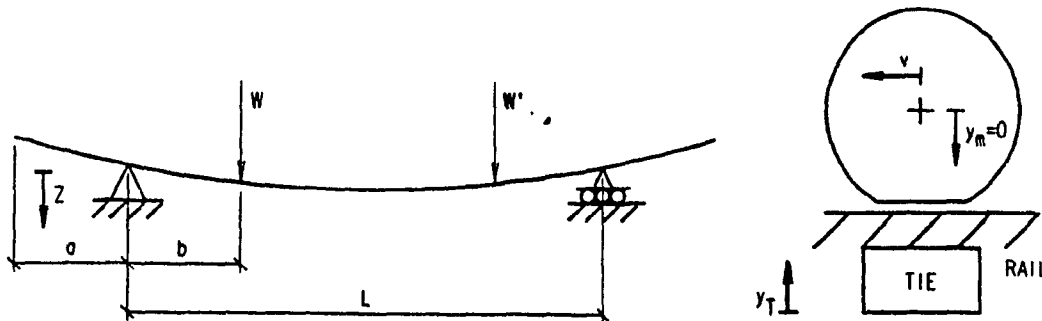
Figure C 1.0   Period of Tie to Close Gap

Compute static deflection to compare with gap distance.

$$Z = \frac{W L^3}{3\,EI}\;\frac{b^2}{L^2}\;\frac{(\ell - b)^2}{L^2} + \frac{WL^3}{6\,EI}\;\frac{(L - b)}{L}\;\frac{b^2}{L^2}\;\frac{b}{L}\left(1 + \frac{L}{b} - \frac{b}{a}\right)$$

$$Z = \frac{W L^3}{3\,EI}\;\frac{b^2}{L^2}\;\frac{(L - b)}{L}\left\{\frac{L - b}{L} + \frac{1}{2}\;\frac{b}{L}\left(1 + \frac{L}{b} - \frac{b}{a}\right)\right\}$$

a = 24" (610 mm), b = 18" (457 mm), c = 96" (2,438 mm)

E = 4.42 x 10^6 psi (3,048 MPa)

I = 1,560 in^4 (6.49 x 10^8 mm^4)

$$W = \frac{64{,}000}{8} = 8{,}000\,lbs \;(35.6\,kN)$$

$$Z = \frac{8{,}000\,(96)^2}{3 \times 5 \times 10^6 \times 1{,}600}\left(\frac{18}{96}\right)^2 \frac{78}{96}\left\{\frac{78}{96} + \frac{1}{2}\;\frac{18}{96}\left(1 + \frac{96}{18} - \frac{18}{24}\right)\right\}$$

Z = 0.0131" (0.3318 mm) for W = 8,000 lbs (35.6 kN)

Z = 0.0539" (1.3688 mm) for W = 33,000 lbs (146.8 kN)

The gap "Δ" due to d = 1" (25.4 mm) "skid" flat is:

214

$$\Delta - r \ (1 - \cos \Theta_0)$$

$$\Delta - r \left(1 - \sqrt{1 - (0.5d/r)^{2}}\ \right)$$

$$\Delta - 0.00174'' \ (0.044 \ mm)$$

$$\frac{\Delta}{Z_{8,000}} - 13 \ percent \qquad \frac{\Delta}{Z_{33,000}} - 3 \ percent$$

Therefore, when tie is vibrating at a fundamental frequency of 85 Hz, its period for a half cycle is 0.0059 sec. Assume a linear relationship between time and distance, then the time to close the gap is:

For a load of 8,000 lbs (35.6 kN) 13 percent of 0.0059 = 0.0008 sec.

For a load of 33,000 lbs (146.8 kN) 3 percent of 0.0059 = 0.0002 sec.

Evaluate The Attenuation Property of Truck Springs
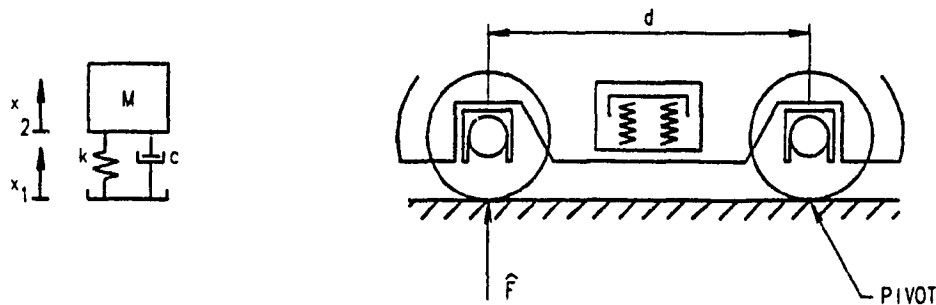
Figure C 1.1   Attenuation Properties of Railway Vehicle Springs

$$\frac{I_0 \, \Theta^2}{2} + \frac{M \ (\Theta d/2)^2}{2} - Mg \, \Theta \frac{d}{2} + \frac{1}{2} \ k \ (\Theta d/2)^2$$

ignoring gravity for dynamic analysis

$$M[C + d^2]\,\Theta^2 - k\,\frac{d^2}{4}\,\Theta^2$$

in harmonic motion $\Theta - -\omega\Theta$

Therefore:

$$\omega^2 - \frac{kd^2/4}{M\left[C + \dfrac{d^2}{4}\right]}$$

or

$$F - \frac{1}{2\pi}\sqrt{\frac{kd^2/4}{\left(I_0 + M\,\dfrac{d^2}{4}\right)}}$$

Where I pivot $- I_0 + \dfrac{Md^2}{4}$

d = 5'6" = 66" (152.4 mm)

k = 37,000 lbs/in. (6.48 kN/mm) (for springs on 1 truck)

M = (1 axle + 2 side frames) = 6.68 + 2 x 2.98 = 12.64 slug

I pivot = M axle x d^2 + I side frames + M side frames x $(d/2)^2$

I pivot = 6.68 x 66^2 + 2 x 1370 + 2 x 2.98 x 33^2

I pivot = 38,328 slug-in^2

$$F - \frac{1}{2\pi}\sqrt{\frac{k\,d^2/4}{I\ pivot}} \ - \ \frac{1}{2\pi}\sqrt{\frac{37,000\ 66^2/4}{38,328}}$$

F = 5.2 Hz resonant frequency.

Conclusion: for impact forces of period from 2 to 5 m.sec most of the frequency is well above the resonant frequency, and is cut off.

Evaluate Duration of Motion of:

Wheel Fall; Rotation of Flat; Spring Up of Tie
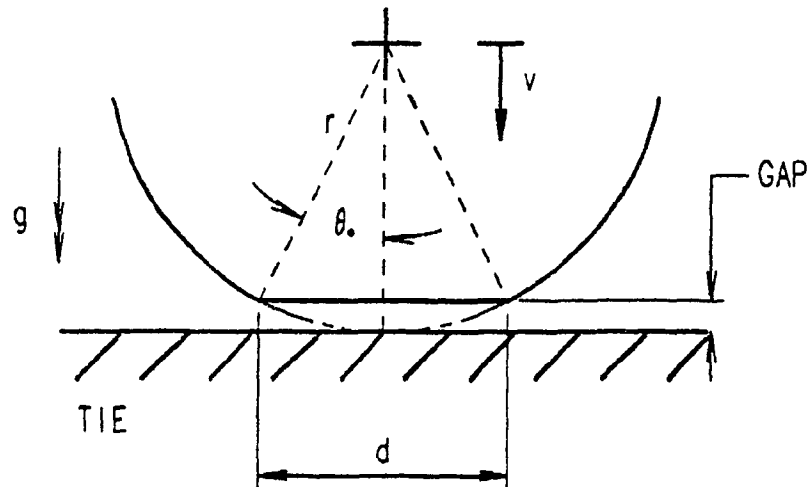
Figure C 1.2   Duration of Motion of Wheel Vertically

A - Duration of Fall of Wheel

in closing gap created by skid flat

d = 1" (25.4 mm)

r = 18" (457.2 mm)

$$r\ (1 - \cos \Theta_0) = \frac{1}{2}\ g t^2 \ ; \quad \sin \Theta_0 = \frac{d/2}{r} \ ; \quad \cos \Theta_0 \sqrt{1 - \left(\frac{d/2}{r}\right)}$$

$$t = \sqrt{\frac{2r\left[1 - \sqrt{1 - \left(\frac{d/2}{r}\right)^2}\right]}{g}} = \sqrt{\frac{2 \times 18 \times \left[1 - \sqrt{1 - \left(\frac{0.5}{18}\right)^2}\right]}{386.4}}$$

t = 0.0060 sec
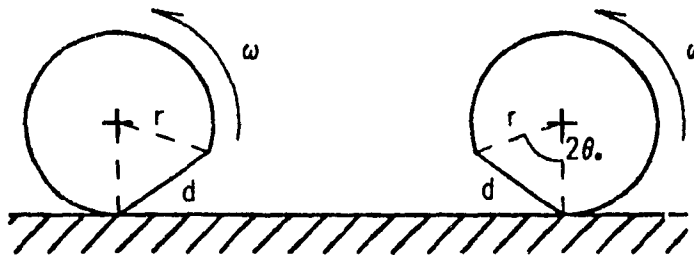
Figure C 1.3   Duration of Motion of Wheel Horizontally

B - <u>Duration of Rotation of Wheel Flat</u>

$$t = \frac{2\,\Theta_0}{\omega} \; ; \quad \omega = \frac{V}{r}$$

$V = 40$ *mph or* 720 *in/*sec

$$\Theta_0 = \sin^{-1}\left(\frac{d/2}{r}\right) = \left(\frac{0.5}{18}\right)$$

$\Theta_0 = 0.02778$ *radians*

$$t = \frac{2\,\Theta_0\,r}{V} = \frac{2 \times 0.02778 \times 18}{720}$$

$t = 0.0010$ sec

APPENDIX D

DOCUMENTATION ON ELONGATION

OF WIRE STRANDS

(COURTESY OF MONARCH PRECO LTD.)

Figure D 1.0   Production Drawing of Type 1 Tie

220

Réléve Des Opérations
de Mise en Tension

Eléments # __TYPE #1 (BEAM #1)__
__T.B.__

Contrat # __CON. U.__

Date __5 FEV-1991__

Description des Eléments __TIE (BEAMS)__
(e.g. Poutres, Double-T. Colonnes)

Identification des torons

Torons		
Diamètre	Fabriquant	Résistance maximale
3/8 "	STELCO	270,000 psi

Capacité du Béton lb/po²		
Coupage des torons		28 Jours
6 FEV.-91	4417 psi (30.46 MR)	5 MAR- 91 / psi

Toron#	Séquence pour la mise en tension	Lecture du manomètre	(lb) Tension			(po.) Elongation		Séquence pour le coupage		Δ_R (po.)
			Initiale	Exigée Finale		Calculée	Mesurée			
1	3		760	15210	15220	0.8725	3/4	11	1 - 1	1/16
2	2		840	15210	15220	0.8676	7/8	1	2 - 2	1/16
3	1		760	15210	15220	0.8725	7/8	5	3 - 3	1/16
4	1		760	15210	15220	0.8725	5/8	6	4 - 4	1/16
5	2		840	15210	15220	0.8676	13/16	2	5 - 5	1/32
6	3		760	15210	15220	0.8725	13/16	12	6 - 6	—
7	5		760	15210	15220	0.8725	7/8	7	7 - 7	3/32
8	4		760	15210	15220	0.8725	7/8	9	8 - 8	1/16
9	5		760	15210	15220	0.8725	13/16	8	9 - 9	1/16
10	4		760	15210	15220	0.8725	13/16	10	10 - 10	1/16
11	7		760	15210	15220	0.8725	13/16	3	11 - 11	3/32
12	6		760	15210	15220	0.8725	7/8	13	12 - 12	—
13	6		760	15210	15220	0.8725	3/4	4	13 - 13	—
14	7		760	15210	15220	0.8725	13/16	14	14 - 14	3/32
15										
16										
17										
18										
19										
20										

_____
Superviseur

_____
Approuvé par

Table D 1.0   Elongation Measurements for T... T1B1

Monarch Préco Ltée

Rélève Des Opérations de Mise en Tension
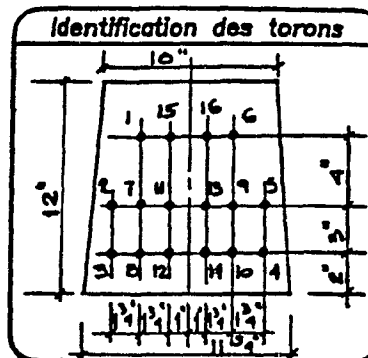
Eléments # __TYPE #1__ __(BEAM #2)__
__T₁ B₂__

Contrat # __CON. U.__

Date __7 FÉV. -1991__

Description des Eléments __TIE (BEAMS)__
(a.g. Poutres, Double-T, Colonnes)

Torons		
Diamètre	Fabriquant	Résistance maximale
3/8"	STELCO	270, 000 psi

Capacité du Béton lb/po²	
Coupage des torons	28 Jours
8 FÉV. / 4297	7 mar /

Identification des torons

Toron#	Séquence pour la mise en tension	Lecture du manomètre	Tension			Elongation		Séquence pour le coupage		ΔR (po)
			Initiale	Exigée	Finale	Calculée	Mesurée			
1	3		760	15210	15220	0.8725	7/8	11	1-1	1/32
2	2		760	15210	15240	0.8736	3/4	1	2-2	1/32
3	1		760	15210	15240	0.8736	4/16	5	3-3	1/32
4	1		760	15210	15240	0.8736	25/32	6	4-4	1/16
5	2		760	15210	15240	0.8736	13/16	2	5-5	1/32
6	3		760	15210	15220	0.8725	15/16	12	6-6	1/32
7	5		760	15210	15220	0.8725	13/16	7	7-7	1/32
8	4		760	15210	15220	0.8725	3/4	9	8-8	1/32
9	5		760	15210	15220	0.8725	13/16	8	9-9	1/32
10	4		760	15210	15220	0.8725	3/4	10	10-10	5/16
11	7		760	15210	15240	0.8736	3/4	3	11-11	1/32
12	6		760	15210	15220	0.8736	11/16	13	12-12	5/16
13	6		760	15210	15220	0.8736	13/16	4	13-13	1/32
14	7		760	15210	15240	0.8736	13/16	14	14-14	5/16
15										
16										
17										
18										
19										
20										

_____
Superviseur

_____
Approuvé par

Table D 1.1   Elongation Measurements for Tie T1B2

222

Réléve Des Opérations
de Mise en Tension

Eléments # __TYPE #1___ (BEAM #3)
___T1 B3___

Contrat # __CON. U.__

Date __8 FEV. -1991__

Description des Eléments __TIE (BEAMS)__
(e.g. Poutton, Double-T, Colonnes)
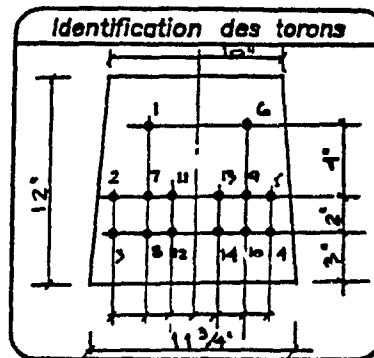
Identification des torons

Torons		
Diametre	Fabriquant	Résistance maximale
3/8"	STELCO	270, 000 psi

Capacité du Béton lb/po²	
Coupage des torons	28 Jours
11 Fev- 91 /5889 psi	8 mar-91 / ___ psi

Toron#	Séquence pour la mise en tension	Lecture du manometre	(Lb) Tension			(po) Elongation		Séquence pour le coupage		ΔR (po)
			Initiale	Exigée Finale		Calculée	Mesurée			
1	3		760	15210	15220	0.8725	3/4	11	1-1	1/32
2	2		760	15210	15220	0.	7/8	1	2-2	1/16
3	1		760	15210	15220	0.	13/16	5	3-3	1/32
4	1		760	15210	15220	0.	3/4	6	4-4	1/32
5	2		760	15210	15220	0.	13/16	2	5-5	1/32
6	3		760	15210	15220	0.	3/4	12	6-6	1/32
7	5		760	15210	15220	0.	7/8	7	7-7	1/16
8	4		760	15210	15220	0.	3/4	9	8-8	1/32
9	5		760	15210	15220	0.	7/8	8	9-9	1/32
10	4		760	15210	15220	0.	3/4	10	10-10	1/32
11	7		760	15210	15220	0.	11/16	3	11-11	1/16
12	6		760	15210	15220	0.	13/16	13	12-12	1/32
13	6		760	15210	15220	0.	3/4	4	13-13	1/16
14	7		760	15210	15220	0.	19/16	14	14-14	1/32
15										
16										
17										
18										
19										
20										

Superieur

Approuvé par

Table D 1.2   Elongation Measurements for Tie T1B3

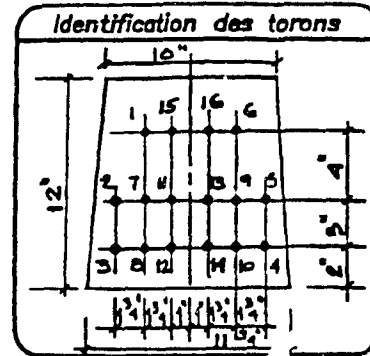**Réléve Des Opérations de Mise en Tension**

Eléments # __TYPE #1 (BEAM #4)__
__T₁ B₄__

Contrat # __Con. U.__

Date __11 FÉV.-1991__

Description des Eléments __TIE (BEAMS)__
(e.g. Preston, Double-T, Colonnes)
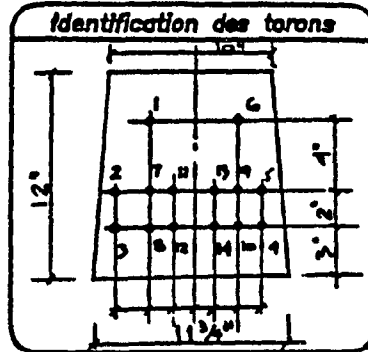
Identification des torons

Torons		
Diametre	Fabriquant	Résistance maximale
3/8"	STELCO	270, 000 psi.

Capacité du Béton lb/po²	
Coupage des torons	28 Jours
12 FÉV / 3899 psi	11 MAR. / psi

Toron#	Séquence pour la mise en tension	Lecture du manometre	Tension			Elongation		Séquence pour le coupage		Δ (f
			Initiale	Exigée	Finale	Calculée	Mesurée			
1	3		760	15210	15220	0.8725	7/8	11	1 - 1	1/2
2	2		760	15210	15240	0.8737	29/32	1	2 - 2	1/2
3	1		760	15210	15220	0.8725	3/4	5	3 - 3	1/2
4	1		760	15210	15220	0.8725	29/32	6	4 - 4	1/2
5	2		760	15210	15240	0.8737	29/32	2	5 - 5	1/2
6	3		760	15210	15220	0.8725	7/8	12	6 - 6	1/2
7	5		760	15210	15220	0.8725	13/16	7	7 - 7	1/2
8	4		760	15210	15220	0.8726	13/16	9	8 - 8	1/2
9	5		760	15210	15220	0.8725	13/16	8	9 - 9	1/2
10	4		760	15210	15220	0.8725	3/4	10	10 - 10	1/2
11	7		760	15210	15220	0.8725	23/32	3	11 - 11	1/2
12	6		760	15210	15220	0.8725	3/4	13	12 - 12	1/2
13	6		760	15210	15220	0.8725	23/32	4	13 - 13	1/2
14	7		760	15210	15220	0.8725	23/32	14	14 - 14	1/2
15										
16										
17										
18										
19										
20										

Superviseur

Approuvé par

Table D 1.3   Elongation Measurements for Tie T1B4

Eléments # __TYPE # 1__ __(BEAM #5)__
__T₁B₅__ __T₁B₅__

Contrat # __CON. U.__

Date __12 FEV - 1991__

Description des Eléments (e.g. Poutre, Double-T, Colonne) __TIE (BEAMS)__

Identification des torons

Torons		
Diamètre	Fabriquant	Résistance maximale
3/8"	STELCO	270,000 psi

Capacité du Béton lb/po²	
Coupage des torons	28 Jours
13 FEV / 4854 psi	12 MAR. /

Toron #	Séquence pour la mise en tension	Lecture du manomètre	Tension			Elongation		Séquence pour le coupage		Δ_R
			Initiale	Exigée	Finale	Calculée	Mesurée			
1	3		760	15210	15220	0.8725	13/16	11	1-1	1/16
2	2		760	15210	15220	0.8725	27/32	1	2-2	1/16
3	1		760	15210	15220	0.8725	13/16	5	3-3	1/32
4	1		760	15210	15220	0.8725	7/8	6	4-4	1/16
5	2		760	15210	15220	0.8725	7/8	2	5-5	0
6	3		760	15210	15220	0.8725	7/8	12	6-6	1/16
7	5		760	15210	15220	0.8725	27/32	7	7-7	1/16
8	4		760	15210	15220	0.8725	29/32	9	8-8	0
9	5		760	15210	15220	0.8725	27/32	8	9-9	1/32
10	4		760	15210	15220	0.8725	13/16	10	10-10	1/16
11	6		760	15210	15220	0.8725	7/8	3	11-11	0
12	7		760	15210	15220	0.8725	7/8	13	12-12	0
13	7		760	15210	15220	0.8725	13/16	4	13-13	1/32
14	6		760	15210	15220	0.8725	13/16	14	14-14	0
15				*MAKE						
16				ADJUSTMENT						
17				FOR TENSION						
18				DUE TO SLIP LOSS						
19				P PULLED <15220 US						
20				ACTUAL						

Signature L = 159.25 m

Superviseur

Approuvé par

Table D 1.4 Elongation Measurements for Tie T1B5

Réléve Des Opérations de Mise en Tension

Eléments # __TYPE #1__ (BEAM #6)
__T.B₆__

Contrat # __Con. U.__

Date __13 FEV -1991__

Description des Eléments __TIE (BEAMS)__
(e.g. Poutres, Cochie-f. Colonne)

Identification des torons
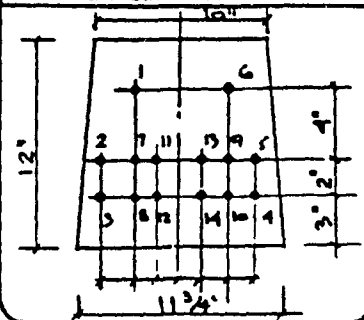
Torons		
Diametre	Fabriquant	Résistance maximale
3/8"	STELCO	270, 000 psi

Capacité du Béton lb/po²	
Coupage des torons	28 Jours
14 FEV. / 4138 psi	13 MAR / psi

Toron#	Séquence pour la mise en tension	Lecture du manometre	Tension			Elongation		Séquence pour le coupage		Δ R
			Initiale	Exigée	Finale	Calculée	Mesurée			
1	2		760	15210	16000	0.9195	7/8	11	1-1	1/16
2	3		760	15210	16000	0.9195	11/16	1	2-2	∅
3	1		760	15210	15220	0.8725	13/16	5	3-3	1/32
4	1		760	15210	15220	0.8725	25/32	6	4-4	∅
5	3		760	15210	16000	0.9195	27/32	2	5-5	∅
6	2		760	15210	16000		27/32	12	6-6	1/32
7	5		760	15210	16000		15/16	7	7-7	1/32
8	4		760	15210	16000		27/32	9	8-8	1/32
9	5		760	15210	16000		15/16	8	9-9	1/32
10	4		760	15210	16000		13/16	10	10-10	∅
11	7		760	15210	16000		13/16	3	11-11	1/32
12	6		760	15210	16000		27/32	13	12-12	1/32
13	6		760	15210	16000		7/8	4	13-13	1/32
14	7		760	15210	16000		27/32	14	14-14	1/32
15										
16										
17										
18										
19										
20										

L= 159.25 in.

Superviseur

Approuvé par

Table D 1.5   Elongation Measurements for Tie T1B6

Tie Type No.2 (Eccentric Prestress)

1) 16 - 3/8"ø DIA. - 7 WIRE STRAND. WITH PRESTRESSING FORCE OF 16,021 LBS EACH.

2) 16,021 LBS = 0.70 fpu As

3) TOTAL PRESTRESSING FORCE = 256,337 LBS.

4) EFFECTIVE PRESTRESSING FORCE = 187,126 LBS.

5) STRESSES IN CONCRETE AFTER TRANSFER:

   ft = 1000 psi Compression
   fb = 1850 psi Compression

6) ECCENTRICITY (e) = 0.59 IN.

STIRRUPS 1/4"ø - Fy (44 ksi)

4 STRANDS

6 STRANDS

6 STRANDS

END VIEW

144"

STRANDS 3/8"ø

1/4"ø STIRRUPS

SIDE VIEW

pcn. # T₂   qu. 6

ph qu. description
4 STIRRUPS 1/4"ø

EK

CONCORDIA UNIV.

TEST

TYPE #2

227

Figure D 1.1 Production Drawing of Type 2 Tie

Réléve Des Opérations de Mise en Tension

Eléments # __TYPE #2 (BEAM #1)__
__T₂ B₁__

Contrat # __CON. 4.__

Date __15 FÉV. 1991__

Description des Eléments __TIE (BEAMS)__
(e.g. Poutre, Double-T, Colonne)

Identification des torons

Torons		
Diametre	Fabriquant	Résistance maximale
3/8"	STELCO	270,000 psi

Capacité du Béton lb/po²	
Coupage des torons	28 Jours
FÉV./ 4695 psi	/ psi

LOSS AFTER COST
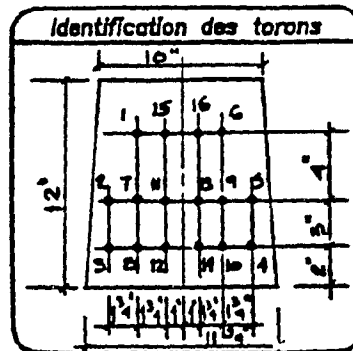
Loss Slip	Toron #	Séquence pour la mise en tension	Lecture du manometre	Tension Initiale	Tension Exigée	Tension Finale	Elongation Calculée	Elongation Mesurée	Séquence pour le coupage		Δ
5/16	1	1		1000	16021	19000	0.9063	1 1/16	1	1-1	∅
3/16	2	2		1000	16021	19000	0.9063	1 8/32	3	2-2	∅
3/16	3	3		1000	16021	19000	0.9063	1 7/32	5	3-3	1/16
3/16	4	3		1000	16021	19000	0.9063	1 3/32	6	4-4	1/16
3/16	5	2		1000	16021	19000	0.9063	1 3/16	4	5-5	∅
7/32	6	1		1000	16021	19000	0.9063	7/32	2	6-6	∅
3/16	7	4		1000	16021	19000	0.9063	1 3/32	7	7-7	∅
3/16	8	5		1000	16021	19000	0.9063	1 4/32	9	8-8	1/16
3/16	9	4		1000	16021	19000	0.9063	1 5/32	8	9-9	∅
7/32	10	5		1000	16021	19000	0.9063	1 7/32	10	10-10	1/16
3/32	11	6		1000	16021	19000	0.9063	1 1/16	11	11-11	∅
3/16	12	7		1000	16021	19000	0.9063	1 6/32	13	12-12	1/16
3/16	13	7		1000	16021	19000	0.9063	1 3/32	12	13-13	∅
3/16	14	6		1000	16021	19000	0.9063	1 3/32	14	14-14	1/16
4/16	15	8 (PULLED AT	1000	16021	19000	0.9063	1 1/32	15	15-15	1/32
3/32	16	9 SLOPE of ≈ 1/20	1000	16021	19000	0.9063	31/32	16	16-16	1/32
	17										
	18										
	19										
	20										

EKarosan
Superviseur

_____
Approuvé par

Table D 2.0 Elogation Measurements for Tie T2B1

228

Réléve Des Opérations de Mise en Tension

Eléments # __TYPE #2 (BEAM #2)__
T₂ B₂

Contrat # __CON. 4.__

Date __18 FÉV. 1991__

Description des Eléments (ex. Poutres, Double-T, Colonnes) __TIE (BEAMS)__

Identification des torons

Torons		
Diametre	Fabriquant	Résistance maximale
3/8"	STELCO	270,000 psi

Capacité du Béton lb/po²	
Coupage des torons	28 Jours
FÉV./ 3223 psi	/ psi

Δ(in)/sup	Toron #	Séquence pour la mise en tension	Lecture du manometre	(lb) Tension Initiale	Exigée	Finale	(in) Elongation Calculée	Mesurée	Séquence pour le coupage		ΔR
5/32	1	1		1000	16021	19000	0.9063	1 5/32	1	1-1	1/32
5/32	2	2		1000	16021	19000	0.9063	1 5/32	3	2-2	1/32
3/16	3	3		1000	16021	19000	0.9063	1 6/32	5	3-3	1/16
3/16	4	3		1000	16021	19000	0.9063	1 4/32	6	4-4	1/16
1/16	5	2		1000	16021	19000	0.9063	3/32	4	5-5	1/16
3/32	6	1		1000	16021	19000	0.9063	1 5/32	2	6-6	∅
1/16	7	4		1000	16021	19000	0.9063	1 3/32	7	7-7	1/32
	8	5		1000	16021	19000	0.9063	1 3/32	9	8-8	1/16
3/16	9	4		1000	16021	19000	0.9063	1 5/32	8	9-9	1/16
	10	5		1000	16021	19000	0.9063	1 3/32	10	10-10	1/16
	11	6		1000	16021	19000	0.9063	1" ∅	11	11-11	∅
	12	7		1000	16021	19000	0.9063	1 1/32	13	12-12	1/16
	13	7		1000	16021	19000	0.9063	1 3/32	12	13-13	∅
	14	6		1000	16021	19000	0.9063	1 1/32	14	14-14	1/16
3/16	15	8		1000	16021	19000	0.9063	1 1/16	15	15-15	1/16
1/16	16	9		1000	16021	19000	0.9063	1 1/32	16	16-16	1/16
	17										
	18										
	19										
	20										

P/D: PAS DISPONIBLE

Superieur

Approuvé par

Table D 2.1 Elogation Measurements for Tie T2B2

**Réléve Des Opérations
de Mise en Tension**

Eléments # __TYPE #2 (BEAM #3)__
__T2 B3__

Contrat # __CON. 4.__

Date __20 FÉV. 1991__

Description des Eléments __TIE (BEAMS)__
(e.g. Poutre, Double-T, Colonne)

Identification des torons

Torons		
Diametre	Fabriquant	Résistance maximale
3/8"	STELCO	270, 000 psi

Capacité du Béton lb/po²	
Coupage des torons	28 Jours
21 FÉV./ 4576 psi	/ psi

SUP LOSS (in)	Toron#	Séquence pour la mise en tension	Lecture du manometre	(lb) Initiale	Exigée	Finale	Calculée	Mesurée	Séquence pour le coupage		Δ F (in)
3/16	1	1		8000	16021	19000	0.9063	18/32	1	1 - 1	1/16
3/16	2	2		1000	16021	19000	0.	5/32	3	2 - 2	1/16
	3	3		1000	16021	19000	0.	2/32	5	3 - 3	1/3:
	4	3		1000	16021	19000	0.	3/32	6	4 - 4	1/16
7/16	5	2		1000	16021	19000	0.	5/32	4	5 - 5	1/16
3/16	6	1		8000	16021	19000	0.	18/32	2	6 - 6	1/16
7/16	7	4		1000	16021	19000	0.	2/32	7	7 - 7	1/16
	8	5		1000	16021	19000	0.	∅	9	8 - 8	1/16
7/16	9	4		1000	16021	19000	0.	1/32	8	9 - 9	1/3:
	10	5		1000	16021	19000	0.	4/32	10	10-10	1/16
	11	6		1000	16021	19000	0.	2/32	11	11 - 11	1/32
	12	7		1000	16021	19000	0.	1/32	13	12-12	1/3:
	13	7		1000	16021	19000	0.	∅	12	13-13	1/32
	14	6		1000	16021	19000	0.	3/32	14	14-14	1/16
7/16	15	8		1000	16021	19000	0.	1/32	15	15-15	1/16
3/16	16	9		1000	16021	19000	0.	1/32	16	16-16	1/8
	17										
	18										
	19										
	20										

Superviseur

Approuvé par

Table D 2.2   Elogation Measurements for Tie T2B3

Réléve Des Opérations de Mise en Tension

Eléments # __TYPE #2 (BEAM #4)__
__T2B4__

Contrat # __CON. 4.__

Date __21 FÉV. 1991__

Description des Eléments __TIE (BEAMS)__
(e.g. Poutres, Double-T, Colonnes)

Torons		
Diametre	Fabriquant	Résistance maximale
3/8"	STELCO	270,000 psi

Capacité du Béton lb/po²	
Coupage des torons	28 Jours
22 FÉV./ 4576 psi	/ psi

Identification des torons

SLIP LOSS (in)	Toron #	Séquence pour la mise en tension	Lecture du manometre	Tension (lb)			(in) Elongation		Séquence pour le coupage		Δ_F (in)
				Initiale	Exigée	Finale	Calculée	Mesurée			
1/32	1	1		1000	16021	19000	0.9063	1 1/32	1	1-1	1/16
1/32	2	2		1000	16021	19000	0.	1 1/32	3	2-2	1/16
—	3	3		1000	16021	19000	0.	1 3/32	5	3-3	1/16
—	4	3		1000	16021	19000	0.	1 3/32	6	4-4	1/16
1/32	5	2		1000	16021	19000	0.	1 1/32	4	5-5	1/16
1/32	6	1		1000	16021	19000	0.	1 1/32	2	6-6	1/16
3/16	7	4		1000	16021	19000	0.	1 1/32	7	7-7	1/16
	8	5		1000	16021	19000	0.	1 3/32	9	8-8	1/16
1/4	9	4		1000	16021	19000	0.	1 1/32	8	9-9	1/16
—	10	5		1000	16021	19000	0.	1 1/32	10	10-10	1/16
—	11	6		1000	16021	19000	0.	1 ∅	11	11-11	1/16
—	12	7		1000	16021	19000	0.	1 1/16	13	12-12	1/16
—	13	7		1000	16021	19000	0.	3 9/32	12	13-13	1/16
—	14	6		1000	16021	19000	0.	1 1/32	14	14-14	1/16
—	15	8		1000	16021	19000	0.	1 1/32	15	15-15	1/16
1/32	16	9		1000	16021	19000	0.	3/32	16	16-16	1/16
	17										
	18										
	19										
	20										

Superieur

Approuvé par

Table D 2.3   Elogation Measurements for Tie T2B4

Rélève Des Opérations de Mise en Tension

Eléments # __TYPE #2 (BEAM #5)__   Contrat # __CON. U.__

__T2B5__

Date __25 FÉV. 1991__

Description des Eléments (ex. Poutres, Double-T, Colonnes) __TIE (BEAMS)__

Torons

Diamètre	Fabriquant	Résistance maximale
3/8"	STELCO	270,000 psi

Capacité du Béton lb/po²

Coupage des torons		28 Jours	
26 FÉV. / 4380 psi		/	psi

Identification des torons

SLIP pos (in)	Toron #	Séquence pour la mise en tension	Lecture du manomètre	Tension (lb) Initiale	Exigée	Final	Elongation (in) Calculée	Mesurée	Séquence pour le coupage		ΔR (in)
3/16	1	1		1000	16021	19000	0.9063	1 3/32	1	1-1	1/16
3/16	2	2		1000	16021	19000		1 3/32	3	2-2	/
	3	3		1000	16021	19000		1 1/32	5	3-3	/
	4	3		1000	16021	19000		1 1/32	6	4-4	/
1/4	5	2		1000	16021	19000		1 ∅	4	5-5	/
5/32	6	1		1000	16021	19000		1 3/32	2	6-6	/
3/16	7	5		1000	16021	19000		1 1/32	7	7-7	/'
	8	4		1000	16021	19000		1 3/32	9	8-8	/
3/16	9	5		1000	16021	19000		1 2/32	8	9-9	/
	10	4		1000	16021	19000		1 1/32	10	10-10	/
	11	6		1000	16021	19000		1 ∅	11	11-11	/
	12	7		1000	16021	19000		30/32	13	12-12	/
	13	7		1000	16021	19000		29/32	12	13-13	/'
	14	6		1000	16021	19000		1 ∅	14	14-14	/
3/16	15	8		1000	16021	19000		1 1/32	15	15-15	/
7/32	16	9		1000	16021	19000		1 1/32	16	16-16	/
	17										
	18										
	19										
	20										

EKaresan

Superviseur   Approuvé par

Table D 2.4   Elogation Measurements for Tie T2B5

Monarch Préco Ltée

*Relévé Des Opérations de Mise en Tension*

Eléments # __TYPE #2 (BEAM #6)__
__T2B6__

Contrat # __CON. 4.__

Date __26 FÉV. 1991__

Description des Eléments __TIE (BEAMS)__
(e.g. Poutres, Double-T, Colonnes)

Identification des torons

Torons

Diametre	Fabriquant	Résistance maximale
3/8"	STELCO	270,000 psi

Capacité du Béton lb/po²

Coupage des torons	28 Jours
1AM. 28 FÉV. / ⟶ psi	/ psi
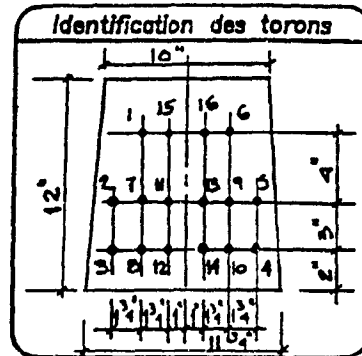
3PM: 27 FÉV. f'c = 2950 psi (20.3 MPa)

SLIP DAS	Toron#	Séquence pour la mise en tension	Lecture du manometre	(lb) Tension Initiale	Exigée	Finale	(in) Elongation Calculée	Mesurée	Séquence pour le coupage		ΔF (in)
5/50	1	1		1000	16023	19000	0.9063	1/32	1	1-1	1/16
5/32	2	2		1000	16021	19000		14/32	3	2-2	
	3	3		1000	16021	19000		1/32	5	3-3	
	4	3		1000	16021	19000		∅	6	4-4	
5/60	5	2		1000	16021	19000		14/32	4	5-5	
6/32	6	1		1000	16021	19000		1/32	2	6-6	
3/16	7	5		1000	16021	19000		13/32	7	7-7	
	8	4		1000	16021	19000		3/32	9	8-8	
1/4	9	5		1000	16021	19000		1/32	8	9-9	
	10	4		1000	16021	19000		∅	10	10-10	
	11	6		1000	16021	19000		12/32	11	11-11	
	12	7		1000	16021	19000		3/32	13	12-12	
	13	7		1000	16021	19000		39/32	12	13-13	
	14	6		1000	16021	19000		31/32	14	14-14	
7/32	15	8		1000	16021	19000		1∅	15	15-15	
5/32	16	9		1000	16021	19000		1∅	16	16-16	
	17										
	18										
	19										
	20										

Superviseur _____

Approuvé par _____

Table D 2.5   Elogation Measurements for Tie T2B6

Tie Type No3 (Eccentric Prestress)

1) 20-3/8" ∅ dia.- 7 wire strand. with prestressing force of 16,510 lbs each.

2) 16,510 lbs = 0.72 fpu A_s

3) Total Prestressing Force = 330,162 lbs

4) Effective Prestressing Force = 241,046 lbs

5) Stresses in Concrete After Transfer:

   $f_t = f_b = 1850$ psi Compression

6) Eccentricity (e) = 0

END VIEW

SIDE VIEW

Figure D 1.2   Production Drawing of Type 3 Tie

234

Monarch Préco Ltée

Réléve Des Opérations de Mise en Tension

Eléments # __TYPE #3 (BEAM #1)__
__T3B1__

Contrat # __Con LL__

Date __1 MARS 1991__

Description des Eléments __TIE (BEAMS)__
(e.g. Poutre, Double-T, Colonne)

Torons		
Diametre	Fabriquant	Résistance maximale
3/8"	STELCO	270.000 psi

Capacité du Béton lb/po²	
Coupage des torons	28 Jours
4-03/4655 psi	1-04/ psi

Identification des torons

Δ up pss	Toron#	Séquence pour la mise en tension	Lecture du manometre	Tension			Elongation		Séquence pour le coupage		Δf (in)
				Initiale	Exigée	Finale	Calculée	Mesurée			
3/16	1	7		1000	16510	19400	0.9358	1 1/32	1	1-1	1/16
5/32	2	8		1000	16510	19400	.	31/32	11	2-2	
3/16	3	7		1000	16510	19400	.	1 1/32	12	3-3	
1/4	4	8		1000	16510	19400	.	1 ø	2	4-4	
1/4	5	2		1000	16510	19400	.	1 3/32	5	5-5	
5/32	6	5		1000	16510	19400	.	1 4/32	15	6-6	
4/32	7	6		1000	16510	19400	.	31/32	16	7-7	
5/16	8	2		1000	16510	19400	.	1 3/32	6	8-8	
1/4	9	1		1000	16510	19400	.	1 3/32	9	9-9	
1/4	10	3		1000	16510	19400	.	30/32	19	10-10	
5/16	11	4		1000	16510	19400	.	31/32	20	11-11	
3/16	12	1		1000	16510	19400	.	1 1/32	10	12-12	
	13	2		1000	16510	19400	.	1 2/32	7	13-13	
	14	6		1000	16510	19400	.	1 3/32	17	14-14	
	15	5		1000	16510	19400	.	31/32	18	15-15	
	16	2		1000	16510	19400	.	1 3/32	8	16-16	
	17	1		1000	16510	19400	.	1 2/32	3	17-17	
	18	4		1000	16510	19400	.	31/32	13	18-18	
	19	3		1000	16510	19400	.	31/32	14	19-19	
	20	1		1000	16510	19400	.	1 ø	4	20-20	

E. Karoosan

T. of 16510 lb increased to 19400 due to Δ_{AVE} slip loss 5/32"

Superviseur

Approuvé par

Table D 3.0 Elongation Measurements for Tie T3B1

235

Réléve Des Opérations de Mise en Tension
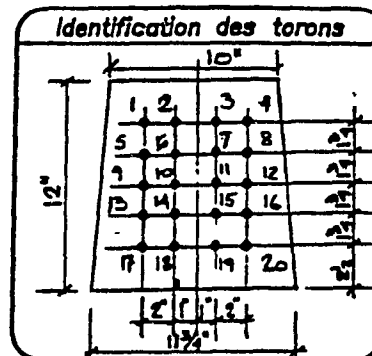
Eléments # _TYPE #3 (BEAM #2)_
_T3 B2_

Contrat # _Cou L_

Date _5-03 1991_

Description des Eléments _TIE (BEAMS)_
(e.g. Poutre, Double-T, Colonne)

Identification des torons

Torons		
Diametre	Fabriquant	Résistance maximale
3/8"	STELCO	270,000 psi

Capacité du Béton lb/po²	
Coupage des torons	28 Jours
6-03 / 5695 psi	2-04 / psi
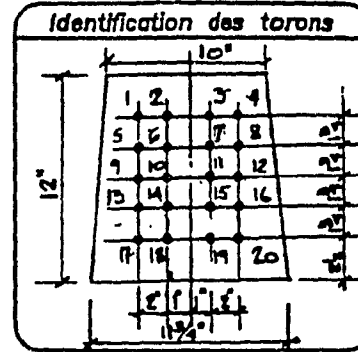
Δ cb	Toron#	Séquence pour la mise en tension	Lecture du manometre	Tension			Elongation		Séquence pour le coupage		ΔR (in)
				Initiale	Exigée	Finale	Calculée 15/16	Mesurée			
5/32	1	7		1000	16510	19400	0.9358	31/32	1	1-1	1/16
3/16	2	8		1000	16510	19400	.	29/32	11	2-2	
8/32	3	7		1000	16510	19400	.	30/32	12	3-3	
8/30	4	8		1000	16510	19400	.	28/32	2	4-4	
5/32	5	2		1000	16510	19400	.	31/32	5	5-5	
6/32	6	5		1000	16510	19400	.	30/32	15	6-6	
3/32	7	6		1000	16510	19300	.	31/32	16	7-7	
6/32	8	2		1000	16510	19400	.	1 1/32	6	8-8	
6/32	9	1		1000	16510	19400	.	1 ∅	9	9-9	
7/32	10	3		1000	16510	19400	.	31/32	19	10-10	
5/32	11	4		1000	16510	19400	.	1 1/32	20	11-11	
4/32	12	1		1000	16510	19400	.	1 1/32	10	12-12	
	13	2		1000	16510	19400	.	1 ∅	7	13-13	
	14	6		1000	16510	19400	.	31/32	17	14-14	
	15	5		1000	16510	19400	.	29/32	18	15-15	
	16	2		1000	16510	19400	.	31/32	8	16-16	Y
	17	1		1000	16510	19400	.	31/32	3	17-17	1/32
	18	4		1000	16510	19400	.	1 1/32	13	18-18	1/16
	19	3		1000	16510	19400	.	1 1/32	14	19-19	1/32
	20	1		1000	16510	19400	.	31/32	4	20-20	

Superviseur _____

Approuvé par _____

Table D 3.1   Elongation Measurements for Tie T3B2

236

Monarch Préco Ltée

Réléve Des Opérations de Mise en Tension

Eléments # **TYPE #3 (BEAM #3)**
T₃B₃

Contrat # **COU LL**

Date **6-03 1991**

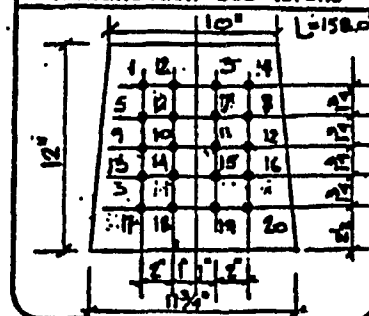Description des Eléments (e.g. Poutre, Double-T, Colonne) **TIE (BEAMS)**

Torons

Diametre	Fabriquant	Résistance maximale
3/8"	STELCO	270.000 psi

Capacité du Béton lb/po²

Coupage des torons	28 Jours
7-03 / 4496 psi	3-04 / psi

Identification des torons

10"

1	2	3	4
5	6	7	8
9	10	11	12
13	14	15	16
17	18	19	20

12" 11¼"

Δ LiP pss	Toron#	Séquence pour la mise en tension	Lecture du manometre	Tension Initiale	Tension Exigée	Tension Finale	Elongation Calculée TG	Elongation Mesurée	Séquence pour le coupage		Δ, Un
4/32	1	7		1000	16510	19400	0.9358	1 1/32	1	1- 1	1/16
6/32	2	8		1000	16510	19400	.	1 3/32	11	2- 2	
5/32	3	7		1000	16510	19400	.	30/32	12	3- 3	
2/32	4	8		1000	16510	19400	.	1 φ	2	4- 4	
5/32	5	2		1000	16510	19400	.	3/32	5	5- 5	
6/32	6	5		1000	16510	19400	.	29/32	15	6- 6	
5/30	7	6		1000	16510	19500	.	31/32	16	7- 7	
6/32	8	2		1000	16510	19400	.	31/32	6	8- 8	
4/32	9	1		1000	16510	19400	.	1 φ	9	9- 9	
6/32	10	3		1000	16510	19400	.	1 φ	19	10- 10	
6/32	11	4		1000	16510	19400	.	30/32	20	11- 11	
4/32	12	1		1000	16510	19400	.	30/32	10	12- 12	
	13	1		1000	16510	19400	.	1 1/32	7	13- 13	
	14	6		1000	16510	19400	.	31/32	17	14- 14	
	15	5		1000	16510	19400	.	30/32	18	15- 15	
	16	2		1000	16510	19400	.	30/32	8	16- 16	
	17	1		1000	16510	19400	.	31/32	3	17- 17	
	18	4		1000	16510	19400	.	1 φ	13	18-18	
	19	3		1000	16510	19400	.	31/32	14	19-19	
	20	1		1000	16510	19400	.	31/32	4	20-20	

Superviseur

Approuvé par

Table D 3.2 Elongation Measurements for Tie T3B3

237

Monarch Préco Ltée

Relévé Des Opérations de Mise en Tension

Eléments # _TYPE #3 (BEAM #4)_
_T3B4_

Contrat # _Cou IL_

Date _21-03-1991_

Description des Eléments (4.4 Poutres, Double-T, Colonnes) _TIE (BEAMS)_

Identification des torons

Torons		
Diamètre	Fabriquant	Résistance maximale
3/8"	STELCO	270,000 psi

REEL PS-12823-1

Capacité du Béton lb/po²	
Coupage des torons	28 Jours
22-03 / 4539 psi	18-04 / 7947 psi

ΔUP oss	Toron#	Séquence pour la mise en tension	Lecture du manomètre	Tension			Elongation		Séquence pour le coupage		
				Initiale	Exigée	Finale	Calculée	Mesurée			
4/32	1	7		1000	16510	19460	0.928	∅	1	1-1	
7/32	2	8		1000	16510	19400		∅	11	2-2	
8/32	3	7		1000	16510	19400		∅	12	3-3	
5/32	4	8		1000	16510	19400		∅	2	4-4	
6/32	5	2		1000	16510	19400		2/32	5	5-5	
8/32	6	5		1000	16510	19400		3/32	15	6-6	
6/32	7	6		1000	16510	19400		3/32	16	7-7	
4/32	8	2		1000	16510	19400		2/32	6	8-8	
4/32	9	1		1000	16510	19400		7/32	9	9-9	
5/32	10	3		1000	16510	19500		4/32	19	10-10	
5/32	11	4		1000	16510	19400		4/32	20	11-11	
6/32	12	1		1000	16510	19400		3/32	10	12-12	
	13	2		1000	16510	19400		1/32	7	13-13	
	14	6		1000	16510	19400		∅	17	14-14	
	15	5		1000	16510	19400		4/32	18	15-15	
	16	2		1000	16510	19400		1/32	8	16-16	
	17	1		1000	16510	19400		2/32	3	17-17	
	18	4		1000	16510	19400		2/32	13	18-18	
	19	3		1000	16510	19400		∅	14	19-19	
	20	1		1000	16510	19500	C.	1/32	4	20-20	

L = 158.0"

EKawsan
Consultant

Approuvé par

Table D 3.3   Elongation Measurements for Tie T3B4

238

Monarch Preco Ltée

Rélevé Des Opérations de Mise en Tension

Éléments # __TYPE #3 (BEAM #5)__
__T₃B₅__

Contrat # __COU LL__

Date __26-3-1991__

Description des Éléments __TIE (BEAMS)__

Identification des torons

Torons		
Diametre	Fabriquant	Résistance maximale
3/8"	STELCO	270,000 psi

REEL PS 12823-1

Capacité du Béton lb/po²	
Coupage des torons	28 Jours
27-3 / 4336 psi	23/4 / 7628 psi

	Toron#	Séquence pour la mise en tension	Lecture du manometre	Tension			Elongation		Séquence pour le coupage	
				Initiale	Exigee	Finale	Calculée	Mesu 1		
1/4	1	7		1000	16510	19800	0.928	30/32	1	1- 1
5/16	2	8		1000	16510	19800		1 2/32	11	2- 2
3/16	3	7		1000	16510	19800		1 2/32	12	3- 3
7/32	4	8		1000	16510	19800		31/32	2	4- 4
1/4	5	2		1000	16510	19800		30/32	5	5- 5
3/16	6	5		1000	16510	19800		31/32	15	6- 6
1/32	7	6		1000	16510	19800		30/32	16	7- 7
1/4	8	2		1000	16510	19800		30/32	6	8- 8
3/16	9	1		1000	16510	19800		1 3/32	9	9- 9
1/4	10	3		1000	16510	19800		30/32	19	10- 10
3/32	11	4		1000	16510	19800		1 1/32	20	11- 11
3/16	12	1		1000	16510	19800		31/32	10	12- 12
	13	2		1000	16510	19800		30/32	7	13- 13
	14	6		1000	16510	19800		1 1/32	17	14- 14
	15	5		1000	16510	19800		1 3/32	18	15- 15
	16	2		1000	16510	19800		31/32	8	16- 16
	17	1		1000	16510	19800		31/32	3	17- 17
	18	4		1000	16510	19800		31/32	13	18- 18
	19	3		1000	16510	19800		1 1/32	14	19- 19
	20	1		1000	16510	19800	0.	31/32	4	20- 20

E. Karaban

Table D 3.4   Elongation Measurements for Tie T3B5

Monarch Préco Liée

Réléve Des Opérations de Mise en Tension

Eléments # __TYPE #3 (BEAM #6)__
__T.B.__

Contrat # __COU LL__

Date __28-3-1991__

Description des Eléments __TIE (BEAMS)__
(e.g. Poutre, Double-T, Colonne)

Torons		
Diamétre	Fabriquant	Résistance maximale
3/8"	STELCO	270,000 psi

REEL F3 12823-1

Capacité du Béton lb/po²	
Coupage des torons	28 Jours
29-3 / 4452 psi	25/4 / 7628 psi

Identification des torons

10"

1	2	3	4
5	6	7	8
9	10	11	12
13	14	15	16
3	18		
17	18	19	20

12"

11¼"

LIP ass	Toron#	Séquence pour la mise en tension	Lecture du manometre	Tension			Elongation		Séquence pour le coupage	
				Initiale	Exigée	Finale	Calculée/2	Mesurée		
7/32	1	7		1000	16510	19400	0.928	31/32	1	1-1
5/16	2	8		1000	16510	19400		1 2/32	11	2-2
3/32	3	7		1000	16510	19400		31/32	12	3-3
3/16	4	8		1000	16510	19400		31/32	2	4-4
7/16	5	2		1000	16510	19400		1 1/32	5	5-5
3/16	6	5		1000	16510	19400		1 1/32	15	6-6
7/32	7	6		1000	16510	19400		31/32	16	7-7
5/16	8	2		1000	16510	19400		30/32	6	8-8
8/32	9	1		1000	16510	19400		28/32	9	9-9
1/32	10	3		1000	16510	19400		1 1/32	19	10-10
7/32	11	4		1000	16510	19400		31/32	20	11-11
4/32	12	1		1000	16510	19400		1 1/32	10	12-12
	13	2		1000	16510	19400		30/32	7	13-13
	14	6		1000	16510	19400		31/32	17	14-14
	15	5		1000	16510	19400		1 1/32	18	15-15
	16	2		1000	16510	19400		31/32	8	16-16
	17	1		1000	16510	19400		1 1/32	3	17-17
	18	4		1000	16510	19400		31/32	13	18-18
	19	3		1000	16510	19400		30/32	14	19-19
	20	1		1000	16510	19400	0.	1 0	4	20-20

E. Caroban

Approuvé par

Table D 3.5   Elongation Measurements for Tie T3B6

APPENDIX E

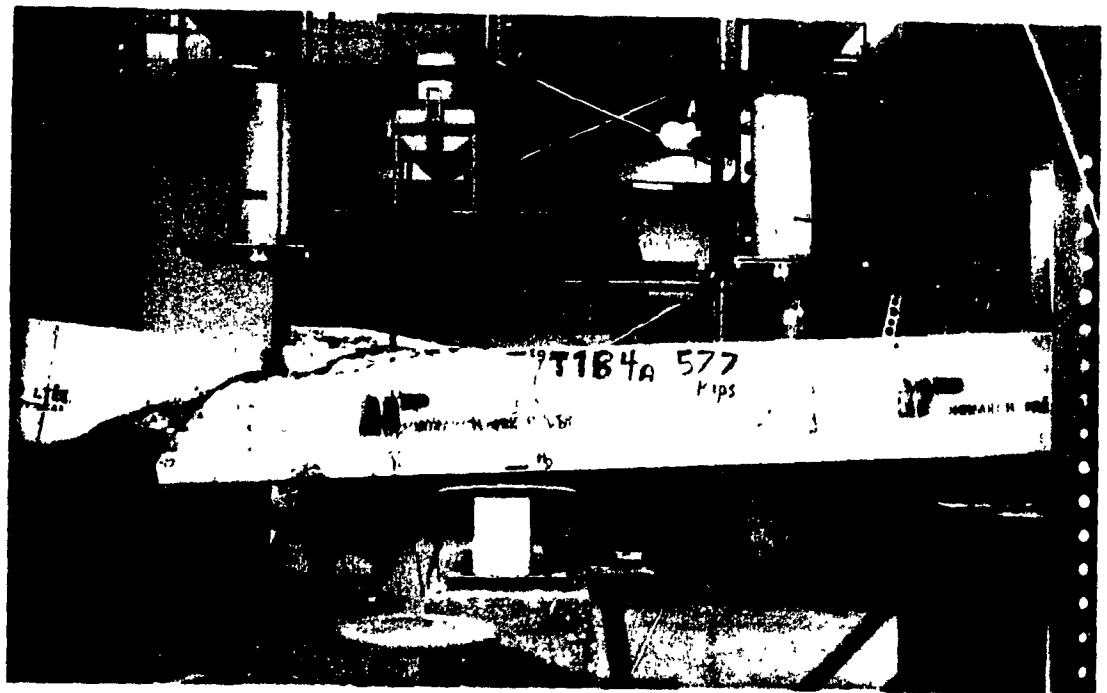## PHOTOGRAPHS OF FAILURE MODE

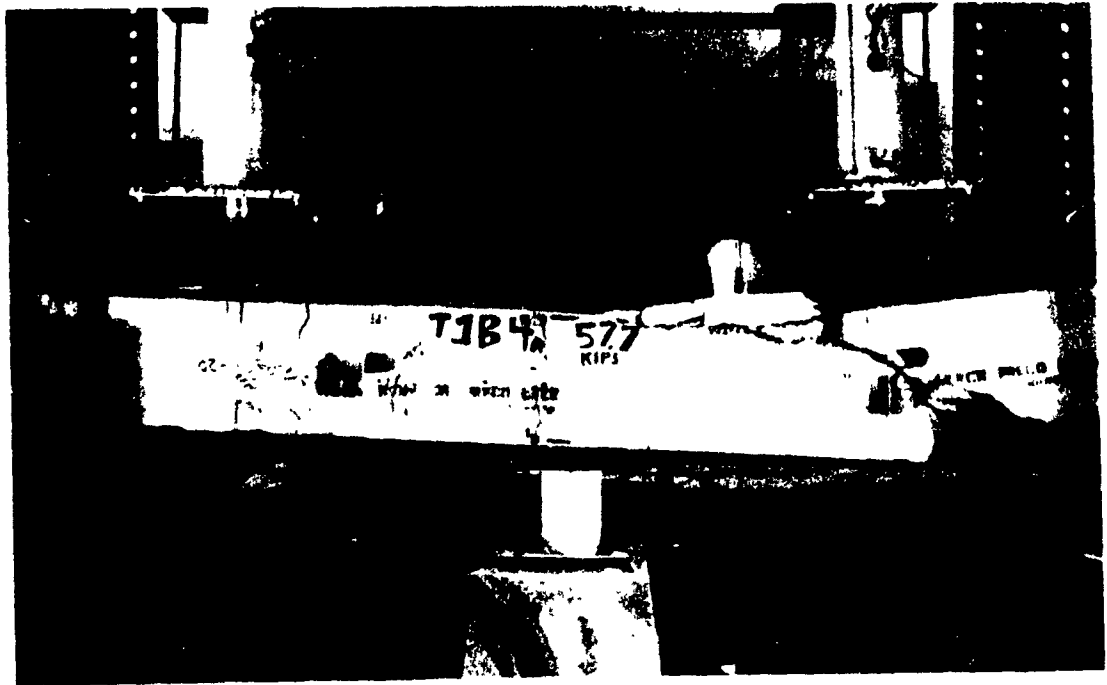## OF LABORATORY TESTED TIES

Figure E 1.0 Photographs of Failure Mode of Tie T1B4
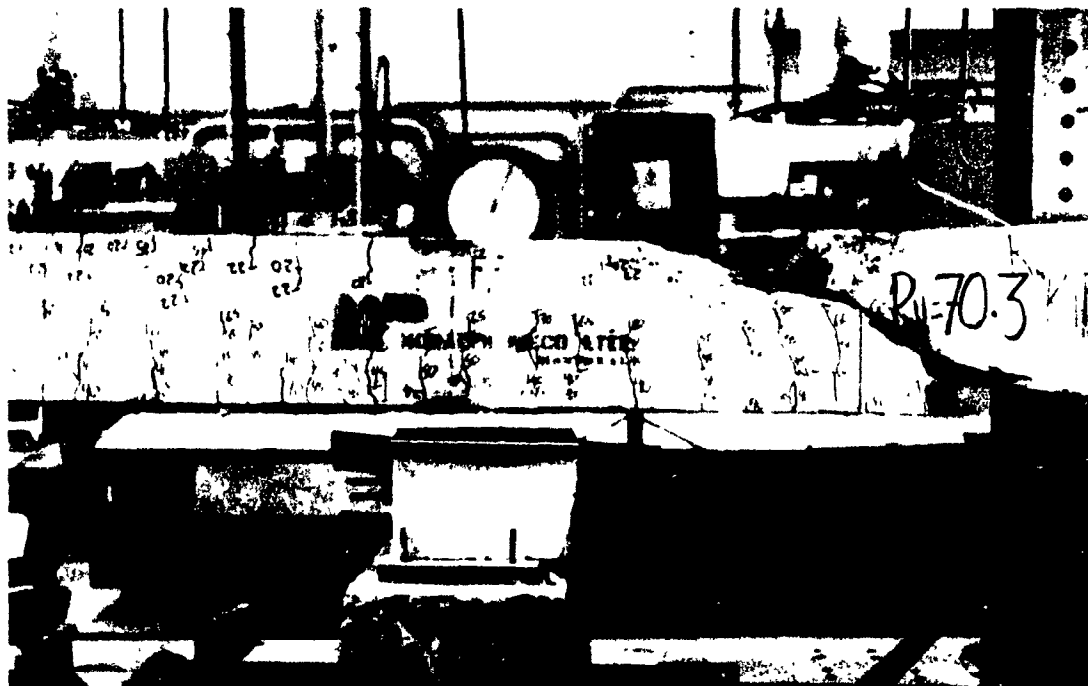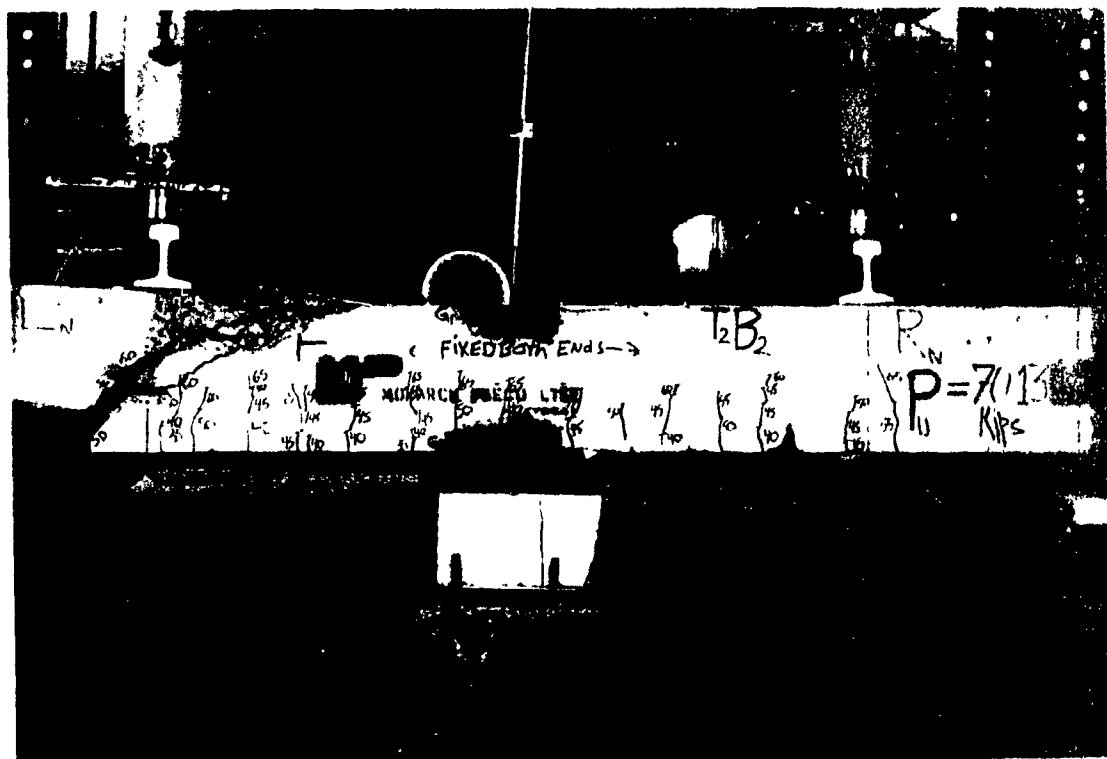
Figure E 1.1   Photographs of Failure Mode of Tie T2B1
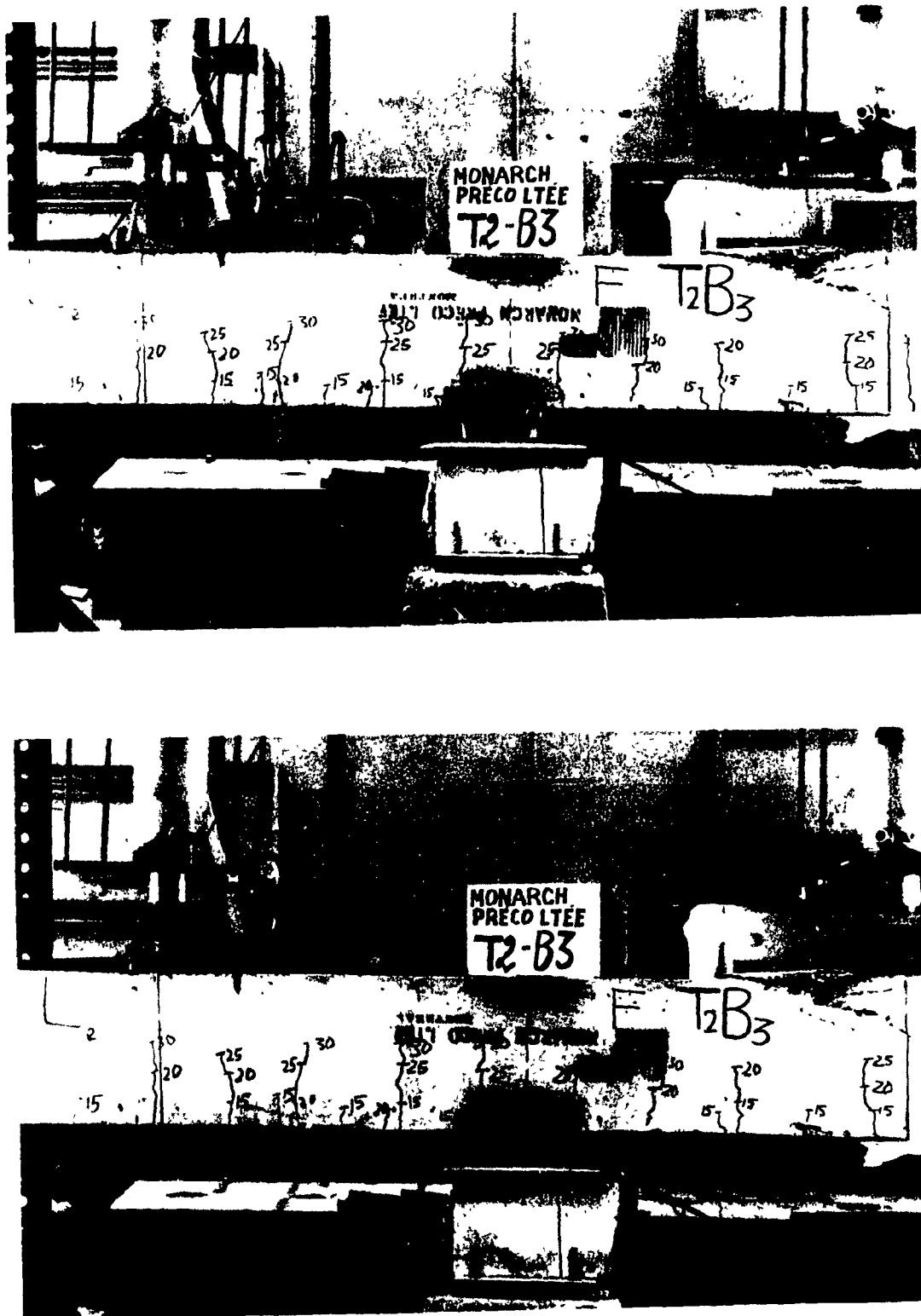
Figure E 1.2   Photograph of Failure Mode of Tie T2B2

244

Figure E 1.3   Photographs of Failure Mode of Tie T2B3